

**POCN-type Pincer Complexes of Ni^{II} and Ni^{III}:
Synthesis, Reactivities, Catalytic Activities and
Physical Properties.**

présentée par: Denis M. Spasyuk

Département de chimie
Faculté des arts et des sciences

Thèse présentée à la Faculté des études supérieures
en vue de l'obtention du grade de Philosophiæ Doctor (Ph.D.)
en chimie

Août, 2010

© Denis M. Spasyuk, 2010.

Cette thèse intitulée:

**POCN-type Pincer Complexes of Ni^{II} and Ni^{III}:
Synthesis, Reactivities, Catalytic Activities and
Physical Properties.**

présentée par: Denis M. Spasyuk

a été évaluée par un jury composé des personnes suivantes:

Garry Hanan, président-rapporteur
Davit Zargarian, directeur de recherche
Frank Schaper, membre du jury
Tom Baker, examinateur externe
Alain Vincent, représentant du Doyen de la Faculté

Résumé

Cette thèse décrit la synthèse, la caractérisation, les réactivités, et les propriétés physiques de complexes divalents et trivalents de Ni formés à partir de nouveaux ligands «pincer» de type POCN. Les ligands POCN de type amine sont préparés d'une façon simple et efficace via l'amination réductrice de 3-hydroxybenzaldéhyde avec NaBH_4 et plusieurs amines, suivie par la phosphination de l'amino alcool résultant pour installer la fonction phosphinite (OPR_2); le ligand POCN de type imine 1,3-(*i*-Pr) $_2\text{PC}_6\text{H}_4\text{C(H)=N(CH}_2\text{Ph)}$ est préparé de façon similaire en faisant usage de PhCH_2NH_2 en l'absence de NaBH_4 . La réaction de ces ligands «pincer» de type POCN avec $\text{NiBr}_2(\text{CH}_3\text{CN})_x$ en présence d'une base résulte en un bon rendement de la cycloméatation du lien C-H situé en *ortho* aux fonctions amine et phosphinite. Il fut découvert que la base est essentielle pour la propreté et le haut rendement de la formation des complexes «pincer» désirés. Nous avons préparé des complexes «pincer» plan-carrés de type POCN, $(\text{POCN}^{\text{RR}'})\text{NiBr}$, possédant des fonctions amines secondaires et tertiaires qui démontrent des réactivités différentes selon les substituants R et R'. Par exemple, les complexes possédant des fonctions amines tertiaires ArCH_2NR_2 ($\text{NR}_2 = \text{NMe}_2, \text{NEt}_2, \text{and morpholinyl}$) démontrent des propriétés rédox intéressantes et pourraient être convertis en leurs analogues trivalents $(\text{POCN}^{\text{R}^2})\text{NiBr}_2$ lorsque réagis avec Br_2 ou *N*-bromosuccinimide (NBS). Les complexes trivalents paramagnétiques à 17 électrons adoptent une géométrie de type plan-carré déformée, les atomes de Br occupant les positions axiale et équatoriale. Les analyses «DSC» et «TGA» des ces composés ont démontré qu'ils sont thermiquement stables jusqu'à ~ 170 °C; tandis que la spectroscopie d'absorption en solution a démontré qu'ils se décomposent thermiquement à beaucoup plus basse température pour régénérer les complexes divalents ne possédant qu'un seul Br; l'encombrement stérique des substitutants amines accélère cette route de décomposition de façon significative. Les analogues NMe_2

et N(morpholinyl) de ces espèces de Ni^{III} sont actifs pour catalyser la réaction d'addition de Kharasch, de CX₄ à des oléfines telles que le styrène, tandis qu'il fut découvert que l'analogue le moins thermiquement stable (POCN^{Et2})Ni est complètement inerte pour catalyser cette réaction.

Les complexes (POCN^{RH})NiBr possédant des fonctions amines secondaires permettent l'accès à des fonctions amines substituées de façon non symétrique via leur réaction avec des halogénures d'alkyle. Un autre avantage important de ces complexes réside dans la possibilité de déprotonation pour préparer des complexes POCN de type amide. De telles tentatives pour déprotoner les fonctions NRH nous ont permis de préparer des espèces dimériques possédant des ligands amides pontants. La nature dimérique de ces complexes [$\kappa^P, \kappa^C, \kappa^N, \mu^N$ -(2,6-(*i*-Pr)₂PC₆H₃CH₂NR)Ni]₂ (R= PhCH₂ et Ph) fut établie par des études de diffraction des rayons-X qui ont démontré différentes géométries pour les cœurs Ni₂N₂ selon le substituant N : l'analogue (PhCH₂)N possède une orientation *syn* des substitutants benzyles et un arrangement ressemblant à celui du cyclobutane du Ni et des atomes d'azote, tandis que l'analogue PhN adopte un arrangement de type diamant quasi-planaire des atomes du Ni et des atomes d'azote et une orientation *anti* des substituants phényles. Les espèces dimériques ne se dissocient pas en présence d'alcools, mais elles promouvoient l'alcoolyse catalytique de l'acrylonitrile. De façon intéressante, les rendements de ces réactions sont plus élevés avec les alcools possédant des fonctions O-H plus acides, avec un nombre de «turnover» catalytique pouvant atteindre 2000 dans le cas de *m*-cresol. Nous croyons que ces réactions d'alcoolyse procèdent par activation hétérolytique de l'alcool par l'espèce dimérique via des liaisons hydrogènes avec une ou deux des fonctions amides du dimère.

Les espèces dimériques de Ni (II) s'oxydent facilement électrochimiquement et par réaction avec NBS ou Br₂. De façon surprenante, l'oxydation chimique mène à l'isolation de nouveaux produits monomériques dans lesquels le centre métallique et le ligand sont oxydés. Le mécanisme

d'oxydation fut aussi investigué par RMN, «UV-vis-NIR», «DFT» et spectroélectrochimie.

Mots-clés: nickel (II), nickel (III), complexes «pincer» de type POCN, activation C-H, diffraction des rayons-X, RMN, voltampérométrie cyclique (CV), analyse thermogravimétrique (TGA), «differential scanning calorimetry» (DSC), spectroélectrochimie, addition de Kharash, hydroalkoxylation des oléfines.

Abstract

This thesis describes the synthesis, characterization, reactivities, and physical properties of divalent and trivalent complexes of Nickel based on new POCN-type pincer ligands. The amino-type POCN ligands were prepared in a simple and efficient manner via reductive amination of 3-hydroxybenzaldehyde with NaBH₄ and various amines, followed by phosphination of the resulting amino alcohol to install the phosphinite (OPR₂) functionality. The imino-type POCN ligand 1,3-(*i*-Pr)₂PC₆H₄C(H)=N(CH₂Ph) was prepared similarly using PhCH₂NH₂ in the absence of NaBH₄. Reaction of these POCN-type pincer ligands with NiBr₂(CH₃CN)_x in the presence of a base results in the high yield cyclometalation of the C-H bond which is *ortho* to the amine and phosphinite functionalities.

The base was found to be essential for a clean and high yield formation of the desired pincer complexes. We have thus prepared square planar POCN-type pincer complexes (POCN^{RR'})NiBr featuring tertiary or secondary amine moieties that exhibit different reactivities as a function of amine substituents R and R'. For instance, complexes bearing the tertiary amine moieties ArCH₂NR₂ (NR₂= NMe₂, NEt₂, and morpholinyl) displayed interesting redox properties and could be converted into their trivalent analogues (POCN^{R2})NiBr₂ when reacted with Br₂ or *N*-bromosuccinimide (NBS). These 17-electron, paramagnetic trivalent complexes adopt a distorted square pyramidal geometry with Br atoms at axial and equatorial positions. DSC and TGA analyses of these compounds revealed them to be thermally stable up to ~170 °C; whereas absorption spectroscopy in solution showed that they undergo thermal decomposition at much lower temperatures to regenerate the monobromo divalent complexes; increased steric bulk of the amine substituents accelerate this decomposition pathway significantly. The NMe₂ and N(morpholinyl) analogues of these Ni^{III} species are active catalysts for the Kharasch addition of CX₄ to olefins such as styrene, whereas the least thermally stable analogue (POCN^{Et2})Ni was found to be completely inert for this reaction.

The complexes (POCN^{RH})NiBr featuring secondary amine moieties allow access to unsymmetrically substituted amine moieties via reaction with alkyl halides. Another important advantage of these complexes lies in the possibility of deprotonation to prepare amide-type POCN complexes. Such attempts at deprotonating the NRH moieties have allowed us to prepare dimeric species featuring bridging amido ligands. The dimeric nature of these complexes [$\kappa^P, \kappa^C, \kappa^N, \mu^N$ -(2,6-(*i*-Pr)₂PC₆H₃CH₂NR)Ni]₂ (R= PhCH₂ and Ph) was established through X-ray diffraction studies that showed different geometries for the Ni₂N₂ cores as a function of *N*-substituent: the (PhCH₂)N analogue featured a *syn* orientation of the benzyl substituents and a cyclobutane-like arrangement of Ni and of the nitrogen atoms, whereas the PhN analogue adopted a nearly planar diamond-like arrangement of the Ni and of the nitrogen atoms and an *anti* orientation of the phenyl substituents. These dimeric species do not dissociate in the presence of alcohols, but they promote the catalytic alcoholysis of acrylonitrile. Interestingly, yields of these reactions are higher with alcohols possessing more acidic O-H moieties, with a catalytic turnover number reaching up to 2000 in the case of *m*-cresol. These alcoholysis reactions are believed to proceed through heterolytic activation of the alcohol by dimeric species via hydrogen bonding with one or two amido moieties in the dimer.

The dimeric Ni (II) species were found to undergo facile oxidation both electrochemically and in reaction with NBS or Br₂. Surprisingly, chemical oxidation led to isolation of new monomeric products in which both the metallic center and the ligand were oxidized, giving a trivalent species featuring an imine-type POCN ligand. Oxidation mechanism was investigated in detail by NMR, UV-vis-NIR, DFT and spectroelectrochemistry.

Keywords: nickel (II), nickel (III), POCN-type pincer complexes, C-H activation, X-ray diffraction, NMR, cyclic voltammetry (CV), thermogravimetric analysis

(TGA), differential scanning calorimetry (DSC), spectroelectrochemistry, Kharasch addition, olefin hydroalkoxylation.

Acknowledgements

I would like to thank **Davit Zargarian** for being a great supervisor and giving me the chance to visit several scientific conferences. I would like to thank him also for his “How-tos” on writing the papers and at the same time I take all blame for any possible linguistic errors I might (or might not) have committed in them.

My thanks to the great people I’ve met in Davit’s group and particularly **Annie Castonguay** who helped me start my project, benefit from her knowledge and for finding time to kindly and promptly translate the thesis abstract to French. During these long 3.5 years of my Ph.D, I have collaborated with many colleagues in our department for whom I have great regard. I want to thank all members of our chemistry department for providing an excellent and inspiring working atmosphere. I’m also thankful to all professors in our department who helped me during my studies and provided their valuable suggestion concerning my project.

I’m in debt to professors **Garry Hanan** and **Hein Schaper** from whom I have sometimes borrowed some chemicals. I am deeply grateful to my crystallography teachers **Hein Schaper**, **André Beauchamp** and **Michel Simard** for their extremely useful knowledge which was and I believe will be very useful in the future. Additional thanks to **Michel Simard** who allowed me to play with the “million dollar machine” and for his valuable help in solving couple of problematic crystal structures.

I would like to acknowledge all collaborators I had the pleasure to interact during my studies and particularly **Art van der Est** who provided me with the knowledge of EPR spectroscopy. It has been a great pleasure for me to collaborate with you!

I would also like to acknowledge the **evaluation committee** of this thesis for the careful reviewing of the manuscript and for the insightful comments.

VIII

My deep thanks to **Nadezhina Elena** for conducting all my elemental analysis and for great discussions over a cup of tea.

My thanks to the 11 **great summer students** I supervised during my Ph.D. who helped me practice my teaching skills and taught me the French language. I'm deeply sorry for not publishing results of your work guys, but I promise to do so shortly after my thesis defense.

My special gratitude is for the administration of our great department of chemistry and to its director **Robert Prud'homme** who accepted me in this amazing university and provided me with opportunity to work here. I am grateful to Université de Montréal and government of Canada for sponsoring this work and for helping me to explore this chemistry.

My last but not least thanks to my Mother, thanks to whom I am here accomplish what I have accomplished and to all my family who have greatly supported my desire for exploration.

Table of Contents

Résumé.....	I
Abstract.....	IV
Acknowledgements.....	VII
Table of Contents.....	IX
List of Tables.....	XIV
List of Figures.....	XVI
List of Schemes.....	XXI
List of Abbreviations.....	XXIII
Chapter 1: Introduction.....	1
1.1 Pincer ligands and complexes.....	1
1.2 Strategy for ligand cyclometallation.....	6
1.2.1 Formation of pincer complexes via C-X activation with low oxidation state of the metal precursors.....	6
1.2.2 Formation of pincer complexes with high valent metal precursors.....	8
1.2.3 Transmetallation and transcyclometallation.....	10
1.3 Transformations of the ligand backbone in pincer complexes.....	11
1.4 Application of pincer chemistry.....	14
1.4.1 Catalytic activities.....	14
1.4.2 Other applications.....	21
1.5 Nickel Pincer complexes: an overview.....	24
1.6 History and objectives of current research.....	26
1.7 References.....	27
Chapter 2: New POCN-Type Pincer Complexes of Ni ^{II} and Ni ^{III}	33
2.1 Abstract.....	34
2.2 Introduction.....	35

2.3	Results and Discussion	36
2.3.1	Synthesis of complexes.....	36
2.3.2	Characterization of 2.3(a-c)	40
2.3.3	Characterization of 3.5(a-c)	45
2.3.4	Thermal stabilities of 2.3 and 2.5	50
2.3.5	Kharasch addition.	54
2.4	Conclusions.....	56
2.5	Experimental Section	57
2.5.1	General.....	57
2.5.2	Synthesis of Pre-ligands 2.1a-c	58
2.5.3	Synthesis of POCN ligands 2.2a-c	60
2.5.4	Synthesis of complexes 2.3-2.5	62
2.5.5	Cyclic voltammetry.....	65
2.5.6	Crystal Structure Determinations.....	65
2.6	Acknowledgment.....	66
2.7	Supporting Information.....	66
2.8	References.....	72
Chapter 3: Monomeric and Dimeric Nickel Complexes Derived from a Pincer Ligand Featuring a Secondary Amine Donor Moiety		77
3.1	Abstract.....	78
3.2	Introduction	79
3.3	Results and Discussion	81
3.3.1	Syntheses.....	81
3.3.2	Characterization	83
3.3.3	Reactivity survey for 3.5	94
3.3.4	Catalytic hydroalkoxylation of acrylonitrile.....	96
3.4	Conclusion	100
3.5	Experimental Section	100
3.5.1	General.....	100
3.5.2	Ligand Synthesis.....	101

3.5.3	Synthesis of Complexes 3.1-3.5	103
3.5.4	General procedure for the reactivity survey.....	106
3.5.5	Typical procedure used for catalytic hydroalkoxylation of acrylonitrile.	107
3.5.6	Crystal Structure Determinations.....	108
3.6	Acknowledgements.....	109
3.7	Supporting Information.....	109
3.8	References.....	113
Chapter 4: Characterization of Divalent and Trivalent Species Generated in The Chemical and Electrochemical Oxidation of a Dimeric Nickel (II) Pincer Complex		121
4.1	Abstract.....	122
4.2	Introduction	123
4.3	Results and Discussions.....	125
4.3.1	Electrochemical oxidation of 4.1	125
4.3.2	Chemical oxidation of 4.1	128
4.3.3	Monitoring oxidation of 1 by NMR spectroscopy.....	130
4.3.4	Detection of oxidation products by EPR spectroscopy.....	132
4.3.5	UV-Vis studies on oxidation of complexes 4.1 , 4.3 , and 4.4 with NBS..	134
4.3.6	Computational studies.....	139
4.3.7	Characterization of 4.2 and 4.3 by NMR and X-ray diffraction analysis.	148
4.3.8	Conclusions.....	153
4.4	Experimental Section	156
4.4.1	General.....	156
4.4.2	Electrochemical measurements.....	159
4.4.3	EPR Spectroscopy.....	160
4.4.4	Computational Details.	161
4.4.5	Crystal Structure Determinations.....	161
4.5	Acknowledgment.....	162
4.6	Supporting Information.....	162
4.7	References.....	162

Chapter 5: Isonitrile Transformation to Carbene in Reaction With POCN Nickel Dimeric Species.....	168
5.1 Abstract.....	168
5.2 Introduction	168
5.3 Results and Discussions.....	169
5.4 Conclusion	176
5.4.1 General.....	177
5.4.2 Synthesis of the complex 5.1	178
5.4.3 Cyclic voltammetry.....	179
5.4.4 Crystal Structure Determinations.....	179
Chapter 6: POCN pincer complexes of nickel featuring secondary amine ligand arm.	182
6.1 Introduction	182
6.2 Results and Discussion	183
6.2.1 Syntheses.....	183
6.2.2 Characterisation	184
6.3 Conclusion.....	195
6.4 Experimental Section.....	195
6.4.1 General.....	195
6.4.2 Synthesis of ligands.....	196
6.4.3 Synthesis of Complexes 6.1–6.5	198
6.4.4 Crystal Structure Determinations.....	202
6.4.5 References.....	203
Chapter 7: Conclusions and perspectives.....	205
7.1 General.....	205
7.2 Synthesis of ligands and complexes.....	205
7.3 Tertiary amine-based POCN pincer complexes of nickel and their properties	208
7.4 Secondary amine-based POCN pincer complexes of nickel and their properties	210

7.5	References.....	214
Chapter 8: Appendixes		215
8.1	General.....	215
8.2	LinXTL	215
8.2.1	General introduction to LinXTL.....	215
8.2.2	Installation.....	216

List of Tables

Table 2.1. Crystal Data Collection and Refinement Parameters for Complexes 2.3a-c	43
Table 2.2. Selected Bond Distances (Å) and Angles (deg) for Complexes 2.3a-c	44
Table 2.3. Crystal Data Collection and Refinement Parameters for Complexes 2.5a-c	46
Table 2.4. Selected Bond Distances (Å) and Angles (deg) for Complexes 2.5a-c	47
Table 3.1 Crystal Data Collection and Refinement Parameters for Complexes 3.1, 3.3	87
Table 3.2. Crystal Data Collection and Refinement Parameters for Complexes 3.4, 3.5	88
Table 3.3. Selected Bond Distances (Å) and Angles (deg) for Complexes 3.1, 3.3, and 3.4	89
Table 3.4. Selected Bond Distances (Å) and Angles (deg) for Complex 3.5	90
Table 3.5. Alcoholysis of Acrylonitrile Catalyzed by Complex 3.5^a	98
Table 4.1. Spin-allowed absorption bands calculated for 4.1 and [4.1]⁺ . ^a	144
Table 4.2. Frontier molecular orbital energies and compositions (%) for 4.1 and [4.1]⁺	145
Table 4.3. Crystal Data Collection and Refinement Parameters for Complexes 4.2 and 4.3	151
Table 4.4. Selected Bond Distances (Å) and Angles (deg) for Complexes 4.2 and 4.3	152
Table 5.1. Crystal Data Collection and Refinement Parameters for Complexes 5.1	174
Table 5.2. Selected Bond Distances (Å) and Angles (deg) for Complexes 5.1 ..	175
Table 6.1. Crystal Data Collection and Refinement Parameters for Complex 6.1 and 6.5	192

Table 6.2. Crystal Data Collection and Refinement Parameters for Complex 6.2-6.4	193
Table 6.3. Selected Bond Distances (Å) and Angles (deg) for Complexes 6.1–6.4	194
Table 6.4. Selected Bond Distances (Å) and Angles (deg) for Complex 6.5	194

List of Figures

Figure 1.1. Example of Pincer ligand.	1
Figure 1.2. Example of symmetric and asymmetric pincer ligand.....	2
Figure 1.3. First pincer complexes made by Shaw.....	2
Figure 1.4. NCN ligand of van Koten.	3
Figure 1.5. PNP pincer system demonstrated by Fryzuk.....	4
Figure 1.6. Series of symmetric pincer ligands.	4
Figure 1.7. Several asymmetric pincer ligands.	5
Figure 1.8. Mechanism of amidation reaction.....	14
Figure 1.9. Examples of Heck catalysts.....	16
Figure 1.10. Mechanism of Kumada Coupling.	17
Figure 1.11. Examples of catalyst for Kumada coupling.....	18
Figure 1.12. Mechanism of Kharasch addition reported by van Koten.	19
Figure 1.13. Mechanism of dehydrogenation reaction proposed by Goldman.....	21
Figure 1.14. NCN platinum complex reported by Connick.....	21
Figure 1.15. Examples of NCN and SCS platinum pincer system.	22
Figure 1.16. 4,4'-stilbenoid NCN-Pincer Platinum(II) complexes.....	22
Figure 1.17. Retaining crystallinity during chemical transformation.	24
Figure 1.18. Examples of the nickel pincer complexes.	25
Figure 1.19. Example of POCN ligand.	27
Figure 2.1. Cyclic voltammograms of 1mM solutions of complexes 2.3(a-c) in dichloromethane containing 0.1M tetrabutylammonium hexafluorophosphate at 25 °C at a scan rate of 100 mV/s on a glassy carbon working electrode...	39
Figure 2.2. ORTEP diagram for complexes 2.3a (a), 2.3b (b), and 2.3c (c). Thermal ellipsoids are shown at the 50% probability level. Hydrogen atoms are omitted for clarity.	42
Figure 2.3. ORTEP diagram for complexes 2.5a (a), 2.5b (b), and 2.5c (c). Thermal ellipsoids are shown at the 50% probability level. Hydrogen atoms are omitted for clarity.	48

- Figure 2.4.** X-band (9 GHz) EPR spectrum of **2.5a** in toluene at 120 K. Microwave frequency 9.405102 GHz, microwave power 2 mW, modulation amplitude 1.0 G 50
- Figure 2.5.** The DSC curve of complexes **2.5(a-c)**: nitrogen flow of 20 mL/min, heating rate of 10 °C/min, ca. 8 mg samples weighed in an alumina crucible 52
- Figure 2.6.** The UV-vis spectra of 0.001 M toluene solutions of **2.5a** (70 °C) **2.5b** (70 °C) and **2.5c** (30 °C) as a function of time..... 54
- Figure 2.7.** TGA thermogram for complexes **2.3a-c** recorded at 20 °C/min using a platinum crucible..... 68
- Figure 2.8.** Cyclic voltammograms of 1 mM solutions of compound **2.1a** and **2.2a** in dichloromethane containing 0.1 M tetrabutylammonium hexafluorophosphate at 25 °C at a scan rate of 100 mV/s on a glassy carbon working electrode..... 69
- Figure 2.9.** Cyclic voltammograms of 1mM solutions of complexes **2.3(a-c)** and {2,6-(*i*-PrPO)₂C₆H₃}NiBr in dichloromethane containing 0.1 M tetrabutylammonium hexafluorophosphate at 25 °C at a scan rate of 100 mV/s on a glassy carbon working electrode. 70
- Figure 2.10.** Cyclic voltammograms of 1 mM solutions of complexes **2.5(a-c)** in dichloromethane containing 0.1 M tetrabutylammonium hexafluorophosphate at 25°C at a scan rate of 100 mV/s on a glassy carbon working electrode. The minor oxidation peak seen at ca. 1.08 V in the voltammogram of **2.5c** is due to the Ni^{II}→Ni^{III} process which is detectable since **2.5c** undergoes ready decomposition to 2.3c. The CV measurements were carried out using CH₂Cl₂ solutions containing Bu₄NPF₆ as electrolyte; different starting potentials were employed for **2.5a** and **2.5b** (0 V, Ag/Ag⁺) vs. the equilibrium potential for **2.5c**, with the same result. 71
- Figure 3.1.** Examples of POCOP and POCN pincer systems. 80
- Figure 3.2.** The methylene region in the ¹H-NMR spectra (C₆D₆) of complexes **3.1** (bottom), **3.5** (middle), and **3.4** (top)..... 85

- Figure 3.3.** ORTEP diagrams for complex **3.1** (a), **3.3** (b), and **3.4** (c). Thermal ellipsoids are set at the 50% probability level. Calculated hydrogen atoms are omitted for clarity..... 91
- Figure 3.4.** ORTEP diagram for complex **3.5** (view a, b). Thermal ellipsoids are set at the 50% probability level. Hydrogen atoms (phenyl groups view a), isopropyl groups view b) are omitted for clarity..... 92
- Figure 3.5.** The aliphatic region (1.9 to 4.7 ppm) of the ^1H -NMR spectrum (C_6D_6) right after mixing complex **3.5** (10 mg, 0.013 mmol) and m-cresol (100 μL , 0.013 mol/ dm^3 in C_6D_6)..... 110
- Figure 3.6.** The ^1H -NMR spectrum of the above mixture (same spectral region) after about 10 min of reaction 111
- Figure 3.7.** the ^1H -NMR spectrum of the above mixture with additional 7 equivalents of m-cresol (same spectral region) after about 10 min of reaction. 112
- Figure 4.1.** Dimeric species **4.1**..... 124
- Figure 4.2.** Cyclic voltammogram measured at 25 $^\circ\text{C}$ for a 1 mM dichloromethane solution of **4.1** containing tetrabutylammonium hexafluorophosphate as supporting electrolyte (0.1 M). The measurements were conducted using a glassy carbon working electrode at a scan rate of 100 mV/s. See Experimental Section for full details on the electrochemical studies. 126
- Figure 4.3.** Absorption spectra of **4.1** in dichloromethane before (a) and after (b) the electrochemical oxidation at $E_{\text{ox}} = 550$ mV. 127
- Figure 4.4.** X-band (9 GHz) EPR spectra (toluene, 120 K) of the oxidation product(s) of **4.1** with 1 equiv of NBS (A) and compound 2 (B). The solid lines are experimental spectra, the dashed curves are simulations. Simulation parameters A: $g_{xx}=g_{yy}=g_{\perp}=2.22$, $g_{zz}=g_{\parallel}=2.01$, $I=3/2$ nucleus $A_{xx}=A_{yy}=A_{\perp}=30$ G, $A_{zz}=170$ G; B: $g_{xx}=2.23$ $g_{yy}=2.19$, $g_{zz}=2.01$, $I=3/2$ nucleus $A_{xx}=A_{yy}=30$ G, $A_{zz}=170$ G. Microwave frequency: 9.401599 GHz; microwave power: 2 mW; modulation amplitude: 1.0 G..... 134

- Figure 4.5.** UV-Vis spectra of nickel complexes (0.4 mM in DCM, 25 °C) with or without NBS: (a) **4.1** + 4 equiv NBS; (b) **4.3** + **4.4** + 1.1 equiv NBS; (c) complex **4.2** alone; (d) **4.4** + 1.1 equiv NBS. 136
- Figure 4.6.** UV-Vis spectra (25 °C) of the divalent complexes **4.3** (a) and **4.4** (b); both samples ca. 0.4 mM. 136
- Figure 4.7.** UV-Vis spectra (25 °C) of **4.1** (2.5 mL of a 0.4 mM solution in DCM, spectrum 0) with 50 μ L aliquots of a 4 mM solution of NBS in DCM (spectra 1-14). 137
- Figure 4.8.** UV-Vis spectra (25 °C) recorded during the initial stage of the titration of **4.1** with NBS. See main text for titration details. 138
- Figure 4.9.** UV-Vis spectra (25 °C) recorded during the second stage of the titration of **4.1** with NBS. See main text for titration details. 138
- Figure 4.10.** Frontier molecular orbitals of **4.1**: LUMO (a) and HOMO (b). Isosurface value of 0.04 a.u. Spheres are coloured to signify the atoms in keeping with convention: grey for carbon, blue for nitrogen, orange for phosphorus, red for oxygen, light-blue for nickel. H atoms are not shown for clarity. 141
- Figure 4.11.** Spin density and frontier molecular orbitals of [**4.1**]⁺: spin density (a; isosurface value of 0.004 a.u.), β -spin LUMO (b; isosurface value of 0.04 a.u.), β -spin HOMO-10 (c; isosurface value of 0.04 a.u.). Spheres are coloured to signify the atoms in keeping with convention: grey for carbon, blue for nitrogen, orange for phosphorus, red for oxygen, light-blue for nickel. H atoms are not shown for clarity. 143
- Figure 4.12.** TD-DFT-calculated visible absorption spectra of **4.1** (solid line) and [**4.1**]⁺ (dash line), calculated at the B3LYP/TZVP level of theory. 147
- Figure 4.13.** ORTEP diagrams for complex **4.2** (a) and **4.3** (b). Thermal ellipsoids are set at the 50% probability level. Hydrogen atoms are omitted for clarity. 150
- Figure 4.14.** Mixvalent species. 156

Figure 5.1. The methylene region in the $^1\text{H-NMR}$ spectra (C_6D_6) of complexes 5.1	171
Figure 5.2. ORTEP diagram for complexes 5.1 . Thermal ellipsoids are shown at the 50% probability level. Hydrogen atoms and benzyl group (C31) are omitted for clarity.....	173
Figure 5.3. Cyclic voltammogram of 1 mmol/dm ³ solutions of complex 5.1 , in dichloromethane containing 0.1 mol/dm ³ tetrabutylammonium hexafluorophosphate at 25 °C at a scan rate of 100 mV/s on a glassy carbon working electrode.....	176
Figure 6.1. The methylene region in the $^1\text{H-NMR}$ spectra (C_6D_6) of complexes 6.1-6.4	185
Figure 6.2. Structural features of POCN pincer complexes.....	187
Figure 6.3. ORTEP diagrams for complexes 6.1 (a), 6.2 (b), 6.3 (c) and 6.4 (d). Thermal ellipsoids are set at the 50% probability level. Calculated hydrogen atoms are omitted for clarity.....	189
Figure 6.4. ORTEP diagrams for complex 6.5 . Thermal ellipsoids are set at the 50% probability level.....	191
Figure 7.1. Structural features of (POCN)Ni complexes.....	208
Figure 7.2. Comparison of Ni^{III} stability.	209
Figure 8.1. Screenshot of LinXTL	216

List of Schemes

Scheme 1.1. Example of Kharasch addition.	3
Scheme 1.2. Pincer hemilabile effect with PCN Pt (II) complexes.	5
Scheme 1.3. Cyclometalation reported by Ozerov.	6
Scheme 1.4. Cyclometalation by Milstein.	7
Scheme 1.5. C-C activation with osmium precursor.	7
Scheme 1.6. Oxidative addition pathway from Pt(II) to Pt(IV).	8
Scheme 1.7. Cyclometalation of NCN ligand reported by Richards.	9
Scheme 1.8. Side product formation with PCsp ² P ligand.	9
Scheme 1.9. Cyclometalation of PCP ligand by Adams.	10
Scheme 1.10. Example of transmetallation.	10
Scheme 1.11. Example of transcyclometallation.	11
Scheme 1.12. Alkylation and acylation of OH group in pincer ligand backbone.	12
Scheme 1.13. Carboxylation of pincer ligand backbone.	13
Scheme 1.14. The amination and reduction of aldehyde group in ligand backbone.	13
Scheme 1.15. Example of Heck reaction.	15
Scheme 1.16. Example of Kumada coupling.	16
Scheme 1.17. Kharasch addition.	18
Scheme 1.18. Example of dehydrogenation reaction.	20
Scheme 1.19. Reversible association of SO ₂ to the NCN pincer complex.	23
Scheme 1.20. First C-H activation with Nickel.	24
Scheme 2.1. Synthesis of ligands and complexes.	37
Scheme 2.2. Effect of the base in cyclometallation.	38
Scheme 2.3. Kharasch addition.	55
Scheme 3.1. Possible transformation pathways of (POCNHR)Ni complexes.	80
Scheme 3.2. Synthesis of ligands and complexes.	82
Scheme 3.3. Reactivities of complex 3.1.	83
Scheme 3.4. Reactivity survey for complex 3.5.	94
Scheme 3.5. Hydroalkoxylation reaction	97

Scheme 4.1. Electrochemical oxidation of 4.1	126
Scheme 4.2. Chemical oxidation of 4.1	128
Scheme 4.3. Alternative synthesis of 4.2	130
Scheme 4.4. Monitoring chemical oxidation by NMR.....	131
Scheme 4.5. Thermal decomposition of 4.2	148
Scheme 4.6. Mechanism of oxidation of 4.1	153
Scheme 5.1. Synthesis of complex 5.1	170
Scheme 6.1. Synthesis of POCN-type ligand.....	183
Scheme 6.2. Cyclometallation reaction	184
Scheme 6.3. Transformation of 6.1 to 6.5	184
Scheme 7.1. Synthesis of POCN pincer ligand.....	205
Scheme 7.2. Reductive amination with bulkier amines.	206
Scheme 7.3. Phosphination of primary amine adducts.....	206
Scheme 7.4. POCN pincer complex formation.	207
Scheme 7.5. Reactivities of secondary amine complexes.	210
Scheme 7.6. Hydroalkoxylation reaction.	211
Scheme 7.7. Oxidation of dimeric POCN complex.....	213
Scheme 7.8. Transformation of complex 3.5 in reaction with 2,6-CH ₃ C ₆ H ₃ isocyanide.	214

List of Abbreviations

Å	Ångstrom
Bn	Benzyl group (-CH ₂ C ₆ H ₅)
br	Broad (spectral)
calcd	Calculated
COD	Cyclooctadiene (ligand)
COSY	Correlation spectroscopy (NMR)
d; h	Day(s), doublet (spectral); hours
DCM	Dichloromethane
dd	Doublet of doublet
DEPT	Distortionless Enhancement by Polarisation Transfer (NMR)
Equiv./eq.	Equivalents
Et ₂ O	Diethyl ether
EtOAc	Ethyl acetate
GC/MS	Gas chromatography with mass spectrometry
HMBC	Heteronuclear Multiple Bond Correlation (NMR)
HMQC	Heteronuclear Multiple Quantum Coherence (NMR)
<i>in situ</i>	Latin, in the place
<i>i</i> -Pr	Isopropyl group
Lg	Leaving group
NBS	N-bromosuccinimide
n-Bu	Primary butyl group
vs	Versus
nm	Nanometres
MP	Melting point
PCsp ² P	1,3-bis(phosphino)benzene
PCsp ³ P	1,5-bis(phosphino)pentane
Ph, Ar	Phenyl group (-C ₆ H ₅)
pKa	Acid dissociation constant

POCN	3-((alkylamino)methyl)phosphinitobenzene
POCsp ² OP	1,3-bis(phosphinito)benzene
POCsp ³ OP	1,3-bis(phosphinito)propane
R	Generic group
rt	Room temperature
s	Singlet (spectral), second(s)
TBDMS	tert-Butyldimethylsilyl
t	Triplet (spectral)
TON	Turnover number
<i>t</i> -Bu	Tertiary butyl group
THF	Tetrahydrofuran

Chapter 1: Introduction

1.1 Pincer ligands and complexes

A pincer ligand is a type of tridentate chelating organic compound that generally consists of two coordinating functionalities like amine, phosphine, ether, thioether, carbene etc. and one anionic functionality like alkyl, aryl, silyl, boryl, amide, phosphide between them (Figure 1.1). Together, these functionalities allow the ligand to bind metal in a tridentate meridional chelating manner.

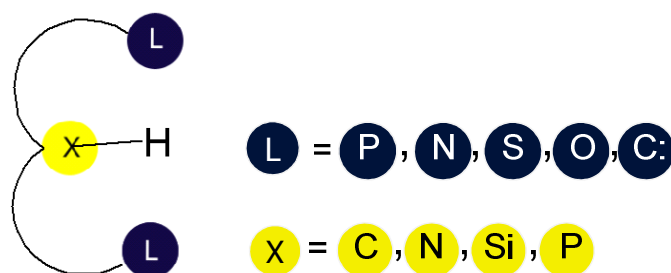


Figure 1.1. Example of Pincer ligand.

There are many different types of pincer ligands known in the literature and all of them could be separated into two primary types: symmetric and asymmetric pincer ligands (Figure 1.2).

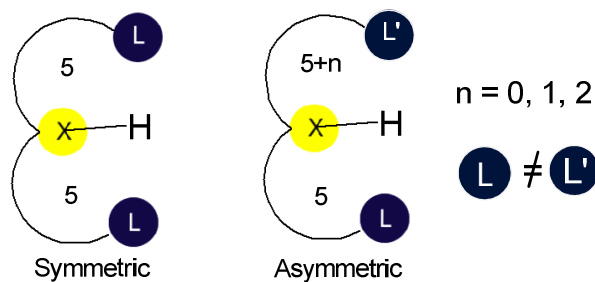


Figure 1.2. Example of symmetric and asymmetric pincer ligand.

Symmetric pincer ligands have been known for a long time since the original introduction of pincer complexes in 1976 by Shaw¹ and coworkers. First pincer complexes featured a series of transition metals, primary late transition metals, such as Ni, Pd, Pt, Rh, Ir and were based on the PCsp²P pincer system shown below (Figure 1.3).

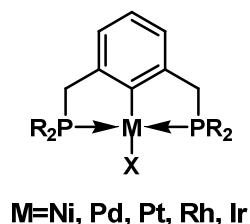


Figure 1.3. First pincer complexes made by Shaw.

Shaw noticed potential use of these complexes in the catalytic applications and highlighted their important features such as thermal stability and ability to sustain the unusual oxidation state of the metal.

After introduction of pincer complexes by Shaw, this chemistry was forgotten for few years and in 1979 pincer topic was continued by van Koten who concentrated his work primarily on newly developed NCN pincer type ligand (Figure 1.4).

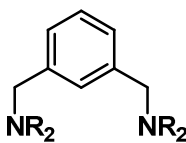
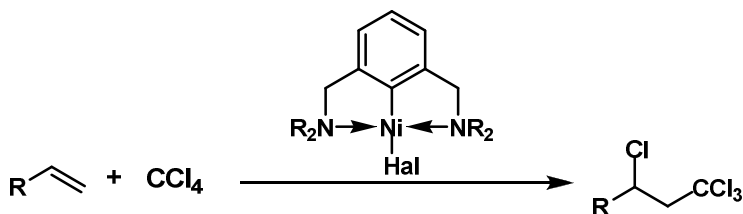


Figure 1.4. NCN ligand of van Koten.

Thus, van Koten's group synthesized a series of complexes based on Ni, Pt and Pd and for the first time, structurally characterized these complexes and reported their chemical reactivities and catalytic activities in the reaction of Kharasch² addition. Also, this was the first group to report stable Ni^{III} complexes featuring Ni-C linkage and to highlight a great importance of this oxidation state of the Nickel for catalytic activities in Kharasch addition reaction (Scheme 1.1).



Scheme 1.1. Example of Kharasch addition.

First decades of pincer chemistry have witnessed the development of many other pincer ligands. Thus, Fryzuk³ reported an interesting example of “hybrid” PNP-type pincer ligand, featuring soft phosphine donors and hard anionic nitrogen ligand. Additionally, this ligand was incorporating two dimethylsilane linkages which were protecting metal from reductive elimination or oxidation (Figure 1.5) Complexes of this type were synthesized with nickel and palladium, and were structurally characterized. More recent advances of this chemistry demonstrated by Caulton's group will be discussed later on.

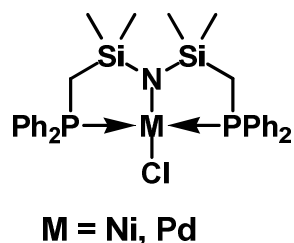


Figure 1.5. PNP pincer system demonstrated by Fryzuk.

Majority of the earlier pincer complexes were based on the symmetric pincer ligands with aromatic backbone featuring not only phosphines or amines as coordination ligands but also sulfur, oxygen or even selenium atoms were used (Figure 1.6). Thus NCN,⁴ POCOP,⁵ PNCNP,⁶ SCS, CCC⁷ pincer ligands were developed and their complexes were structurally characterized.

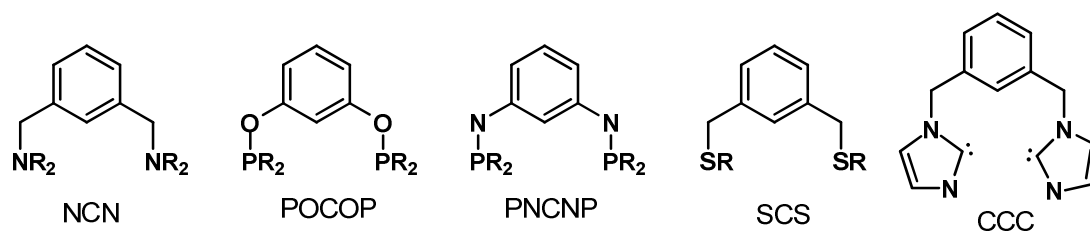


Figure 1.6. Series of symmetric pincer ligands.

Some extensive studies in symmetric pincer ligand were done using POCOP pincer system which was originally introduced by Jensen in 1998.⁸ Eventually, interesting reactivities of this type of system was discovered based on Ir for dehydrogenation of alkanes to olefins.

Later, a number of asymmetric pincer ligands were developed containing mixed donor atoms PCN,⁹ NCS¹⁰ and PCS¹⁰-type pincer ligands. The chemistry of these ligands remains significantly less developed compared to the chemistry of symmetric ones (Figure 1.7) but the number of reports concerning the nonsymmetrical pincer ligands grows every year.¹¹

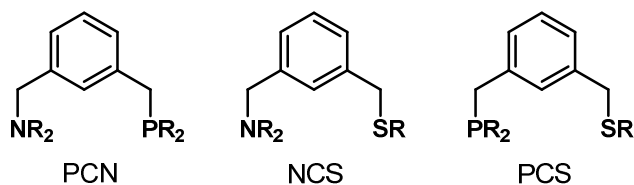
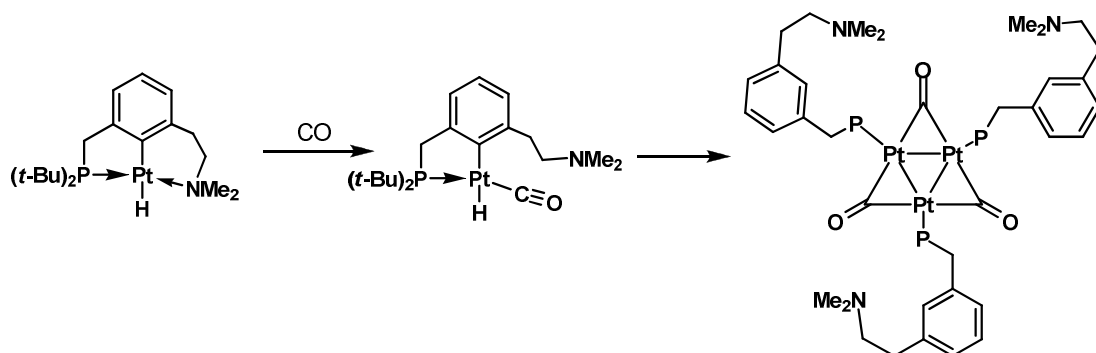


Figure 1.7. Several asymmetric pincer ligands.

Aside from the interesting structural features of non symmetric pincer ligands, there are interesting possibilities of tuning electronic properties of the metal by changing donor substituents. Additionally, use of hemilabile ligands¹² such as oxygen or nitrogen in unsymmetrical pincer ligand structure allows to achieve control over other possible catalytic reaction pathway and this significantly increases the numbers of active sites on the metal center thereby increasing its performance. However, use of hemilabile ligand sometimes presents a drawback where the ligand undergoes irreversible dissociation from the metal core and decomposition ensues. For example, the reaction of a platinum hydride PCN pincer complex with CO_{gas} , reported by Milstein and coworkers, leads to reductive elimination and a formation of a structurally characterized cluster (Scheme 1.2).



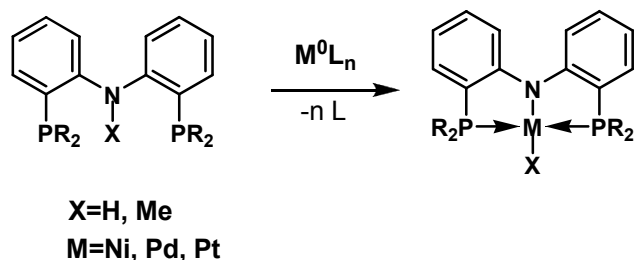
Scheme 1.2. Pincer hemilabile effect with PCN Pt (II) complexes.

1.2 Strategy for ligand cyclometallation

The cyclometallation is a process during which the metal precursor undergoes reaction with a chelating ligand and forms a metallacycle. In the case of pincer ligands, the cyclometallation proceeds through formation of two metallacycles arranged in a B-shaped formation. Generally, the most complicated process in pincer complex formation is the XH activation and so many methods have been developed to achieve such transformation.

1.2.1 Formation of pincer complexes via C-X activation with low oxidation state of the metal precursors

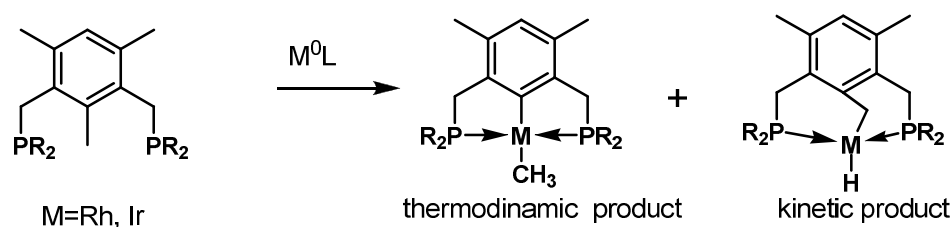
Cyclometallation, could be achieved through different pathways. There are a number of reports in the literature describing the use of low oxidation state metal precursors in cyclometallation reaction which generally lead to formation of corresponding metallacycles with a metal-X (X=H, CH₃, Cl, etc.) moiety in the resulting complex.^{13,14,15} For instance, Ozerov^{13a} and coworkers have reported the formation of pincer complexes based on PNP pincer type ligands via activation of NX (X=H, CH₃) bond (Scheme 1.3).



Scheme 1.3. Cyclometallation reported by Ozerov.

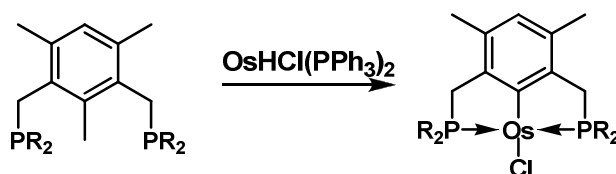
Using the metal precursor based on a group 10 metal, Ozerov's group was able to achieve good to moderate yields of the hydrido- and methyl- complexes. Interestingly, the best conversion in this case, was displayed with nickel and palladium while platinum shows somewhat sluggish conversion.

Formation of pincer complexes via activation of C-C bonds has been studied by Milstein's group. In his pioneering report regarding cyclometalation chemistry of PC(CH₃)P ligand Milstein demonstrated both activation of aliphatic C-H bond as well as C-C bond activation by Rh and Ir precursors at room temperature.¹⁶ Interestingly enough, the C-H bond activation adduct was reported irreversibly converted to the C-C activation complex which is eventually, after investigation of mechanistic details of this reaction, found to be the thermodynamically favorable product. (Scheme 1.4).



Scheme 1.4. Cyclometalation by Milstein.

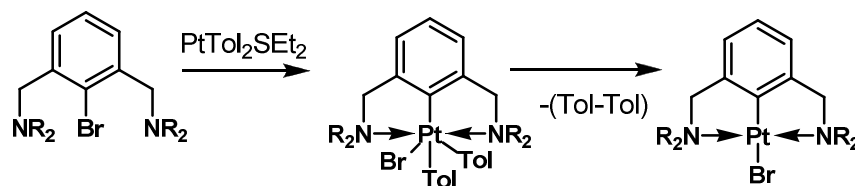
Similar findings were reported by performing computational studies on mechanism of the reaction.¹⁷ On the other hand, using OsHCl(PPh₃)₂ precursor with PC(CH₃)P ligand furnished PCPOsClPPh₃ by elimination of methane via C-C activation while C-H activation and formation of CH₃Cl were not observed¹⁸ (Scheme 1.5).



Scheme 1.5. C-C activation with osmium precursor.

Although formation of pincer complexes via C-H or N-H oxidative addition is fairly rare in literature, the oxidative addition of C-Hal is more common and strongly exploited in van Koten's chemistry¹⁹. Similar to C-H oxidative addition, C-Hal activation reaction generally proceeds through

oxidation of metal from 0 to 2 oxidation state and formation of M-Hal precursor which is more stable than corresponding M-H species and usually much easier to manipulate with. At the same time, cyclometalation of pincer ligand by high-valent metal precursors such as bis(tolyl)platinum was also reported in literature and in this case the oxidative addition pathway from Pt(II) to Pt(IV) was proposed²⁰ (Scheme 1.6).

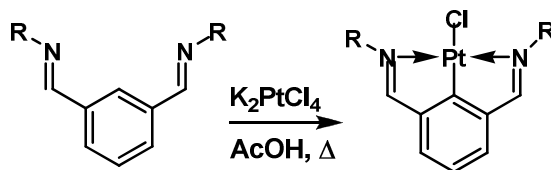


Scheme 1.6. Oxidative addition pathway from Pt(II) to Pt(IV).

1.2.2 Formation of pincer complexes with high valent metal precursors

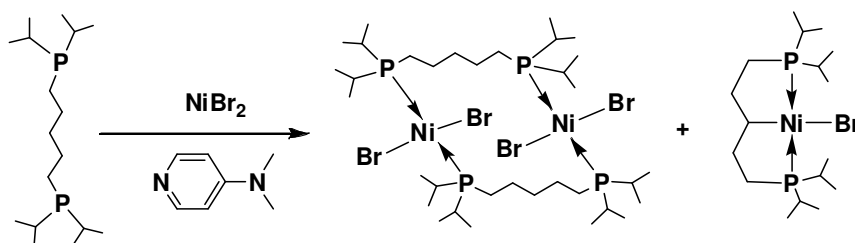
One of the biggest disadvantages of the above method for formation of pincer complexes formation is the need to preactivate the ligands prior to reaction with metal precursors. Generally, halogenation in position 2 of aromatic core is used. Additionally, use of highly reactive low-valent metal precursors is required for which special conditions of manipulation and handling are necessary. From economic point of view, low valent metal precursors are more expensive than their high valent versions. Moreover, precursors with higher oxidation state of the metal are much easier to handle since most of them are air stable and does not require special inert atmosphere. On the other hand, sometimes it is almost impossible to achieve cyclometalation of ligand with high valent precursors due to their insufficient reactivity or domination of other side processes. For example NC(H)N pincer ligand developed in van Koten's group is almost impossible to cyclometallate by the use of high-valent metal precursors. Just recently, using pincer systems similar to van Koten's NCN ligands, Richard's group has reported a new way to potentially overcome cyclometalation problem. In their work, they used 1,3-diimino substituted NCN-type pincer ligand and K_2PtCl_4 in glacial acetic

acid as a solvent to achieve the final complex in about 30-50 % yield.²¹ These findings are of great interest since they provide a relatively cheap synthetic pathway toward one of the most used types of the pincer ligand (Scheme 1.7).



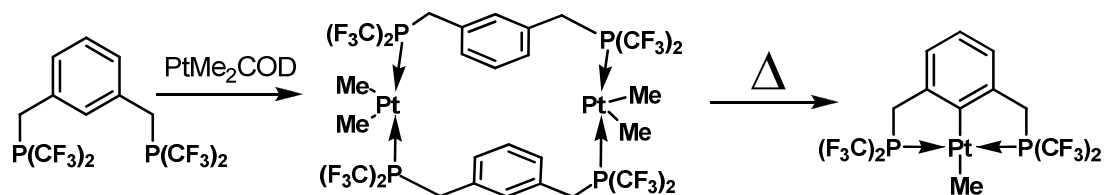
Scheme 1.7. Cyclometalation of NCN ligand reported by Richards.

Similar issues were addressed in some of our group's earlier publications, particularly with aliphatic PCsp³P ligands.²² During cyclometalation of these ligands, significant amounts of side products such as dimeric Ni^{II} species were formed and eventually recovered from reaction mixture (Scheme 1.8)



Scheme 1.8. Side product formation with PCsp²P ligand.

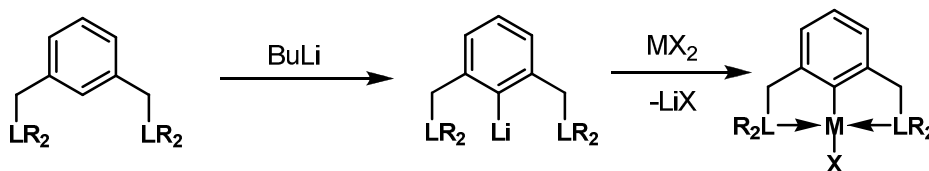
Contrary to NCsp²N pincer systems, PCsp²P type ligand was reported having no difficulty to cyclometallate with various types of late transition metal precursors. Use of pincer complexes based on this type of ligand with Ni, Pd, Pt, Ir, and Rh was the pioneering work in the pincer chemistry originated by Shaw and coworkers back in 1976. However, formation of dimers by using high valent metal precursors, similar to that described above for nickel, can be spotted in literature. Roddick²³ have reported a PCsp²P ligand which undergoes the formation of dimer prior to cyclometalation (Scheme 1.9).



Scheme 1.9. Cyclometalation of PCP ligand by Adams.

1.2.3 Transmetallation and transcyclometallation

Aside from the direct metallation of pincer ligands, there are a number of reports in the literature dealing with the preparation of pincer complexes via transmetallation and this pathway is reported to be successful in cases where direct cyclometalation route has failed. Generally, transmetallation is referred to substitution reaction of one metal, usually lithium, by transition metals²⁴ (Scheme 1.10).



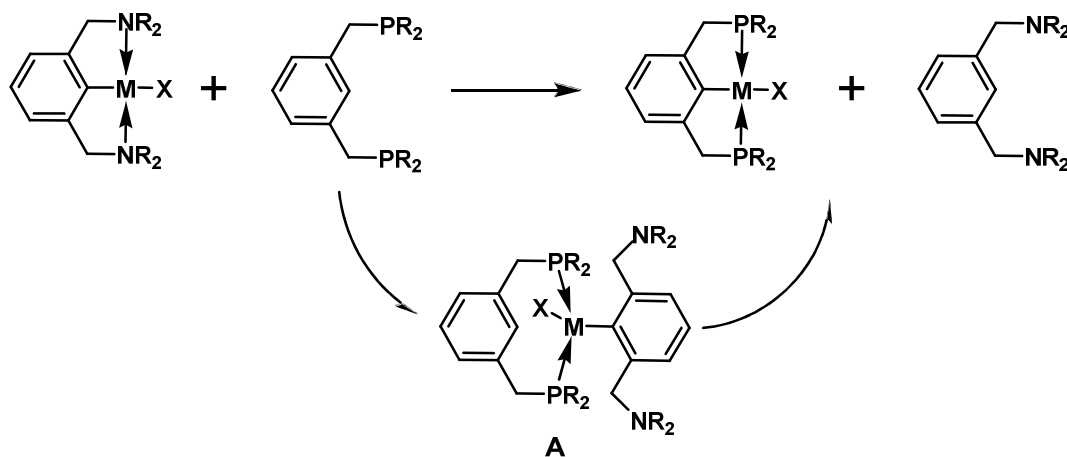
Scheme 1.10. Example of transmetallation.

The major use of transmetallation can be found in the chemistry of LXL (X=N, P) ligands. The X-H activation in these systems is complicated by the formation of M-XH coordination bond, which is the kinetic intermediate of cyclometalation reaction. Further X-H activation is somewhat sluggish and reported to take place only with certain types of transition metals. In these cases lithiation or use of other strong bases, such as sodium or potassium alkyl or alkoxide reagents are required in order to generate the metallation product.

The transmetallation approach for pincer complex formation was used by several researchers with transition metals or ligands where the conventional direct

cyclometalation route was found to be ineffective or impossible. For example, NCN²⁵ and PNP¹³ type pincer ligand systems are generally very hard to cyclometallate via the direct route and so preactivation of the ligands by lithiation is required in order to achieve desirable complexation. Overall, use of transmetallation pathway is proven to be successful and sometimes unique for preparation of pincer complexes.

Recently, van Koten's group introduced to the pincer chemistry another way of ligand transmetallation as transcyclometallation or TCM.²⁶ However the use of this method is limited for a narrow range of ligands. Original investigation of TCM was conducted with NCN and PCP pincer ligands where (NCN)Ru complex was used.²⁷ According to literature examples, nitrogen containing ligands can be easily displaced by more strongly coordinating ligands such as phosphines. As stated by van Koten, (PCP)Ru pincer complex can be smoothly prepared by transcyclometallation route from (NCN)Ru system. Intermediate **A** (Scheme 1.11) was not only observed but also was isolated and structurally characterized.



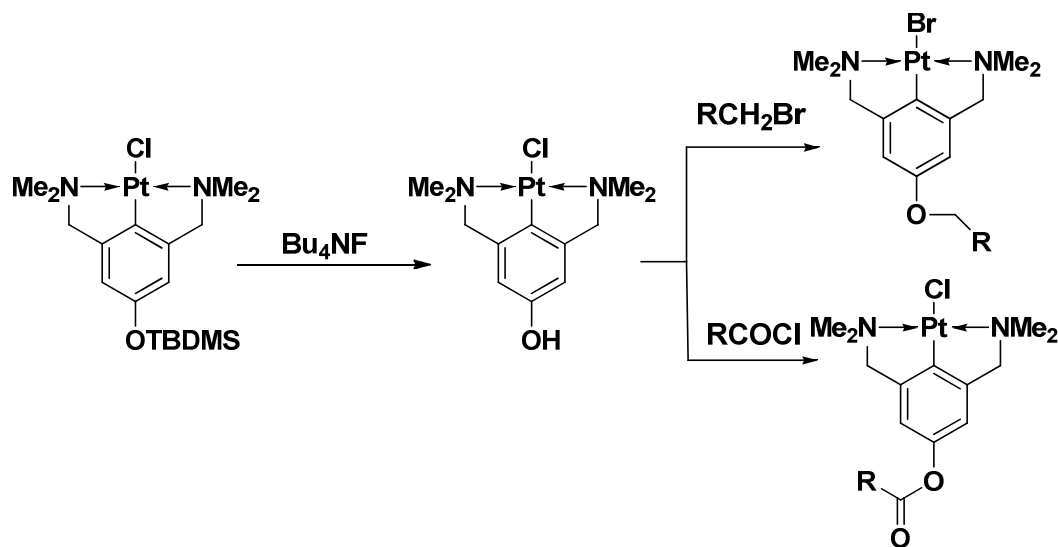
Scheme 1.11. Example of transcyclometallation.

1.3 Transformations of the ligand backbone in pincer complexes

One of the promising areas of the pincer chemistry is modification of ligand backbone in the pincer complex. This would allow derivatization of the pincer complexes and perhaps creation of new materials and more complex catalytic systems. Most of the literature available on this subject, generally, deals with ligand modification prior to the cyclometallation.²⁸ This approach helps to avoid the possible complication which might arise from using reactive reagents.

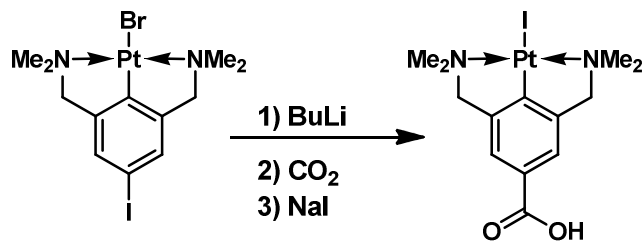
Unfortunately, presence of highly reactive metal center does not allow the use of common reagents, which are necessary for organic transformation to take place. Radical reactions, electrophilic substitutions in aryl cores and nucleophilic substitutions are hard to imagine in pincer chemistry. Most of these reactions utilize very strong acids, bases or highly active oxidants which, could damage or transform the metal and its surroundings and perhaps lead to intractable mixtures of products. Nevertheless, some of these transformations are possible and have been illustrated previously by several research groups.

Remarkable reactivities in this area of research were demonstrated by Rodriguez²⁹ and Suijkerbuijk,³⁰ based on (NCN)Pt complexes. Interestingly, the platinum complexes reported in these papers undergo multistep modifications of the ligand backbone without having significant influence on the platinum center (Scheme 1.12).²⁹



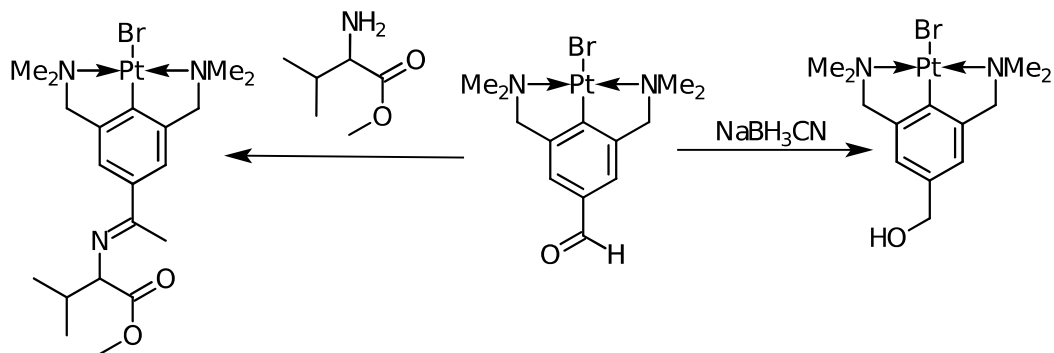
Scheme 1.12. Alkylation and acylation of OH group in pincer ligand backbone.

Interesting reactivities were demonstrated in the reaction of complex 4-I-(NCN)PtCl with BuLi, which undergoes transformation of both metal Pt-Br and ligand C-I bonds. However reactions with CO₂ and salt methathesis with NaI subsequently introduces carboxylic group to the ligand structure and regenerates platinum surrounding (Scheme 1.13).



Scheme 1.13. Carboxylation of pincer ligand backbone.

Another interesting reactivity reported in these papers is the reduction of aldehyde group, in the NCN pincer complex to an alcohol group with NaBH₃CN in the presence of acetic acid (Scheme 1.14).



Scheme 1.14. The amination and reduction of aldehyde group in ligand backbone.

In some cases, the ligand transformation was found to be crucial in catalytic activities of the Ru-based PNN pincer complex which is reported by Milstein and coworkers.³¹ In this paper, the author elegantly demonstrated the use

of ligand transformation for catalytic formation of amides and molecular hydrogen from alcohol and amine³² (Figure 1.8).

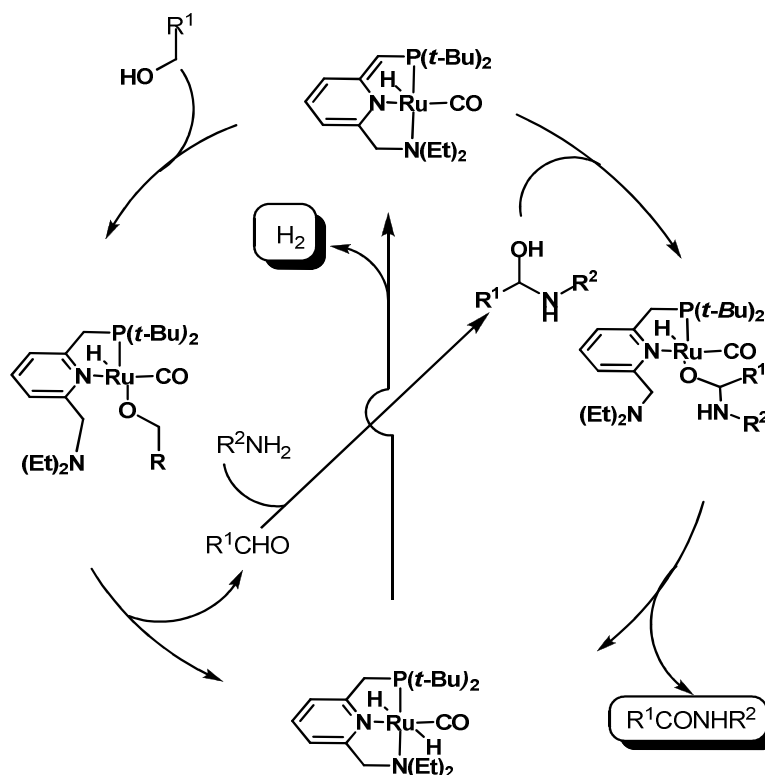


Figure 1.8. Mechanism of amidation reaction.

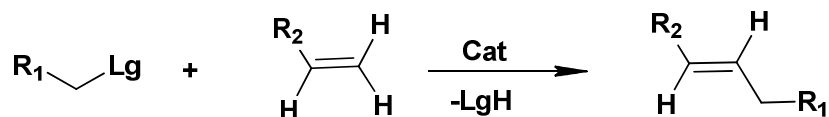
1.4 Application of pincer chemistry

Thermal stability combined with robust ligand structure made pincer complexes of interest for practical applications. Most of the applications of pincer chemistry highlighted in the literature are catalytic applications. However, there are several other studies describing use of these organometallic objects in light harvesting, OLED devices as well as molecular sensors and switches.

1.4.1 Catalytic activities

1.4.1.1 Heck coupling

Heck reaction or olefination reaction as it sometimes called, is the transformation of alkyl halide (or OTs, OTf) and alkenes to substituted alkenes. The basic concept of this reaction can be illustrated by the following equation:



Scheme 1.15. Example of Heck reaction.

Heck reaction has long attracted much attention in the scientific community especially in the past decade. This reaction provides access to the substituted alkenes and is very useful for preparation of highly conjugated and luminescent organic materials that find use in OLED displays.

One of the best series of catalysts for Heck coupling is the palladium based pincer complexes. Different ligand structure and type of coordinated ligand seem to have a dramatic influence on the performance of the palladium catalyst. One of the first effective catalysts was reported by Shibasaki,³³ who showed up to $8.9 \cdot 10^6$ TON with some substrates. Another catalyst reported by Takenaka³⁴ is one of the most promising catalysts to date which in a way is comparable with palladium catalyst reported by Liang³⁵ (Figure 1.9). It is worth mentioning that the catalytic system reported by Chung³⁶ is somewhat similar to Takenaka's (Figure 1.9), but use of aromatic instead of aliphatic amines as coordinating ligand in this pincer complex leads to a decrease in performance of Chung's catalysts.

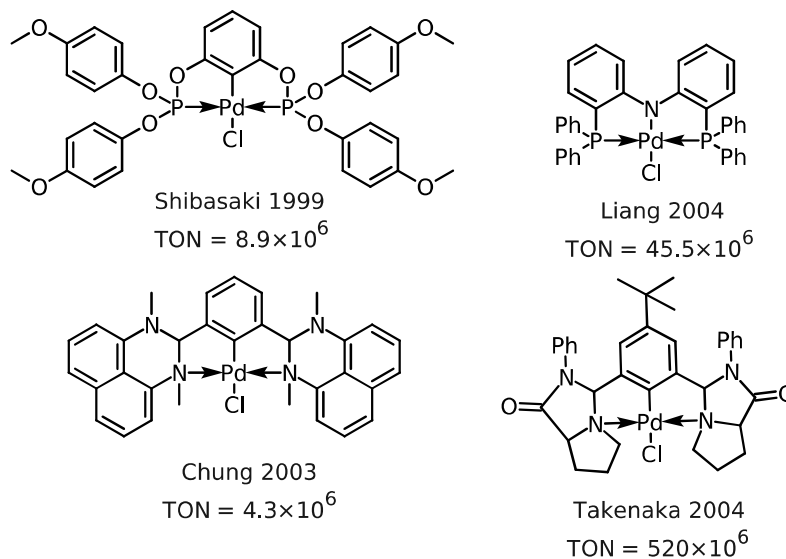


Figure 1.9. Examples of Heck catalysts.

Although it is difficult to compare reactivities of all catalysts due to the different conditions of catalytic tests, the following observation could be noted from the literature. First of all, the reaction seems to proceed more easily with more electron donating pincer ligands, which make palladium more electron rich and render the requisite oxidative addition easier. Secondly, electron withdrawing groups (EWG) in aryl or alkyl halide or olefinic substrate facilitate the olefination reaction.

1.4.1.2 Kumada-Tamao-Corriu coupling.



Scheme 1.16. Example of Kumada coupling.

Kumada coupling is the coupling reaction of aryl or alkyl halides with Grignard reagents (Scheme 1.16). Initially, this reaction was conducted with nickel precursor but subsequently many other late transition metals were used as well. The mechanism of this reaction is believed to go through the following steps: oxidative addition of alkyl or aryl halide to the metal precursor, followed

by transmetalation with RMgX , and eventually the elimination of the coupling product and the regeneration of metal precursor (Figure 1.10).

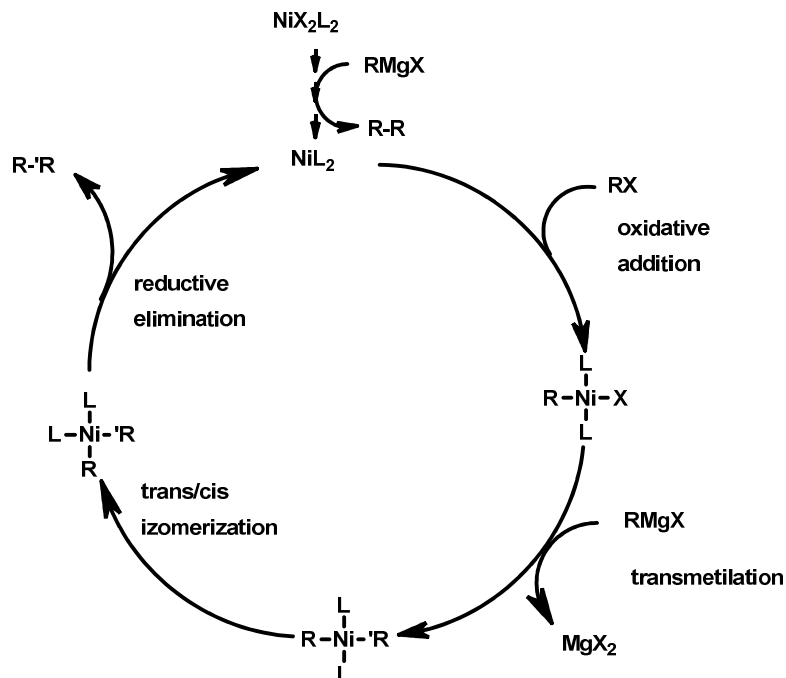


Figure 1.10. Mechanism of Kumada Coupling³⁷.

Nowadays, the mechanism of this reaction is becoming more and more of interest among researchers especially with use of pincer complexes as catalyst, where the reductive elimination from M^{2+} to M^0 is improbable. At the same time, the metathesis or M^{4+} to M^{2+} reductive pathway was proposed by several research groups.³⁸ Interesting advantages of using pincer complexes over conventional catalysts were highlighted in several studies. Thus, the use of pincer complexes can reduce or fully eliminate possible products of β -hydride elimination and significantly improve regioselectivity of the reaction. Most promising class of catalyst, for Kumada transformation among pincer chemistry are the pincer complexes based on Nickel (Figure 1.11).

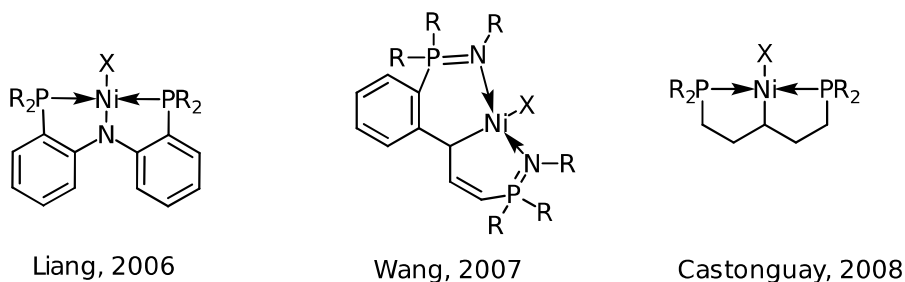
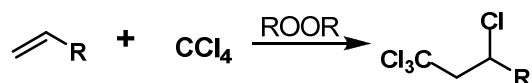


Figure 1.11. Examples of catalyst for Kumada coupling^{38a-c}.

For most of these complexes, the metal center is reported to be very electron rich and can undergo reversible alkyl-halogen exchange, a property that can make these systems suitable for catalytic transformation in Kumada coupling.

1.4.1.3 Kharasch addition

Back to 1938, Kharasch and Mayo³⁹ have reported the example of anti-Markovnikov C-Cl addition to olefins catalyzed by peroxides (Scheme 1.17).



Scheme 1.17. Kharasch addition.

One of the key problems of this transformation is the formation of undesirable products such as polymeric materials, products of olefination and low regioselectivity of the process. Since then, many more catalysts have been developed for this reaction.

One of the most efficient and selective class of catalyst in Kharasch transformation are the Ni based NCN pincer complexes described by van Koten⁴⁰. These compounds were proven to be very efficient catalysts for the Kharasch transformation with various olefinic substrates and different polyhalogenated reagents. This reaction is possible under mild conditions around 40 °C in various solvents and in some cases reaches up to 2000 catalytic turnovers. van Koten's

group extensively studied this reaction and found that Ni^{II} undergoes oxidation to Ni^{III} via reaction with polychlorinated alkanes which transfer one of the halogens to the metal ($\text{Ni}^{\text{II}} \rightarrow \text{Ni}^{\text{III}}$) and create a cage trapped $\cdot\text{CX}_3$ radical (A in Figure 1.12). This radical is believed to be an active intermediate in this transformation and it eventually reacts with the olefin to form the radical cage intermediate $\text{CCl}_3\text{CH}_2\text{-CHR}_1\cdot$ (B in Figure 1.12) that undergoes reductive elimination of the product and regenerates the active catalyst (Figure 1.12)

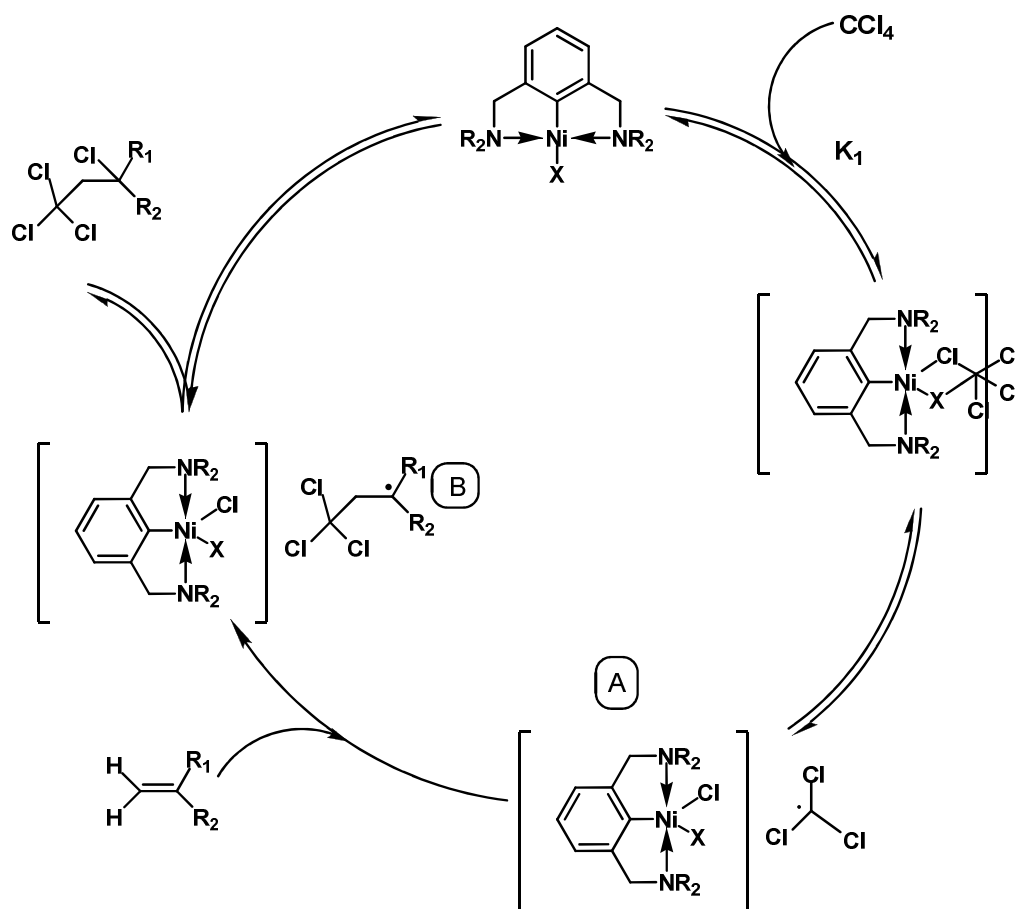
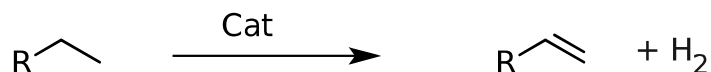


Figure 1.12. Mechanism of Kharasch addition reported by van Koten.

Interestingly, use of bulkier alkyl substituents like Et and n-Bu in the amine moiety ligand of the (NCN)Ni complexes were significantly inhibiting the reactivity of the catalyst. Eventually, van Koten's group developed the

heterogeneous catalyst based on a dendrimer backbone with multiple (NCN)Ni pincer moieties⁴¹ to test it for possible industrial use.

1.4.1.4 Dehydrogenation of alkanes.



Scheme 1.18. Example of dehydrogenation reaction.

There are several types of dehydrogenation reactions known in literature. The most challenging is the transformation of alkanes to alkenes (Scheme 1.18). The transformation of alkanes to alkenes is an organic reaction which presents interesting possibilities for preparation of olefinic monomers for synthesis of polyolefins and involves elimination of hydrogen gas. In general, this reaction requires intense heat, photochemical activation or catalyst. For example, Cr_2O_3 was used at 500 °C in order to transform pentane to pentene. Much milder condition was shown to be effective by using Iridium PCP pincer system described by Goldman^{42,43} (Figure 1.13).

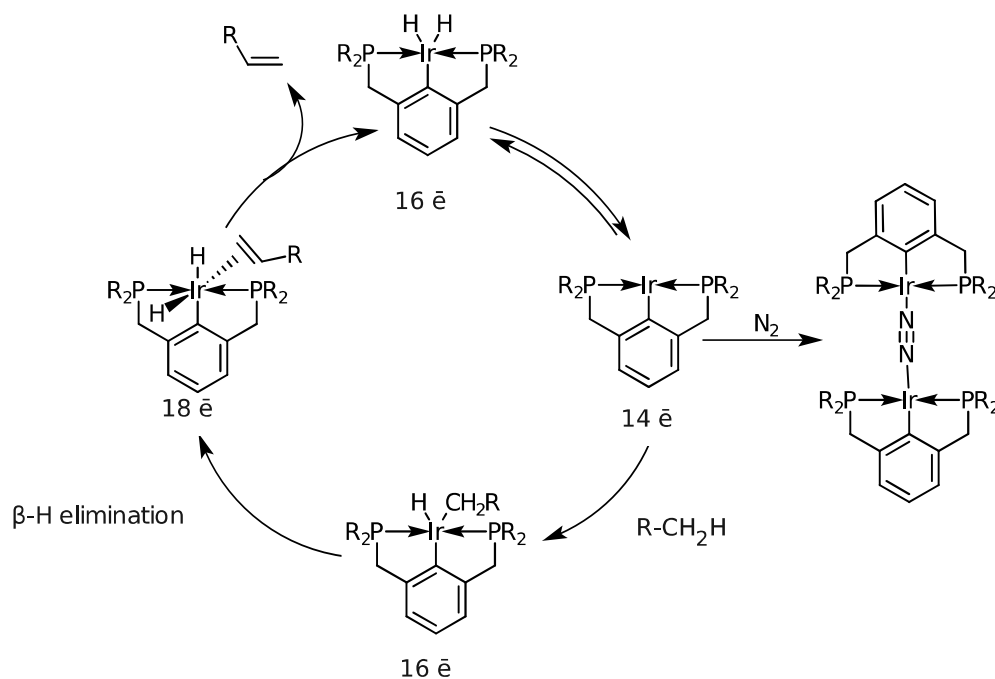


Figure 1.13. Mechanism of dehydrogenation reaction proposed by Goldman.

Interestingly, *t*-butylethylene was used as the hydrogen acceptor in order to successfully convert alkanes to alkenes. Furthermore, iridium based PCP system was found to be nitrogen sensitive and appropriate argon atmosphere was needed for this transformation to proceed.

1.4.2 Other applications

Thermal stability of the pincer complex is one of the most important attributes of the pincer chemistry, especially in the area of materials science. Thus, light-emitting devices, sensors and switches were developed using pincer complexes.

Square planar complexes are often found to be light emissive, and so can be potentially used in OLED as an emissive layer. Most of the publications in this area describe the platinum based pincer systems. Thus, Connick⁴⁴ and coworkers have reported platinum based pincer complexes displaying strong emission in 640-765 nm (Figure 1.14) wavelength range at the temperature of liquid nitrogen.

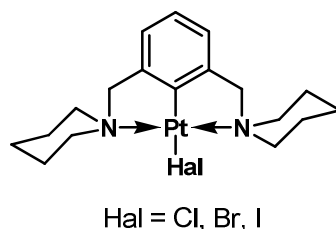


Figure 1.14. NCN platinum complex reported by Connick.

Similar findings were presented in 2006 by Yamamoto⁴⁵ and coworkers with their NCN and SCS pincer system (Figure 1.15).

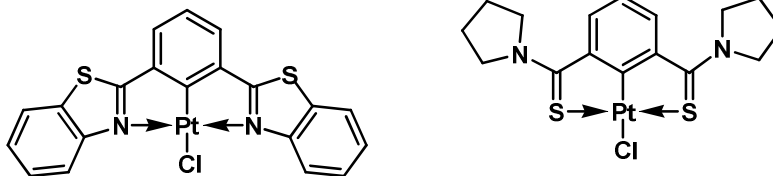


Figure 1.15. Examples of NCN and SCS platinum pincer system.

Together with spectroscopic investigations of this chemistry, there were some examples of manufacturing of an actual OLED⁴⁶ and testing its electro luminescence. In this context, van Koten and coworkers have reported differently substituted 4,4'-stilbenoid NCN-pincer Platinum(II) complexes (Figure 1.16).

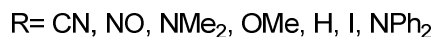
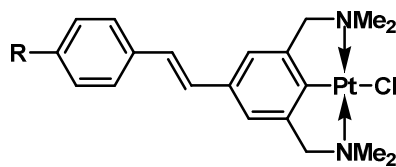
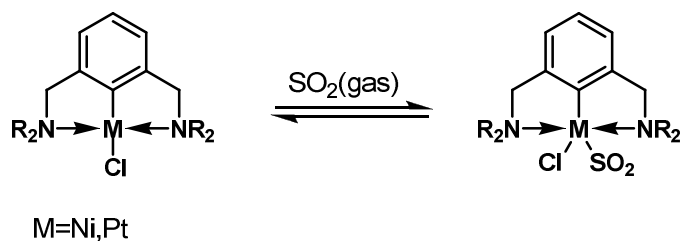


Figure 1.16. 4,4'-stilbenoid NCN-Pincer Platinum(II) complexes.

These compounds display an intense luminescence band at ~ 480 nm in solution and a somewhat weaker band at 640 nm in electroluminescence spectra. In addition, several stilbene substituted complexes were tested and promising luminescence properties were found for complexes that contained accepting or donating (CN, NO₂, NR₂) groups in the stilbene core. The actual OLED device was assembled in sandwich-like five layers formation, where the most promising cyano-substituted stilbene (NCN) complex was used as an emissive layer. Van Koten has shown that, overall, electroluminescence of this device is significant at liquid nitrogen temperature, but almost absent at room temperature and so unsuitable for practical use.

Other interesting properties of NCN pincer system were noted by van Koten's group. It appears that an NCN system based on Nickel or Platinum could

strongly bind SO_2^{47} gas to its metal center and lead to dramatic color changes. Thus, Platinum and Nickel based systems reversibly associate the SO_2 gas while changing color from colorless or yellow to bright orange and therefore they can be used as gas sensors (Scheme 1.19).



Scheme 1.19. Reversible association of SO_2 to the NCN pincer complex.

In the case of Nickel based pincer complexes, the association with SO_2 was partially leading to degradation of the complex while platinum showed good reversibility upon prolonged exposure to SO_2 . In the case of the platinum complex, the observed color changes were from colorless to intense orange; the color depth depends on the gas concentration. These properties of the platinum based NCN pincer complex allowed the determination of SO_2 gas not only qualitatively but quantitatively. Van Koten has noticed that increase of bulk of nitrogen donating ligand, from NMe_2 to NMeEt , significantly lowering the sensor's response. Interestingly, presence of another gas like HCl or CO together with SO_2 had no effect on detection of the latter. Noteworthy, that the platinum based NCN complex self-assembled in a polymer-like matrix, reported by van Koten, undergoes association with SO_2 in solid state without significantly perturbing the crystallinity of this material and reversibly transforming back to the original complex in similar fashion.

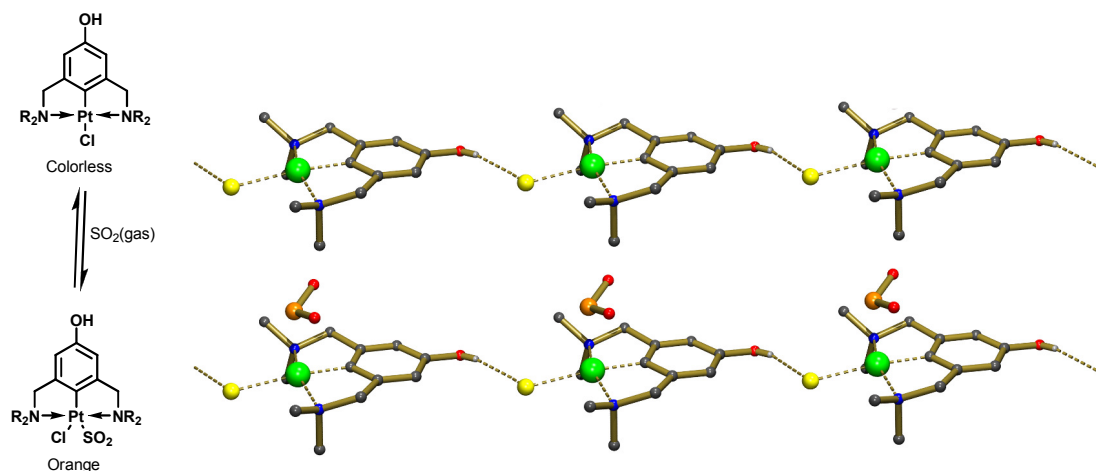
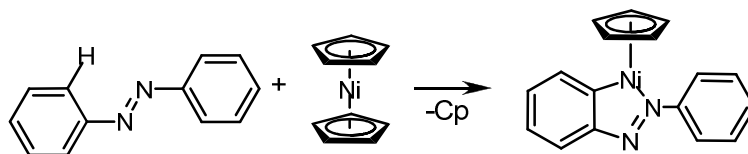


Figure 1.17. Retaining crystallinity during chemical transformation.

1.5 Nickel Pincer complexes: an overview.

Nickel has long been an attractive metal for ligand assisted C-H activation as well as catalytic applications associated with these reactivities. The history of nickel metallacycles goes back to 1963 when Kleimen and Dubeck⁴⁸ reported the first Nickel-promoted C-H activation. In their work, nickelocene undergoes C-H activation of azobenzene and formation of 5-membered metallacycle of nickel (Scheme 1.20)



Scheme 1.20. First C-H activation with Nickel.

This was a significant achievement that lay the foundation of nickel pincer chemistry. As noted earlier, the first pincer-like metallacycle of nickel was introduced in 1976 by the work of Shaw and coworkers who prepared various metal PCP pincer complexes. Continuation of nickel chemistry by Fryzuk and van Koten's group brought many more advances in nickel pincer chemistry

development and broadened the application to not only nickel chemistry but also pincer chemistry in general. Remarkable work in nickel pincer chemistry was done by Grove in van Koten's group. He reported not only a series of different NiX substituted pincer complexes,⁴⁹ but also the first example of an octahedral Ni^{III} pincer complex⁵⁰ (Figure 1.18) and highlighted the use of this family of complexes as catalysts in the Kharasch addition.

In our group's first studies of pincer chemistry conducted by Annie Castonguay and Valerica Pandarus, a series of Nickel pincer complexes were prepared based on PCsp³P and POCsp³OP pincer ligands⁵¹ (Figure 1.18). It is important to mention that these studies constituted some of the earliest examples of pincer complexes conducted with aliphatic ligands. Another interesting work was reported by Doux where he demonstrated new nickel pincer complexes based on original SPPPS pincer ligand^{52,53} and underlined basic mechanistic details of such cyclometalation.

Yet another rare example of nickel complexes was highlighted by Ingleson and Caulton. Based on a PNP pincer ligand with very bulky coordinating substituents, they reported first example of Ni^I pincer species (Figure 1.18). The complex was isolated and structurally characterized⁵⁴.

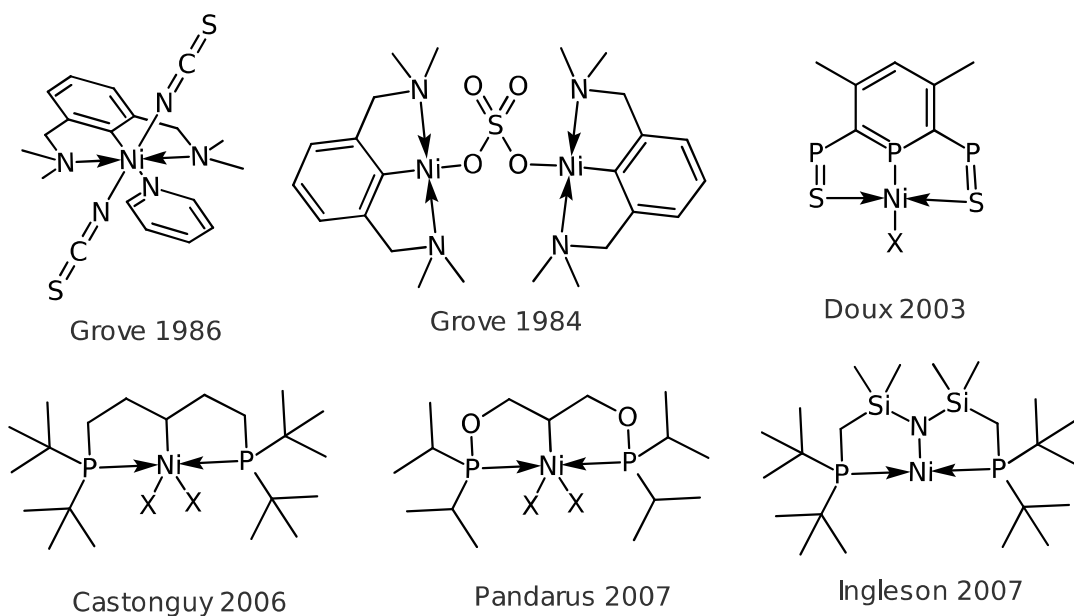


Figure 1.18. Examples of the nickel pincer complexes.

1.6 History and objectives of current research

The central theme of my Ph. D. studies is the use of POCN type pincer ligands in the chemistry of nickel complexes. The development of POCN-type pincer ligands and complexes were based on previously conducted research in our group as well as several studies reported in the literature. Prior studies with POCOP and PCP nickel systems described by Valerica Pandarus and Annie Castonguay have shown that the electron richness of the nickel metal in these complexes is much greater with PCP system while cyclometalation of these ligands is much easier with POCOP. Both these studies have shown that metal complexes featuring both PCP and POCOP ligands are durable and stable even with use of harsh organolithium reagents which allowed synthesis of stable alkyl complexes without visible decomposition. Contrary to PCsp²P and POCsp²OP ligands, the PCsp³P and POCsp³OP systems have shown a greater ability to stabilize Ni^{III} complexes, many examples of which were synthesized and structurally characterized. However, the nature of these ligands did not allow much variation in its structure and it restricted the possibility to investigate more detailed properties of Ni^{III} complexes. In addition, based on reactivity studies of these complexes, the catalytic application in reactions of hydrosilylation of olefins, Kumada coupling and Kharasch addition were explored.

While POCOP and PCP pincer systems were proven to be interesting and stable, their reactivities were found to be somewhat limited by only one reaction center located on a nickel core. Also, presence of bulky substituents in the phosphine ligands somewhat limits exploration of mechanistic details of catalytic reactions in which these compounds get involved. On the other hand, using nitrogen as one of the coordination ligand could potentially eliminate these problems since vast varieties of amines are readily available commercially. Moreover, amines are significantly cheaper than their phosphorus analogs and do not require special handling. Use of NCN pincer ligand, on the other hand, is shown to have difficulties to cyclometallate with nickel and, overall, has proven

less attractive due to absence of phosphine moiety, which is not only a very good ligand, but also helps characterization and monitoring of reactions by using ^{31}P NMR technique.

On the basis of the above considerations, preparation of a new POCN (Figure 1.19) pincer ligand (Figure 1.19) was proposed to allow easy variation of nitrogen moiety and explore the properties of POCN complexes in catalytic reactions and perhaps to answer some of the fundamental questions of pincer complex formation.

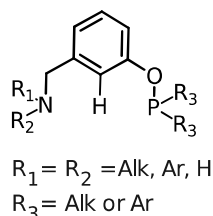


Figure 1.19. Example of POCN ligand.

The next few chapters of this thesis will describe the properties of POCN-type pincer nickel complexes.

1.7 References

-
- ¹ Moulton, C. J.; Shaw, B. L. *J. Chem. Soc., Dalton Trans.* **1976**, 1020-1024.
- ² Kharasch, M. S.; Engelmann, H.; Mayo, F. R. *J. Org. Chem.* **1938**, 2, 288.
- ³ Fryzuk, M. D.; MacNell, P. A.; Rettig, S. J.; Secco, A. S.; Trotter, J. *Organometallics* **1982**, 1, 918-930
- ⁴ (a) van Koten, G.; Timmer, K.; Noltes, J. G.; Spek, A. L. *J. Chem. Soc., Chem. Commun.* **1978**, 250. (b) Grove, D. M.; van Koten, G.; Ubbels, H. J. C.; Zoet, R.; Spek, A. L. *Organometallics* **1984**, 3, 1003 (c) Grove, D. M.; van Koten, G.; Verschuuren, A. H. M. *J. Mol. Catal.* **1988**, 45, 169

-
- ⁵ (a) Morales-Morales, D.; Redón, R.; Yung, C.; Jensen, C. M. *Chem. Commun.* **2000**, 1619. (b) Morales-Morales, D.; Grause, C.; Kasaoka, K.; Redón, R.; Cramer, R. E.; Jensen, C. M. *Inorg. Chim. Acta* **2000**, 300, 958. (c) Morales-Morales, D.; Lee, D. W., Wang Z.; Jensen, C. M. *Organometallics*, **2001**, 20, 1144. (d) Salem, H.; Ben-David, Y.; Shimon, L. J. W.; Milstein, D. *Organometallics* **2006**, 25, 2292. (e) Sykes, A. C.; White, P.; Brookhart, M. *Organometallics* **2006**, 25, 1664
- ⁶ Benito-Garagorri, D.; Bocokić, V.; Mereiter, K.; Kirchner, K. *Organometallics* **2006**, 25, 3817
- ⁷ Gründemann, S.; Albrecht, M.; Loch, J. A.; Faller, J. W.; Crabtree, R. H. *Organometallics* **2001**, 20, 5485.
- ⁸ Lee, D. W.; Kaska, W. C.; Jensen, C. M. *Organometallics* **1998**, 17, 1-3
- ⁹ Poverenov, E.; Gandelman, M.; Shimon, L. J. W.; Rozenberg, H.; Ben-David, Y.; Milstein, D. *Chem. - A Eur. J.* **2004**, 10, 4673-4684.
- ¹⁰ Gagliardo, M.; Selander, N.; Mehendale, N.; van Koten, G.; KleinGebbinck, R.; Szab, K. *Chem. - A Eur. J.* **2008**, 14, 4800-4809.
- ¹¹ (a) Zhang, J.; Gandelman, M.; Herrman, D.; Leitus, G.; Shimon, L. J.; Ben-David, Y.; Milstein, D. *Inorg. Chim. Acta* **2006**, 359, 1955-1960. (b) Fischer, J.; Schurmann, M.; Mehring, M.; Zachwieja, U.; Jurkschat, K. *Organometallics* **2006**, 25, 2886-2893. (c) Debono, N.; Iglesias, M.; Sánchez, F. *Adv. Syn. & Cat.* **2007**, 349, 2470-2476. (d) Durand, J.; Gladiali, S.; Erre, G.; Zangrando, E.; Milani, B. *Organometallics* **2007**, 26, 810-818. (e) Boronat, M.; Corma, A.; González-Arellano, C.; Iglesias, M.; Sánchez, F. *Organometallics* **2010**, 29, 134-141.
- ¹² Poverenov, E.; Gandelman, M.; Shimon, L. J. W.; Rozenberg, H.; Ben-David, Y.; Milstein, D. *Organometallics* **2005**, 24, 1082-1090.
- ¹³ (a) Ozerov, O. V.; Guo, C.; Fan, L.; Foxman, B. M. *Organometallics* **2004**, 23, 5573-5580. (b) Liang, L.; Chien, P.; Huang, Y. *J. Am. Chem. Soc.* **2006**, 128, 15562-15563.

-
- ¹⁴ Grove, D. M.; Van Koten, G.; Ubbels, H. J. C.; Zoet, R.; Spek, A. L. *Organometallics* **1984**, *3*, 1003-1009.
- ¹⁵ Meijer, M. D.; Ronde, N.; Vogt, D.; van Klink, G. P. M.; van Koten, G. *Organometallics* **2001**, *20*, 3993-4000.
- ¹⁶ Rytchinski, B.; Vigalok, A.; Ben-David, Y.; Milstein, D. *J. Am. Chem. Soc.* **1996**, *118*, 12406-12415.
- ¹⁷ Sundermann, A.; Uzan, O.; Martin, J. M. L. *Organometallics* **2001**, *20*, 1783-1791.
- ¹⁸ Gauvin, R. M.; Rozenberg, H.; Shimon, L. J. W.; Milstein, D. *Organometallics* **2001**, *20*, 1719-1724.
- ¹⁹ (a) Van der Ploeg, A. F. M. J.; Van Koten, G.; Vrieze, K.; Spek, A. L.; Duisenberg, A. J. M. *Organometallics* **1982**, *1*, 1066-1070. (b) Terheijden, J.; Van Koten, G.; De Booy, J. L.; Ubbels, H. J. C.; Stam, C. H. *Organometallics* **1983**, *2*, 1882-1883. (c) Grove, D. M.; Van Koten, G.; Ubbels, H. J. C.; Zoet, R.; Spek, A. L. *Organometallics* **1984**, *3*, 1003-1009. (d) Grove, D. M.; Van Koten, G.; Mul, P.; Van der Zeijden, A. A. H.; Terheijden, J.; Zoutberg, M. C.; Stam, C. H. *Organometallics* **1986**, *5*, 322-326. (e) van de Kuil, L. A.; Grove, D. M.; Gossage, R. A.; Zwikker, J. W.; Jenneskens, L. W.; Drenth, W.; van Koten, G. *Organometallics* **1997**, *16*, 4985-4994. (f) Gossage, R. A.; van de Kuil, L. A.; van Koten, G. *Accounts of Chemical Research* **1998**, *31*, 423-431. (g) Gossage, R. A.; Jastrzebski, J. T. B. H.; van Ameijde, J.; Mulders, S. J. E.; Brouwer, A. J.; Liskamp, R. M. J.; van Koten, G. *Tetrahedron Let.* **1999**, *40*, 1413-1416.
- ²⁰ Cauty, A. J.; Patel, J.; B. W. Skelton, A. H. White, A. H. *J. Organomet. Chem.* **2000**, *599*, 195.
- ²¹ Fossey, J. S.; Richards, C. J. *Organometallics* **2002**, *21*, 5259-5264.
- ²² Castonguay, A.; Sui-Seng, C.; Zargarian, D.; Beauchamp, A. L. *Organometallics* **2006**, *25*, 602.
- ²³ Adams, J.J.; Lau, L.; Arulsamy, N.; Roddick, D. *Inorg. Chem.*, **2007**, *46* (26), 11328-11334.
- ²⁴ Pape, A.; Lutz, M.; Müller, G., *Angew. Chem.* **1994**, *106*, 2375

-
- ²⁵ Albrecht, M.; Kocks, B. M.; Spek, A. L.; van Koten G. *J. Organomet. Chem.* **2001**, *624*, 271.
- ²⁶ Kleij, A. W.; Gossage, R. A.; Klein Gebbink, R. J. M.; Brinkmann, N.; Reijerse, E. J.; Kragl, U.; Lutz, M.; Spek, A. L.; van Koten, G. *J. Am. Chem. Soc.* **2000**, *122*, 12112
- ²⁷ Dani, P.; Albrecht, M.; van Klink, G. P. M.; van Koten, G. *Organometallics* **2000**, *19*, 4468-4476.
- ²⁸ (a) Dani, P.; Karlen, T.; Gossage, R. A.; Gladiali, S.; van Koten, G. *Angew. Chem. Int. Ed.* **2000**, *39*, 743–745. (b) Naota, T.; Takaya, H.; Murahashi, S.-I. *Chem. Rev.* **1998**, *98*, 2599. (c) Dani, P.; Albrecht, M.; van Klink, G. P. M.; van Koten, G. *Organometallics* **2000**, *19*, 4468. (d) Jeon, S. L.; Loveless, D. M.; Yount, W. C.; Craig, S. L. *Inorg. Chem.* **2006**, *45*, 11060-11068. (e) Gorla, F.; Togni, A.; Venanzi, L. M.; Albinati, A.; Lianza, F. *Organometallics* **1994**, *13*, 1607. (f) Gorla, F.; Venanzi, L. M.; Albinati, A. *Organometallics* **1994**, *13*, 43. (g) (1) Kleij, A. W.; Gossage, R. A.; Klein Gebbink, R. J. M.; Brinkmann, N.; Reijerse, E. J.; Kragl, U.; Lutz, M.; Spek, A. L.; van Koten, G. *J. Am. Chem. Soc.* **2000**, *122*, 12112-12124.
- ²⁹ Rodriguez, G.; Albrecht, M.; Schoenmaker, J.; Ford, A.; Lutz, M.; Spek, A. L.; van Koten, G. *J. Am. Chem. Soc.* **2002**, *124*, 5127-5138.
- ³⁰ Suijkerbuijk, B. M.; Slagt, M. Q.; Klein Gebbink, R. J.; Lutz, M.; Spek, A. L.; van Koten, G. *Tetrahedron Lett.* **2002**, *43*, 6565-6568.
- ³¹ (a) Gunanathan, C.; Ben-David, Y.; Milstein, D. *Science* **2007**, *317*, 790-792. (b) Zhang, J.; Gandelman, M.; Shimon, L. J. W.; Milstein, D. *Dalton Trans.* **2007**, 107-113. (c) Gnanaprakasam, B.; Zhang, J.; Milstein, D. *Angew. Chemie, Int. Ed. Engl.* **2010**, *49*, 1468-1471.
- ³² Gunanathan, C.; Ben-David, Y.; Milstein, D. *Science* **2007**, *317*, 790-792.
- ³³ Miyazaki, F.; Shibasaki, M., *Tetrahedron Lett.* **1999**, *40*, 7379
- ³⁴ Takenaka, K.; Uozumi, Y. *Adv. Syn. & Cat.* **2004**, *346*, 1693-1696.
- ³⁵ Huang, L.-C. Liang, *Organometallics* **2004**, *23*, 2813.

-
- ³⁶ Jung, I. G.; Son, S. U.; Park, K. H.; Chung, K.-C.; Lee, J. W.; Chung, Y. K. *Organometallics* **2003**, *22*, 4715
- ³⁷ (a) Tamao, K.; Sumitani, K.; Kumada, M. *J. Am. Chem. Soc.* **1972**, *94*, 4374.
(b) Tamao, K.; Kiso, Y.; Sumitani, K.; Kumada, M. *J. Am. Chem. Soc.* **1972**, *94*, 9268.
- ³⁸(a) Liang, L.; Chien, P.; Lin, J.; Huang, M.; Huang, Y.; Liao, J. *Organometallics* **2006**, *25*, 1399-1411. (b) Wang, Z.; Wang, L. *Chem. Commun.* **2007**, 2423. (c) Castonguay, A.; Beauchamp, A. L.; Zargarian, D. *Organometallics* **2008**, *27*, 5723-5732. (d) Vechorkin, O.; Csok, Z.; Scopelliti, R.; Hu, X. *Chem. - Eur. J.* **2009**, *15*, 3889-3899. (e) Sun, K.; Wang, L.; Wang, Z. *Organometallics* **2008**, *27*, 5649-5656. (f) Gu, S.; Chen, W. *Organometallics* **2009**, *28*, 909-914 (g) Csok, Z.; Vechorkin, O.; Harkins, S. B.; Scopelliti, R.; Hu, X. *J. Am. Chem. Soc.* **2008**, *130*, 8156-8157.
- ³⁹ Kharasch, M. S.; Engelmann, H.; Mayo, F. R. *J. Org. Chem.* **1938**, *2*, 288.
- ⁴⁰ (a) Grove, D. M.; van Koten, G.; Verschuuren, A. H. M. *J. Mol. Catal.* **1988**, *45*, 169. (b) Grove, D. M.; van Koten, G.; Mul, W. P.; van der Zeijden, A. A. H.; Terheijden, J.; Zoutberg, M. C.; Stam, C. H. *Organometallics* **1986**, *5*, 322.
- ⁴¹ Kleij, A. W.; Gossage, R. A.; Klein Gebbink, R. J. M.; Brinkmann, N.; Reijerse, E. J.; Kragl, U.; Lutz, M.; Spek, A. L.; van Koten, G. *J. Am. Chem. Soc.* **2000**, *122*, 12112-12124.
- ⁴² Renkema, K. B.; Kissin, Y. V.; Goldman, A. S. *J. Am. Chem. Soc.* **2003**, *125*, 7770-7771.
- ⁴³ Kundu, S.; Choliy, Y.; Zhuo, G.; Ahuja, R.; Emge, T. J.; Warmuth, R.; Brookhart, M.; Krogh-Jespersen, K.; Goldman, A. S. *Organometallics* **2009**, *28*, 5432-5444.
- ⁴⁴ Jude, H.; Bauer, J.A.K.; Connick, W.B. *Inorg. Chem.*, **2002**, *41*, 2275-2281
- ⁴⁵ a) Kanbara, T.; Okada, K.; Yamamoto, T.; Ogawa, H.; Inoue, T. *J. of Organomet. Chem.* **2004**, *689*, 1860-1864. b) Okamoto, K.; Kanbara, T.; Yamamoto, T.; Wada, A. *Organometallics* **2006**, *25*, 4026-4029.

-
- ⁴⁶ Batema, G. D.; Lutz, M.; Spek, A. L.; van Walree, C. A.; Donegá, C. D. M.; Meijerink, A.; Havenith, R. W. A.; Pérez-Moreno, J.; Clays, K.; Büchel, M.; Dijken, A. V.; Bryce, D. L.; van Klink, G. P. M.; van Koten, G. *Organometallics* **2008**, *27*, 1690-1701.
- ⁴⁷ Spek, A. L.; van Koten, G. *Nature* **2000**, *406*, 970
- ⁴⁸ J. P. Kleiman, M. Dubeck, *J. Am. Chem. Soc.* **1963**, *85*, 1544.
- ⁴⁹ Grove, D. M.; Van Koten, G.; Ubbels, H. J. C.; Zoet, R.; Spek, A. L. *Organometallics* **1984**, *3*, 1003-1009.
- ⁵⁰ Grove, D. M.; Van Koten, G.; Mul, P.; Van der Zeijden, A. A. H.; Terheijden, J.; Zoutberg, M. C.; Stam, C. H. *Organometallics* **1986**, *5*, 322-326.
- ⁵¹ Castonguay, A.; Sui-Seng, C.; Zargarian, D.; Beauchamp, A. L. *Organometallics* **2006**, *25*, 602-608.
- ⁵² Doux, M.; Mézailles, N.; Ricard, L.; Le Floch, P. *Eur. J. Inorg. Chem.* **2003**, *21*, 3878-3894.
- ⁵³ Pandarus, V.; Zargarian, D. *Chem. Commun.* **2007**, 978-980.
- ⁵⁴ Ingleson, M. J.; Fullmer, B. C.; Buschhorn, D. T.; Fan, H.; Pink, M.; Huffman, J. C.; Caulton, K. G. *Inorg. Chem.* **2008**, *47*, 407-409.

Chapter 2: New POCN-Type Pincer Complexes of Ni^{II} and Ni^{III}

Article 1

Denis M. Spasyuk[†], Davit Zargarian[†] and Art van der Est[‡]

[†] Département de Chimie, Université de Montréal, Montréal, QC, Canada H3C 3J7 [‡]

Department of Chemistry, Brock University, St. Catharines, ON, Canada L2S 3A1

Organometallics, **2009**, 28, 6531–6540

2.1 Abstract

Unsymmetrical POC(H)N-type pincer ligands react with $\text{NiBr}_2(\text{NCMe})_x$ to give the complexes $(\text{POCN})\text{Ni}^{\text{II}}\text{Br}$ ($\text{POCN} = \kappa^{\text{P}}, \kappa^{\text{C}}, \kappa^{\text{N}}\text{-}\{2\text{-}(i\text{-Pr}_2\text{PO}), 6\text{-}(\text{NR}_2\text{CH}_2)\text{-C}_6\text{H}_3\}$; $\text{NR}_2 = 3\text{-morpholino}$ (**2.3a**), NMe_2 (**2.3b**), and NEt_2 (**2.3c**)). The presence of an added base such as NEt_3 in these metallation reactions maximizes the yields of the target pincer complexes by suppressing the formation of side-products arising from protonation of the ligand by the in-situ generated HBr . The cyclic voltammograms of **2.3** exhibit a quasi-reversible, one-electron oxidation at ca. +1.0 V, in addition to an irreversible oxidation at higher potentials likely due to ligand oxidation. Reaction of the 16-electron, yellow complexes **2.3** with Br_2 , *N*-Bromosuccinimide, or CBr_4 gives black crystalline compounds identified as the 17-electron complexes $(\text{POCN})\text{Ni}^{\text{III}}\text{Br}_2$ (**2.5**). Complexes **2.3** and **2.5** adopt square planar and distorted square pyramidal geometries, respectively. The Ni-Br bond lengths in **2.5** are significantly longer for the Br atom occupying the axial position (2.43-2.46 vs. 2.37 Å), consistent with the repulsive interactions expected between the bromide lone pair and the singly-occupied d_{z^2}/d_{pz} hybrid MO. In agreement with this picture, the *g*-values obtained from the EPR spectrum of **2.5a** are $g_{xx} \sim g_{yy} \sim 2.2$, $g_{zz} \sim 2.00$, and strong Br hyperfine coupling is observed on the g_{zz} component. Our preliminary studies indicate that the thermal stabilities of **2.5**, both in the solid state (as probed by differential scanning calorimetry) and in solution (as probed by UV-vis spectroscopy), vary in the order **2.5a** ~ **2.5b** > **2.5c**; this order of stability is consistent with the relative steric demands of the *N*-moiety. Complexes **2.5a** (or **2.3a**) and **2.5b** (or **2.3b**) promote the Kharasch addition of CX_4 ($\text{X} = \text{Cl}, \text{Br}$) to styrene at 80 °C, giving $\text{PhC}(\text{X})\text{CH}_2\text{CX}_3$, the product of an anti-Markovnikov addition, in up to 50 catalytic turnovers.

2.2 Introduction

Since their initial introduction by Shaw's group over 30 years ago,¹ pincer type complexes have been shown to promote many interesting and useful reactivities.² The initial phase in the development of the chemistry of pincer complexes was dominated by complexes featuring monoanionic, terdentate ligands based on bis(phosphine) (PCP)¹ and bis(amine) (NCN)³ donor moieties. More recent years have witnessed the introduction of complexes based on a large variety of new ligands, including bis(phosphino)amides (PNP),⁴ bis(phosphinites) (POCOP),⁵ bis(phosphinidines) (PNCNP),⁶ and bis(carbenes) (CCC),⁷ as well as nonsymmetrical pincer ligands such as PCN,^{8,9} CNS,¹⁰ NNN,¹¹ etc. The relatively facile access to such a diverse array of new ligands has accelerated the exploration of the reactivities of their metal complexes, which has led in turn to discovery of novel reactivities.¹²

Our long-standing interest in the chemistry of organonickel complexes¹³ combined with van Koten's landmark reports on NCN-Ni complexes^{3b,c,d} and the emerging chemistry of PCP-Ni complexes¹⁴ inspired us to investigate the synthesis and reactivities of Ni compounds with various pincer-type ligands. In earlier reports, we have described the chemistry of the $\text{PC}_{\text{sp}^2}\text{P-Ni}^{\text{II}}$ species $\{1,3\text{-}(\text{Ph}_2\text{PCH}_2\text{CH}_2)_2\text{-2-indenyl}\}\text{NiCl}^{15}$ and the $\text{PC}_{\text{sp}^3}\text{P-Ni}^{\text{II}}$ complexes $\{(\text{t-Bu}_2\text{PCH}_2\text{CH}_2)_2\text{CH}\}\text{-NiX}$ ($\text{X} = \text{Cl, Br, I, Me, H}$) and $[\{(\text{t-Bu}_2\text{PCH}_2\text{CH}_2)_2\text{CH}\}\text{NiL}]^+$ ($\text{L} = \text{CH}_3\text{CN, CH}_2=\text{CHCN}$).¹⁶ Recently, we have described new $\text{POC}_{\text{sp}^2}\text{OP}$ and $\text{POC}_{\text{sp}^3}\text{OP}$ complexes of Ni^{II} and Ni^{III} as well as their catalytic activities in hydroamination (Michael addition) and Kharasch addition.^{17,18} Our studies to date indicate that the nature of the pincer ligand has a major influence on the metallation step as well as the stabilities and reactivities of the ensuing pincer complexes. For instance, metallation of the ligand's central C-H bond is more facile with POCOP vs. PCP and with ligands based on aromatic vs. aliphatic linkers. Furthermore, stable and isolable trivalent species are accessible with $\text{POC}_{\text{sp}^3}\text{OP}$ - and $\text{PC}_{\text{sp}^3}\text{P}$ -type ligands, whereas ligands based on

aromatic linkers ($\text{POC}_{\text{sp}^2}\text{OP}$ - or $\text{PC}_{\text{sp}^2}\text{P}$ -type ligands) have not yielded high-valent nickel complexes.¹⁸

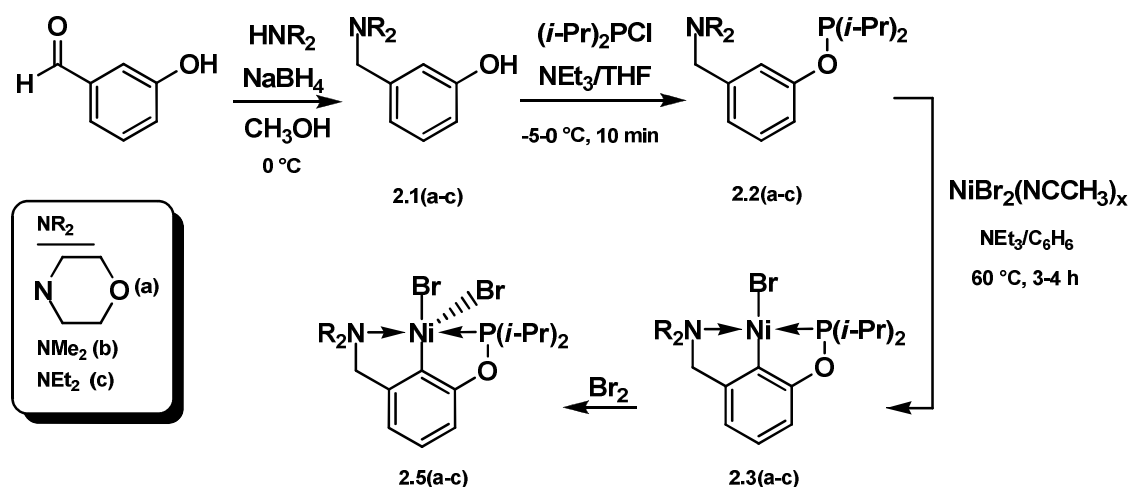
The latter observation, that PCP and POCOP ligands based on an aromatic linker do not yield Ni^{III} species, is in direct contrast to the relatively facile preparation of trivalent species based on aromatic NCN ligands, as reported by van Koten's group.^{3b,c,d} The discrepancy between the chemistry of PCP/ POCOP vs. NCN ligands featuring an aromatic skeleton prompted us to investigate the preparation of high-valent nickel complexes based on unsymmetrical PCN-type ligands. Since bis(phosphinite) ligands have been found to undergo metallation more readily than their bis(phosphine) counterparts, our initial studies have been focused on the phosphinite-amine ligands $\text{R}_2\text{PO-C}_6\text{H}_4\text{-CH}_2\text{NR}_2$ (POCN). The present report describes the preparation of POCN-type pincer ligands and their di- and trivalent complexes of nickel.

2.3 Results and Discussion

2.3.1 Synthesis of complexes

The synthetic route leading to the new complexes **2.3(a-c)** is illustrated in Scheme 2.1. The aminophenol precursors for the POCN ligands **2.2** were prepared by condensation of 3-hydroxybenzaldehyde with the corresponding secondary amines, followed by reduction of the in situ formed imine with NaBH_4 in methanol.¹⁹ Formation of the amino phenols **2.1** is quite exothermic, requiring stepwise addition of NaBH_4 and cooling of the reaction mixture to avoid forming side products such as 3-(hydroxymethyl)phenol that complicate separation of pure **2.1**. The pre-ligands **2.1** were isolated in good yields as white solids (**2.1a** and **2.1b**) or a pale yellow oil (**2.1c**); the identities of these compounds were established by elemental analysis and NMR spectroscopy. The phosphination of **2.1** with chlorodiisopropylphosphine and triethylamine gave the corresponding POC(H)N-type pincer ligands **2.2**, which were isolated in high yields as colorless oils and characterized by NMR spectroscopy and elemental analysis. All ligands proved to be quite sensitive to residual moisture, but relatively inert to oxygen.

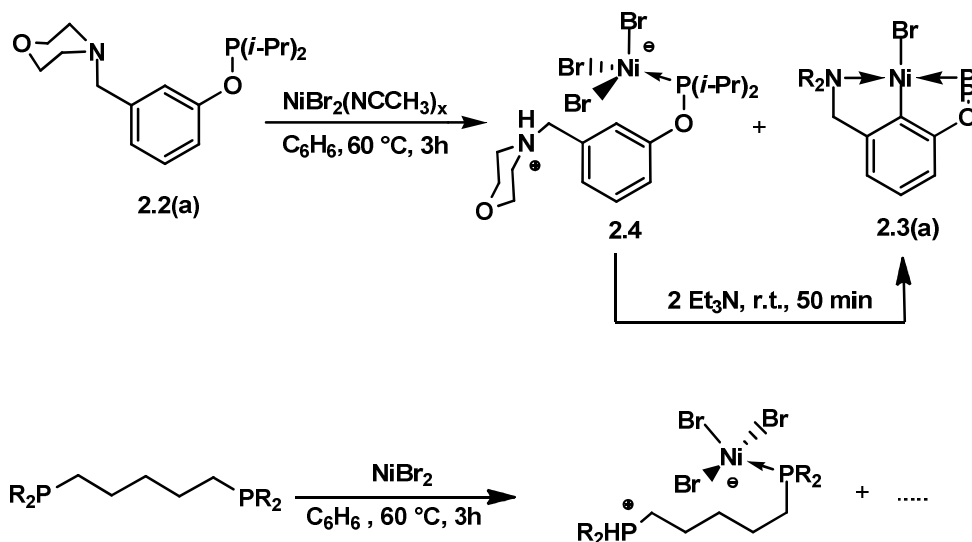
Heating **2.2** with $\text{NiBr}_2(\text{MeCN})_x$ ²⁰ in the presence of triethylamine (benzene, 60 °C, 3-4 h) led to the metallation of the ligands and gave the new complexes **2.3** in ~86% yields as yellow solids. Use of different precursors such as $\text{NiBr}_2(\text{THF})_x$ or NiBr_2 , or different bases such as *N,N*-dimethylaminopyridine (DMAP), led to significantly lower yields of the complexes (~35%). Pd and Pt complexes based on similar POCN ligands have been reported previously,²¹ but complexes **2.3** are, to our knowledge, the first examples of POCN-type complexes of nickel.



Scheme 2.1. Synthesis of ligands and complexes.

It is noteworthy that the use of a base was found to be necessary in order to maximize the reaction yield of complexes **2.3(a-c)**. When the reaction of **2.2a** was performed without any added base, we obtained the desired pincer complex **2.3a** in poor yields (< 50%) along with variable amounts of a sparingly soluble, NMR-silent turquoise-green solid **2.4**. Interestingly, the latter side-product generates the desired pincer complex **2.3a** when treated with two equivalents of Et_3N . Unfortunately, we have not succeeded in growing suitable single crystals of this compound due to its poor solubility in common aprotic and non-coordinating solvents and its decomposition in coordinating solvents. Nevertheless, the above observations and the results of a combustion analysis carried out on this solid allow us to propose the structure shown in Scheme 2.2 (**2.4**). It should be noted

that anionic, tetrahedral species analogous to **2.4** have been detected previously during the preparation of $\text{PC}_{\text{sp}^3}\text{P}$ -type pincer complexes of Ni (Scheme 2).^{16a} Such side-products likely arise from the reaction of the HBr, liberated at the cyclometallation stage of the synthesis, with the amino moiety of the ligand, prior to or after the latter's coordination to the metal center.



Scheme 2.2. Effect of the base in cyclometallation.

The redox properties of complexes **2.3** were investigated by cyclic voltammetry measurements in CH_2Cl_2 . The voltammograms (Figure 2.1) showed quasi-reversible redox waves at ca. 1.0 V; this redox process is assigned to oxidation of the Ni center ($\text{Ni}^{\text{II}} \rightarrow \text{Ni}^{\text{III}}$).²² Comparison of the oxidation potentials of these POCN complexes to that of the previously reported complex $(\text{POC}_{\text{sp}^2}\text{OP})\text{NiBr}$ ^{17,18} suggests that high-valent compounds should be easier to prepare and isolate with these POCN-based complexes. This is borne out by the successful chemical oxidation of **2.3** and the isolation of Ni^{III} species (vide infra). We conclude, therefore, that POCN ligands are more effective than their POCOP homologues in stabilizing high-valent nickel species, which can be understood both in terms of the greater nucleophilicity and “hardness” of amine moieties relative to OPR_2 moieties.

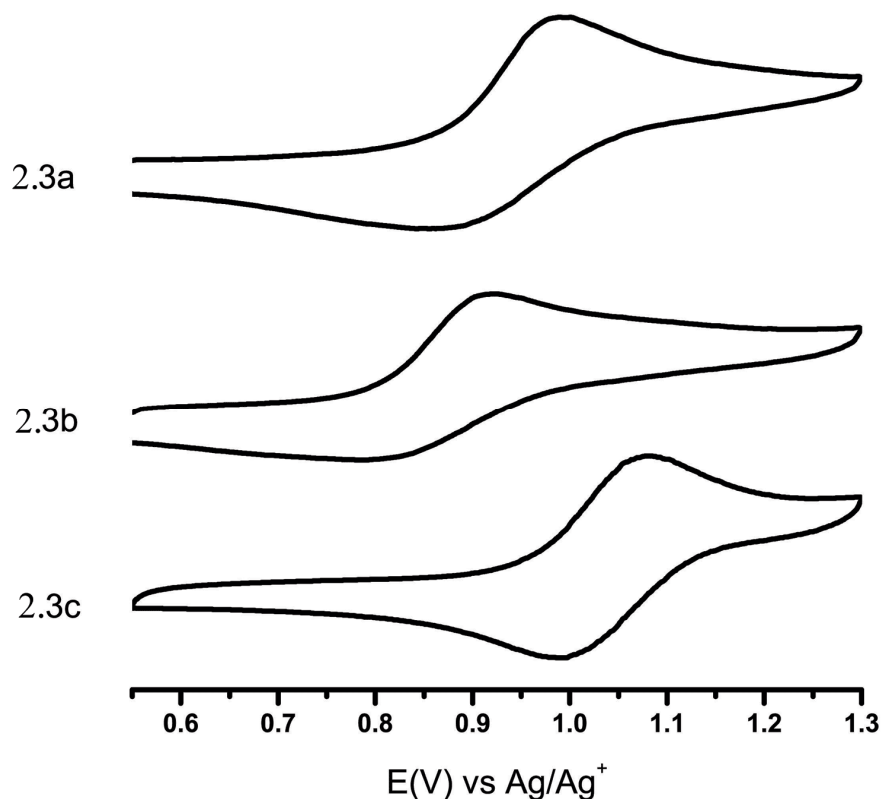


Figure 2.1. Cyclic voltammograms of 1mM solutions of complexes **2.3(a-c)** in dichloromethane containing 0.1M tetrabutylammonium hexafluorophosphate at 25 °C at a scan rate of 100 mV/s on a glassy carbon working electrode.

Chemical oxidation of **2.3** to their Ni^{III} counterparts was achieved by reaction with bromine in dry diethyl ether, which gave the corresponding $(POCN)Ni^{III}Br_2$ complexes (**2.5a-c**) as black solids in greater than 90% yields (Scheme 1). The relative thermal instability of **2.5c** (vide infra) required that its synthesis be performed at $-78\text{ }^\circ\text{C}$ (in dry solvents) over 10 minutes, followed by addition of cold hexane to precipitate the product. N-bromosuccinimide (NBS) and CBr_4 were also competent oxidants for generation of Ni^{III} species, but these reagents furnished lower yields of the products (50-70%). The NBS reaction led to formation of succinimide that has solubility properties similar to those of **2.5**, which complicated the isolation of pure products. Complexes **2.5** are soluble in Et_2O , THF, CH_2Cl_2 , and CH_3CN . Et_2O or CH_2Cl_2 solutions of complexes **2.5a** and

2.5b were found to be fairly stable at room temperature, whereas solutions of complex **2.5c** were significantly less stable and had to be handled rapidly and at significantly lower temperatures (*vide infra*).

2.3.2 Characterization of **2.3(a-c)**

The diamagnetic Ni^{II} complexes **2.3** were fully characterized by NMR spectroscopy, elemental analysis, and single crystal X-ray diffraction studies. The ³¹P{¹H} NMR spectra of **2.3** were straight forward, each consisting of a single resonance at about 200 ppm; this signal is significantly downfield of the corresponding signal for the free ligands (147 ppm) but close to the chemical shift region where we find the ³¹P signal for the analogous (POCOP)NiBr compounds (186 ppm).¹⁸ The ¹H and ¹³C{¹H} NMR spectra were much more complex, but ¹H-COSY and HMQC correlation experiments allowed us to assign all ¹H and ¹³C signals. Together, these spectra indicate that complexes **2.3** possess a plane of symmetry in solution, as reflected in the equivalence of the two CHMe₂ and the NCH₂Ar protons in **2.3a-c**, the two NCH₂ and OCH₂ carbons in **2.3a**, and the two signals for N(CH_{2CH₃) (**2.3c**) and N(CH₃) (**2.3b**). The plane of symmetry, which coincides with the plane of coordination, also renders the following nuclei (sitting above and below the plane) pair-wise equivalent: CH(CH₃)₂ in **2.3a-c**; morpholine protons in **2.3a**; and NCH₂CH₃ signals in **2.3c**.}

Single crystal X-ray diffraction studies of **2.3** showed that these complexes adopt moderately distorted square planar geometries in the solid state (Figure 2.2), the greatest structural distortions appearing in the angles P-Ni-N (162-167°) and P-Ni-C (82°) (Table 2.2); these distortions away from ideal geometry arise presumably from the terdentate nature of the pincer ligand. The Ni center and the aromatic ring are only slightly out of the coordination plane, which is consistent with the existence in solution of a plane of symmetry. The Ni-P distances in these POCN-type complexes are shorter than the corresponding distances in the analogous (POCOP)Ni-X compounds (ca. 2.11 vs. 2.15-2.16 Å),¹⁸ implying a greater trans influence for the OPR₂ moieties vs. the amine ligands. Moreover, in

comparison to their POCOP-type counterparts, the POCN-type complexes **2.3** display somewhat shorter Ni-C distances (ca. 1.85-1.86 vs. 1.88 Å) and longer Ni-Br (ca. 2.33-2.36 vs. 2.32 Å) distances.

Figure 2.2. ORTEP diagram for complexes **2.3a** (a), **2.3b** (b), and **2.3c** (c). Thermal ellipsoids are shown at the 50% probability level. Hydrogen atoms are omitted for clarity.

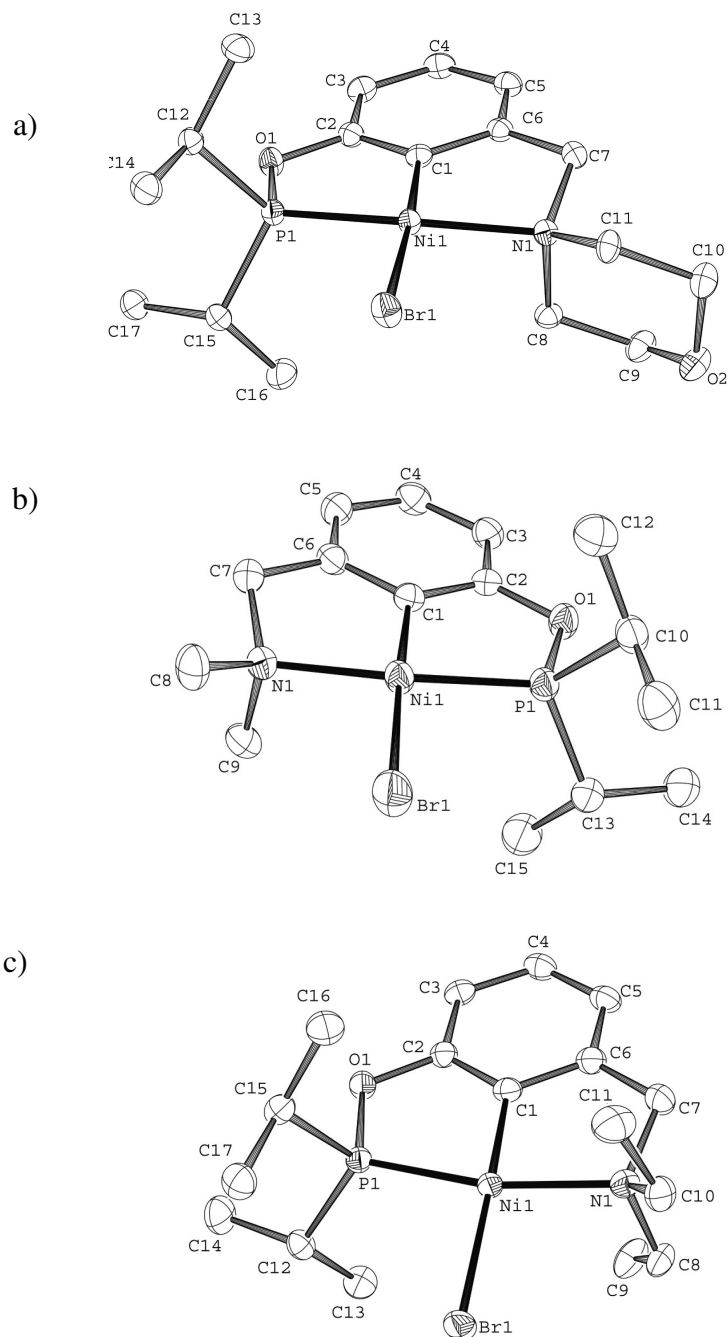


Table 2.1. Crystal Data Collection and Refinement Parameters for Complexes **2.3a-c**.

	2.3a	2.3b	2.3c
chemical formula	C ₁₇ H ₂₇ NO ₂ PNiBr	C ₁₅ H ₂₅ NOPNiBr	C ₁₇ H ₂₉ NOPNiBr
<i>F</i> _w	446.99	409.00	433.00
<i>T</i> (K)	150	150	150
wavelength (Å)	1.54178	1.54178	1.54178
space group	P2 ₁ /n	P-1	Pna2 ₁
<i>a</i> (Å)	9.9289(2)	9.3512(2)	20.5409(5)
<i>b</i> (Å)	8.2128(2)	9.4406(2))	8.1439(2)
<i>c</i> (Å)	23.0832(4)	10.7745(2)	11.5377(3)
α (deg)	90	67.668(1)	90
β (deg)	98.695(1)	79.819(2)	90
γ (deg)	90	75.681(1)	90
<i>Z</i>	4	2	4
<i>V</i> (Å ³)	1860.66(7)	847.19(2)	1930.06(8)
ρ _{calcd} (g cm ⁻³)	1.596	1.587	1.490
μ (cm ⁻¹)	48.94	52.60	46.56
θ range (deg)	3.87 – 67.94	4.46 – 67.81	4.30 – 68.13
R1 ^a [I > 2σ(I)]	0.0293	0.0296	0.0218
wR2 ^b [I > 2σ(I)]	0.0763	0.0781	0.0576
R1 [all data]	0.0293	0.0301	0.0219
wR2 [all data]	0.0763	0.0784	0.0576
GOF	1.143	1.060	1.102

^a $R1 = \frac{\sum(|F_o| - |F_c|)}{\sum|F_o|}$

^b $wR2 = \left\{ \frac{\sum[w(F_o^2 - F_c^2)^2]}{\sum[w(F_o^2)^2]} \right\}^{1/2}$

Table 2.2. Selected Bond Distances (Å) and Angles (deg) for Complexes **2.3a-c**.

	(2.3a)	(2.3b)	(2.3c)
Ni-C(1)	1.853(2)	1.859(2)	1.856(2)
Ni-P(1)	2.1107(6)	2.1119(7)	2.1088(7)
Ni-N(1)	2.043(2)	2.021(2)	2.025(2)
Ni-Br	2.3319(4)	2.3407(5)	2.3615(4)
C(1)-Ni-Br	176.26(7)	177.16(8)	172.47(7)
P(1)-Ni-N(1)	162.20(6)	163.81(6)	166.63(5)
P(1)-Ni-Br	95.08(2)	95.56(2)	95.53(2)
N(1)-Ni-Br	99.65(5)	98.34(6)	97.82(5)
P(1)-Ni-C(1)	81.72(7)	81.99(9)	81.51(8)
N(1)-Ni-C(1)	83.85(9)	83.89(9)	85.15(9)

2.3.3 Characterization of 3.5(a-c).

The identities of the Ni^{III} complexes **2.5a-c** were established by elemental analyses and single crystal X-ray diffraction studies. As can be seen from their ORTEP diagrams (Figure 2.3), these 17-electron compounds adopt square pyramidal structures displaying a slight pyramidal distortion reflected in the out-of-plane displacement of the Ni center from the basal plane defined by the atoms P1, C1, N1, and Br1 (by ca. 0.31 (**2.5a**), 0.34 (**2.5b**), and 0.30 (**2.5c**) Å). This distortion results in trans angles of 158-162° and cis angles of 80-98°, in addition to significantly longer (> 10 e.s.d.) Ni-X bonds relative to the corresponding distances in the Ni^{II} species **2.3**: for Ni-C, ca. 1.89-1.90 vs. 1.85-1.86 Å; for Ni-P, ca. 2.19-2.21 vs. 2.11 Å; and for Ni-N, 2.05-2.07 vs. 2.02-2.04 Å (Table 2.4). The Ni-Br bond for the Br atom occupying the axial position is also much longer than that involving the basal Br atom (2.43-2.46 vs. 2.37 Å); this is consistent with the repulsive interactions anticipated between the bromide lone pair and the half-filled d_{z^2}/d_{p_z} hybrid MO. Unequal axial and basal Ni-X bonds have been observed in POCOPNi^{III}X₂¹⁸ and the closely related (but divalent) complex PCP-Ni^{II}(catecholate) (Ni-O1= 1.92 Å vs. Ni-O2= 2.06 Å),^{14c} whereas the two Ni-I bond distances in van Koten's NCN-Ni^{III}(I)₂ complex are fairly similar (2.61 and 2.63 Å)²³ and identical for NCN-Ni^{III}(Cl)₂ (2.30 Å).²⁴ Finally, close inspection of the structural details for **2.5** reveals significant steric repulsions between the axial Br and the N-alkyl substituents; this repulsion appears to be greatest in complex **2.5c**, which displays the longest Ni-Br2 bond and the least thermal stability (vide infra).

We have subjected the Ni^{III} complexes **2.5** to cyclic voltammetry measurements and compared the results to those obtained with the divalent species **2.3**. The voltammograms (Fig. 2.10) show an irreversible reduction wave (Ni^{III} → Ni^{II}) and an irreversible oxidation peak, which we assign to a ligand-based oxidation process.

Table 2.3. Crystal Data Collection and Refinement Parameters for Complexes **2.5a-c**.

	2.5a	2.5b	2.5c
chemical formula	C ₁₇ H ₂₇ NO ₂ PNiBr ₂	C ₁₅ H ₂₅ NOPNiBr ₂	C ₁₇ H ₂₉ NOPNiBr ₂
<i>F</i> _w	526.90	484.86	512.91
<i>T</i> (K)	150	150	150
wavelength (Å)	1.54178	1.54178	1.54178
space group	Pna2 ₁	P2 ₁ /n	P2 ₁ /n
<i>a</i> (Å)	21.1300(2)	9.3685(2)	8.1481(2)
<i>b</i> (Å)	9.8048(8)	11.2260(3)	19.8813(4)
<i>c</i> (Å)	9.3608(9)	18.1186(4)	12.9752(3)
<i>α</i> (deg)	90	90	90
<i>β</i> (deg)	90	100.817(1)	104.770(1)
<i>γ</i> (deg)	90	90	90
<i>Z</i>	4	4	4
<i>V</i> (Å ³)	1939.3(3)	1871.69(8)	2032.46(8)
<i>ρ</i> _{calcd} (g·cm ⁻³)	1.805	1.721	1.676
<i>μ</i> (cm ⁻¹)	71.30	72.84	67.43
<i>θ</i> range (deg)	4.18–68.38	4.66–67.69	4.17–67.84
R1 ^a [I > 2σ(I)]	0.0362	0.0229	0.0220
wR2 ^b [I > 2σ(I)]	0.0869	0.0581	0.0580
R1 [all data]	0.0358	0.0259	0.0221
wR2 [all data]	0.0873	0.0593	0.0581
GOF	1.044	1.062	1.133

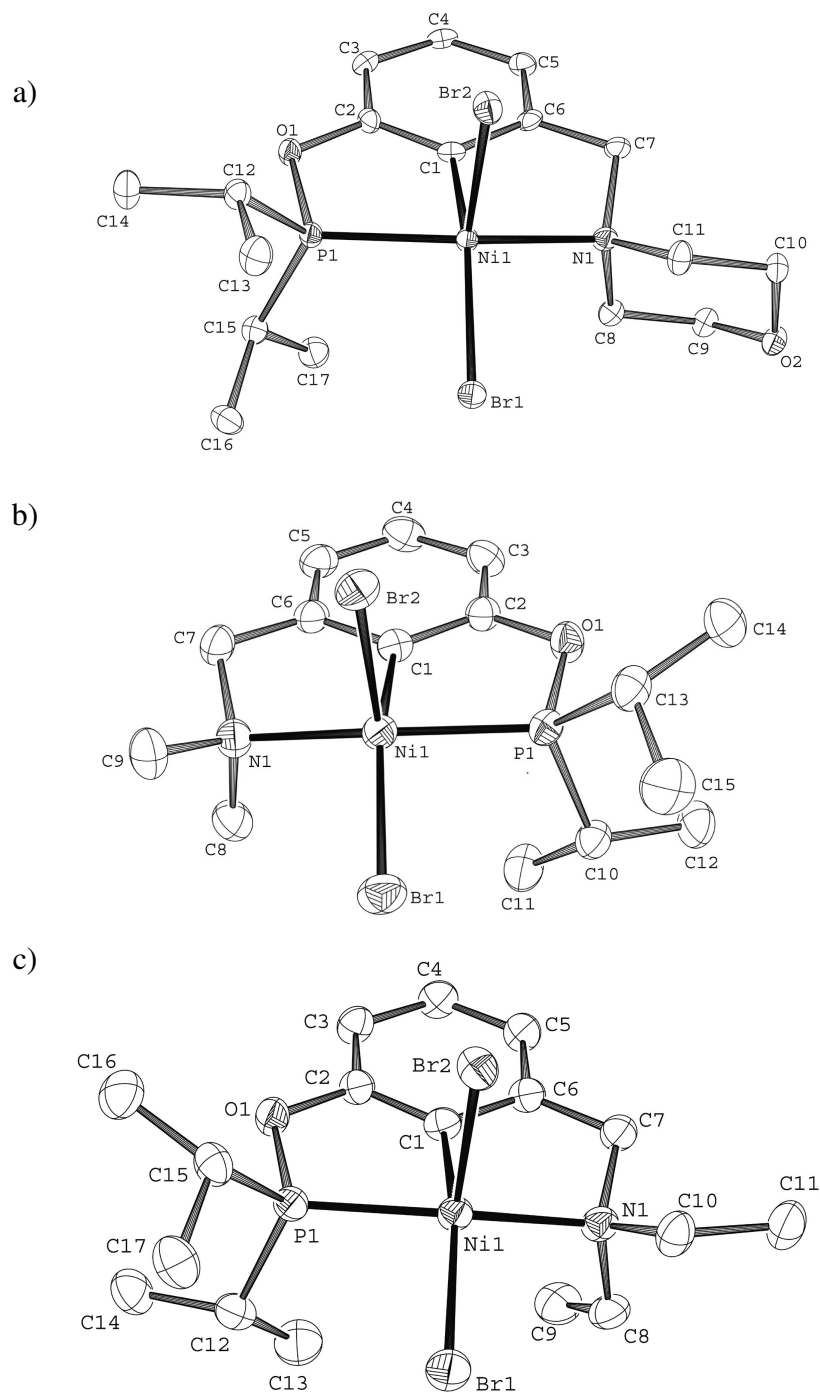
^a $R1 = \frac{\sum(|F_o| - |F_c|)}{\sum|F_o|}$

^b $wR2 = \left\{ \frac{\sum[w(F_o^2 - F_c^2)^2]}{\sum[w(F_o^2)]} \right\}^{1/2}$

Table 2.4. Selected Bond Distances (Å) and Angles (deg) for Complexes **2.5a-c**.

	2.5a	2.5b	2.5c
Ni-C(1)	1.883 (4)	1.897(2)	1.891(2)
Ni-P(1)	2.201 (1)	2.1905(6)	2.2078(5)
Ni-N(1)	2.072(3)	2.051(2)	2.069(2)
Ni-Br(1)	2.3673(7)	2.3710(4)	2.3688(4)
Ni-Br(2)	2.4339(9)	2.4350(4)	2.4638(3)
C(1)-Ni-Br(1)	161.2(1)	159.60(6)	162.27(6)
C(1)-Ni-Br(2)	91.3(1)	95.24(6)	90.98(5)
P-Ni-N	159.9(1)	158.08(6)	159.42(5)
P-Ni-Br(1)	94.23(3)	92.43(2)	92.27(2)
N-Ni-Br(2)	95.8(1)	98.29(5)	98.09(4)
P-Ni-C(1)	80.1(1)	79.92(7)	80.31(6)
N-Ni-C(1)	83.9(1)	83.52(8)	84.47(7)

Figure 2.3. ORTEP diagram for complexes **2.5a** (a), **2.5b** (b), and **2.5c** (c). Thermal ellipsoids are shown at the 50% probability level. Hydrogen atoms are omitted for clarity.



The bonding and electronic structure of **2.5a** were investigated further by EPR analysis. The EPR spectrum of this compound (Figure 2.4) is typical of Ni^{III} pincer compounds with halogen ligands^{3d,23,25} and shows a nearly axial g-tensor with strong hyperfine coupling to the halogen nucleus on the g_{zz} component. The splitting due to the spin 3/2 Br nucleus is shown schematically above the spectrum. The z-component of the g-tensor is close to the free electron g-value (2.0023) while the x- and y- components are in the vicinity of $g = 2.2$. The deviation of the g-tensor from axial symmetry is hard to estimate accurately from the spectrum, because the Br hyperfine coupling on the g_{zz} component is of similar magnitude to the g-anisotropy and a so-called “anomalous line” similar to that found in many Cu^{II} spectra²⁶ is expected. Hence, it is not clear whether the low-field peak is due to the g_{xx} component or the anomalous line. In any case, this combination of g-factors ($g_{xx} \approx g_{yy} > g_{zz} = 2.0023$) is expected for a low-spin d^7 metal ion with tetragonally elongated octahedral symmetry such that the unpaired electron resides in the d_{z^2} orbital^{3d,27}. The strong Br hyperfine splitting seen only on the g_{zz} component indicates that the d_{z^2} orbital is involved in bonding to Br and is consistent with a bonding scheme in which the MOs involved in the axial Br bond are derived from d_{z^2} and p_z orbitals of the Ni^{III} and hold three electrons. Closer inspection of the spectrum reveals a large number of small partially resolved hyperfine splittings due to coupling to the phosphorus (spin 1/2), nitrogen (spin 1) and/or in-plane Br (spin 3/2). In principle, these couplings could provide a clearer picture of the spin density distribution and, by extension, the bonding in the molecular plane; without additional information, however, the large number of unknown parameters precludes a meaningful simulation of the spectrum.

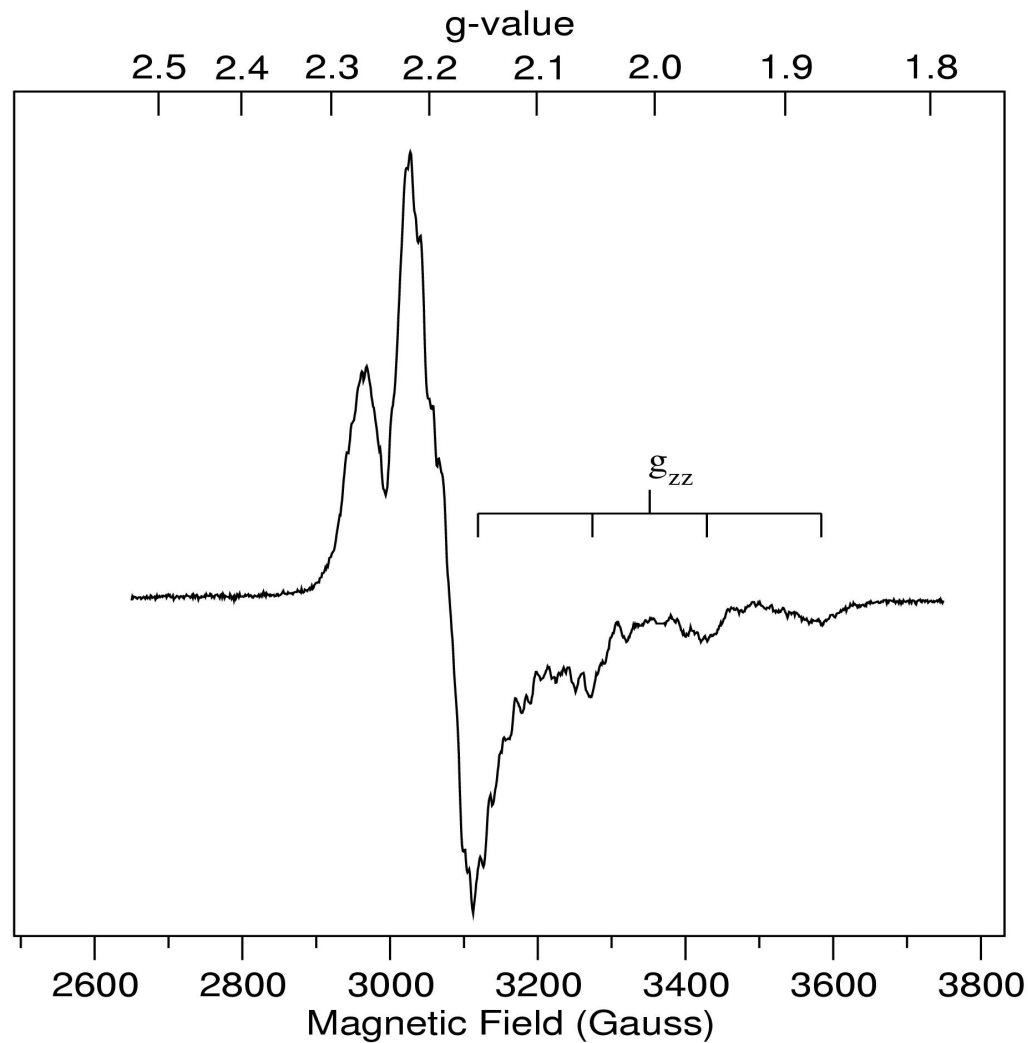


Figure 2.4. X-band (9 GHz) EPR spectrum of **2.5a** in toluene at 120 K. Microwave frequency 9.405102 GHz, microwave power 2 mW, modulation amplitude 1.0 G

2.3.4 Thermal stabilities of **2.3** and **2.5**.

The thermal stability of Ni^{II} complexes was examined by thermogravimetric analysis (TGA). The results showed no decomposition of Ni^{II} complexes **2.3** even above their melting points; the compounds simply evaporated without leaving any significant amount of residue (see TGA thermograms in the supporting information). The thermal stabilities of the Ni^{III} complexes in solid

state were established by studying their thermal profiles using Differential Scanning Calorimetry (DSC). As can be seen in Figure 2.5, complexes **2.5a** and **2.5b** appear to be stable to well above 130 °C, showing exothermic decomposition only above 150 and 140 °C, respectively. The onset of decomposition (exothermic) for these complexes appears to coincide with an endothermic process at ca. 165-173 °C (**2.5a**) and 160-165 °C (**2.5b**), which we attribute to the melting of **2.3a** (observed at 175-177 °C) and **2.3b** (observed at 166-168 °C). A second endothermic process is observed for **2.5b** above 190 °C, which we attribute to the evaporation of the decomposition product **2.3b**. In contrast, **2.5c** appears to be stable only up to 60 °C, beginning to decompose significantly at ca. 80 °C; for this sample, too, there was an endothermic process at 105-110 °C, which we attribute to the melting of the decomposition product **2.3c** (observed at 110-111 °C).

An examination of the thermal stabilities of complexes **2.5** in solution was conducted by variable temperature UV-vis spectroscopy (Figure 2.6), and the results point to the same order of thermal stability as in the solid state, namely: **2.5a**~ **2.5b**> **2.5c**. Thus, **2.5a** and **2.5b** display a $t_{1/2}$ of about 4 h and 3h, respectively, at 70 °C, whereas **5c** begins to decompose upon dissolution at room temperature and displays a $t_{1/2}$ of about 20 minutes at 30 °C. It is noteworthy that the solution decomposition is faster in more concentrated solutions, implying a bimolecular pathway.

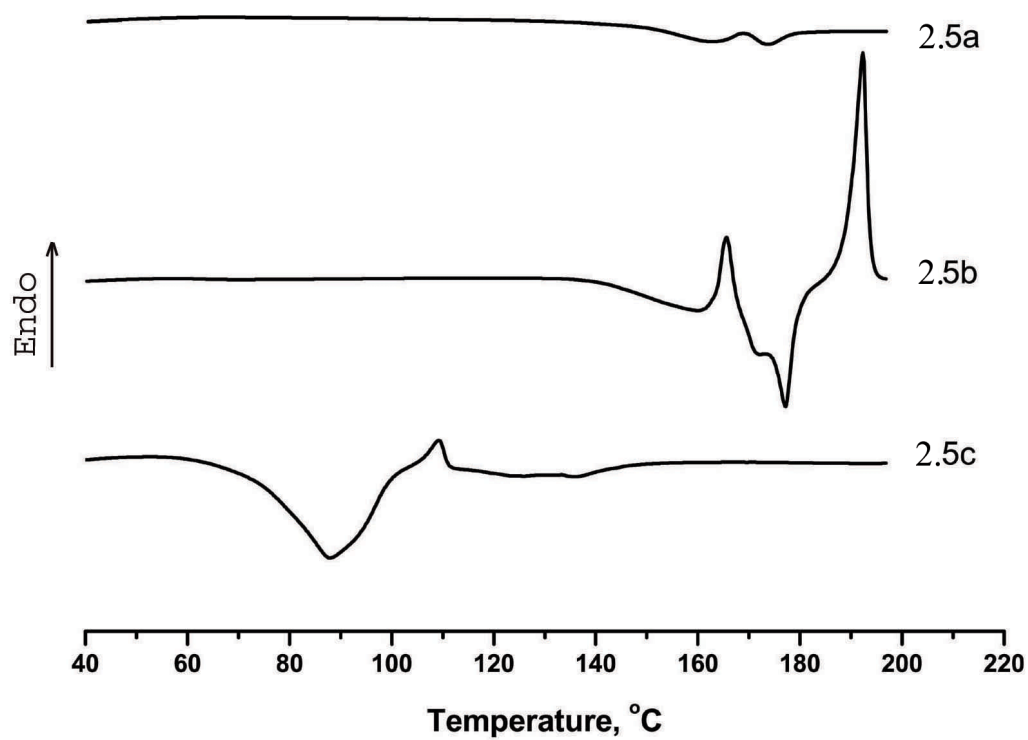
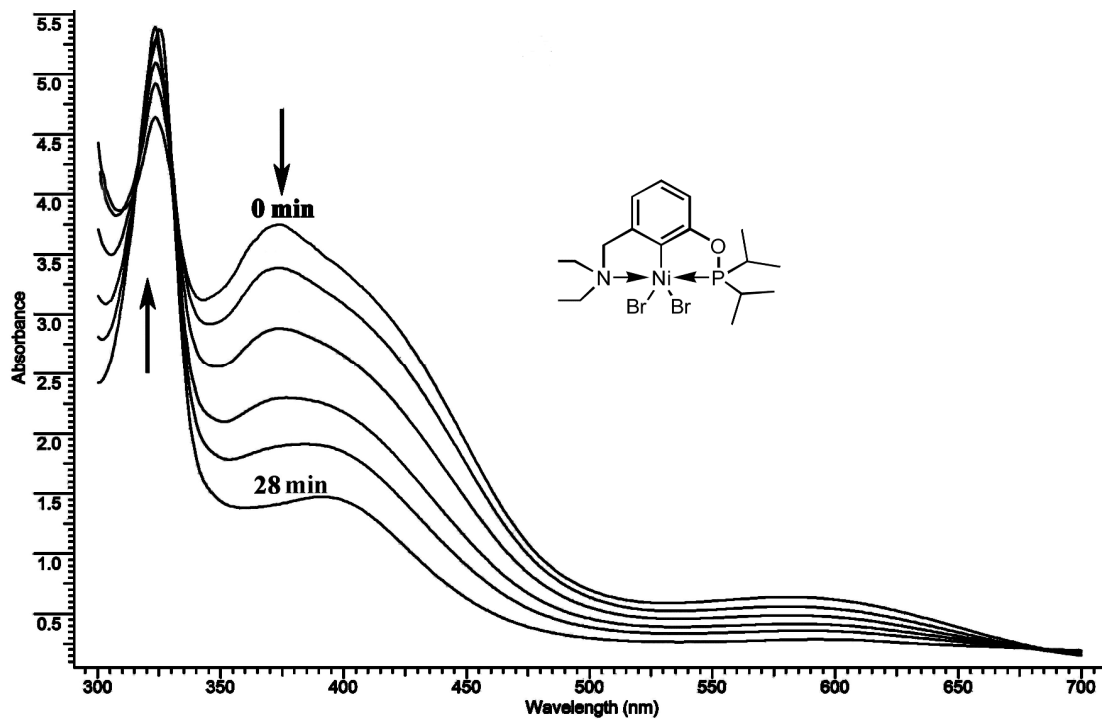
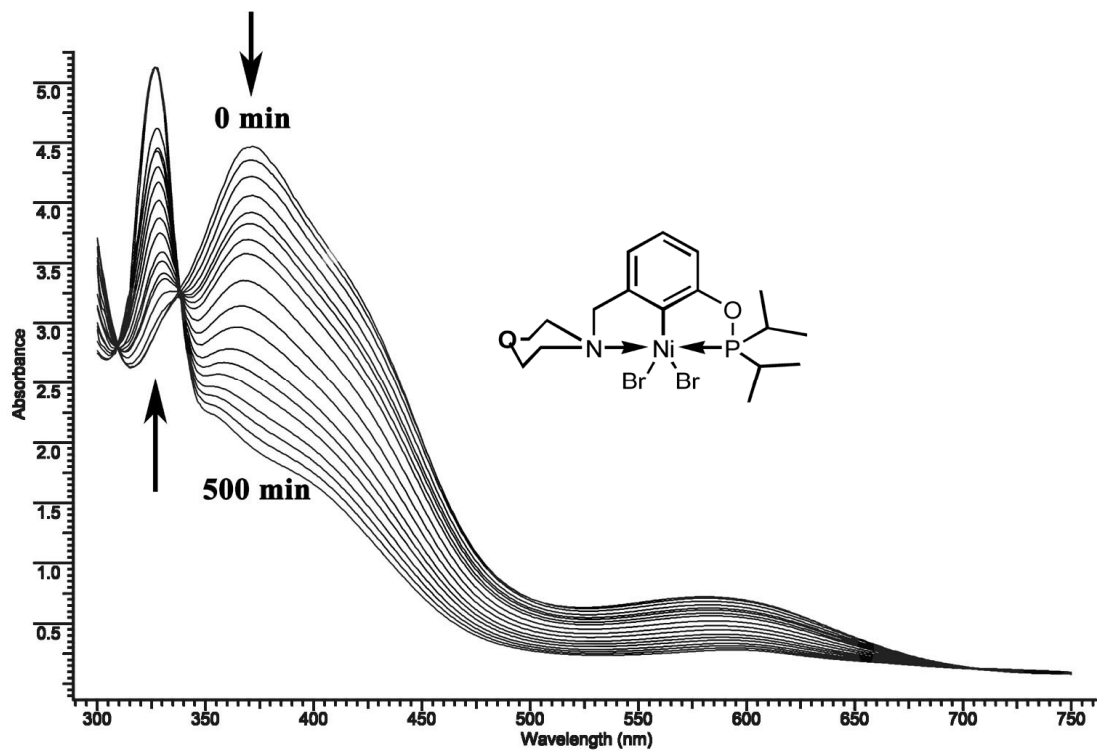


Figure 2.5. The DSC curve of complexes **2.5(a-c)**: nitrogen flow of 20 mL/min, heating rate of 10 °C/min, ca. 8 mg samples weighed in an alumina crucible



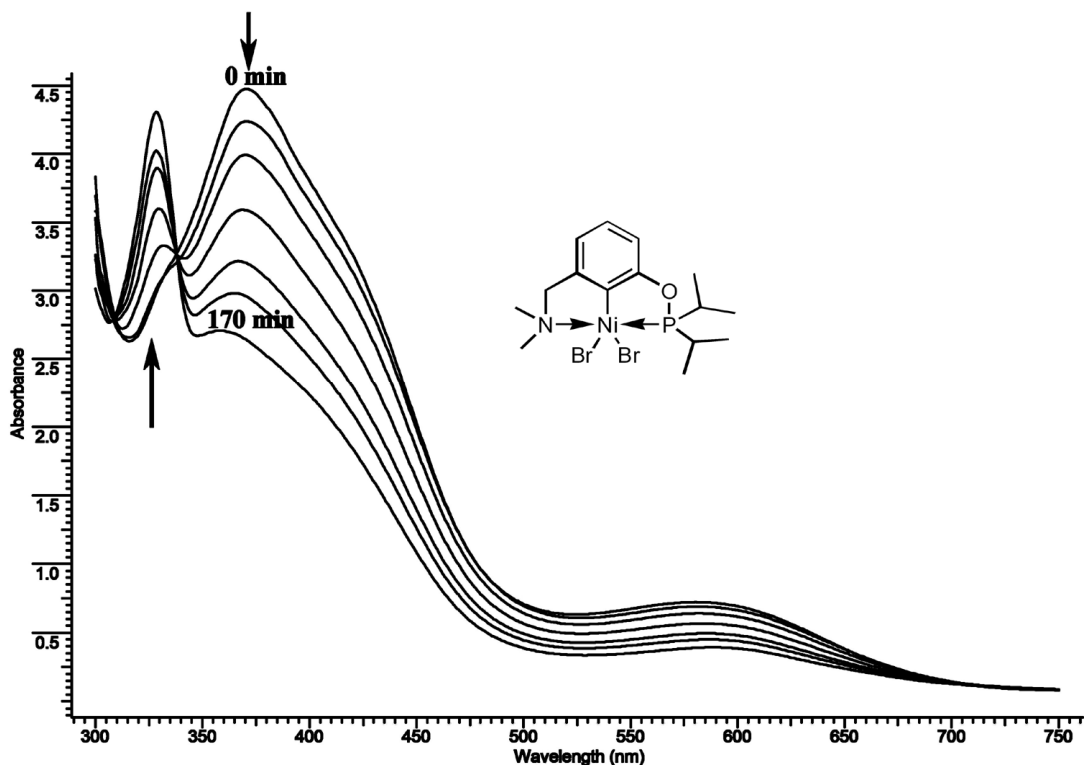


Figure 2.6. The UV-vis spectra of 0.001 M toluene solutions of **2.5a** (70 °C) **2.5b** (70 °C) and **2.5c** (30 °C) as a function of time.

2.3.5 Kharasch addition.

A wide variety of paramagnetic metal complexes are known to promote the Kharasch addition of CCl_4 to various olefins.²⁸ Of relevance to our studies, van Koten's group has shown that Ni complexes based on NCN-type pincer ligands are efficient promoters of the addition of polyhalogenated alkanes to olefins, giving the anti-Markovnikov product (Scheme 2.3). Mechanistic studies by this group have concluded that this reaction proceeds through a non-chain cycle wherein the carbon-based radical entities are held within the solvent cage of the Ni^{III} complex $(\text{NCN})\text{NiX}_2$, thereby favoring 1:1 additions over radical chain type polymerization or telomerisation reactions.



Scheme 2.3. Kharasch addition.

We have reported recently that the $(\text{POC}_{\text{sp}^3}\text{OP})\text{Ni}^{\text{II}}\text{X}/(\text{POC}_{\text{sp}^3}\text{OP})\text{Ni}^{\text{III}}\text{X}_2$ systems promote the Kharasch addition of CCl_4 to a number of olefins, but the catalytic efficacy of these systems are inferior to the reactivities displayed by van Koten's $(\text{NCN})\text{Ni}^{\text{II}}\text{X}$ system. For example, the latter catalyzes the addition of CCl_4 to styrene and methyl methacrylate with catalytic turnover numbers (TON) of up to 1700 and an initial turnover frequency (TOF) of 400 h^{-1} at room temperature, compared to TON of 1000 over 24 h displayed by our $\text{POC}_{\text{sp}^3}\text{OP}$ systems in refluxing acetonitrile.¹⁸ Access to isolable samples of the $(\text{POCN})\text{Ni}^{\text{III}}\text{X}_2$ complexes via the relatively facile oxidation of $(\text{POCN})\text{Ni}^{\text{II}}\text{Br}$ complexes **2.3** with CCl_4 prompted us to screen the reactivities of these complexes for the Kharasch addition reaction. The results of a preliminary study on the addition of CCl_4 to styrene are described below.

The catalytic runs were conducted over 18 h in acetonitrile at $80 \text{ }^\circ\text{C}$ with a Ni: styrene: CCl_4 ratio of 1:50:250. We obtained 95% yields of the anti-Markovnikov addition product when using **2.3a/2.5a** or **2.3b/2.5b** as precursors (TON= 45, TOF~ 2.5/h), but no conversion was noted when using **2.3c/2.5c** as precursor. Analysis of the reaction mixture by NMR spectroscopy and GC-MS showed nearly total conversion to the expected product and no side-products arising from telomerization or oligomerization of styrene. In contrast to what was observed in van Koten's NCN system and our $\text{POC}_{\text{sp}^3}\text{OP}$ system, we found that virtually identical catalytic results are obtained whether or not the catalysis is carried out in air or in an inert atmosphere.

The progress of the catalytic reactions can be monitored by the colors of the catalytic mixtures: depending on whether divalent or trivalent Ni precursors were used, the initial colors of the catalytic mixtures are yellow (when using **2.3a**

or **2.3b**) or dark-brown (**2.5a** or **2.5b**), but all mixtures become yellow-green as the catalysis progresses. No color change is observed and no conversion takes place over days when reaction mixtures are kept at room temperature. NMR monitoring of the catalytic reactions in which **2.3a** or **2.3b** was the Ni precursor revealed that the ^{31}P signals of these species disappeared ca. 10 min after the start of the reaction, whereas reaction mixtures in which **2.3c** or **2.5c** was used as the Ni precursor displayed the ^{31}P signal expected for **2.3c** throughout the reaction. These observations indicate that promotion of the Kharasch addition requires relatively stable and long-lived Ni^{III} intermediates, which is consistent with the generally accepted mechanism for this type of reaction.²⁹

2.4 Conclusions

The current study has shown that POCN-type pincer ligands serve as very attractive templates for preparing organonickel complexes: they undergo relatively facile nickellation and form thermally robust $(\text{POCN})\text{Ni}^{\text{II}}\text{Br}$ derivatives that can, in turn, stabilize the high-valent species $(\text{POCN})\text{Ni}^{\text{III}}\text{Br}_2$. Two of the latter, **2.5a** and **2.5b**, are thermally stable yet fairly reactive in the promotion of the Kharasch addition of CCl_4 to styrene

It is instructive to review the factors affecting the catalytic efficacy for the Kharasch additions catalyzed by pincer-nickel complexes. van Koten has established that the catalytic activities of $(\text{NCN})\text{NiX}$ complexes for the Kharasch addition correlate reasonably well with the redox potential for the one-electron oxidation of these complexes, the more easily oxidizable systems being more effective catalysts. This correlation appears to hold across the series NCN, POCOP, and POCN as the ease of oxidation ($\text{Ni}^{\text{II}} \rightarrow \text{Ni}^{\text{III}}$) and catalytic efficacy in the Kharasch addition follow the order $\text{NCN} > \text{POC}_{\text{sp}^3}\text{OP} > \text{POCN}$, whereas $(\text{POC}_{\text{sp}^2}\text{OP})\text{NiBr}$ does not form isolable high-valent species and does not promote the Kharasch addition. Another important factor is the steric bulk of the donor moieties in these systems, the highest catalytic activities in the NCN systems being observed with the NMe_2 analogue. A similar phenomenon is in effect in the

POCN systems, with the more bulky NEt_2 analogue **2.5c** displaying the lowest thermal stability and being inactive in the Kharasch addition. By extension, we speculate that the greater steric bulk of the $i\text{-Pr}_2\text{P}$ moiety in our $\text{POC}_{\text{sp}^3}\text{OP}$ and POCN systems might be an important factor contributing to their lower levels of catalytic activities and the lower stabilities of the high-valent species $\text{LNi}^{\text{III}}\text{X}_2$ in comparison to van Koten's NCN systems. These considerations might serve as guiding principles for the design of a new generation of catalysts for the Kharasch addition based on systems with less bulky donor moieties or larger and more flexible metallacycle rings.

2.5 Experimental Section

2.5.1 General

All manipulations were carried out using standard Schlenk and glove box techniques under nitrogen atmosphere. Solvents were degassed and dried using standard procedures. The following were purchased from Aldrich and used without further purification: Ni (metal), chlorodiisopropylphosphine, 3-hydroxybenzaldehyde, triethylamine, and C_6D_6 . A Bruker AV 400 spectrometer was used for recording ^1H , $^{13}\text{C}\{^1\text{H}\}$ (101 MHz), and $^{31}\text{P}\{^1\text{H}\}$ (162 MHz) NMR spectra. ^1H and ^{13}C chemical shifts are reported in ppm downfield of TMS and referenced against the residual C_6D_6 signals (7.15 ppm for ^1H and 128.02 ppm for ^{13}C); ^{31}P chemical shifts are reported in ppm and referenced against the signal for 85% H_3PO_4 (external standard, 0 ppm). Coupling constants are reported in Hz. The correlation and assignment of ^1H and ^{13}C NMR resonances were aided by 2D COSY, HMQC, HMBC, DEPT and $^1\text{H}\{^{31}\text{P}\}$ experiments when necessary. GC/MS measurements were made on an Agilent 6890N spectrometer. UV/Vis spectra were recorded on Varian Bio 300 equipped with temperature controlling system using standard sampling cells (1 cm optical path length). The EPR spectra of **2.5a** were collected on a Bruker Elexsys E580 spectrometer operating in cw mode. A solution of **2.5a** in toluene (~1 mM) was prepared, filtered and placed in a 4 mm o.d. EPR tube. The solution was then degassed by repeated freeze-pump-thaw

cycles and the tube was sealed under vacuum. The sample was frozen to 120 K in the spectrometer resonator. DSC curves were obtained using a PerkinElmer Jade Thermoanalyser system with a nitrogen flow of 20 mL/min, a heating rate of 10 °C/min and with samples weighing about 8 mg; an alumina crucible was used in the DSC measurements and samples were prepared by using standard techniques. The elemental analyses were performed by the Laboratoire d'Analyse Élémentaire (Université de Montréal). Melting points for complexes **2.3a**, **2.3b**, **2.3c** were determined with a Mel-TEMP 1010 melting point apparatus equipped with digital thermometer. Thermal gravimetric analysis (TGA) was performed using a 2950 TGA HR V5.4A system with nitrogen as purge gas and a heating rate of 20°C/min; a platinum crucible was used in the TGA measurements and samples were prepared by using standard techniques.

2.5.2 Synthesis of Pre-ligands 2.1a-c

2.5.2.1 [3-((morpholino)methyl)phenol], **2.1a**

To a solution of 3-hydroxybenzaldehyde (0.500 g, 4.10 mmol) in 10 mL of methanol at r.t. was added a solution of morpholine (0.714 g, 8.20 mmol) in 6 mL of methanol. The resulting mixture was stirred for one hour to obtain a yellow solution. The latter was then cooled to -5 °C and NaBH₄ (0.200 g, 5.26 mmol) was added portionwise during one hour. The pre-ligand was purified in one of two ways.

Purification Method A.

The reaction mixture was concentrated under reduced pressure and then treated with 10% HCl until pH=1, washed with a 1:1 mixture of EtOAc and Et₂O (3×10 mL), and finally treated with concentrated aqueous ammonia solution until pH=10. This mixture was then extracted with a 1:1 mixture of EtOAc and Et₂O (5×10 mL), the extracts combined and dried over MgSO₄, filtered through a glass frit and evaporated to give a colorless oil, which crystallized over time to give a white powder (0.664 g, 84%).

Purification Method B.

The reaction mixture was evaporated and the residue re-solubilized in 20 mL of benzene, filtered through a short column of silica gel, and evaporated under dynamic vacuum to give a white powder. (0.736 g, 93%).

^1H NMR (δ , CDCl_3): 2.49 (m, 4H, $2\times\text{NCH}_2$), 3.46 (s, 2H, ArCH_2N), 3.72 (t, $^3J=5$, 4H, $2\times\text{CH}_2\text{O}$), 6.70 (dd, $^3J=8$, $J=3$, 1H, $\{\text{Ar}\}H^6$), 6.75 (s, 1H, $\{\text{Ar}\}H^2$), 6.84 (d, $^3J=8$, 1H, $\{\text{Ar}\}H^4$), 7.15 (t, $^3J=8$, 1H, $\{\text{Ar}\}H^5$), 7.84 (br s, 1H, OH).

$^{13}\text{C}\{^1\text{H}\}$ NMR (δ , CDCl_3): 53.48 (s, 2C, $2\times\text{NCH}_2$), 63.22 (s, 1C, ArCH_2N), 66.68 (s, 2C, $2\times\text{OCH}_2$), 114.64 (s, 1C, $\{\text{Ar}\}C^6$), 116.38 (s, 1C, $\{\text{Ar}\}C^2$), 121.48 (s, 1C, $\{\text{Ar}\}C^4$), 129.45 (s, 1C, $\{\text{Ar}\}C^5$), 138.70 (s, 1C, $\{\text{Ar}\}C^3$), 156.03 (s, 1C, $\{\text{Ar}\}C^1$).
Anal. Calcd for $\text{C}_{11}\text{H}_{15}\text{NO}_2$: C, 68.44; H, 7.96; N, 7.18; Found: C, 68.37; H, 7.82; N, 7.25.

2.5.2.2 [3-((*N,N*-dimethylamino)methyl)phenol], 2.1

The procedure described above for the preparation of pre-ligand **2.1a** (Purification Method B) was used with dimethylammonium chloride (1.174 g, 12.3 mmol) and triethylamine (1.71 mL, 12.3 mmol) to prepare 3-((*N,N*-dimethylamino)methyl)phenol (**2.1b**), which was isolated as a white powder (0.390 g, 63%).

^1H NMR (δ , C_6D_6): 2.26 (s, 6H, $2\times\text{CH}_3$), 3.41 (s, 2H, ArCH_2N), 6.74-6.67 (m, 2H, $\{\text{Ar}\}H^{2,6}$), 6.76 (d, $^3J=8$, 1H, $\{\text{Ar}\}H^4$), 7.13 (t, $^3J=8$, 1H, $\{\text{Ar}\}H^5$), 8.42 (br s, 1H, OH).

$^{13}\text{C}\{^1\text{H}\}$ NMR (δ , C_6D_6): 44.72 (s, 2C, $2\times\text{CH}_3$), 63.78 (s, 1C, ArCH_2N), 115.44 (s, 1C, $\{\text{Ar}\}C^6$), 117.19 (s, 1C, $\{\text{Ar}\}C^2$), 121.24 (s, 1C, $\{\text{Ar}\}C^4$), 129.36 (s, 1C, $\{\text{Ar}\}C^5$), 138.15 (s, 1C, $\{\text{Ar}\}C^3$), 157.09 (s, 1C, $\{\text{Ar}\}C^1$).

Anal. Calcd for $\text{C}_9\text{H}_{13}\text{NO}$: C, 71.49; H, 8.67; N, 9.26; Found: C, 71.55; H, 8.75; N, 9.13.

2.5.2.3 [3-((*N,N*-diethylamino)methyl)phenol], 2.1c

The procedure described above for the preparation of pre-ligand **2.1a** (Purification method A) was used with diethyl amine to prepare 3-((*N,N*-

diethylamino)methyl)phenol, **2.1c**, which was isolated as an off-white oil (0.594 g, 81%).

^1H NMR (δ , C_6D_6): 1.01 (t, $^3J=7$, 6H, $2\times\text{CH}_3$), 2.50 (q, $^3J=7$, 4H, $2\times\text{NCH}_2$), 3.49 (s, 2H, ArCH_2N), 6.83 (dd, $^3J=8$, $J=2$, 1H, $\{\text{Ar}\}H^6$), 6.96 (d, $^3J=8$, 1H, $\{\text{Ar}\}H^4$), 7.03 (br s, 1H, OH), 7.06 (s, 1H, $\{\text{Ar}\}H^2$), 7.17 (t, $^3J=8$, 1H, $\{\text{Ar}\}H^5$).

$^{13}\text{C}\{^1\text{H}\}$ NMR (δ , C_6D_6): 11.29 (s, 2C, $2\times\text{CH}_3$), 46.61 (s, 2C, $2\times\text{NCH}_2$), 57.69 (s, 1C, ArCH_2N), 115.03 (s, 1C, $\{\text{Ar}\}C^6$), 116.93 (s, 1C, $\{\text{Ar}\}C^2$), 121.15 (s, 1C, $\{\text{Ar}\}C^4$), 129.59 (s, 1C, $\{\text{Ar}\}C^5$), 140.79 (s, 1C, $\{\text{Ar}\}C^3$), 157.36 (s, 1C, $\{\text{Ar}\}C^1$).
Anal. Calcd for $\text{C}_{11}\text{H}_{17}\text{NO}$: C, 73.70; H, 9.56; N, 7.81; Found: C, 73.3; H, 9.62; N, 7.38.

2.5.3 Synthesis of POCN ligands 2.2a-c

2.5.3.1 [3-((morpholino)methyl)phosphinitobenzene], **2.2a**

A solution of chlorodiisopropyl phosphine (0.427 mL, 2.59 mmol, 96%) in THF (15 mL) was added to a solution of **2.1a** (0.500 g, 2.59 mmol) and triethylamine (0.400 mL, 2.85 mmol) in THF (35 mL) stirring at 0-5 °C. The resulting mixture was allowed to warm to room temperature and stirred for 1 additional hour. Evaporation of the solvent and extraction of the residue with Et_2O (3x25 mL) followed by filtration of the combined extracts and evaporation gave the desired product as a colorless oil (0.768 g, 96%).

^1H NMR (δ , C_6D_6): 0.72 (dd, $^3J_{\text{HP}}=9$, $J_{\text{HH}}=7$, 3H, CHCH_3), 0.73 (dd, $^3J_{\text{HP}}=8$, $J_{\text{HH}}=7$, 3H, CHCH_3), 0.93-0.85 (m, 6H, $2\times\text{CHCH}_3$), 1.57-1.47 (m, 2H, CH), 1.90-1.92 (m, 4H, $2\times\text{NCH}_2$), 2.95 (s, 2H, NCH_2), 3.28-3.30 (m, 4H, $2\times\text{OCH}_2$), 6.67 (d, $^3J_{\text{HH}}=7$, 1H, $\{\text{Ar}\}H^6$), 6.85 (t, $^3J_{\text{HH}}=8$, 1H, $\{\text{Ar}\}H^5$), 6.89 (s, 1H, $\{\text{Ar}\}H^2$), 6.95 (d, $^3J_{\text{HH}}=8$, 1H, $\{\text{Ar}\}H^4$).

$^{13}\text{C}\{^1\text{H}\}$ NMR (δ , C_6D_6): 17.17 (d, $^2J_{\text{CP}}=8$, 2C, $2\times\text{CHCH}_3$), 17.89 (d, $^2J_{\text{CP}}=20$, 2C, $2\times\text{CHCH}_3$), 28.64 (d, $^1J_{\text{CP}}=19$, 2C, $2\times\text{CH}$), 53.99 (s, 2C, $2\times\text{NCH}_2$), 63.42 (s, 1C, ArCH_2N), 67.10 (s, 2C, $2\times\text{OCH}_2$), 117.56 (d, $^3J_{\text{CP}}=11$, 1C, $\{\text{Ar}\}C^6$), 119.41 (d, $^3J_{\text{CP}}=10$, 1C, $\{\text{Ar}\}C^2$), 122.56 (s, 1C, $\{\text{Ar}\}C^4$), 129.48 (s, 1C, $\{\text{Ar}\}C^5$), 140.58 (s, 1C, $\{\text{Ar}\}C^3$), 160.11 (d, $^2J_{\text{CP}}=9$, 1C, $\{\text{Ar}\}C^1$).

$^{31}\text{P}\{^1\text{H}\}$ NMR (δ , C_6D_6): 147.5 (s).

Anal. Calcd for $\text{C}_{17}\text{H}_{28}\text{NO}_2\text{P}$ C, 66.00; H, 9.12; N, 4.53; Found: C, 66.18; H, 9.36; N, 4.32.

2.5.3.2 [3-((*N,N*-dimethylamino)methyl)phosphinitobenzene], **2.2b**.

The procedure described above for the preparation of **2.2a** was used to prepare 3-((*N,N*-diethylamino)methyl)phosphinitobenzene, **2.2b**, which was isolated as a colorless oil (0.799 g, 91%).

^1H NMR (δ , C_6D_6): 0.68 (dd, $^3J_{\text{HP}}=15$, $^3J_{\text{HH}}=7$, 6H, $2\times\text{CHCH}_3$), 0.84 (dd, $^3J_{\text{HP}}=10$, $^3J_{\text{HH}}=7$, 6H, $2\times\text{CHCH}_3$), 1.46 (m, 2H, $2\times\text{CH}$), 1.76 (s, 6H, $2\times\text{NCH}_3$), 2.94 (s, 2H, ArCH_2), 6.68 (d, $^3J_{\text{HH}}=7$, 1H, $\{\text{Ar}\}H^6$), 6.81 (t, $^3J_{\text{HH}}=8$, 1H, $\{\text{Ar}\}H^5$), 6.85 (s, 1H, $\{\text{Ar}\}H^2$), 6.89 (d, $^3J_{\text{HH}}=8$, 1H, $\{\text{Ar}\}H^4$).

$^{13}\text{C}\{^1\text{H}\}$ NMR (δ , C_6D_6): 17.17 (d, $^2J_{\text{CP}}=9$, 2C, $2\times\text{CH}_3$), 17.87 (d, $^2J_{\text{CP}}=21$, 2C, $2\times\text{CH}_3$), 28.64 (d, $^1J_{\text{CP}}=19$, 2C, $2\times\text{CH}$), 45.34 (s, 2C, $2\times\text{CH}_3\text{N}$), 64.29 (s, 1C, ArCH_2N), 117.48 (d, $^3J_{\text{CP}}=11$, 1C, $\{\text{Ar}\}C^6$), 119.29 (d, $^3J_{\text{CP}}=10$, 1C, $\{\text{Ar}\}C^2$), 122.43 (s, 1C, $\{\text{Ar}\}C^4$), 129.44 (s, 1C, $\{\text{Ar}\}C^5$), 160.08 (d, $^2J_{\text{CP}}=9$, 1C, $\{\text{Ar}\}C^6$).

$^{31}\text{P}\{^1\text{H}\}$ NMR (δ , C_6D_6): 147.4 (s).

Anal. Calcd for $\text{C}_{15}\text{H}_{26}\text{NOP}$: C, 67.39; H, 9.80; N, 5.24; Found: C, 66.97; H, 9.96; N, 4.91.

2.5.3.3 [3-((*N,N*-diethylamino)methyl)phosphinitobenzene], **2.2c**.

The procedure described above for the preparation of **2.2a** was used to prepare 3-((*N,N*-diethylamino)methyl)phosphinitobenzene **2.2c**, which was isolated as a colorless oil (0.730 g, 89%).

^1H NMR (δ , C_6D_6): 0.56 (t, $^3J_{\text{HH}}=7$, 6H, $2\times\text{CH}_2\text{CH}_3$), 0.63 (dd, $^3J_{\text{HP}}=16$, $J_{\text{HH}}=7$, 6H, $2\times\text{CHCH}_3$), 0.79 (dd, $^3J_{\text{HP}}=11$, $J_{\text{HH}}=7$, 6H, $2\times\text{CHCH}_3$), 1.51-1.26 (m, 2H, $2\times\text{CH}$), 2.03 (q, $^3J_{\text{HH}}=7$, 4H, $2\times\text{CH}_2$), 3.06 (s, 2H, ArCH_2N), 6.67 (d, $^3J_{\text{HH}}=8$, 1H, $\{\text{Ar}\}H^6$), 7.03-6.92 (m, 3H, $\{\text{Ar}\}H^{4,2,5}$).

$^{13}\text{C}\{^1\text{H}\}$ NMR (δ , C_6D_6): 12.00 (s, 2C, $2\times\text{CH}_2\text{CH}_3$), 14.76 (d, $^2J_{\text{CP}}=3$, 2C, $2\times\text{CHCH}_3$), 15.85 (d, $^2J_{\text{CP}}=2$, 2C, $2\times\text{CHCH}_3$), 24.82 (d, $^1J_{\text{CP}}=64$, 2C, $2\times\text{CH}$), 46.96 (s, 2C, $2\times\text{CH}_2\text{CH}_3$), 58.15 (s, 1C, ArCH_2N), 114.73 (s, 1C, $\{\text{Ar}\}C^6$), 116.67

(s, 1C, {Ar}C²), 119.93 (s, 1C, {Ar}C⁴), 129.44 (s, 1C, {Ar}C⁵), 158.86 (s, 1C, {Ar}C¹).

³¹P{¹H} NMR (δ, C₆D₆): 147.1 (s).

Anal. Calcd for C₁₇H₃₀NOP: C, 69.12; H, 10.24; N, 4.74; Found: C, 69.32 ; H, 10.37 ; N, 4.48.

2.5.4 Synthesis of complexes 2.3-2.5

2.5.4.1 $\kappa^P, \kappa^C, \kappa^N$ -{2,6-(*i*-Pr₂PO)(C₆H₃)(CH₂[c-N(CH₂)₄O])}NiBr, **2.3a**

Slow addition of a solution of **2.2a** (0.500 g, 1.62 mmol) and NEt₃ (0.23 mL, 1.62 mmol) in 20 mL of benzene to the suspension of NiBr₂(CH₃CN)_x (0.485 g, 1.618 mmol) in benzene (10 mL) resulted in a dark brown mixture, which was heated for 3 h at 60 °C. Filtration of the final mixture through a pad of silica gel followed by evaporation of the volatiles gave the desired product as a yellow powder (0.659g, 91%).

¹H NMR (δ, C₆D₆): 1.16 (dd, ³J_{HP}= 15, ³J_{HH}= 7, 6H, CH₃) 1.47 (dd, ³J_{HP}= 18, ³J_{HH}= 7, 6H, CH₃), 2.27-2.12 (m, 2H, CH), 2.31 (d, ³J_{HH}= 13, 2H, NCH₂CH₂), 3.14 (dd, ³J_{HH}= 12 & 3, 2H, NCH₂CH₂), 3.20 (td, ³J_{HH}= 12 & 2, 2H, OCH₂), 3.62 (s, 2H, ArCH₂N), 4.18 (m, 2H, OCH₂), 6.44 (d, ³J_{HH}= 8, 1H, {Ar}H⁵), 6.61 (d, ³J_{HH}= 8, 1H, {Ar}H³), 6.92 (t, ³J_{HH}= 8, 1H, {Ar}H⁴).

¹³C{¹H} NMR (δ, C₆D₆): 16.90 (s, 2C, 2×CH₃) 18.34 (d, ²J_{CP} = 4, 2C, 2×CH₃), 28.61 (s, 2C, 2×CH), 54.13 (s, 2C, 2×NCH₂), 60.98 (s, 2C, 2×OCH₂), 62.99 (s, 1C, ArCH₂N), 108.29 (d, ³J_{CP}= 12, 1C, {Ar}C³), 108.42 (s, 1C, {Ar}C⁵), 115.92 (s, 1C, {Ar}C⁴), 142.15 (d, ²J_{CP} = 35, 1C, {Ar}C¹-Ni), 150.75 (s, 1C, {Ar}C⁶), 165.96 (d, ²J_{CP} = 9, 1C, {Ar}C²).

³¹P{¹H} NMR (δ, C₆D₆): 201.48 (s).

Anal. Calcd for C₁₇H₂₇P₁O₂NiBr: C, 45.68; H, 6.09; N, 3.13; Found: C, 45.69; H, 6.04; N, 3.04.

2.5.4.2 $\kappa^P, \kappa^C, \kappa^N$ -{2,6-(*i*-Pr₂PO)(C₆H₃)(CH₂NMe₂)}NiBr, **2.3b**.

The procedure described above for the preparation of **2.3a** was used to prepare this complex, which was isolated as a yellow powder (0.583 g, 77%).

¹H NMR (δ, C₆D₆): 1.17 (dd, ³J_{HP} = 15, ³J_{HH} = 7, 6H, 2×CH₃), 1.47 (dd, ³J_{HP} = 18, ³J_{HH} = 7, 6H, 2×CH₃), 2.19 (m, 2H), 2.44 (d, ³J_{HH} = 2, 6H, 2×NCH₃), 3.25 (s, 2H, NCH₂), 6.40 (d, ³J_{HH} = 7, 1H, {Ar}H⁵), 6.62 (d, J_{HH} = 8, 1H, {Ar}H³), 6.93-6.87 (m, 1H, {Ar}H⁴). ¹³C{¹H} NMR (δ, C₆D₆): 16.87 (s, 2C, 2×CH₃), 18.26 (d, ²J_{CP} = 4, 2C, 2×CH₃), 28.49 (d, ¹J_{CP} = 24, 2C, 2×CH), 49.11 (s, 2C, 2×NCH₃), 71.84 (s, 1C, CH₂), 108.38 (d, ³J_{CP} = 13, 1C, {Ar}C³), 115.67 (s, 1C, {Ar}C⁵), 127.04 (s, 1C, {Ar}C⁴), 143.11 (d, ²J_{CP} = 33, 1C, {Ar}C¹-Ni), 151.09 (s, 1C, {Ar}C⁶), 166.16 (d, ²J_{CP} = 11, 1C, {Ar}C²).

³¹P{¹H} NMR (δ, C₆D₆): 199.16 (s, P).

Anal. Calcd for C₁₅H₂₇P₁O₂NiBr: C, 44.50; H, 6.22; N, 3.46; Found: C, 44.56; H, 6.41; N, 3.53.

2.5.4.3 $\kappa^P, \kappa^C, \kappa^N$ -{2,6-(*i*-Pr₂PO)(C₆H₃)(CH₂NEt₂)}NiBr, **2.3c**.

The procedure described above for the preparation of **2.3a** was used to prepare this complex, which was isolated as a yellow powder (0.616 g, 84%).

¹H NMR (δ, C₆D₆): 1.12 (dd, ³J_{HP} = 14, ³J_{HH} = 7, 6H, 2×CHCH₃) 1.51-1.37 (m, 12H, 2×CH₂CH₃ and 2×CHCH₃), 2.08-1.96 (m, 2H, 2×CH), 2.17 (m, 2H, CH₂CH₃), 3.41-3.28 (m, 2H, CH₂CH₃), 3.43 (s, 2H, ArCH₂N), 6.35 (d, ³J_{HH} = 8, 1H, {Ar}H⁵), 6.56 (d, ³J_{HH} = 8, 1H, {Ar}H³), 6.85 (t, ³J_{HH} = 8, 1H, {Ar}H⁴).

¹³C{¹H} NMR (δ, C₆D₆): 13.34 (s, 2C, 2×CH₂CH₃) 16.85 (d, ²J_{CP} = 2, 2C, 2×CH₃), 18.19 (d, ²J_{CP} = 4, 2C, 2×CH₃), 28.6 (d, ¹J_{CP} = 24, 2C, 2×CH), 56.3 (d, ³J_{CP} = 2, 2C, 2×CH₂CH₃), 64.7 (d, ³J_{CP} = 2, 1C, ArCH₂N), 107.96 (d, ³J_{CP} = 13, 1C, {Ar}C³), 114.3 (d, ⁴J_{CP} = 2, C, {Ar}C⁵), 126.8 (s, 1C, {Ar}C⁴), 142.1 (d, ²J_{CP} = 33, 1C, {Ar}C¹-Ni), 154.1 (s, 1C, {Ar}C⁶), 165.8 (d, ²J_{CP} = 11, 1C, {Ar}C²).

³¹P{¹H} NMR (δ, C₆D₆): 197.92 (s).

Anal. Calcd for C₁₇H₂₉OPNNiBr: C, 47.16; H, 6.75; N, 3.23;. Found: C, 47.71; H, 6.68; N, 3.26.

2.5.4.4 κ^P -[1,3- $\{(i\text{-Pr}_2\text{PO})(\text{C}_6\text{H}_4)(\text{CH}_2[\text{c-NH}(\text{CH}_2)_4\text{O}])\}] \text{NiBr}_3$, **2.4**

A solution of **2.2a** (0.500 g, 1.618 mmol) in benzene (15 ml) was added to $\text{NiBr}_2(\text{CH}_3\text{CN})_x$ (0.486 g, 1.62 mmol). The resulting brown mixture was stirred at 60 °C for 3 h, which resulted in the precipitation of a blue-green solid. Filtration through a glass frit (under inert atmosphere) and washing the solid on a filter with benzene followed by drying under vacuum gave a turquoise-green solid (0.423 g, 43%). The filtrate was passed through a pad of silica gel followed by removal of solvent to give **2.3a** as a yellow powder (0.333 g, 46%).

Anal. Calcd for $\text{C}_{17}\text{H}_{29}\text{O}_2\text{P}_1\text{NiBr}_3$: C, 33.54; H, 4.80; N, 2.30; Found: C, 33.58; H, 4.81; N, 2.39.

2.5.4.5 $\kappa^P, \kappa^C, \kappa^N$ -{2,6- $(i\text{-Pr}_2\text{PO})(\text{C}_6\text{H}_3)(\text{CH}_2[\text{c-N}(\text{CH}_2)_4\text{O}])$ } NiBr_2 , **2.5a**

A solution of Br_2 (6.5 μL , 0.123 mmol) in E_2O (5 mL) was cooled to -15 °C and then added to a solution of **3a** (0.100 g, 0.224 mmol) in 10 mL of a 5:1 mixture of Et_2O and CH_2Cl_2 . The resulting mixture was stirred for 20 min and then concentrated under reduced pressure to ~ 3-5 mL. The final mixture was layered with cold hexane (5 mL) and placed in a -15 °C freezer to obtain black crystals, which were collected by filtration (112 mg, 95%).

Anal. Calcd for $\text{C}_{17}\text{H}_{27}\text{O}_2\text{PNNiBr}_2$: C, 38.75; H, 5.17; N, 2.66. Found: C, 38.47; H, 5.05; N, 2.57.

2.5.4.6 $\kappa^P, \kappa^C, \kappa^N$ -{2,6- $(i\text{-Pr}_2\text{PO})(\text{C}_6\text{H}_3)(\text{CH}_2\text{NMe}_2)$ } NiBr_2 , **2.5b**

The procedure described above for the preparation of **5a** was used to prepare this complex, which was isolated as black crystals (114 mg, 96%).

Anal. Calcd for $\text{C}_{15}\text{H}_{25}\text{OPNNiBr}_2$: C, 37.16.; H, 5.20; N, 2.89. Found: C, 37.13; H, 5.23; N, 2.97

2.5.4.7 $\kappa^P, \kappa^C, \kappa^N$ -{2,6- $(i\text{-Pr}_2\text{PO})(\text{C}_6\text{H}_3)(\text{CH}_2\text{NEt}_2)$ } NiBr_2 , **2.5c**

A modified version of the procedure described above for the preparation of **5a** (reaction temperature -78 °C) was used to prepare this complex, which was isolated as black crystals (93 mg, 80%).

Anal. Calcd for $C_{17}H_{29}OPNNiBr_2$: C, 39.81; H, 5.70; N, 2.73. Found: C, 39.34; H, 5.86; N, 2.73.

2.5.5 Cyclic voltammetry

Cyclic voltammetry measurements were performed using a BAS Epsilon potentiostat. The electrochemical properties of these compounds were measured at room temperature in dichloromethane using a standard three electrode system consisting of a glassy carbon working electrode, a Pt auxiliary electrode, and a Ag/AgCl reference electrode. Bu_4NPF_6 was used as electrolyte (0.1 mol/L) and the solutions were bubbled with nitrogen before each experiment. Reversible redox waves of the ferrocenyl moieties were observed under these conditions ($E_{1/2}$ { $FeCp_2^+/FeCp_2$ } = +0.47 V).

2.5.6 Crystal Structure Determinations

Single crystals of **3a-3c** were grown by slow diffusion of hexanes into saturated benzene solutions of the complexes. Single crystals of **5a-5c** were grown from dichloromethane-hexane mixtures at -20 °C. The crystallographic data for complexes **3a-3c** and **5a-5c** were collected on a Bruker Microstar generator (micro source) equipped with a Helios optics, a Kappa Nonius goniometer and a Platinum135 detector. Cell refinement and data reduction were done using SAINT.³⁰ An empirical absorption correction, based on the multiple measurements of equivalent reflections, was applied using the program SADABS.³¹ The space group was confirmed by XPREP routine³² in the program SHELXTL.³³ The structures were solved by direct-methods and refined by full-matrix least squares and difference Fourier techniques with SHELX-97.³⁴ All non-hydrogen atoms were refined with anisotropic displacement parameters. Hydrogen atoms were set in calculated positions and refined as riding atoms with a common thermal parameter.

2.6 Acknowledgment

The authors gratefully acknowledge financial support received from Université de Montréal (fellowships to D.M. S.) and NSERC of Canada (Research Tools and Instruments grants to D.Z. and Discovery grants to D.Z. and AvdE). Profs. D. Rochefort and M. S. Workentin are thanked for their valuable help with electrochemical studies.

2.7 Supporting Information

TGA for **2.3a-c** and cyclic voltammograms for complexes **2.3**, ligand **2.2a**, and pre-ligand **2.1a**. This material is available free of charge via the Internet at <http://pubs.acs.org>. Complete details of the X-ray analyses for complexes **2.3a-c** and **2.5a-c** have been deposited at The Cambridge Crystallographic Data Centre (CCDC 713853 (**2.3a**), 713858 (**2.3b**), 713854 (**2.3c**), 713856 (**2.5a**), 713855 (**2.5b**), 713857 (**2.5c**)). These data can be obtained free of charge via www.ccdc.cam.ac.uk/data_request/cif, or by emailing data_request@ccdc.cam.ac.uk, or by contacting The Cambridge Crystallographic Data Centre, 12, Union Road, Cambridge CB2 1EZ, UK; fax: +44 1223 336033.

Supporting information

New POCN-Type Pincer Complexes of Ni^{II} and Ni^{III}

Denis M. Spasyuk and Davit Zargarian*

Département de chimie, Université de Montréal, Montréal (Québec), Canada H3C
3J7

1. TGA for **2.3(a-c)**
2. CV of **2.1a** and **2.2a**
3. CV of **2.3(a-c)** and **2.5(a-c)**

Figure 2.7. TGA thermogram for complexes **2.3a-c** recorded at 20 °C/min using a platinum crucible.

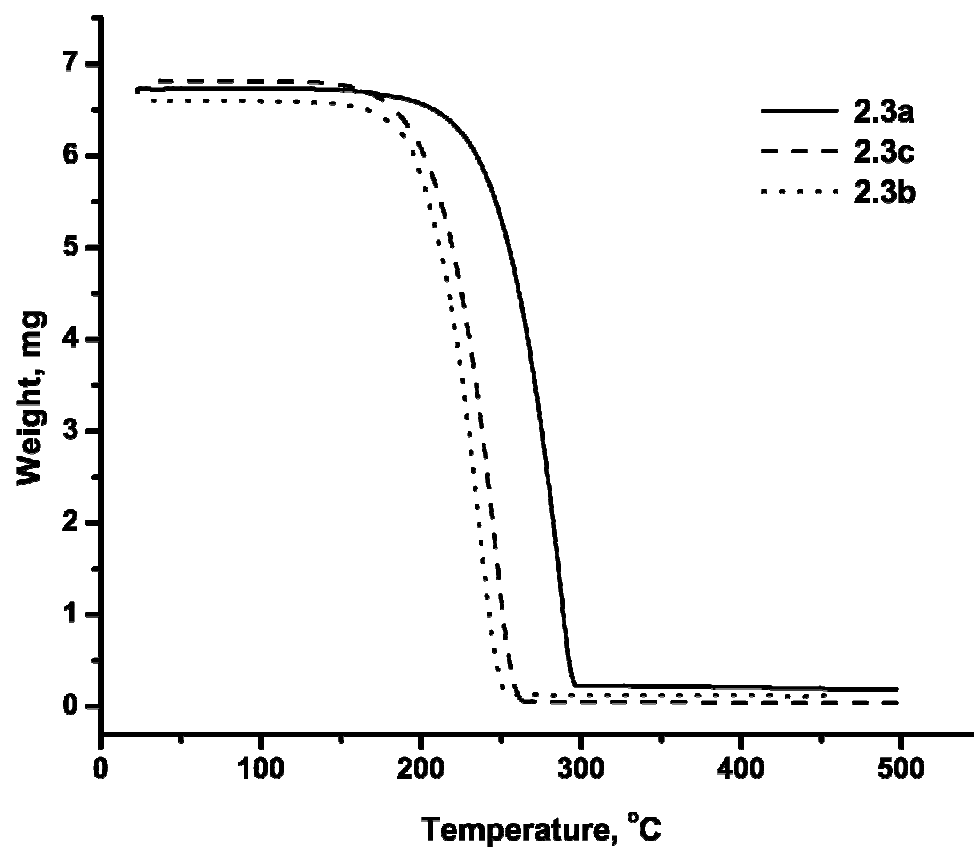


Figure 2.8. Cyclic voltammograms of 1 mM solutions of compound **2.1a** and **2.2a** in dichloromethane containing 0.1 M tetrabutylammonium hexafluorophosphate at 25 °C at a scan rate of 100 mV/s on a glassy carbon working electrode.

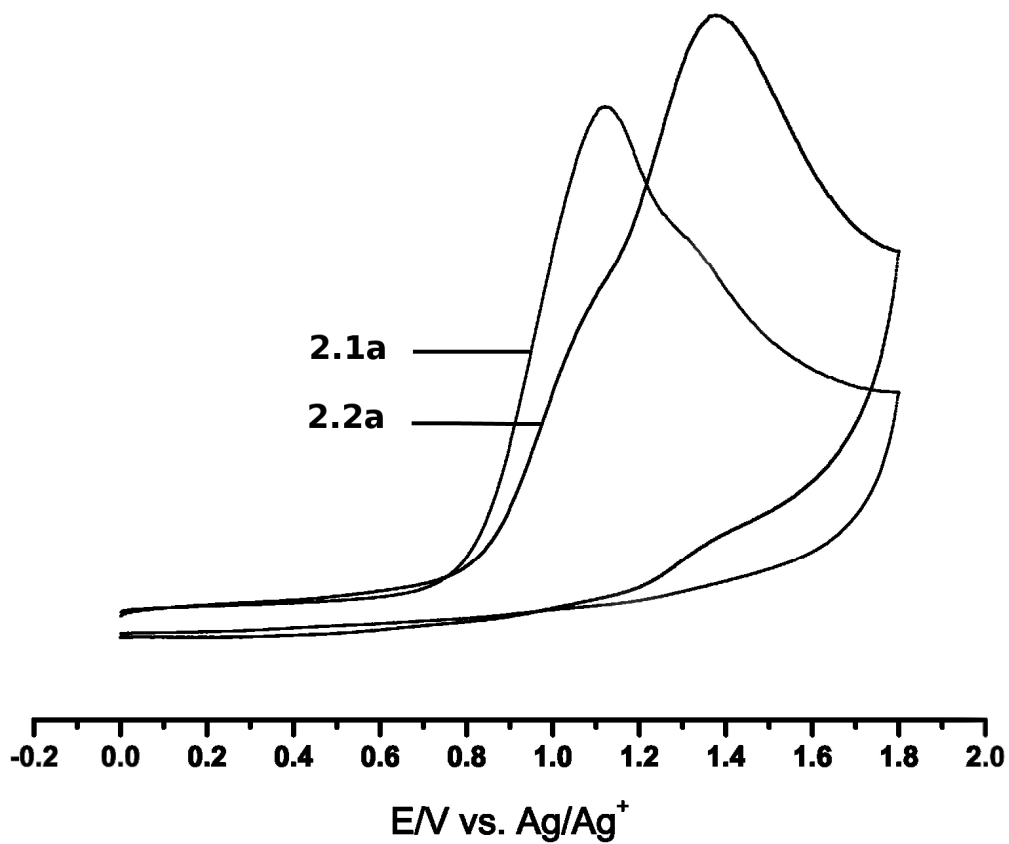


Figure 2.9. Cyclic voltammograms of 1mM solutions of complexes **2.3(a-c)** and $\{2,6-(i\text{-PrPO})_2\text{C}_6\text{H}_3\}\text{NiBr}$ in dichloromethane containing 0.1 M tetrabutylammonium hexafluorophosphate at 25 °C at a scan rate of 100 mV/s on a glassy carbon working electrode.

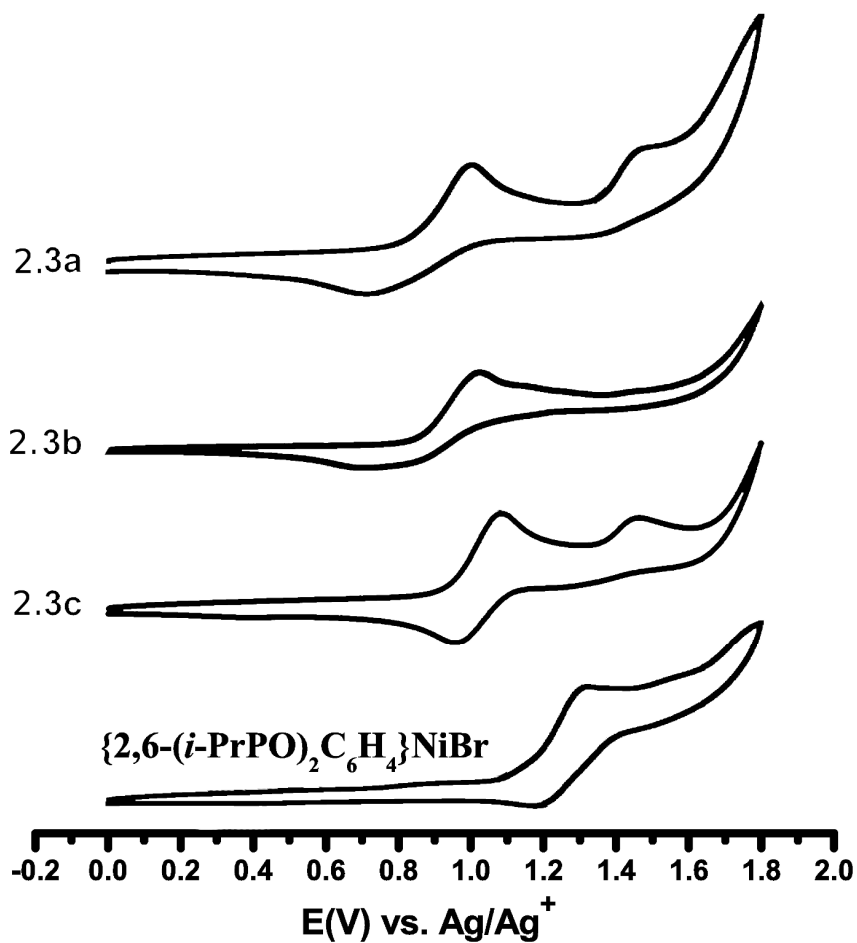
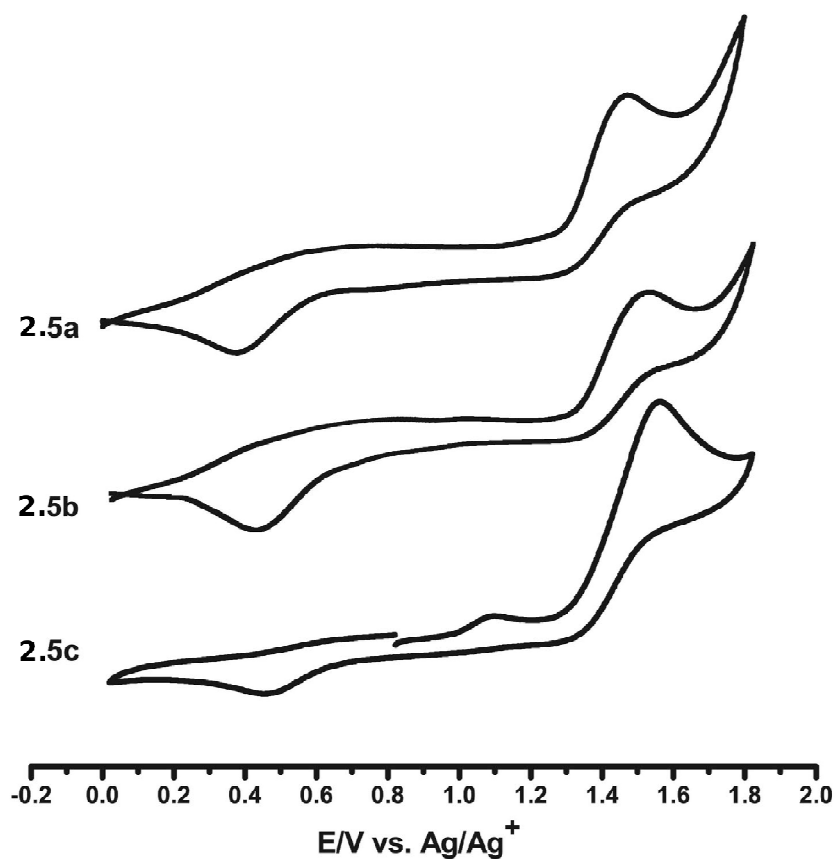


Figure 2.10. Cyclic voltammograms of 1 mM solutions of complexes **2.5(a-c)** in dichloromethane containing 0.1 M tetrabutylammonium hexafluorophosphate at 25°C at a scan rate of 100 mV/s on a glassy carbon working electrode. The minor oxidation peak seen at ca. 1.08 V in the voltammogram of **2.5c** is due to the $\text{Ni}^{\text{II}} \rightarrow \text{Ni}^{\text{III}}$ process which is detectable since **2.5c** undergoes ready decomposition to **2.3c**. The CV measurements were carried out using CH_2Cl_2 solutions containing Bu_4NPF_6 as electrolyte; different starting potentials were employed for **2.5a** and **2.5b** (0 V, Ag/Ag^+) vs. the equilibrium potential for **2.5c**, with the same result.



2.8 References

¹ a) Moulton, C. J.; Shaw, B. L. *J. Chem. Soc., Dalton Trans.* 1976, 1020. b) Crocker, C.; Errington, R. J.; McDonald, W. S.; Odell, K. J.; Shaw, B. L.; Goodfellow, R. J. *J. Chem. Soc., Chem. Commun.* **1979**, 498.

² Reviews: (a) M. Albrecht and G. Van Koten, *Angew. Chem., Int. Ed.*, **2001**, 40, 3750. (b) M. E. van der Boom and D. Milstein, *Chem. Rev.*, **2003**, 103, 1759. (c) G. R. Newcome, *Chem. Rev.*, **1993**, 93, 2067. (d) J. T. Singleton, *Tetrahedron*, **2003**, 59, 1837. (e) L.-C. Liang, *Coord. Chem. Rev.*, **2006**, 250, 1152.

³ (a) van Koten G.; Timmer, K.; Noltes, J. G.; Spek, A. L. *J. Chem. Soc., Chem. Commun.* **1978**, 250. (b) Grove, D. M.; van Koten, G.; Ubbels, H. J. C.; Zoet, R.; Spek, A. L. *Organometallics* **1984**, 3, 1003. (c) Grove, D. M.; van Koten, G.; Verschuuren, A. H. M. *J. Mol. Cat.* **1988**, 45, 169. (d) Grove, D. M.; van Koten, G.; Mul, W. P.; van der Zeijden, A. A. H.; Terheijden, J.; Zoutberg, M. C.; Stam, C. H. *Organometallics* **1986**, 5, 322.

⁴ (a) Fryzuk, M. D.; MacNeil, P. A. *J. Am. Chem. Soc.* **1981**, 103, 3592. (b) Weng, W., Guo, C., Moura, C., Yang, L., Foxman, B. M. and Ozerov, O. V. *Organometallics*, **2005**, 24, 3487.

⁵ (a) Morales-Morales, D.; Redón, R.; Yung, C.; Jensen, C. M. *Chem. Commun.* **2000**, 1619. (b) Morales-Morales, D.; Grause, C.; Kasaoka, K.; Redón, R.; Cramer, R. E.; Jensen, C. M. *Inorg. Chim. Acta* **2000**, 300, 958. (c) Morales-Morales, D., Lee, D. W., Wang Z. and Jensen, C. M. *Organometallics*, **2001**, 20, 1144. (d) Salem, H., Ben-David, Y., Shimon, L. J. W., Milstein, D. *Organometallics* **2006**, 25, 2292. (e) Sykes, A. C.; White, P.; Brookhart, M. *Organometallics* **2006**, 25, 1664

⁶ Benito-Garagorri, D.; Bocokić, V.; Mereiter, K.; Kirchner, K. *Organometallics* **2006**, 25, 3817

⁷ Gründemann, S.; Albrecht, M.; Loch, J. A.; Faller, J. W.; Crabtree, R. H. *Organometallics* **2001**, 20, 5485.

⁸ (a) Poverenov, E.; Gandelman, M.; Shimon, L. J. W.; Rozenberg, H.; Ben-David, Y.; Milstein, D. *Chem. Eur. J.* **2004**, *10*, 4673. (b) Gong, J.; Zhang, Y.; Song, M.; Xu, C. *Organometallics* **2007**, *26*, 6487. (1) Inés, B.; SanMartin, R.; Churruca, F.; Domínguez, E.; Urriaga, M. K.; Arriortua, M. I. *Organometallics* **2008**, *27*, 2833.

⁹ van der Made, A. W.; van der Made, R. H. *J. Org. Chem.* **1993**, *58*, 1262.

¹⁰ Amoedo, A.; Grana, M.; Martinez, J.; Pereira, T.; Lopez-Torres, M.; Fernández, A.; Fernández, J. J.; Vila, J. M. *Eur. J. Inorg. Chem.* **2002**, 613.

¹¹ Vechorkin, O.; Csok, Z.; Scopelliti, R.; Hu, X. *Chem. Eur. J.* **2009**, *15*, 3889-3899 and references therein.

¹² (a) Gozin, M.; Aizenberg, M.; Liou, S.-Y.; Weisman, A.; Ben-David, Y.; Milstein, D. *Nature* **1994**, *370*, 42. (b) Kanzelberger, M.; Singh, B.; Czerw, M.; Krogh-Jespersen, K.; Goldman, A. S. *J. Am. Chem. Soc.* **2000**, *122*, 11017. (c) Gusev, D. G.; Fonatine, F.-G.; Lough, A. J.; Zargarian, D. *Angew. Chem. Int. Ed. Engl.* **2003**, *42*, 216. (d) Zhao, J.; Goldman, A. S.; Hartwig, J. F. *Science* **2005**, *307*, 1080. (e) Goldman, A. S.; Roy, A. H.; Huang, Z.; Ahuja, R.; Schinski, W.; Brookhart, M. *Science* **2006**, *312*, 257. (f) Ingleson, M.; Fan, H.; Pink, M.; Tomaszewski, J.; Caulton, K. G. *J. Am. Chem. Soc.*, **2006**, *128*, 1804. (g) Gunanathan, C.; Ben-David, Y.; Milstein, D. *Science* **2007**, *317*, 790. (h) Kohl, S. W.; Weiner, L.; Schwartsburd, L.; Konstantinovski, L.; Shimon, L. J. W.; Ben-David, Y.; Iron, M. A.; Milstein, D. *Science* **2009**, *324*, 74.

¹³ (a) Baho, N.; Zargarian, D. *Inorg. Chem.* **2007**, *46*, 299. (b) Gareau, D.; Sui-Seng, C.; Groux, L. F.; Brisse, F.; Zargarian, D. *Organometallics* **2005**, *24*, 4003. (c) Chen, Y.; Sui-Seng, C.; Zargarian, D. *Angew. Chem., Int. Ed. Engl.* **2005**, *44*, 7721. (d) Boucher, S.; Zargarian, D. *Can. J. Chem.* **2005**, *84*, 233. (e) Chen, Y.; Sui-Seng, C.; Boucher, S.; Zargarian, D. *Organometallics* **2005**, *24*, 149. (f) Fontaine, F.-G.; Zargarian, D. *J. Am. Chem. Soc.* **2004**, *126*, 8786. (g) Groux, L. F.; Zargarian, D. *Organometallics* **2003**, *22*, 4759. (h) Fontaine, F.-G.; Nguyen, R.-V.; Zargarian, D. *Can. J. Chem.* **2003**, *81*, 1299. (i) Groux, L. F.; Zargarian, D. *Organometallics* **2003**, *22*, 3124. (j) Groux, L. F.; Zargarian, D.; Simon, L. C.;

Soares, J. B. P. *J. Mol. Catal. A* **2003**, *19*, 51. (k) Rivera, E.; Wang, R.; Zhu, X. X.; Zargarian, D.; Giasson, R. *J. Mol. Catal. A* **2003**, *204-205*, 325. (l) Zargarian, D. *Coord. Chem. Rev.* **2002**, *233-234*, 157. (m) Wang, R.; Groux, L. F.; Zargarian, D. *J. Organomet. Chem.* **2002**, *660*, 98. (n) Fontaine, F.-G.; Zargarian, D. *Organometallics* **2002**, *21*, 401. (o) Dubois, M.-A.; Wang, R.; Zargarian, D.; Tian, J.; Vollmerhaus, R.; Li, Z.; Collins, S. *Organometallics* **2001**, *20*, 663. (p) Groux, L. F.; Zargarian, D. *Organometallics* **2001**, *20*, 3811. (q) Groux, L. F.; Zargarian, D. *Organometallics* **2001**, *20*, 3811. (r) Fontaine, F.-G.; Dubois, M.-A.; Zargarian, D. *Organometallics* **2001**, *20*, 5156. (s) Wang, R.; Bélanger-Gariépy, F.; Zargarian, D. *Organometallics* **1999**, *18*, 5548. (t) Fontaine, F.-G.; Kadkhodazadeh, T.; Zargarian, D. *Chem. Commun.* **1998**, 1253. (u) Vollmerhaus, R.; Bélanger-Gariépy, F.; Zargarian, D. *Organometallics* **1997**, *16*, 4762. (v) Huber, T. A.; Bayrakdarian, M.; Dion, S.; Dubuc, I.; Bélanger-Gariépy, F.; Zargarian, D. *Organometallics* **1997**, *16*, 5811. (w) Bayrakdarian, M.; Davis, M. J.; Reber, C.; Zargarian, D. *Can. J. Chem.* **1996**, *74*, 2194. (x) Huber, T. A.; Bélanger-Gariépy, F.; Zargarian, D. *Organometallics* **1995**, *14*, 4997.

¹⁴ (a) Kennedy, A. R.; Cross, R. J.; Muir, K. W. *Inorg. Chim. Acta* **1995**, *231*, 195. (b) Bachechi, F. *Struct. Chem.* **2003**, *14(3)*, 263. (c) Kozhanov, K. A.; Bupnov, M. P.; Cherkasov, V. K.; Fukin, G. K.; Abakumov, G. A. *Chem. Commun.* **2003**, 2610. (d) Cámpora, J.; Palma, P.; del Río, D.; Canejo, M. M.; Alvarez, E. *Organometallics*, **2004**, *23*, 5653. (e) Cámpora, J.; Palma, P.; del Río, D.; Alvarez, E. *Organometallics*, **2004**, *23*, 1652. (f) Van der Boom, M. E.; Liou, S.-Y.; Shimon, L. J.W.; Ben-David, Y.; Milstein, D. *Inorg. Chim. Acta* **2004**, *357*, 4015.

¹⁵ Groux, L.F.; Bélanger-Garlépy, F.; Zargarian, D. *Can. J. Chem.* **2005**, *83*, 634.

¹⁶ (a) Castonguay, A.; Sui-Seng, C.; Zargarian, D.; Beauchamp, A. L. *Organometallics* **2006**, *25*, 602. (b) Castonguay, A.; Beauchamp, A. L.; Zargarian, D. *Acta Cryst.* **2007**, *E63*, m196. (c) Sui-Seng, C.; Castonguay, A.; Chen, Y.; Gareau, D.; Groux, L. F.; Zargarian, D. *Topics in Catalysis* **2006**, *37*, 81.

¹⁷ Castonguay, A.; Spasyuk, D. M.; Madern, N.; Beauchamp, A.L.; Zargarian, D.; *Organometallics* **2009**, 28, 2134.

¹⁸ (a) Pandarus, V.; Zargarian, D. *Chem. Commun.* **2007**, 978. (b) Pandarus, V.; Zargarian, D. *Organometallics* **2007**, 26, 4321.

¹⁹ Abdel-Magid, A. F.; Carson, K. G.; Harris, B. D.; Maryanoff, C. A.; Shah, R. D. *J. Org. Chem.* **1996**, 61, 3849.

²⁰ Hathaway, B. J. and Holah, D. G. *J. Chem. Soc.* **1964**, 2400.

²¹ (a) Motoyama, Y.; Shimozone, K.; Nishiyama, K. *Inorg. Chim. Acta* **2006**, 359, 1725. (b) Gong, J.-F.; Zhang, Y.-H.; Song, M.-P.; Xu, C. *Organometallics* **2007**, 26, 6487.

²² It should be noted that these redox processes appear to be more complex for **2.5a** and **2.5b**, as judged by the less symmetrical shapes of these waves; changing the cut-off potential or varying the scan rates (100-300 mV/s) did not produce more symmetrical redox couples. Moreover, complexes **2.3** undergo other (irreversible) oxidative processes at higher potentials; comparisons to the CV of the free ligands indicate that these processes are ligand-based. See the supporting information for the full CV plots of **2.3**, the pre-ligand **2.1a**, and ligand **2.2a**.

²³ Grove, D. M.; van Koten, G.; Zoet, R. *J. Am. Chem. Soc.* **1983**, 105, 1379.

²⁴ Kleij, A.W.; Gossage, R.A.; Gebbink, K.; Brinkmann, N.; Reijerse, E.J.; Kragl, U.; Lutz, M. Spek A.L.; van Koten, G. *J. Am. Chem. Soc.* **2000**, 122, 12112

²⁵ (a) Grove, D. M.; van Koten, G.; Mul, P.; Zoet, R.; van der Linden, J. G. M.; Legters, J.; Schmitz, J. E. J.; Murrall, N. W.; Welch, A. J., *Inorg. Chem.* **1988**, 27, 2466-2473. (b) Kozhanov, K. A.; Bubnov, M. P.; Cherkasov, V. K.; Fukin, G. K.; Vavilina, N. N.; Efremova, L. Y.; Abakumov, G. A., *J. Mag. Res.* **2009**, 197, 36-39.

²⁶ Kivelson, D.; Neiman, R., *J. Chem. Phys.* **1961**, 35, 156-161.

²⁷ (a) Maki, A. H.; Davison, A.; Edelstein, N.; Holm, R. H., *J. Amer. Chem. Soc.* **1964**, 86, 4580-4587. (b) Lappin, A. G.; Murray, C. K.; Margerum, D. W., *Inorg. Chem.* **1978**, 17, 1630-1634. (c) Chmielewski, P. J.; Latos-Grazynski, L., *Inorg. Chem.* **1997**, 36, 840-845.

²⁸ For recent reviews on metal-catalyzed Kharasch additions see : Severin, K. *Curr. Org. Chem.* **2006**, *10*, 217-224. (b) Delaude, L.; Demonceau, A.; Noels, A. F. *Top. Organomet. Chem.* **2004**, *11*, 155-171.

²⁹ van de Kuil, L. A.; Grove, D. M.; Gossage, R. A.; Zwikker, J. W.; Jenneskens, L. W.; Drenth, W.; van Koten, G. *Organometallics* **1997**, *16*, 4985.

³⁰ SAINT (**1999**) Release 6.06; Integration Software for Single Crystal Data. Bruker AXS Inc., Madison, Wisconsin, USA.

³¹ Sheldrick, G.M. (**1999**). SADABS, Bruker Area Detector Absorption Corrections. Bruker AXS Inc., Madison, Wisconsin, USA.

³² XPREP (**1997**) Release 5.10; X-ray data Preparation and Reciprocal space Exploration Program. Bruker AXS Inc., Madison, Wisconsin, USA.

³³ SHELXTL (**1997**) Release 5.10; The Complete Software Package for Single Crystal Structure Determination. Bruker AXS Inc., Madison, Wisconsin, USA.

³⁴ (a) Sheldrick, G.M. (**1997**). SHELXS97, Program for the Solution of Crystal Structures. Univ. of Gottingen, Germany. (b) Sheldrick, G.M. (**1997**). SHELXL97, Program for the Refinement of Crystal Structures. University of Gottingen, Germany.

**Chapter 3: Monomeric and Dimeric Nickel
Complexes Derived from a Pincer Ligand
Featuring a Secondary Amine Donor Moiety**

Article 2

Denis M. Spasyuk, Davit Zargarian

† Département de Chimie, Université de Montréal, Montréal, QC, Canada
H3C 3J7

Inorg. Chem., **2010**, *49*, 6203

3.1 Abstract

Reaction of $\text{NiBr}_2(\text{CH}_3\text{CN})_x$ with the unsymmetrical pincer ligand $m\text{-(i-Pr}_2\text{PO)(CH}_2\text{NHBn)C}_6\text{H}_4$ ($\text{Bn} = \text{CH}_2\text{Ph}$) gives the complex $(R,S)\text{-}\kappa^{\text{P}},\kappa^{\text{C}},\kappa^{\text{N}}\text{-}\{2\text{-(i-Pr}_2\text{PO),6-(CH}_2\text{NHBn)-C}_6\text{H}_3\}\text{Ni}^{\text{II}}\text{Br}$, **3.1**, featuring an asymmetric secondary amine donor moiety. Deprotonation of the latter with methyl lithium gave a dark brown compound that could not be characterized directly, but fully characterized derivatives prepared from this compound indicate that it is the LiBr adduct of the 14-electron amido species $[\kappa^{\text{P}},\kappa^{\text{C}},\kappa^{\text{N}}\text{-}\{2\text{-(i-Pr}_2\text{PO),6-(CH}_2\text{NBn)-C}_6\text{H}_3\}\text{Ni}]$, **3.2**. Thus, **3.2·LiBr** reacts with water to regenerate **3.1**, while reaction with excess benzyl or allyl bromide gave the POCN-type pincer complexes **3.3** and **3.4**, respectively, featuring tertiary amine donor moieties. On the other hand, heating **2·LiBr** at 60 °C led to loss of LiBr and dimerization to generate the orange crystalline compound $[\mu^{\text{N}};\kappa^{\text{P}},\kappa^{\text{C}},\kappa^{\text{N}}\text{-}\{2\text{-(i-Pr}_2\text{PO),6-(CH}_2\text{NBn)-C}_6\text{H}_3\}\text{Ni}]_2$, **3.5**. Solid state structural studies show that **3.1**, **3.3**, and **3.4** are monomeric, square planar complexes involving one Ni-N interaction, whereas complex **3.5** is a C_2 -symmetric dimer involving four Ni-N interactions and a Ni_2N_2 core featuring a short Ni-Ni distance (2.51 Å). Preliminary reactivity tests have shown that **3.5** is stable toward weak nucleophiles such as acetonitrile but reacts with strong nucleophiles such as CO or 2,6- $\text{Me}_2(\text{C}_6\text{H}_3)\text{NC}$. Reactions with protic reagents showed that phthalimide appears to break the dimer to generate a monomeric species, whereas alcohols appear to leave the dimer intact, giving rise instead to adducts through $\text{N}\cdots\text{H}\cdots\text{O}$ interactions. These ROH adducts of **3.5** were found to be active precatalysts for the alcoholysis of acrylonitrile with up to 2000 catalytic turnover numbers.

3.2 Introduction

The chemistry of pincer complexes has experienced much progress over the past three decades as it has been shown that various metal-pincer ligand combinations can generate compounds that act as versatile catalysts, molecular sensors and switches, and diverse functional materials.¹ Pincer ligands can impart enhanced reactivity or thermal stability to the metals they bind, thus facilitating difficult reactions or allowing the isolation of rare reaction intermediates featuring unusual oxidation states or bonding patterns;² this capacity to modulate reactivities of metals is helping advance our fundamental understanding of organometallic chemistry. During the early years following their introduction,³ the most commonly studied pincer ligands were LXL-type ligands (monoanionic, terdentate) featuring tertiary phosphine or amine donor moieties linked to each other through an aliphatic or aromatic skeleton encompassing a carbon- or nitrogen-bound anionic anchor,⁴ but a variety of ligand types has been introduced recently (L= carbenes, alkenes, RSR, κ^O -R₃P=O, RSeR, etc.; X= alkyl, aryl, SiR₃, BR₂, etc.).⁵

Our group has investigated the chemistry of nickel complexes based on symmetrical and unsymmetrical pincer ligands featuring tertiary phosphine, phosphinite, and amine donor moieties (Figure 3.1.) and reported on their reactivities in catalytic transformations such as Kumada-Corriu coupling, hydroamination of acrylonitrile derivatives, Kharasch additions to olefins, as well as oligomerization of PhSiH₃ and its addition to styrene.⁶ As an extension of these studies, we set out to prepare POCN-type complexes of nickel featuring secondary amine donor moieties that might offer two attractive advantages over their tertiary amine homologues.¹⁵ⁱ First, alkylation of the N-H moiety in these complexes should, in principle, provide an alternative pathway for the preparation of difficult-to-access tertiary amine derivatives, including species featuring tetradentate ligands encapsulating the Ni center (Scheme 3.1).⁷ Second, dehydrohalogenation of (POCN)NiX complexes featuring a secondary amine donor moiety (X= halide) might generate 14-electron Ni-amido species that would

be expected to display unique reactivities. The latter possibility was particularly intriguing since, to the best of our knowledge, all previously reported pincer-type compounds of Ni have more than 14 valence electrons (15,⁸ 16,⁹ or 17¹⁰).

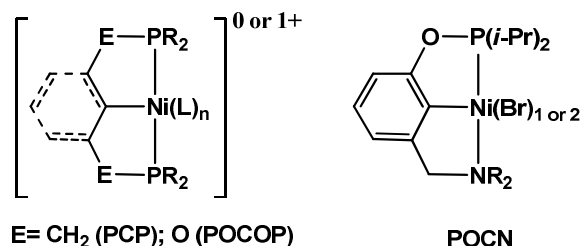
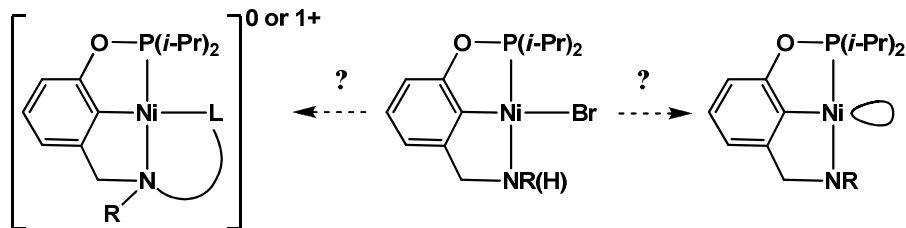


Figure 3.1. Examples of POCOP and POCN pincer systems.



Scheme 3.1. Possible transformation pathways of (POCNHR)Ni complexes.

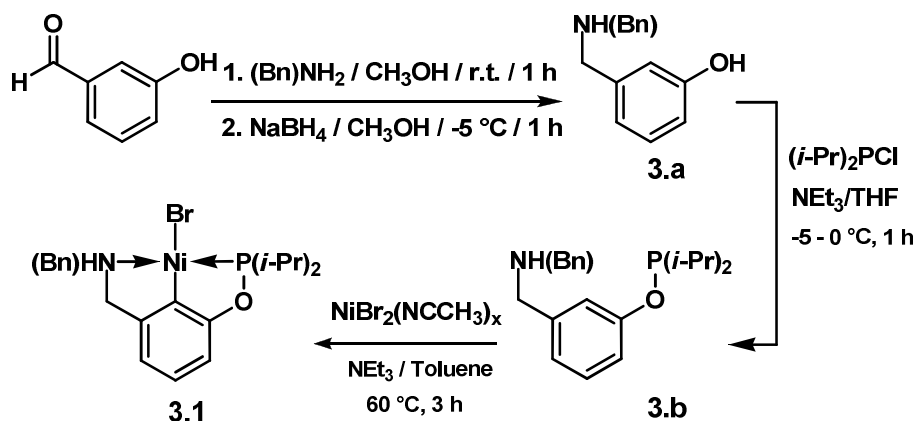
Whereas 14-electron species are expected to be highly reactive due to the presence of two empty valence orbitals on the metal,¹¹ many of these compounds are only nominally unsaturated, because their operational unsaturation is usually “quenched” by extraneous interactions that can be either intermolecular (e.g., solvent/anion association or dimerization) or intramolecular (e.g., π -donation or agostic interactions).^{11a} We were, therefore, mindful of the possibility that our plan to generate a highly reactive 14-electron species (Scheme 1) might be thwarted by the propensity of the amido ligand to form a dimer. Initial tests showed that dimerization does indeed take place, but the resulting dimer is fairly reactive nonetheless. The present contribution describes the synthesis and

reactivities of the dimeric species $[\mu^N; \kappa^P, \kappa^C, \kappa^N\text{-}\{2\text{-}(i\text{-Pr}_2\text{PO}), 6\text{-}(\text{CH}_2\text{NBn})\text{-C}_6\text{H}_3\}\text{Ni}]_2$, **3.5**, which was obtained from deprotonation of the monomeric (R,S)- $\kappa^P, \kappa^C, \kappa^N\text{-}\{2\text{-}(i\text{-Pr}_2\text{PO}), 6\text{-}(\text{CH}_2\text{NHBn})\text{-C}_6\text{H}_3\}\text{Ni}^{\text{II}}\text{Br}$, **3.1**; also reported are the synthesis and characterization of complexes **3.3** and **3.4**, the N-allyl and N-benzyl derivatives of **3.1**, respectively.

3.3 Results and Discussion

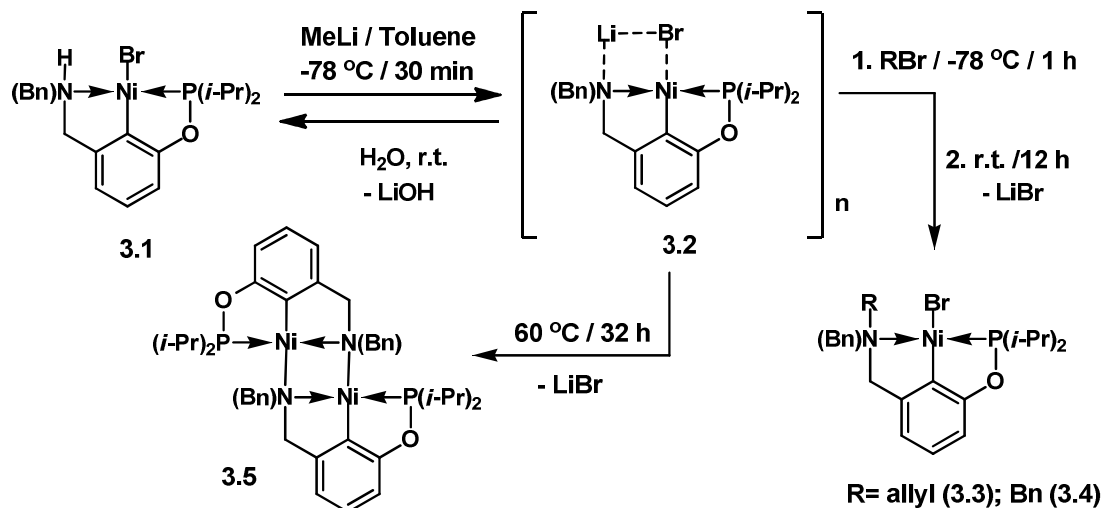
3.3.1 Syntheses

The POCN-type ligand **3.b** was prepared following a procedure used for the preparation of analogous ligands featuring 3° amines¹⁵ⁱ. Thus, reaction of 3-hydroxybenzaldehyde with benzyl amine followed by reduction of the in situ formed Schiff base with NaBH₄ in methanol gave 3-((N-Benzylamino)methyl)phenol, **3.a** (Scheme 3.2). Reaction of the latter with *i*-Pr₂PCL in the presence of NEt₃ led to exclusive phosphination at the O-H (vs. N-H) moiety, thus facilitating isolation of the new pincer-type ligand **3.b** as an analytically pure colorless oil in 96% yield. It is worth noting that the phosphinite moiety in **3.b** is quite sensitive to hydrolysis but relatively stable toward oxidation. Finally, heating a toluene suspension of **3.b** and NiBr₂(CH₃CN)_x at 60 °C in the presence of NEt₃ led to cyclometallation of **3.b** and formation of the new pincer complex **3.1**. The presence of an added base in such metallation reactions maximizes the yields of the target pincer complexes by suppressing the formation of side-products arising from protonation of the ligand by the in situ generated HBr¹⁵ⁱ.



Scheme 3.2. Synthesis of ligands and complexes

Reaction of **3.1** with MeLi in toluene at -78°C gave an air-sensitive, oily material which could not be characterized directly, but its conversion to unambiguously characterized derivatives **3.3** and **3.4** has allowed us to identify this substance as the LiBr adduct of the 14-electron species generated from deprotonation of the NH moiety in **3.1** (Scheme 3.3).¹² For instance, the in situ generated **3.2** reacted readily with water or benzyl bromide to give analytically pure samples of the starting material **3.1** or its Bn_2N analogue **3.4**, respectively. The reaction of **3.2** with allyl bromide was more sluggish and produced significant amounts of intractable materials in addition to the anticipated N-allylated derivative **3.3** (Scheme 3.3); the latter was purified by chromatography on silica gel and isolated in about 60% yield. That **3.2** can be hydrolyzed to regenerate **3.1** and allylated or alkylated to give **3.3** and **3.4** lends strong support for the proposed identity of **3.2**; the formation of **3.3** and **3.4** also indicates that this procedure is a viable synthetic route for modifying a metal-bound pincer ligand.



Scheme 3.3. Reactivities of complex **3.1**.

Solutions of **3.2** lose LiBr slowly (over a week at r.t. or 32 h at 60 °C) to give the dimeric species **3.5** (Scheme 3.3). Attempts to trap the postulated 14 electron intermediate, **3.2**, as isolable monomeric adducts by doing the deprotonation reaction in the presence of N- or P-based ligands led to intractable mixtures of products, whereas running the deprotonation in coordinating solvents (THF, MeCN) gave **3.5**.

3.3.2 Characterization

The identities of the pre-ligand **3.a**, the ligand **3.b**, and the complexes **3.1** and **3.3-3.5** were discerned from NMR and elemental analyses, and corroborated by single crystal structure determination in the case of the complexes. As will be discussed below, the complex spectral features of the new pincer complexes were interpreted on the basis of data from $^1\text{H-COSY}$, $^1\text{H-NOESY}$, and HETCOR experiments as well as by comparisons to the characteristic NMR resonances of the ligand (vide infra).

The $^{31}\text{P}\{^1\text{H}\}$ NMR spectra were straightforward, displaying a single resonance for the ligand **3.b** (147 ppm) and the complexes **3.1** (202 ppm), **3.3** and

3.4 (201 ppm), and **3.5** (192 ppm). Analysis of the ^1H and ^1H -COSY NMR spectra confirmed the presence of an NH proton in **3.1**, indicating that complexation to the Ni center left the NH moiety of **3.b** intact. It is worth noting that complexation /cyclometalation of the POCN ligand **3.b** also leads to asymmetrization of the nitrogen center in **3.1**, which renders the NCH_2 protons diastereotopic and gives rise to complex spin coupling patterns. This is evident when the signal for the NCH_2 protons in the ligand (a singlet resonance at ca. 3.3 ppm) is compared to the multiplets displayed in the spectrum of **3.1** (Figure 3.2). Thus, the signals for NH and the non-equivalent protons 7A and 7B¹³ form an ABX pattern of which the AB portion is centered at ca. 3.4 ppm and displays coupling constants of 16 ($J_{\text{H7A-H7B}}$), 6 ($J_{\text{H7A-NH}}$), and 4 Hz ($J_{\text{H7B-NH}}$), whereas the corresponding signals for the benzylic protons 30A and 30B resonate at significantly different chemical shifts ($\Delta\delta \sim 1$ ppm) but with a similar coupling constant ($J_{\text{H30A-H30B}} = 14$ Hz); interestingly, H30A couples fairly strongly with the NH proton ($J_{\text{H30A-NH}} = 10$ Hz) while H30B does not.

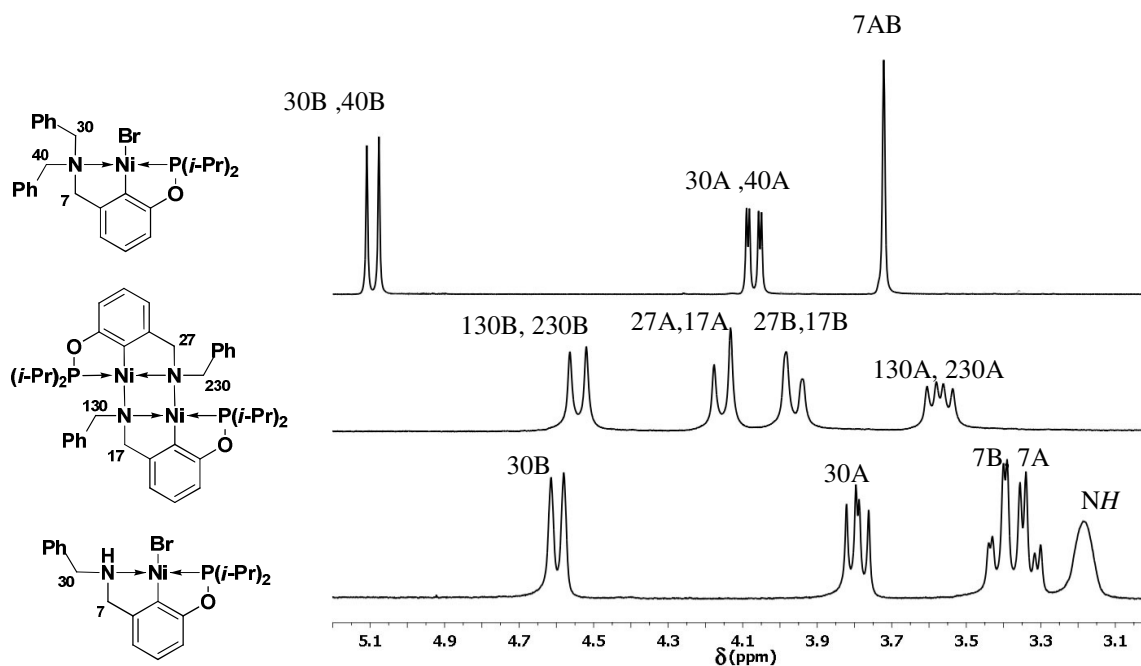


Figure 3.2. The methylene region in the ^1H -NMR spectra (C_6D_6) of complexes **3.1** (bottom), **3.5** (middle), and **3.4** (top).

The ^1H and ^{13}C NMR spectra of complex **3.4** are simpler than those of **3.1**, because the Bn_2N moiety gives rise to a plane of symmetry in **3.4** and renders the symmetry-related nuclei above and below the plane of symmetry equivalent. Hence, we observe one signal for the symmetry-related methylene carbons and protons, two signals for the four methyl groups, one signal for the two benzylic protons labeled 7 (Figure 3.1), and one signal for the benzylic carbons (C30 and C40). Equivalence of the benzylic carbons coupled with the observation of two different signals for their protons (Figure 3.1) implies that the latter are pairwise equivalent (30A/40A, 30B/40B) and should appear as a pair of AB doublets, which is the case (ca. 4.1 and 5.1 ppm; $J \sim 13$ Hz). Interestingly, the more upfield signal is further split into a doublet due to a through-space coupling with the P nucleus ($J_{\text{H-P}} = 3$ Hz). The ^1H NMR spectrum of complex **3.3** is similar to that of complex **3.1** since both of these complexes contain a chiral N center, but there are important differences: absence of NH in **3.3** eliminates a potential source of coupling such that ArCH_2N protons appear as two characteristic AB doublets, whereas coupling due to the P nucleus leads to different multiplicities for the methylene protons of the allyl moiety (ddd, $J_{\text{P-H}} = 4$ Hz) and the benzyl moiety (dd, $J_{\text{P-H}} = 2$ Hz). Finally, the ^1H and ^{13}C NMR spectra of complex **3.5** show the equivalence of all symmetry-related protons and carbon nuclei, indicating that the two halves of this dimer are related by a mirror plane and/or a C_2 axis of rotation. As above, the coupling patterns of the methylene protons indicate the pairwise equivalence of the chemically inequivalent protons (Figure 3.1: 130A/230A vs. 130B/230B; 17A/27A vs. 17B/27B); one of the benzylic protons is also coupled to the P nucleus with a rather large coupling constant ($J_{\text{P-H}} = 10$ Hz).

Single crystals for complex **3.1**, **3.3**, **3.4**, and **3.5** were obtained and subjected to crystallography in order to determine solid state structural parameters. Crystal and data collection details for all complexes are presented in

Table 3.1 and Table 3.2, selected structural parameters are listed in Table 3.3 (**3.1**, **3.3**, and **3.4**) and Table 3.4 (**3.5**), and ORTEP diagrams are shown in Figures 3.2 (**3.3** and **3.4**) and 3 (**3.5**). Complexes **3.1** and **3.3** crystallize in the non-chiral space groups $Pna2_1$ and $P\bar{1}$, respectively. It is noteworthy that complex **3.3** crystallizes with one molecule per asymmetric unit so that the nitrogen atom adopts either S or R configuration to generate a racemic mixture, whereas **3.1** crystallizes with two molecules per asymmetric unit and both molecules adopt the same configuration (S,S or R,R) at the nitrogen atom. Ironically, the achiral complex **3.4** crystallizes in the chiral space group $P2_1$ due to crystal packing. The NH in complex **3.1** was located in the difference Fourier map, whereas all other hydrogen atoms were placed in calculated positions and refined by using a riding model. Although the amino moiety in complex **3.3** was disordered over two positions, the structure refined quite well ($R1= 2.6\%$).

Table 3.1 Crystal Data Collection and Refinement Parameters for Complexes **3.1**, **3.3**.

	3.1	3.3
chemical formula	C ₂₀ H ₂₇ NOPNiBr	C ₂₃ H ₃₁ NNiOPBr
<i>F</i> _w	467.01	507.08
<i>T</i> (K)	150	150
wavelength (Å)	1.54178	0.71073
space group	Pna2 ₁	P-1
<i>a</i> (Å)	10.7398(2)	8.606(1)
<i>b</i> (Å)	10.8633(2)	11.146(1)
<i>c</i> (Å)	34.2587(5)	13.340(2)
α (deg)	90	79.686(2)
β (deg)	90	73.752(2)
γ (deg)	90	71.897(2)
<i>Z</i>	8 (<i>Z'</i> =2)	2
<i>V</i> (Å ³)	3997.0(1)	1161.6(3)
ρ _{calcd} (g·cm ⁻³)	1.552	1.450
μ (cm ⁻¹)	41.32	26.37
θ range (deg)	2.58–68.16	2.38–27.45
R1 ^a [<i>I</i> > 2σ(<i>I</i>)]	0.0330	0.0259
wR2 ^b [<i>I</i> > 2σ(<i>I</i>)]	0.0875	0.0674
R1 [all data]	0.0337	0.0333
wR2 [all data]	0.0879	0.0694
GOF	1.157	1.037

^a $R_1 = \frac{\sum(|F_o| - |F_c|)}{\sum|F_o|}$

^b $wR_2 = \left\{ \frac{\sum[w(F_o^2 - F_c^2)^2]}{\sum[w(F_o^2)^2]} \right\}^{1/2}$

Table 3.2. Crystal Data Collection and Refinement Parameters for Complexes 3.4, 3.5.

	3.4	3.5
chemical formula	C ₂₇ H ₃₃ NNiOPBr	C ₄₀ H ₅₂ N ₂ Ni ₂ O ₂ P ₂
<i>F</i> _w	557.13	772.20
<i>T</i> (K)	150	150
wavelength (Å)	1.54178	1.54178
space group	P2 ₁	P2 ₁ /n
<i>a</i> (Å)	7.3167(2)	13.0358(2)
<i>b</i> (Å)	11.0759(2)	21.2671(4)
<i>c</i> (Å)	16.2119(3)	13.9931(2)
α (deg)	90	90
β (deg)	101.144(1)	100.920(1)
γ (deg)	90	90
<i>Z</i>	2	4
<i>V</i> (Å ³)	1289.02(5)	3809.1(1)
ρ _{calcd} (g·cm ⁻³)	1.435	1.347
μ (cm ⁻¹)	36.25	22.96
θ range (deg)	2.78–58.00	3.83–67.81
R1 ^a [I > 2σ(I)]	0.0202	0.0344
wR2 ^b [I > 2σ(I)]	0.0520	0.0969
R1 [all data]	0.0204	0.0444
wR2 [all data]	0.0521	0.1017
GOF	1.028	1.028

^a $R_1 = \frac{\sum(|F_o| - |F_c|)}{\sum|F_o|}$

^b $wR_2 = \left\{ \frac{\sum[w(F_o^2 - F_c^2)^2]}{\sum[w(F_o^2)^2]} \right\}^{1/2}$

Table 3.3. Selected Bond Distances (Å) and Angles (deg) for Complexes **3.1**, **3.3**, and **3.4**.

	3.1	3.3	3.4
Ni(1)-C(1)	1.854(5)	1.849(2)	1.856(1)
Ni(1)-P(1)	2.105(1)	2.110(1)	2.100(1)
Ni(1)-N(1)	1.983(4)	2.033(2)	2.043(2)
Ni(1)-Br(1)	2.344(1)	2.344(1)	2.359(1)
C(1)-Ni(1)-Br(1)	171.9(1)	173.53(6)	175.41(8)
P(1)-Ni(1)-N(1)	166.2(2)	166.25(5)	163.86(5)
P(1)-Ni(1)-Br(1)	96.00(4)	95.00(2)	93.95(2)
N(1)-Ni(1)-Br(1)	97.56(2)	98.03(4)	99.51(5)
P(1)-Ni(1)-C(1)	82.1(1)	82.12(6)	82.27(7)
N(1)-Ni(1)-C(1)	84.1(2)	84.5(7)	83.83(9)

Table 3.4. Selected Bond Distances (Å) and Angles (deg) for Complex **3.5**.

	3.5
Ni(1)-C(11)	1.864(2)
Ni(1)-N(1)	1.997(2)
Ni(1)-N(2)	1.970(1)
Ni(1)-Ni(2)	2.512(1)
Ni(1)-P(1)	2.122(1)
C(11)-Ni(1)-N(2)	168.96(8)
C(11)-Ni(1)-P(1)	81.34(7)
C(11)-Ni(1)-N(1)	85.09(8)
N(1)-Ni(1)-N(2)	85.81(6)
N(1)-Ni(2)-N(2)	86.06(6)
N(2)- Ni(1)-P(1)	107.72(5)
N(1)-Ni(1)- P(1)	166.43(5)

Figure 3.3. ORTEP diagrams for complex **3.1** (a), **3.3** (b), and **3.4** (c). Thermal ellipsoids are set at the 50% probability level. Calculated hydrogen atoms are omitted for clarity.

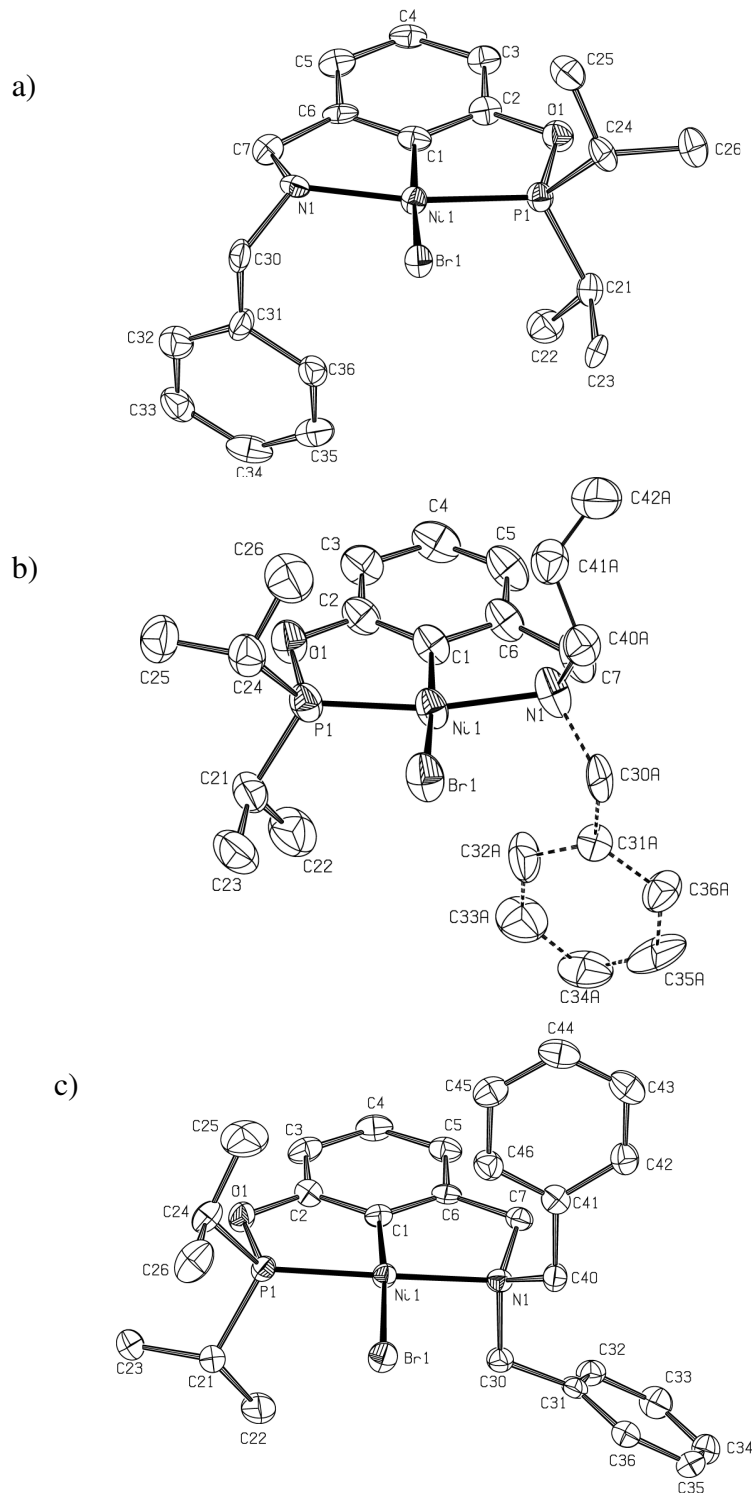
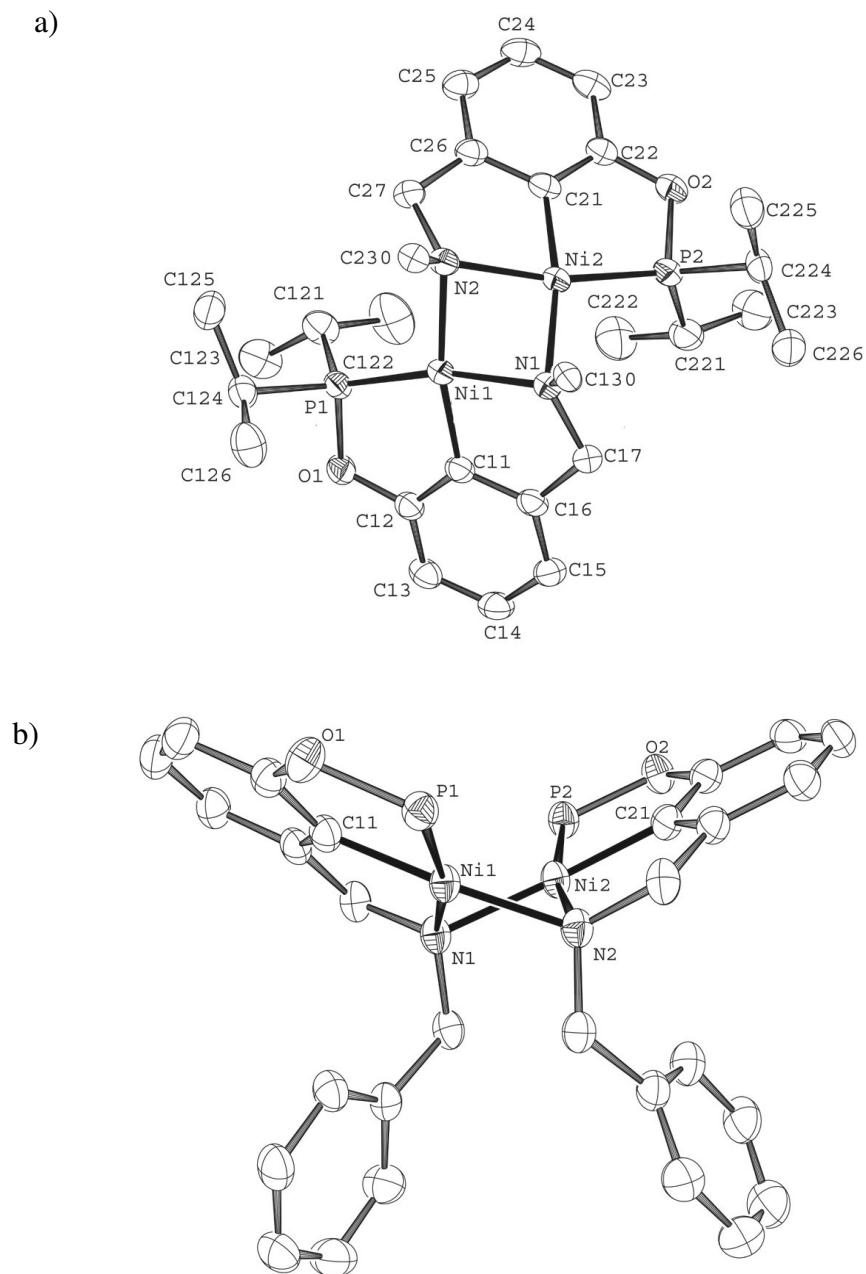


Figure 3.4. ORTEP diagram for complex **3.5** (view a, b). Thermal ellipsoids are set at the 50% probability level. Hydrogen atoms (phenyl groups view a), isopropyl groups view b) are omitted for clarity.



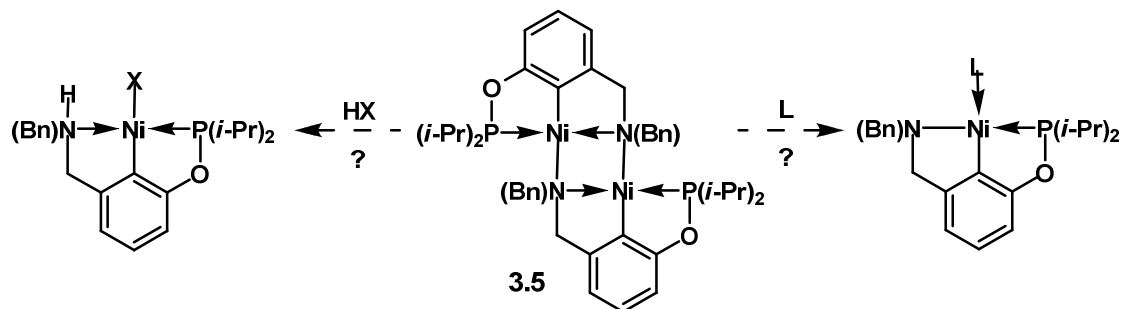
The main structural parameters of the three monomeric complexes **3.1**, **3.3**, and **3.4** are quite comparable and similar to those of previously reported POCN-type complexes of nickel featuring tertiary amines.¹⁵ⁱ Thus, these complexes adopt moderately distorted square planar geometries wherein the nitrogen atom is slightly displaced from the coordination plane (Figure 3.2); similar observations have been reported for other nitrogen-containing pincer complexes.^{4c,d,14} The Ni-C distances in these complexes fall within a narrow range and are very similar to the Ni-C distances in the previously reported analogues (1.849-1.856 Å vs. 1.853-1.859 Å). Similar trends are observed for the Ni-Br (2.343-2.359 vs 2.332-2.362 Å) and Ni-P distances (2.106-2.110 vs 2.109-2.112 Å), but the Ni-N bond is somewhat shorter (by about 10 e.s.d. values) in **3.1** (1.983(4) and 2.016(4) Å) as compared to **3.4** (2.043(2) Å), **3.3** (2.033(2) Å), and the previously reported analogous complexes featuring tertiary amines (2.021-2.043 Å).¹⁵ⁱ Not unexpectedly, the olefinic moiety tethered to the new pincer ligand in **3.3** does not interact with the nickel center.

Single crystal structure analysis of **3.5** revealed a dimeric species that adopts an overall butterfly-like shape (ORTEP diagram in Figure 3.3, views a and b). The structure consists of two T-shaped halves (as defined by the coordination planes involving the Ni, C, P, and N atoms) that are rotated with respect to each other by ca. 70° and connected to each other by two additional Ni-N linkages. The latter create a central Ni₂N₂ core that adopts a cyclobutane-like conformation featuring a Ni-Ni distance of ca. 2.51 Å, which is within one e.s.d. of the sum of the two Ni^{II} covalent radii (1.24(4) Å),¹⁵ four acute angles (Ni-N-Ni~ 79°; N-Ni-N~ 86°), and two Ni/N/Ni planes puckered at the Ni-Ni axis by ca. 124°; the puckering places the two N-benzyl groups syn to each other. In comparison to the monomeric species **3.3** and **3.4**, each half of complex **3.5** displays slightly longer Ni-C (ca. 1.864 vs. 1.856 and 1.849 Å) and Ni-P bonds (ca. 2.122 vs. 2.100 and 2.110 Å), but a shorter Ni-N bond (ca. 1.997 vs. 2.043 and 2.033 Å). Interestingly, the shorter Ni-N distance in the Ni₂N₂ core (Ni-N~ 1.970 Å) involves the Ni and N atoms belonging to different halves of the complex (Δ Ni-N~ 16 e.s.d.).

It is instructive to compare the main structural features of complex **3.5** to those of $[\mu^N, \kappa^P, \kappa^N, \kappa^P\text{-}(\text{PNP})\text{Ni}^I]_2$ ($\text{PNP}^- = \text{N}[2\text{-P}(i\text{-Pr})_2\text{-4-methylphenyl}]_2$),^{8b} to our knowledge the only other structurally characterized pincer-nickel dimer.¹⁶ The two phosphine moieties of each $\mu\text{-PNP}$ ligand in this dimer extend across the Ni^I centers to allow each phosphine to coordinate to a different Ni atom. The Ni_2N_2 core generated in this structure has a planar, diamond-like configuration containing two Ni-N-Ni angles $<70^\circ$ and two N-Ni-N angles of $\sim 111^\circ$, in contrast to complex **3.5** that possesses a cyclobutane-like, puckered Ni_2N_2 core defined by four acute angles. Curiously, the two 17-electron Ni^I centers in $[\mu\text{-PNP}\text{Ni}]_2$ interact only weakly in spite of the rather short intermetallic distance of ca. 2.33 Å; as a result, there is no $\text{Ni}^I\text{-Ni}^I$ bond and the dimer appears to be a diradical in the solid state. On the other hand, a number of observations seem to indicate that a dimer-monomer equilibrium might be operative in solutions of this complex, whereas **3.5** appears to retain its dimeric structure even in solution.

3.3.3 Reactivity survey for **3.5**

A series of NMR test reactions were undertaken in order to assess the reactivities of the dimeric complex **3.5**. Of primary interest is the reactivity with Lewis bases and reagents featuring X-H bonds of varying degrees of acidity, the main question being whether or not the dimer is prone to breaking up into monomeric species (Scheme 3.4).



Scheme 3.4. Reactivity survey for complex **3.5**.

Monitoring ^1H NMR spectra of a 1:1 mixture of **3.5** and m-Cresol at room temperature showed that the OH signal shifted downfield from 3.9 ppm to 4.1 ppm, broadening and partially obscuring one of the doublets due to the methylene protons 130/230 (Figure 3.5 in SI). Other spectral changes were also observed after the mixture was allowed to equilibrate at 50 °C for about 10 min: the cresol methyl group moved from 2.13 ppm to 2.34 ppm and a greater number of multiplets appeared in the methylene region, indicating a loss of symmetry (Figure 3.5 in SI). The $^{31}\text{P}\{^1\text{H}\}$ NMR spectrum of the mixture showed the disappearance of the signal due to **3.5** (191.61 ppm) and emergence of two new peaks at 190.23 ppm and 191.23 ppm.

Adding 7 equivalents of m-cresol to the above sample and allowing ca. 10 min for the mixture to equilibrate at 50 °C led to further spectral changes: the pattern for the methylene signals became simpler and more similar to the original signals for **3.5**, except for protons 130/230 that appeared as two overlapping doublets of doublets (Figure 3.7 in SI); the $^{31}\text{P}\{^1\text{H}\}$ NMR spectrum showed only one signal very close to the original chemical shift for **3.5** (191.43 vs. 191.61 ppm). Similar observations were noted in the reactions of **3.5** with 2,2,2-trifluoroethanol (TFE) or N-hydroxyphthalimide (NHP). For example, the $^{31}\text{P}\{^1\text{H}\}$ NMR spectra of the sample containing 8 equivalents of these reagents showed that the original signal of **3.5** shifted slightly (from 191.61 to 192.46 ppm for TFE and 191.50 for NHP), while the $^{19}\text{F}\{^1\text{H}\}$ NMR spectrum of the mixture containing TFE showed two triplets, one at 78.24 ppm (free TFE) and the other at 77.69 ppm (TFE associated with **3.5**). To sum up, presence of excess m-cresol, TFE, and NHP appears to bring about observable but very subtle changes to the NMR spectra of **3.5**, implying that the original structure of **3.5** is mostly maintained in the presence of alcohols (dimer not broken up). We propose that reacting **3.5** with alcohols gives rise to $\text{N}\cdots\text{H}\cdots\text{O}$ type interactions that only minimally perturb the solution structure of the dimer, while serving to enhance the nucleophilicities of ROH (vide infra).

In contrast to the reactions of ROH described above, distinct color changes were observed when **3.5** was reacted with 5 equivalents of phthalimide (orange→

pale yellow) or phenylacetylene (orange→ dark brown) and new $^{31}\text{P}\{^1\text{H}\}$ signals emerged in a chemical shift region associated with monomeric species (198.4 and 202.9 ppm, respectively). Moreover, GC/MS analysis of the reaction mixture containing phenylacetylene showed the formation of cyclic trimers, 1,3,5- and 1,3,4-triphenylbenzene. Visible color changes were also noted during the reactions with excess phenylsilane (dark-brown) and m-toluidine (deep red). GC/MS analysis of the phenylsilane mixture showed the formation of diphenylsilane, but no new $^{31}\text{P}\{^1\text{H}\}$ signal was observed for this reaction, whereas the reaction with m-toluidine or aniline gave rise to new $^{31}\text{P}\{^1\text{H}\}$ signals at 188.8 or 190.5 ppm, respectively. Finally, reactions with CO or 2,6-dimethyl(phenyl)isonitrile did not cause any color change, but produced two new $^{31}\text{P}\{^1\text{H}\}$ signals at: 186.0 and 179.3 ppm for the reaction with CO, and at 181.0 and 178.2 ppm for the reaction with 2,6-dimethyl(phenyl)isonitrile. ^1H NMR spectra of the latter reaction mixtures indicate two non equivalent pincer moieties that are fairly similar to the spectral pattern of complex **5**. These observations are consistent with the coordination of CO or 2,6-dimethyl(phenyl)isonitrile with only one of the Ni atoms in **3.5** to give inequivalent phosphinite moieties.

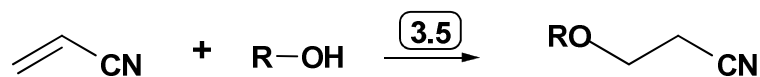
3.3.4 Catalytic hydroalkoxylation of acrylonitrile

Catalytic hydroalkoxylation of olefins or allenes represents an atom-efficient transformation that generates products with multiple commercial uses.¹⁷ Interestingly, hydroalkoxylation of some olefins can be promoted by different acids¹⁸ or bases,¹⁹ and even nucleophilic phosphines,²⁰ but a great variety of hydroalkoxylations are also catalyzed by salts of Al²¹ and complexes of Cu,²² Ag,²³ Au,^{22a,24} Ru,²⁵ Rh,²⁶ Pd,²⁷ and Pt.²⁸ Metal-catalyzed hydroalkoxylation reactions involving activated olefins (Michael receptors) have been investigated more frequently, owing to the possibility of outer-sphere attack by nucleophiles on metal-bound olefins.

In this context, Yi et al. have shown that a Ru(II)-acetamido complex²⁵ promotes hydroalkoxylation of cyanoolefins via a novel bifunctional mechanism

that involves i) the heterolytic activation of the alcohol O-H bond by the acetamido moiety (Lewis basicity) to generate an alkoxide ion, and ii) addition of this in situ generated alkoxide to the C=C moiety of the cyanoolefin that has become activated as a result of κ^N -nitrile binding to an empty coordination site of Ru(II) (Lewis acidity). The observation, in our studies, that alcohol O-H bonds can be activated through O \cdots H \cdots N interactions with the Ni centers in **3.5** raised the possibility that the latter might serve as a pre-catalyst for hydroalkoxylation of activated olefins according to the above-noted bifunctional mechanism. This possibility was borne out by a few initial tests: alcoholysis of acrylonitrile proceeded in the presence of catalytic amounts of **3.5** to give the anti-Markovnikov product (linear ether, Scheme 3.5). Optimization experiments have shown that catalytic efficiency requires an excess of alcohol and elevated temperatures, as described below.

^1H NMR and GC/MS analyses of a 1:1 mixture of acrylonitrile (ACN) and *m*-cresol in benzene (ca. 1.4 M with respect to ACN) that had been stirring in the presence of 0.5% of **3.5** at room temperature indicated little conversion after 5.5 h (ca. 11%), but repeating the reaction at 50 °C for 1 h led to 44% yield of the anti-Markovnikov addition product ArOCH₂CH₂CN (Ar= 3-Me-Ph; Run 1, Table 3.5). Doubling the ACN: *m*-cresol ratio provided a 92% yield in 0.5 h (Run 2), while increasing the reaction time did not appear to have a significant beneficial effect on the yield (Run 3). It is worth noting that good yields can be obtained at ambient temperature if an excess of alcohol and longer reaction times are employed (Run 4), and significantly larger catalytic turnovers can be obtained with smaller catalyst loadings (Runs 5 and 6).



Scheme 3.5. Hydroalkoxylation reaction

Table 3.5. Alcoholysis of Acrylonitrile Catalyzed by Complex **3.5**^a.

Run	ROH	3.5 :ACN:ROH	Time (h)	Yield (%)	TON
1	<i>m</i> -cresol	1 : 200 : 200	1	44	88
2		1 : 200 : 400	0.5	92	184
3			1.0	93	186
4			9.0 ^b	71	142
5		1 : 2000 : 4000	6.0	59	1180
6			36	99	~2000
7	MeOH	1 : 200 : 200	1.0	8	16
8		1 : 200 : 400	1.0	16	32
9		1 : 200 : 2000	0.5	74	148
10			1.0	100	200
11	EtOH	1 : 200 : 200	20	11	22
12		1 : 200 : 2000	0.5	49	98
13			1.0	87	174
14	CF ₃ CH ₂ OH	1 : 200 : 2000	0.5	90	180
15			5.5 ^b	100	200
16	<i>n</i> -PrOH	1 : 200 : 2000	0.5	23	46
17			1.0	43	86
18			8	64	128
19	<i>i</i> -PrOH	1 : 200 : 2000	0.5	Trace	
20		1 : 200 : 2000	24	23	46
21	BnOH	1 : 200 : 2000	0.5	61	122
22		1 : 200 : 2000	1.0	100	200
23	H ₂ O	1 : 200 : 2000	24	Trace ^c	

^a The catalytic reactions were monitored by ¹H-NMR and the final mixtures analyzed by GC/MS; reaction yields were determined on the basis of calibration curves prepared using authentic samples of the anticipated products, as well as by ¹H NMR spectroscopy. ^bCatalysis conducted at ambient temperature. ^c The hydrolysis reaction was conducted in THF or acetone/benzene; product found is: O(CH₂CH₂CN)₂.

When one equivalent of MeOH was used instead of *m*-cresol, the catalysis proceeded to ca. 8% yield over 1 h (Run 7), but much higher yields were obtained with higher MeOH:ACN ratios, up to quantitative yields over 1 h with a 10-fold excess of MeOH (Runs 8-10). Similar results were also obtained for the catalysis with EtOH (Runs 11-13), whereas 1,1,1-trifluoroethanol proved to be more reactive, giving 90% yield over 30 min at 50 °C (Run 14) and a quantitative yield over 5.5 h at ambient temperature (Run 15). These observations indicate that alcohol acidity has a favorable influence for the hydroalkoxylation reaction,²⁹ whereas comparing the catalytic results with MeOH, EtOH, *n*-PrOH, and *i*-PrOH (Runs 10, 13, 17, and 20) implies that the steric bulk of the alcohol is detrimental to its reactivity. Finally, BnOH proved very active (Runs 21 and 22), whereas water proved nearly unreactive, giving traces only of the ether arising from a double addition, O(CH₂CH₂CN)₂.

To our dismay, crotonitrile and methacrylonitrile reacted only very sluggishly (ca. 5%), whereas activated olefins bearing substituents other than nitrile were completely inert for the hydroalkoxylation reaction catalyzed by **3.5**. Benzene and toluene proved to be the most suitable solvents for the alcoholysis reaction, since the catalyst precursor is freely soluble and stable in these solvents. In contrast, little or no conversion was noted for the addition of *m*-cresol to acrylonitrile conducted in chlorinated solvents such as CH₂Cl₂ and CHCl₃; solutions of **3.5** in these solvents undergo a color change from orange to green over minutes, signaling a decomposition. With acetonitrile as co-solvent with benzene,³⁰ the *m*-cresol reaction was found to be much less efficient, giving 23% yield after 1 hour and ca. 60% over 24 h; in contrast, the catalysis proceeded unhindered in ethyl acetate. The observation of inhibition in acetonitrile but not in ethyl acetate, combined with the lack of reactivity observed for activated olefins bearing functionalities other than nitrile, implies that κ^{N} -nitrile binding of acrylonitrile might play an important role in the alcoholysis reaction, as stipulated by Yi.²⁵

3.4 Conclusion

This work has presented a convenient protocol for synthesis of a POCN-type pincer complex of nickel bearing a secondary amine moiety, and shown that the N-H moiety in this complex opens new paths for modification of the pincer ligand via N-alkylation and for synthesis of a dimeric pincer species such as complex **3.5**. N-Ni interactions in **3.5** stabilize the Ni centers sufficiently to allow isolation, but the dimeric species is reactive enough to activate alcohols for the hydroalkoxylation of acrylonitrile with up to 2000 catalytic turnovers. It should be noted that **3.5** is, to our knowledge, the first Ni complex to promote hydroalkoxylation of acrylonitrile. Interestingly, although **3.5** also reacts with aniline and p-toluidine, it appears to be ineffective in promoting hydroamination of acrylonitrile with these amines, which suggests that reaction of amino alcohols with acrylonitrile might proceed selectively with the addition of the O-H bond; this possibility will be probed in future studies. We will also investigate the feasibility of isolating monomeric 14-electron Ni-amido species from POCN-type complexes analogous to **3.1** bearing a sterically bulky N-substituent.

3.5 Experimental Section

3.5.1 General

All manipulations were carried out using standard Schlenk and glove box techniques under nitrogen atmosphere. All solvents used for experiments were dried to water contents of less than 10 ppm (determined using a Mettler Toledo C20 coulometric Karl Fischer titrator) by passage through activated aluminum oxide columns (MBraun SPS) and freeze-thaw degassed. C₆D₆ was dried over 4 Å molecular sieves and then freeze-thaw degassed. The following were purchased from Aldrich and, unless otherwise noted, used without further purification: Ni (metal), chlorodiisopropylphosphine, 3-hydroxybenzaldehyde, triethylamine, and all the alcohols and olefins used in the catalytic studies. A Bruker AV 400 spectrometer was used for recording ¹H, ¹³C{¹H} (101 MHz), and ³¹P{¹H} (162

MHz) and Bruker AV 300 was used to record ^{19}F NMR spectra. ^1H and ^{13}C chemical shifts are reported in ppm downfield of TMS and referenced against the residual C_6D_6 signals (7.15 ppm for ^1H and 128.02 ppm for ^{13}C); ^{31}P chemical shifts are reported in ppm and referenced against the signal for 85% H_3PO_4 (external standard, 0 ppm). Coupling constants are reported in Hz. The correlation and assignment of ^1H and ^{13}C NMR resonances were aided by ^1H COSY, HMQC, HMBC, DEPT, NOESY and $^1\text{H}\{^{31}\text{P}\}$ experiments when necessary. GC/MS measurements were made on an Agilent 6890N spectrometer.

3.5.2 Ligand Synthesis.

3.5.2.1 3-((*N*-Benzylamino)methyl)phenol (**3.a**)

To a solution of 3-hydroxybenzaldehyde (0.500 g, 4.10 mmol) in 10 mL of methanol at r.t. was added a solution of benzylamine (0.439 g, 4.10 mmol) in 10 mL of methanol. The resulting mixture was stirred for one hour to obtain a white suspension (the Schiff base). The suspension was then cooled to $-5\text{ }^\circ\text{C}$ and NaBH_4 (0.30 g, 7.89 mmol) added portionwise over one hour. The resulting mixture was concentrated under reduced pressure, treated with 10% HCl until pH=1, and extracted with a 1:1 mixture of EtOAc : Et_2O (3×10 mL) to remove the components soluble in the organic phase. The remaining mass was then treated with concentrated aqueous ammonia solution until pH=12 to free up the amine pre-ligand, which was extracted with a 1:1 mixture of EtOAc and Et_2O (5×10 mL). The organic extracts were then combined and evaporated to give a caramel-like compound which was crystallized by adding a 1:4 mixture of Et_2O /hexane and scratching the flask walls just under the solvent level. Filtration of the resulting suspension through a glass frit and drying under vacuum for 1 more hour gave an off-white powder. (0.780 g, 89 %).

^1H NMR (δ , C_6D_6): 3.47 (s, 2H, CH_2Ph), 3.55 (s, 2H, CH_2N), 5.40 (br s, 2H, OH, NH), 6.65 (d, $J = 8$, 1H, $\{\text{Ar}\}H^4$), 6.78 (dd, $J = 8$, 2, 1H, $\{\text{Ar}\}H^6$), 6.84 (s, 1H, $\{\text{Ar}\}H^2$), 7.06-6.99 (m, 2H, $\{\text{Ar}\}H^5$, $\{\text{Bn}\}H^{\text{para}}$), 7.11 (t, $J = 7$, 2H, $2\times\{\text{Bn}\}H^{\text{meta}}$), 7.16 (m, 2H, $2\times\{\text{Bn}\}H^{\text{ortho}}$).

$^{13}\text{C}\{^1\text{H}\}$ NMR (δ , C_6D_6): 52.71 (s, 1C, CH_2), 52.85 (s, 1C, CH_2), 115.39 (s, 1C, $\{\text{Ar}\}\text{C}^6$), 116.13 (s, 1C, $\{\text{Ar}\}\text{C}^2$), 120.22 (s, 1C, $\{\text{Ar}\}\text{C}^4$), 127.47 (s, 1C, $\{\text{Ar}\}\text{C}^5$), 128.71 (s, 2C, $2\times\{\text{Bn}\}\text{C}^{\text{ortho}}$), 128.86 (s, 2C, $2\times\{\text{Bn}\}\text{C}^{\text{meta}}$), 129.92 (s, 1C, $\{\text{Bn}\}\text{C}^{\text{para}}$), 139.21 (s, 1C, $\{\text{Ar}\}\text{C}^3$), 140.69 (s, 1C, $\{\text{Bn}\}\text{C}^{\text{ipso}}$), 157.90 (s, 1C, $\{\text{Ar}\}\text{C}^1$).

Anal. Calcd for $\text{C}_{14}\text{H}_{15}\text{NO}$: C, 78.84; H, 7.09; N, 6.57; Found: C, 78.84; H, 7.24; N, 6.59.

3.5.2.2 3-((*N*-Benzylamino)methyl)phosphinitobenzene (**3.b**)

To a solution of **3.a** (0.500 g, 2.34 mmol) and triethylamine (0.360 mL, 2.85 mmol) in THF (35 mL) stirring at 0-5 °C was added a solution of chlorodiisopropyl phosphine (0.385 mL, 2.34 mmol 96%) in THF (15 mL). The resulting mixture was allowed to warm to room temperature, stirred for an additional hour, and evaporated under decreased pressure to give an oily residue, which was extracted with Et_2O (3×25 mL). Evaporation of the combined extracts furnished the product as a colorless oil (0.740g, 96%).

^1H NMR (δ , C_6D_6): 1.00 (dd, $^3J_{\text{HP}} = 16$, $^3J_{\text{HH}} = 7$, 6H, $2\times\text{CHCH}_3$), 1.17 (dd, $^3J_{\text{HP}} = 11$, $^3J_{\text{HH}} = 7$, 6H, $2\times\text{CHCH}_3$), 1.87 – 1.73 (m, 2H, $2\times\text{PCH}$), 3.55 (s, 4H, $2\times\text{CH}_2$) 6.94 (d, $^3J_{\text{HH}} = 8$, 1H, $\{\text{Ar}\}\text{H}^6$), 7.07 – 7.13 (m, 2H, $\{\text{Ar}\}\text{H}^5$ & $\{\text{Ar}\}\text{H}^4$), 7.14 – 7.23 (m, 3H, $2\times\{\text{Bn}\}\text{H}^{\text{meta}}$ & $\{\text{Bn}\}\text{H}^{\text{para}}$, overlapping with $\text{C}_6\text{D}_5\text{H}$), 7.27 (d, $^3J_{\text{HH}} = 7$, 2H, $\{\text{Bn}\}\text{H}^{\text{ortho}}$), 7.43 (s, 1H, $\{\text{Ar}\}\text{H}^2$).

$^{13}\text{C}\{^1\text{H}\}$ NMR (δ , C_6D_6): 17.19 (d, $^2J_{\text{CP}} = 9$, 2C, $2\times\text{CHCH}_3$), 17.90 (d, $^2J_{\text{CP}} = 21$, 2C, $2\times\text{CHCH}_3$), 28.64 (d, $^1J_{\text{CP}} = 18$, 2C, $2\times\text{PCH}$), 53.21 (s, 1C, CH_2), 53.35 (s, 1C, CH_2), 117.26 (d, $^3J_{\text{CP}} = 11$, 1C, $\{\text{Ar}\}\text{C}^6$), 118.60 (d, $^3J_{\text{CP}} = 10$, 1C, $\{\text{Ar}\}\text{C}^2$), 121.70 (s, 1C, $\{\text{Ar}\}\text{C}^4$), 127.01 (s, 1C, $\{\text{Ar}\}\text{C}^5$), 128.42 (s, 2C, $\{\text{Bn}\}\text{C}^{\text{ortho}}$), 128.49 (s, 2C, $\{\text{Bn}\}\text{C}^{\text{meta}}$), 129.52 (s, 1C, $\{\text{Bn}\}\text{C}^{\text{para}}$), 141.11 (s, 1C, $\{\text{Ar}\}\text{C}^3$), 142.94 (s, 1C, $\{\text{Bn}\}\text{C}^{\text{ipso}}$), 160.08 (d, $^2J_{\text{CP}} = 9$, 1C, $\{\text{Ar}\}\text{C}^1$).

$^{31}\text{P}\{^1\text{H}\}$ NMR (δ , C_6D_6): 147.2 (s).

Anal. Calcd for $\text{C}_{20}\text{H}_{28}\text{OPN}$: C, 72.92; H, 8.57; N, 4.25; Found: C, 72.20; H, 8.57; N, 4.60.

3.5.3 Synthesis of Complexes 3.1-3.5

3.5.3.1 $\kappa^P, \kappa^C, \kappa^N$ -{2,6-(*i*-Pr₂PO)(C₆H₃)(CH₂NBnH)}NiBr (**3.1**).

A solution of **3.b** (0.500 g, 1.52 mmol) in 20 mL of benzene was slowly added to the stirring suspension of NiBr₂(CH₃CN)_x (0.503 g, 1.66 mmol) and triethylamine (0.230 mL, 1.66 mmol) in toluene (5 mL) at r. t. The resulting dark brown mixture was then heated for 3 h at 60 °C, washed with water (3x5 mL), and evaporated to dryness to give the crude product as an oily yellow powder (0.656 g, 93 %). Chromatography through a short pad of silica gel (eluents: hexane followed by 50:50 CH₂Cl₂:Hexane) gave an analytically pure sample (0.553 g, 78 %).

¹H NMR (δ, C₆D₆): 1.19 (dd, ³J_{HP} = 14, ³J_{HH} = 7, 3H, CHCH₃) 1.25 (dd, ³J_{HP} = 15, ³J_{HH} = 7, 3H, CHCH₃), 1.50 (dd, ³J_{HP/HH} = 7, 3H, CHCH₃), 1.54 (dd, ³J_{HP/HH} = 6, 3H, CHCH₃), 2.33-2.11 (m, 2H, 2xPCH), 3.22 (br. s, 1H, NH), 3.33 (dd, ²J_{HH} = 16, ³J_{HH} = 6, 1H, ArCH₂N), 3.42 (dd, ²J_{HH} = 16, ³J_{HH} = 4, 1H, ArCH₂N), 3.83 (dd, ²J_{HH} = 14, ³J_{HH} = 10, 1H, {Bn}CH₂), 4.63 (d, ²J_{HH} = 14, 1H, {Bn}CH₂), 6.32 (d, ³J_{HH} = 7, 1H, {Ar}H⁵), 6.62 (d, ³J_{HH} = 8, 1H, {Ar}H³), 6.86 (t, ³J_{HH} = 8, 1H, {Ar}H⁴), 7.04 (m, 3H, 2x{Bn}H^{meta}, {Bn}H^{para}), 7.11 (d, ³J_{HH} = 5, 2H, 2x{Bn}H^{ortho}).

¹³C{¹H} NMR (δ, C₆D₆): 16.61 (d, ²J_{CP} = 2, 1C, CH₃), 17.14 (s, 1C, CH₃), 18.17 (d, ²J_{CP} = 4, 2C, 2xCH₃), 28.36 (d, ¹J_{CP} = 10, 2C, CH), 28.60 (d, ¹J_{CP} = 9, 1C, CH), 54.27 (s, 1C, CH₂), 57.62 (s, 1C, CH₂), 108.27 (d, ³J_{CP} = 13, 1C, {Ar}C³), 115.59 (s, 1C, {Ar}C⁵), 127.10 (s, 1C, {Ar}C⁴), 128.55 (s, 1C, {Bn}C^{para}), 128.83 (s, 2C, 2x{Bn}C^{ortho}), 129.25 (s, 2C, 2x{Bn}C^{meta}), 137.22 (s, 1C, {Bn}C^{ipso}), 143.46 (d, ²J_{CP} = 32, 1C, {Ar}C¹Ni), 152.75 (s, 1C, {Ar}C⁶), 166.16 (d, ²J_{CP} = 10, 1C, {Ar}C²).

³¹P{¹H} NMR (δ, C₆D₆): 201.72 (s).

Anal. Calcd for C₂₀H₂₇OPNNiBr: C, 51.44; H, 5.73; N, 3.00; Found: C, 51.28; H, 5.83; N, 2.90.

3.5.3.2 $\kappa^P, \kappa^C, \kappa^N$ -{2-(*i*-Pr₂PO)(6-(CH₂N(Bn)(allyl)(C₆H₃))}NiBr (**3.3**)

To a stirred solution of **3.1** (0.100 g, 0.216 mmol) in a dry and degassed 1:1 mixture of hexane : THF or dry and degassed toluene (5 mL) at -78 °C was added a MeLi solution in diethoxymethane (0.108 mL, 3 M, 0.323 mmol) and the resulting red mixture stirred for 30 min. Allyl bromide (0.042 mL, 0.485 mmol) was then added and the mixture stirred for one more hour at -78 °C, and then overnight at r.t. Complex **3.3** was isolated by flash chromatography (SiO₂, benzene) as a yellow powder (0.071 g, 64 %).

¹H NMR (δ, C₆D₆): 1.17 (2×dd, ³J_{HP} = 15, ³J_{HH} = 7, 6H, 2×CHCH₃), 1.48 (dd, ³J_{HP} = 11, ³J_{HH} = 7, 3H, CHCH₃), 1.53 (dd, ³J_{HP} = 11, ³J_{HH} = 7, 3H, CHCH₃), 2.24 (m, 2H, 2×PCH), 2.87 (ddd, J_{HH} = 12, 9, J_{HP} = 4, 1H, CH₂CH), 3.65 (d, ²J_{HH} = 16, 1H, ArCH₂), 3.81 (d, ²J_{HH} = 16, 1H, ArCH₂), 4.03 (dd, ²J_{HH} = 13, J_{HP} = 2, 1H, CH₂{Bn}), 4.33 (dd, ²J_{HH} = 13, ³J_{HH} = 5, 1H, CH₂CH), 4.84 (d, ²J_{HH} = 13, 1H, CH₂{Bn}), 4.96 (d, ³J_{HH} = 17, 1H, trans-CH₂=), 5.04 (d, ³J_{HH} = 10, 1H, cis-CH₂=), 6.37 (d, ³J_{HH} = 8, 1H, {Ar}H⁵), 6.58 (d, ³J_{HH} = 8, 1H, {Ar}H³), 6.84 (t, ³J_{HH} = 8, 1H, {Ar}H⁴), 6.83–6.92 (m, 1H, CH₂CH), 7.13–7.02 (m, 3H, 2×{Bn}H^{ortho}, {Bn}H^{para}), 7.58 (d, ³J_{HH} = 6, 2H, {Bn}H^{meta}).

¹³C{¹H} NMR (δ, C₆D₆): 16.88 (d, ²J_{CP} = 22, 2C, 2×CHCH₃), 18.19 (d, ²J_{CP} = 4 Hz, 1C, CHCH₃), 18.24 (d, ²J_{CP} = 4 Hz, 1C, CHCH₃), 28.37 (d, ¹J_{CP} = 25 Hz, 1C, PCH), 28.68 (d, ¹J_{CP} = 25 Hz, 1C, PCH), 61.07 (s, 1C, ArCH₂N), 61.20 (s, 1C, BnCH₂), 61.80 (s, 1C, AllylCH₂), 108.16 (d, ²J_{CP} = 13 Hz, 1C, {Ar}C³), 115.41 (s, 1C, {Ar}C⁵), 120.48 (s, 1C, CH₂=CH), 127.09 (s, 1C, {Ar}C⁴), 128.25 (s, 1C, {Bn}C^{para} found by DEPT), 128.43 (s, 2C, 2×{Bn}C^{meta}), 131.99 (s, 2C, 2×{Bn}C^{ortho}), 133.98 (s, 1C, CH₂=CH), 134.03 (s, 1C, {Bn}C^{ipso}), 142.53 (d, ²J_{CP} = 33 Hz, 1C, {Ar}C¹Ni), 152.21 (s, 1C, {Ar}C⁶), 165.73 (d, ²J_{CP} = 11 Hz, 1C, {Ar}C²).

³¹P{¹H} NMR (δ, C₆D₆): 200.64 (s).

Anal. Calcd for C₂₃H₃₁OPNNiBr : C, 54.48, H, 6.16; N, 2.76; Found: C, 54.70; H, 6.23; N, 2.73.

3.5.3.3 $\kappa^P, \kappa^C, \kappa^N$ -{2,6-(*i*-Pr₂PO)(C₆H₃)(CH₂NBn₂)}NiBr (**3.4**).

The procedure described above for the preparation of **3.3** was used to prepare this complex, which was isolated as a yellow powder (0.068 g, 57 %).

¹H NMR (δ, C₆D₆): 1.17 (dd, ³J_{HP} = 14, ³J_{HH} = 7, 6H, 2×CHCH₃), 1.54 (dd, ³J_{HP} = 18, ³J_{HH} = 7, 6H, 2×CHCH₃), 2.21-2.34 (m, 2H, PCH), 3.73 (s, 2H, ArCH₂), 4.08 (dd, ²J_{HH} = 13, ²J_{HP} = 3, 2H, {Bn}CH₂), 5.09 (d, ²J_{HH} = 13, 2H, {Bn}CH₂), 6.34 (d, ³J_{HH} = 7, 1H, {Ar}H⁵), 6.58 (d, ³J_{HH} = 8, 1H, {Ar}H³), 6.83 (t, ³J_{HH} = 8, 1H, {Ar}H⁴), 7.13-7.07 (m, 6H, 4×{Bn}H^{metha}, 2×{Bn}H^{para}), 7.75-7.67 (m, 4H, 4×{Bn}H^{ortho}).

¹³C{¹H} NMR (δ, C₆D₆): 16.81 (s, 2C, 2×CHCH₃), 18.18 (d, ²J_{CP} = 4, 2C, 2×CHCH₃), 28.42 (d, ¹J_{CP} = 25, 2C, 2×PCH), 58.91 (s, 1C, ArCH₂), 59.49 (s, 2C, 2×BnCH₂), 108.26 (d, ³J_{CP} = 13, 1C, {Ar}C³), 115.94 (d, ²J_{CP} = 2, 1C, {Ar}C⁵), 127.15 (s, 1C, {Ar}C⁴), 128.42 (s, 4C, 4×{Bn}C^{metha}), 128.45 (s, 2C, 2×{Bn}C^{para}), 132.04 (s, 4C, 4×{Bn}C^{ortho}), 134.32 (s, 2C, {Bn}C^{ipso}), 142.60 (d, ²J_{CP} = 34, 1C, {Ar}C¹Ni), 151.56 (s, 1C, {Ar}C⁶), 165.80 (d, ²J_{CP} = 10, 1C, {Ar}C²).

³¹P{¹H} NMR (δ, C₆D₆): 200.87 (s).

Anal. Calcd for C₂₇H₃₃OPNNiBr: C, 58.21, H, 5.97; N, 2.51; Found: C, 58.24; H, 6.03; N, 2.49.

3.5.3.4 [$\kappa^P, \kappa^C, \kappa^N$ -{2,6-(*i*-Pr₂PO)(C₆H₃)(CH₂NBn)}Ni]₂ (**3.5**).

To a stirred solution of **3.1** (0.500 g, 1.07 mmol) in dry and degassed toluene (10 mL) at -78 °C was added MeLi as a solution (0.393 mL of a 3 M solution in diethoxymethane, 1.18 mmol) or a solid (26 mg, 1.18 mmol), and the resulting red mixture was stirred for 30 min, allowed to warm to r.t., and stirred for additional 32 h at 60 °C (or stirred for 1 week at room temperature). Conversion of **3.1** to **3.5** was monitored by ³¹P{¹H} NMR spectroscopy. At the end of reaction, the mixture was washed with water (10 mL×3) and evaporated under reduced pressure to give an orange powder (0.367 g, 89%).

¹H NMR (δ, C₆D₆): 1.12-0.91 (m, 12H, 4×CHCH₃), 1.23 (dd, ³J_{HP} = 17, ³J_{HH} = 7, 6H, 2×CHCH₃), 1.71 (dd, ³J_{HP} = 16, ³J_{HH} = 7, 6H, 2×CHCH₃), 2.13-1.86 (m, 4H,

4×PCH), 3.58 (dd, $^2J_{\text{HH}} = 17$, $J_{\text{HP}} = 10$ 2H, BnCH₂), 3.97 (d, $^2J_{\text{HH}} = 18$, 2H, ArCH₂), 4.16 (d, $^2J_{\text{HH}} = 18$, 2H, ArCH₂), 4.55 (d, $^2J_{\text{HH}} = 17$, 2H, BnCH₂), 6.49 (d, $^3J_{\text{HH}} = 7$, 2H, 2×{Ar}H⁵), 6.67 (d, $^3J_{\text{HH}} = 8$, 2H, 2×{Ar}H³), 6.92 (t, $^3J_{\text{HH}} = 8$, 2H, 2×{Ar}H⁴), 7.06 (t, $^3J_{\text{HH}} = 7$, 2H, 2×{Bn}H^{para}), 7.17 (m, 4H, 4×{Bn}H^{meta}, overlapping with C₆D₅H) 7.77 (d, $^3J_{\text{HH}} = 7$, 4H, 4×{Bn}H^{ortho}).

¹³C{¹H} NMR (δ, C₆D₆): 15.08 (d, $^2J_{\text{CP}} = 6$, 2C, 2×CHCH₃), 16.60 (d, $^2J_{\text{CP}} = 9$, 2C, 2×CHCH₃), 18.57 (s, 2C, 2×CHCH₃), 19.04 (s, 2C, 2×CHCH₃), 28.97 (d, $^1J_{\text{CP}} = 24$, 2C, 2×PCH), 29.15 (d, $^1J_{\text{CP}} = 17$, 2C, 2×PCH), 59.28 (s, 2C, 2×BnCH₂), 72.42 (s, 2C, 2×ArCH₂), 106.75 (d, $^3J_{\text{CP}} = 13$, 2C, 2×{Ar}C³), 114.20 (s, 2C, 2×{Ar}C⁵), 126.09 (s, 2C, 2×{Ar}C⁶), 126.28 (s, 2C, 2×{Bn}C^{para}), 126.94 (s, 4C, 4×{Bn}C^{ortho}), 128.14 (s, 4C, 4×{Bn}C^{meta}, found by DEPT), 142.51 (s, 2C, 2×{Bn}C^{ipso}), 145.80 (d, $^2J_{\text{CP}} = 30$, 2C, 2×{Ar}C¹Ni), 158.31 (s, 2C, 2×{Ar}C⁶), 165.78 (d, $^2J_{\text{CP}} = 11$, 2C, 2×{Ar}C²).

³¹P{¹H} NMR (δ, C₆D₆): 191.6 (s, 2P).

Anal. Calcd for C₄₀H₅₂O₂P₂N₂Ni₂: C, 62.22, H, 6.97; N, 3.63; Found: C, 62.37; H, 6.94; N, 3.48.

3.5.4 General procedure for the reactivity survey.

An NMR tube was charged with a C₆D₆ solution of **3.5** (10.0 mg, 0.013 mmol, in 0.6 mL) and the desired amount of the reagent to be studied as follows: m-toluidine: 4.5 μL, 0.065 mmol; m-cresol: 10 μL of a 0.0013 M solution in C₆D₆ in the first step, followed by 9.5 μL of neat m-cresol, 0.091 mmol; 2,6-dimethyl(phenyl)isonitrile: 8.5 mg, 0.065 mmol; phthalimide: 9.5 mg, 0.065 mmol; CO: excess; TFE 7.5 μL, 0.104 mmol; N-hydroxyphthalimide: 10.6 mg, 0.065 mmol. The NMR tube was capped with a rubber septum and placed in an oil bath at 50 °C for a predetermined period of time. The progress of the reactions was monitored by NMR spectroscopy.

3.5.5 Typical procedure used for catalytic hydroalkoxylation of acrylonitrile.

The catalytic runs were conducted in air. The reaction vessel was charged with acrylonitrile (e.g., 0.100 g, 1.887 mmol), the alcohol (e.g., 0.810 g, 18.87 mmol of EtOH), and dodecane as the internal standard (0.046 g, 0.269 mmol). The catalyst precursor **5** was then added (1.00 mL of a 0.0094 M solution in C₆H₆). The mixture was stirred at 50 °C for a predetermined length of time and then analyzed by GC/MS to identify the products and determine the yield using a previously prepared calibration curve. The products 3-methoxypropionitrile³¹ and 3-benzyloxypropionitrile³² are known compounds; characterization of the remaining products is given below:

3.5.5.1 3-ethoxypropionitrile.

¹H NMR (δ, C₆D₆): 0.92 (t, *J* = 7, 3H, CH₃), 1.60 (t, *J* = 6, 2H, CNCH₂), 2.79 (t, *J* = 6, 2H, CH₂O), 2.97 (q, *J* = 7, 2H, OCH₂).

¹³C{¹H} NMR (δ, C₆D₆): 15.02 (s, 1C, CH₃), 18.39 (s, 1C, CNCH₂), 65.00 (s, 1C, CH₂O), 66.36 (s, 1C, OCH₂) 117.73 (s, 1C, CN).

3.5.5.2 3-(*m*-tolylloxy)propionitrile.

¹H NMR (δ, C₆D₆): 1.67 (t, *J* = 6, 2H, CNCH₂CH₂), 2.08 (s, 3H, CH₃), 3.18 (t, *J* = 6, 2H, CH₂O), 6.44 (dd, *J* = 8, 2, 1H, {Ar}H⁶), 6.51 (s, 1H, {Ar}H²), 6.67 (d, *J* = 7, 1H, {Ar}H⁴), 7.01 (t, *J* = 8, 1H, {Ar}H⁵).

¹³C{¹H} NMR (δ, C₆D₆): 18.00 (s, 1C, CH₃), 21.38 (s, 1C, CNCH₂), 62.39 (s, 1C, CH₂O), 111.73 (s, 1C, {Ar}C), 115.84 (s, 1C, {Ar}C), 117.40 (s, 1C, CN), 122.62 (s, 1C, {Ar}C), 129.53 (s, 1C, {Ar}C), 139.67 (s, 1C, {Ar}C³), 158.26 (s, 1C, {Ar}C¹)

3.5.5.3 3-(2,2,2-trifluoroethoxy)propionitrile.

¹H NMR (δ, C₆D₆) 1.58 (t, ³*J*_{HH} = 6, 2H, CH₂CN), 2.79 (t, ³*J*_{HH} = 6, 2H, OCH₂), 3.10 (q, ³*J*_{HF} = 9, 2H, CF₃CH₂).

$^{13}\text{C}\{^1\text{H}\}$ NMR (δ , C_6D_6): 18.48 (s, 1C, CH_2CN), 67.14 (s, 1C, OCH_2), 68.40 (q, $J_{\text{CF}}=34$, 1C, CF_3CH_2), 117.51 (s, 1C, CN), 124.57 (q, $J_{\text{CF}} = 279$, 1C, CF_3). ^{13}F NMR (300 MHz, δ , C_6D_6) 76.0 (t, $J_{\text{HF}} = 9$, 3F).

3.5.5.4 3-propoxypropionitrile.

^1H NMR (δ , C_6D_6): 0.77 (t, $J = 7$, 3H, CH_3), 1.40-1.30 (m, 2H, CH_2CH_3), 1.63 (t, $J = 6$, 2H, CNCH_2CH_2), 2.83 (t, $J = 6$, 2H, CH_2CN), 2.93 (t, $J = 6$, 2H, OCH_2). $^{13}\text{C}\{^1\text{H}\}$ NMR (δ , C_6D_6): 10.62 (s, 1C, CH_3), 18.37 (s, 1C, CH_2O), 23.02 (s, 1C, CH_2CH_3), 65.24 (s, 1C, CH_2CN), 72.68 (s, 1C, OCH_2), 117.71 (s, 1C, CN).

3.5.6 Crystal Structure Determinations.

Single crystals of **3.1** and **3.3-3.5** were grown by slow diffusion of hexanes into a saturated benzene solution of each complex. The crystallographic data for complexes **3.1**, **3.4**, and **3.5** were collected on a Bruker Microstar generator (rotating anode) equipped with a Helios optics, a Kappa Nonius goniometer and a Platinum135 detector, whereas crystallographic data for complex **3.3** were collected on a Bruker SMART generator (X-ray sealed tube) a Kappa Nonius goniometer and a APEX II detector.

Cell refinement and data reduction were done using SAINT³³. An empirical absorption correction, based on the multiple measurements of equivalent reflections, was applied using the program SADABS.³⁴ The space group was confirmed by XPREP routine³⁵ in the program SHELXTL.³⁶ The structures were solved by direct-methods and refined by full-matrix least squares and difference Fourier techniques with SHELX-97.³⁷ All non-hydrogen atoms were refined with anisotropic displacement parameters. Hydrogen atoms were set in calculated positions and refined as riding atoms with a common thermal parameter, except for those of the NH moiety of complexes **1**, which were positioned from residual peaks in the difference Fourier map.

3.6 Acknowledgements.

The authors gratefully acknowledge financial support received from Université de Montréal (fellowships to D.M.S.) and NSERC of Canada (Research Tools and Instruments and Discovery grants to D.Z.). We are grateful to Drs. S. Gorelsky and F. Schaper for helpful discussions.

3.7 Supporting Information.

¹H NMR spectra for the reactions of **3.5** with m-cresol. This material is available free of charge via the Internet at <http://pubs.acs.org>. Complete details of the X-ray analyses for complexes **3.1**, **3.3**, **3.4**, and **3.5** have been deposited at The Cambridge Crystallographic Data Centre (CCDC) and can be retrieved with the following reference numbers: 699466 (**3.1**), 772484 (**3.3**), 772485 (**3.4**), 699467 (**3.5**). These data can be obtained free of charge via www.ccdc.cam.ac.uk/data_request/cif, or by emailing data_request@ccdc.cam.ac.uk, or by contacting The Cambridge Crystallographic Data Centre, 12, Union Road, Cambridge CB2 1EZ, UK; fax: +44 1223 336033.

Supporting information for:

**Monomeric and Dimeric Nickel Complexes Derived From a Pincer Ligand
Featuring a Secondary Amine Donor Moiety**

Denis M. Spasyuk and Davit Zargarian.

Département de chimie, Université de Montréal, Montréal (Québec), Canada

H3C 3J7

Figure 3.5. The aliphatic region (1.9 to 4.7 ppm) of the ^1H -NMR spectrum (C_6D_6) right after mixing complex **3.5** (10 mg, 0.013 mmol) and m-cresol (100 μL , 0.013 mol/ dm^3 in C_6D_6).

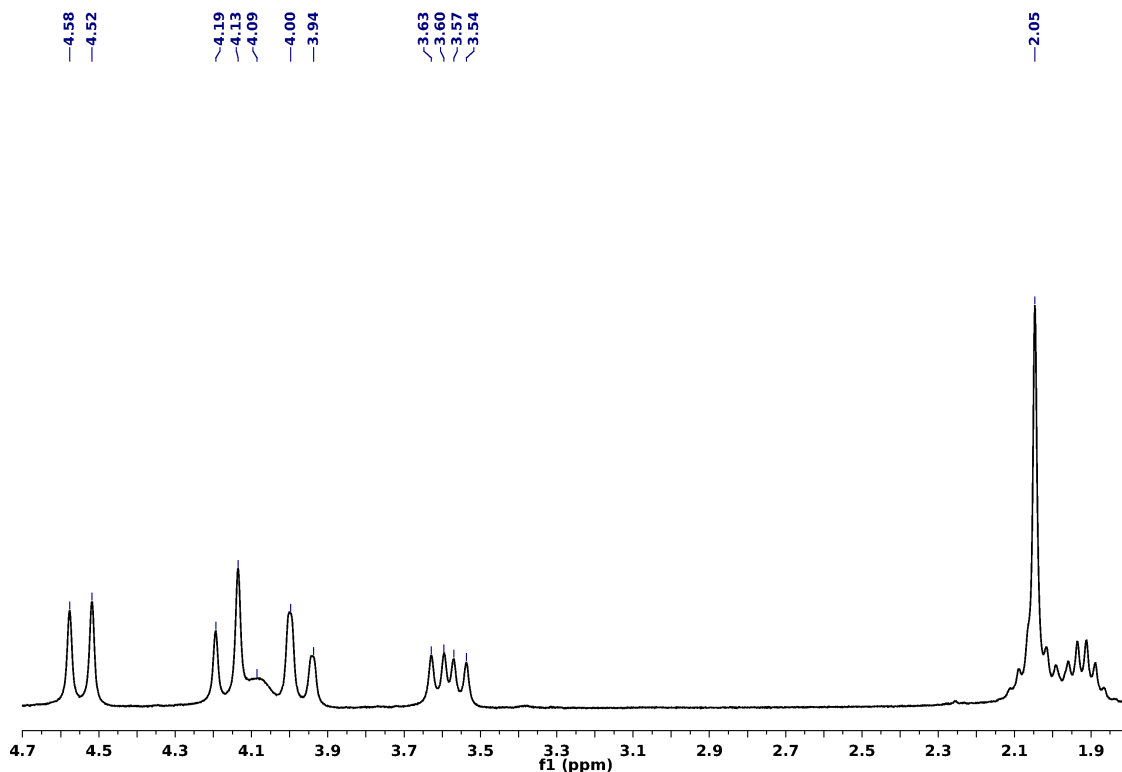


Figure 3.6. The ^1H -NMR spectrum of the above mixture (same spectral region) after about 10 min of reaction

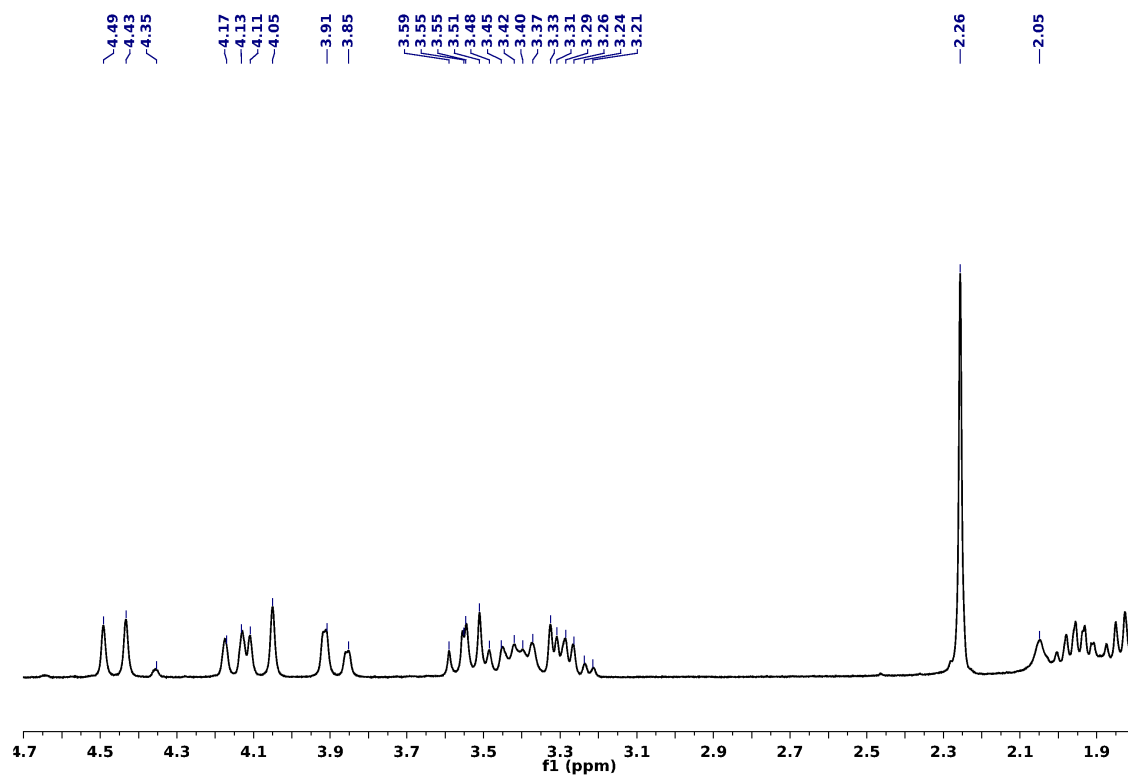
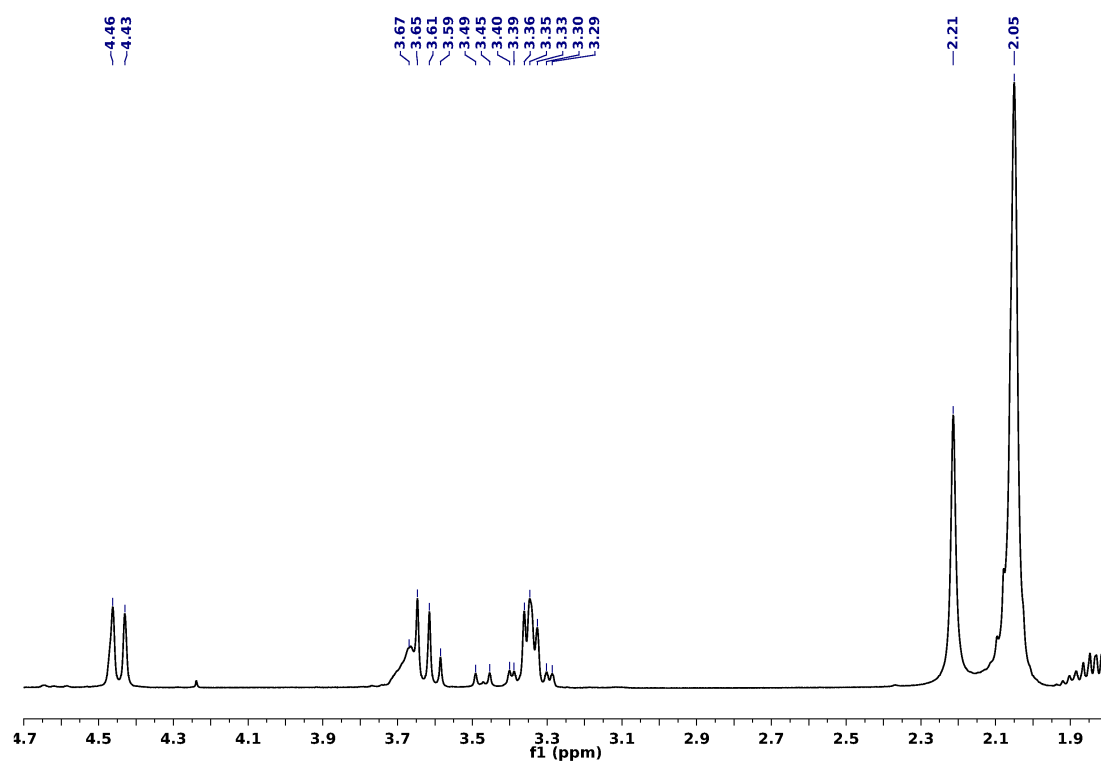


Figure 3.7. the ^1H -NMR spectrum of the above mixture with additional 7 equivalents of m-cresol (same spectral region) after about 10 min of reaction.



3.8 References

¹ For a selection of reviews and primary reports describing some applications of pincer complexes see: (a) Albrecht, M.; van Koten, G. *Angew. Chem., Int. Ed.* **2001**, *40*, 375. (b) van der Boom, M. E.; Milstein, D. *Chem. Rev.* **2003**, *103*, 1759. (c) Singleton, J. T. *Tetrahedron* **2003**, *59*, 1837. (d) Liang, L.-C. *Coord. Chem. Rev.* **2006**, *250*, 1152. (e) Nishiyama, H. *Chem. Soc. Rev.* **2007**, *36*, 1133. (f) Leis, W.; Mayer, H. A.; Kaska, W. C. *Coord. Chem. Rev.* **2008**, *252*, 1787. (g) Goldman, A. S.; Roy, A. H.; Huang, Z.; Ahuja, R.; Schinski, W.; Brookhart, M. *Science* **2006**, *312*, 257. (h) van der Ploeg, A. F. M. J.; van Koten, G.; Brevard, C. *Inorg. Chem.* **1982**, *21*, 2878. (i) Batema, G. D.; Lutz, M.; Spek, A. L.; van Walree, C. A.; Donegá, C. d. M.; Meijerink, A.; Havenith, R. W. A.; Pérez-Moreno, J.; Clays, K.; Büchel, M.; van Dijken, A.; Bryce, D. L.; van Klink, G. P. M.; van Koten, G. *Organometallics* **2008**, *27*, 1690. (j) Zweifel, T.; Naubron, J.-V.; Grützmacher, H. *Angew. Chem., Int. Ed.* **2009**, *48*, 559. (k) Ohff, M.; Ohff, A.; van der Boom, M. E.; Milstein, D. *J. Am. Chem. Soc.* **1997**, *119*, 11687. (l) Miyazaki, F.; Yamaguchi, K.; Shibasaki, M. *Tetrahedron Letters* **1999**, *40*, 7379. (m) Naghipour, A.; Sabounchei, S. J.; Morales-Morales, D.; Canseco-González, D.; Jensen, C. M. *Polyhedron* **2007**, *26*, 1445. (n) Gunanathan, C.; Ben-David, Y.; Milstein, D. *Science* **2007**, *317*, 790. (o) Sebelius, S.; Olsson, V. J.; Szabo, K. J. *J. Am. Chem. Soc.* **2005**, *127*, 10478. Bernskoetter, W. H.; Brookhart, M. *Organometallics* **2008**, *27*, 2036. (p) Dijkstra, H. P.; Meijer, M. D.; Patel, J.; Kreiter, R.; van Klink, G. P. M.; Lutz, M.; Spek, A. L.; Canty, A. J.; van Koten, G. *Organometallics* **2001**, *20*, 3159.

² (a) Rybtchinski, B.; Milstein, D. *Angew. Chem. Int. Ed.* **1999**, *38*, 870. (b) Zhao, J.; Goldman, A. S.; Hartwig, J. F. *Science* **2005**, *307*, 1080. (c) Kanzelberger, M.; Singh, B.; Czerw, M.; Krogh-Jespersen, K.; Goldman, A. S. *J. Am. Chem. Soc.* **2000**, *122*, 11017. (d) Gusev, D. G.; Fontaine, F.-G.; Lough, A. J.; Zargarian, D. *Angew. Chem. Int. Ed. Eng.* **2003**, *42*, 216. (e) Agapie, T.; Bercaw, J. E. *Organometallics* **2007**, *26*, 2957. (f) Ingleson, M. J.; Fullmer, B. C.;

Buschhorn, D. T.; Fan, H.; Pink, M.; Huffman, J. C.; Caulton, K. G. *Inorg. Chem.* **2008**, *47*, 407. (g) Ingleson, M.J.; Fan, H.; Pink, M.; Tomaszewski, J.; Caulton, K. G. *J. Am. Chem. Soc.* **2006**, *128*, 1804. (h) Ingleson, Pink, M.; Caulton, K. G. *J. Am. Chem. Soc.* **2006**, *128*, 4248. (i) Gozin, M.; Aizenberg, M.; Liou, S.-Y.; Weisman, A.; Ben-David, Y.; Milstein, D. *Nature* **1994**, *370*, 42. (j) Grove, D. M.; van Koten, G.; Mul, P.; van der Zeijden, A. A. H.; Terheijden, J.; Zoutberg, M. C.; Stam, C. H. *Organometallics* **1986**, *5*, 322. (k) Gusev, D. G.; Maxwell, T.; Dolgushin, F. M.; Lyssenko, M.; Lough, A. J. *Organometallics* **2002**, *21*, 1095. (l) Gusev, D. G.; Madott, M.; Dolgushin, F. M.; Lyssenko, K. A.; Antipin, M. Y. *Organometallics* **2000**, *19*, 1734.

³ (a) Moulton, C. J.; Shaw, B. L. *J. Chem. Soc., Dalton Trans.* **1976**, 1020. (b) Crocker, C.; Errington, R. J.; McDonald, W. S.; Odell, K. J.; Shaw, B. L.; Goodfellow, R. J. *J. Chem. Soc., Chem. Commun.* **1979**, 498.

⁴ (a) Fryzuk, M. D.; MacNeil, P. A. *J. Am. Chem. Soc.* **1981**, *103*, 3592. (b) Fryzuk, M. D. *Can. J. Chem.* **1992**, *70*, 2839. (c) Grove, D. M.; van Koten, G.; Zoet, R.; Murrall, N. W.; Welch, A. J. *J. Am. Chem. Soc.* **1983**, *105*, 1379. (d) Grove, D. M.; Van Koten, G.; Ubbels, H. J. C.; Zoet, R.; Spek, A. L. *Organometallics* **1984**, *3*, 1003.

⁵ For Si-based systems see the following reports and references therein: (a) Mitton, S.; McDonald, J. R.; Turculet, L. *Angew. Chem., Int. Ed.* **2009**, *48*, 8568. (b) Sangtrirutnugul, P.; Tilley, T. D.; *Organometallics* **2007**, *26*, 5557; (c) MacInnis, M. C.; MacLean, D. F.; Lundgren, R. J.; McDonald, R.; Turculet, L. *Organometallics* **2007**, *26*, 6522. (d) Korshin, E. E.; Leitus, G.; Shimon, L. J. W.; Konstantinovski, L.; Milstein, D. *Inorg. Chem.* **2008**, *47*, 7177. For B-based systems see the following reports: (e) Spokoyny, A. M.; Reuter, M. G.; Stern, C. L.; Ratner, M. A.; Seideman, T.; Mirkin, C. A. *J. Am. Chem. Soc.* **2009**, *131*, 9482. (f) Segawa, Y.; Yamashita, M.; Nozaki, K. *J. Am. Chem. Soc.* **2009**, *131*, 9201. For a OCO (R₃P=O)-type system see: (g) Mehring, M.; Schurmann, M.; Jurkschat, K. *Organometallics* **1998**, *17*, 1227. For recent reports on CC'C-type carbene systems see: (h) Grundemann, S.; Albrecht, M.; Loch, J. A.; Faller, J. W.;

Crabtree, R. H. *Organometallics* **2001**, *20*, 5485. (i) Liu, A.; Zhang, X.; Chen, W. *Organometallics* **2009**, *28*, 4868. For SCS ligand see: (j) Suijkerbuijk, B. M. J. M.; Herreras Martínez, S. D.; Koten, G. V.; Klein Gebbink, R. J. M. *Organometallics* **2008**, *27*, 534.

⁶ (a) Groux, L.F.; Bélanger-Gariépy, F.; Zargarian, D. *Can. J. Chem.* **2005**, *83*, 634. (b) Castonguay, A.; Sui-Seng, C.; Zargarian, D.; Beauchamp, A. L. *Organometallics* **2006**, *25*, 602. (c) Sui-Seng, C.; Castonguay, A.; Chen, Y.; Gareau, D.; Groux, L. F.; Zargarian, D. *Topics in Catalysis* **2006**, *37*, 81. (d) Castonguay, A.; Beauchamp, A. L.; Zargarian, D. *Acta Cryst.* **2007**, *E63*, m196. (e) Pandarus, V.; Zargarian, D. *Chem. Commun.* **2007**, 978. (f) Pandarus, V.; Zargarian, D. *Organometallics* **2007**, *26*, 4321. (g) Castonguay, A.; Beauchamp, A. L.; Zargarian, D. *Organometallics* **2008**, *27*, 5723. (h) Castonguay, A.; Spasyuk, D. M.; Madern, N.; Beauchamp, A. L.; Zargarian, D. *Organometallics* **2009**, *28*, 2134. (i) Spasyuk, D. M.; Zargarian, D.; van der Est, A. *Organometallics* **2009**, *28*, 6531.

⁷ For a report on a Cu complex featuring such an encapsulated ligand see: Ribas, X.; Jackson, D. A.; Donnadieu, B.; Mahía, J.; Parella, T.; Xifra, R.; Hedman, B.; Hodgson, K. O.; Llobet, A.; Stack, T. D. P. *Angew. Chem., Int. Ed.* **2002**, *41*, 2991

⁸ 15-Electron pincer complexes of nickel include the cationic, square planar $[(\text{PNP})\text{Ni}^{\text{III}}\text{Cl}]^+$ (see (a) Adhikari, D.; Mossin, S.; Basuli, F.; Huffman, J. C.; Szilagy, R. K.; Meyer, K.; Mindiola, D. *J. Am. Chem. Soc.* **2008**, *130*, 3676) and the neutral, T-shaped $(\text{PNP})\text{Ni}^{\text{I}}$ (see ref. 2f and (b) Adhikari, D.; Mossin, S.; Basuli, F.; Dible, B. R.; Chipara, M.; Fan, H.; Huffman, J. C.; Meyer, K.; Mindiola, D. *J. Inorg. Chem.* **2008**, *47*, 10479).

⁹ Most pincer complexes of nickel are 16-electron species (Ni^{II} , neutral or cationic, square planar). For a few examples see: (a) Campora, J.; Palma, P.; del Rio, D.; Alvarez, E. *Organometallics* **2004**, *23*, 1652. (b) Spencer, L. P.; Winston, S.; Fryzuk, M. D. *Organometallics* **2004**, *23*, 3372. (c) Melaimi, M.; Thoumazet, C.; Ricard, L.; Floch, P. L. *J. Organomet. Chem.* **2004**, *689*, 2988. (d) Ozerov, O.

V.; Guo, C.; Fan, L.; Foxman, B. M. *Organometallics* **2004**, *23*, 5573. (e) Baldovino-Pantaleón, O.; Hernández-Ortega, S.; Morales-Morales, D. *Inorg. Chem.* **2005**, *8*, 955. (f) Liang, L.; Chien, P.; Lin, J.; Huang, M.; Huang, Y.; Liao, J. *Organometallics* **2006**, *25*, 1399. (g) Liang, L.; Chien, P.; Huang, Y. *J. Am. Chem. Soc.* **2006**, *128*, 15562. (h) Benito-Garagorri, D.; Wiedermann, J.; Pollak, M.; Mereiter, K.; Kirchner, K. *Organometallics* **2007**, *26*, 217. For examples of Ni-PC_{sp}²P complexes see ref. 1a and the following reports : (i) Kennedy, A. R.; Cross, R. J.; Muir, K. W. *Inorg. Chim. Acta* **1995**, *231*, 195. (j) Huck, W. T. S.; Snellink-Ruël, B.; van Veggel, F. C. J. M.; Reinhoudt, D. N. *Organometallics* **1997**, *16*, 4287. (k) Bachechi, F. *Struct. Chem.* **2003**, *14*, 263. (l) Kozhanov, K. A.; Bubnov, M. P.; Cherkasov, V. K.; Fukin, G. K.; Abakumov, G. A. *Dalton Trans.* **2004**, 2957. (m) Cámpora, J.; Palma, P.; del Río, D.; Álvarez, E. *Organometallics* **2004**, *23*, 1652. (n) Cámpora, J.; Palma, P.; del Río, D.; Conejo, M. M.; Álvarez, E. *Organometallics* **2004**, *23*, 5653. (o) van der Boom, M. E.; Liou, S. Y.; Shimon, L. J. W.; Ben-David, Y.; Milstein, D. *Inorg. Chim. Acta* **2004**, *357*, 4015. (p) Boro, B. J.; Duesler, E. N.; Goldberg, K. I.; Kemp, R. A. *Inorg. Chem.* **2009**, *48*, 5081.

¹⁰ The dimer $\{(\mu\text{-PNP})\text{Ni}\}_2$ is a unique example of a 17-electron complex featuring four-coordinate Ni^I centers (see ref. 8b), whereas most 17-electron pincer complexes of Ni are neutral, Ni^{III} complexes of square pyramidal geometry, including refs. 6e-6g, 6i, and the following reports: (a) van de Kuil, L. A.; Grove, D. M.; Gossage, R. A.; Zwikker, J. W.; Jenneskens, L. W.; Drenth, W.; van Koten, G. *Organometallics* **1997**, *16*, 4985. (b) Kozhanov, K. A.; Bubnov, M. P.; Cherkasov, V. K.; Fukin, G. K.; Vavilina, N. N.; Efremova, L. Y.; Abakumov, G. A. *J. Mag. Res.* **2009**, *197*, 36. (c) Kozhanov, K. A.; Bubnov, M. P.; Cherkasov, V. K.; Fukin, G. K.; Abakumov, G. A. *Chem. Commun.* **2003**, 2610. (d) Grove, D. M.; van Koten, G.; Mul, P.; Zoet, R.; van der Linden, J. G. M.; Legters, J.; Schmitz, J. E. J.; Murrall, N. W.; Welch, A. J. *Inorg. Chem.* **1988**, *27*, 2466.

¹¹ (a) Huang, D.; Streib, W. E.; Eisenstein, O.; Caulton, K. G. *Angew. Chem. Int. Ed. Engl.* **1997**, *36*, 2004. (b) Huang, D.; Bollinger, J. C.; Streib, W. E.; Folting, K.; Young, Jr; V.; Eisenstein, O.; Caulton, K. G. *Organometallics* **2000**, *19*, 2281. (c) Scott, N. M.; Pons, V.; Stevens, E. D.; Heinekey, D. M.; Nolan, S. P. *Angew. Chem.* **2005**, *44*, 2512.

¹² It is worth emphasizing that i) NMR spectra of the oily material obtained from reaction of **1** with MeLi allow us to confidently exclude formation of a Ni-Me derivative, and ii) the structure proposed for **2·LiBr** in Scheme 2 is a simplified and tentative one. Alternative postulates might involve cluster-type structures such as those found in the following reports: (a) Aubrecht, K. B.; Lucht, B. L.; Collum, D. B. *Organometallics* **1999**, *18*, 2981. (b) Strohmman, C.; Lehmen, K.; Ludwig, A.; Schildbach, D. *Organometallics* **2001**, *20*, 4138. (c) Sott, R.; Hakansson, M.; Hilmersson, G. *Organometallics* **2006**, *25*, 6047. (d) Paté, F.; Oulyadi, H.; Harrison-Marchand, A.; Maddaluno, J. *Organometallics* **2008**, *27*, 3564.

¹³ Another cause for the non-equivalence of protons 7A and 7B is the absence of a plane of symmetry in complex **1**, which also results in the non-equivalence of the two *i*-Pr substituents of the phosphinite moiety sitting above and below the plane of coordination. Thus, we find four different signals for the proton and carbon nuclei of the Me groups and two different signals for the methyne carbons, whereas the signals for the two methyne CH appear as a poorly resolved multiplet at ca. 2.11-2.33 ppm.

¹⁴ (a) Consorti, C.; Ebeling, G.; Flores, F.; Rominger, F.; Dupont, J. *Adv. Syn. & Cat.* **2004**, *346*, 617. (b) Poverenov, E.; Gandelman, M.; Shimon, L. J. W.; Rozenberg, H.; Ben-David, Y.; Milstein, D. *Organometallics* **2005**, *24*, 1082.

¹⁵ Cordero B., Gómez V., Platero-Prats A. E., Revés M., Echeverría J., Cremades E., Barragán F., Alvarez, C. *Dalton Trans.*, **2008**, 2832.

¹⁶ A recent report from Holm's group describes a dimeric Ni^{II} pincer complex $[\mu^S, \kappa^S, \kappa^N, \kappa^S-(SNS)Ni]_2$ featuring a dianionic XLX-type SNS ligand, but no

structural studies have been conducted on this species due to its limited solubility: Huang, D.; Deng, L.; Sun, J.; Holm, R. *Inorg. Chem.* **2009**, *48*, 6159.

¹⁷ For a few reviews see: (a) J. J. Brunet and D. Neibecke, in *Catalytic Heterofunctionalization*, ed. A. Togni and H. Grützmacher, VCH, Weinheim, **2001**, pp. 91–141. (b) Beller, M.; Seayad, J.; Tillack, A.; Jiao, H. *Angew. Chem. Int. Ed. Engl.* **2004**, *43*, 3368. (c) Nising, C. F.; Brase, S. *Chem. Soc. Rev.* **2008**, *37*, 1218–1228. For a report on hydroalkoxylation of alkynes, see: (d) R. Casado, M. Contel, M. Laguna, P. Romero and S. Sanz, *J. Am. Chem. Soc.*, **2003**, *125*, 11925.

¹⁸ (a) Noyce, D. S.; DeBruin, K. E. *J. Am. Chem. Soc.* **1968**, *90*, 372. (b) Fedor, L. R.; De, N. C.; Gurware, S. K. *J. Am. Chem. Soc.* **1973**, *95*, 2905. (c) Jensen, J. L.; Carre, D. J. *J. Org. Chem.* **1974**, *39*, 2103. (d) Wabnitz, T. C.; Spencer, J. B. *Org. Lett.* **2003**, *5*, 2141. (e) Li, Z.; Zhang, J.; Brouwer, C.; Yang, C.-G.; Reich, N. W.; He, C. *Org. Lett.* **2006**, *8*, 4175. (f) Rosenfeld, D. C.; Shekhar, S.; Takemiya, A.; Utsunomiya, M.; Hartwig, J. F. *Org. Lett.* **2006**, *8*, 4179. (g) Coulombel, L.; Favier, I.; Dunach, E. *Chem. Comm.* **2005**, 2286.

¹⁹ (b) Duffy, J. L.; Kurth, J. A.; Kurth, M. J. *Tet. Lett.* **1993**, *34*, 1259. (c) Dumez, E.; Rodriguez, J.; Dulcère, J.-P. *Chem. Comm.* **1997**, 1831. (d) Murtagh, J.E.; McCooey, S.H.; Cannon S. J.; *Chem. Comm.* **2005**, 227.

²⁰ (a) Stewart, I.C.; Bergman, R.G.; Toste, F. D. *J. Am. Chem. Soc.* **2004**, *125*, 8696. (b) Kisanga, P. B.; Iankumaran, P.; Fetterly, B. M.; Verkade, J. G. *J. Org. Chem.* **2002**, *67*, 3555.

²¹ Coulombel, L.; Rajzmann, M.; Pons, J.; Olivero, S.; Duñach, E. *Chem. Eur. J.* **2006**, *12*, 6356.

²² Corberán, R.; Marrot, S.; Dellus, N.; Merceron-Saffon, N.; Kato, T.; Peris, E.; Baceiredo, A. *Organometallics* **2009**, *28*, 326. (b) Munro-Leighton, C.; Delp, S. A.; Blue, E. D.; Gunnoe, T. B. *Organometallics* **2007**, *26*, 1483. (c) van Lingen, H. L.; Zhuang, W.; Hansen, T.; Rutjes, F. P. J. T.; Jørgensen, K. A. *Org. Biomol. Chem.* **2003**, *1*, 1953.

²³ Gallagher, T. *J. Chem. Soc., Chem. Commun.* **1984**, 1554.

²⁴ (a) Yang, C.-G.; He, C. *J. Am. Chem. Soc.*, **2005**, *127*, pp 6966. (b) Kamiya, I.; Tsunoyama, H.; Tsukuda, T.; Sakurai, H. *Chem. Lett.* **2007**, *36*, 646. (c) Zhang, X.; Corma, A. *Dalton Trans.* **2008**, 397. (d) Volz, F.; Krause, N. *Org. Biomol. Chem.* **2007**, *5*, 1519. (e) Hirai, T.; Hamasaki, A.; Nakamura, A.; Tokunaga, M. *Org. Lett.* **2009**, *11*, 5510.

²⁵ Yi, C. S.; Yun, S. Y.; He, Z. *Organometallics* **2003**, *22*, 3031.

²⁶ (a) Kawamoto, T.; Hirabayashi, S.; Guo, X.; Nishimura, T.; Hayashi, T. *Chem. Commun.* **2009**, 3528. (b) K. Hori, H. Kitagawa, A. Miyoshi, T. Ohta and I. Furukawa, *Chem. Lett.* **1998**, 1083.

²⁷ (a) Hosokawa, T.; Shinohara, T.; Ooka, Y.; Murahashi, S.-I. *Chem. Lett.* **1989**, 2001. (b) Miller, K. J.; Kitagawa, T. T.; Abu-Omar, M. M. *Organometallics* **2001**, *20*, 4403. (c) Matsukawa, Y.; Mizukado, J.; Quan, H.; Tamura, M.; Sekiya, A. *Angew. Chem.* **2005**, *117*, 1152. (d) Gligorich, K. M.; Schultz, M. J.; Sigman, M. S. *J. Am. Chem. Soc.* **2006**, *128*, 2794. (e) Zhang, Y.; Sigman, M. S. *Org. Lett.* **2006**, *8*, 5557. (f) Patil, N. T.; Lutete, L. M.; Wu, H.; Pahadi, N. K.; Gridnev, I. D.; Yamamoto, Y. *J. Org. Chem.* **2006**, *71*, 4270. (g) Lemechko, P.; Grau, F.; Antoniotti, S.; Dunach, E. *Tetrahedron Lett.* **2007**, *48*, 5731.

²⁸ Qian, H.; Han, X.; Widenhoefer, R. A. *J. Am. Chem. Soc.* **2004**, *126*, 9536-9537.

²⁹ The pK_a value for CF_3CH_2OH is estimated to be ca. 11-12: Ballinger, P.; Long, F. A. *J. Am. Chem. Soc.* **1959**, *81*, 1050.

³⁰ Complex **3.3** is insoluble in pure acetonitrile.

³¹ Stewart I.C., Bergman R. G., and Toste F. D. *J. Am. Chem. Soc.*, **2003**, *125*, 8696.

³² Krishna T. R., and Jayaraman N., *J. Org. Chem.* **2003**, *68*, 9694.

³³ SAINT (**1999**) Release 6.06; Integration Software for Single Crystal Data. Bruker AXS Inc., Madison, Wisconsin, USA.

³⁴ Sheldrick, G.M. (**1999**). SADABS, Bruker Area Detector Absorption Corrections. Bruker AXS Inc., Madison, Wisconsin, USA.

³⁵ XPREP (1997) Release 5.10; X-ray data Preparation and Reciprocal space Exploration Program. Bruker AXS Inc., Madison, Wisconsin, USA.

³⁶ SHELXTL (1997) Release 5.10; The Complete Software Package for Single Crystal Structure Determination. Bruker AXS Inc., Madison, Wisconsin, USA.

³⁷ (a) Sheldrick, G.M. (1997). SHELXS97, Program for the Solution of Crystal Structures. Univ. of Gottingen, Germany. (b) Sheldrick, G.M. (1997). SHELXL97, Program for the Refinement of Crystal Structures. University of Gottingen, Germany.

Chapter 4: Characterization of Divalent and Trivalent Species Generated in The Chemical and Electrochemical Oxidation of a Dimeric Nickel (II) Pincer Complex

Article 3

**Denis M. Spasyuk[†], Serge Gorelsky[§]; Art van der Est[‡]
and Davit Zargarian[†]**

[†] Département de chimie, Université de Montréal, Montréal, QC, Canada H3C 3J7

[§] Centre for Catalysis Research and Innovation, Department of Chemistry, University of Ottawa, Ottawa (Ontario), Canada K1N 6N5

[‡] Department of Chemistry, Brock University, St. Catharines, ON, Canada L2S 3A1

J. Am. Chem. Soc., submitted.

4.1 Abstract

The electrolytic and chemical oxidation of the dimeric pincer complex $[\kappa^P, \kappa^C, \kappa^N, \mu^N-(2,6-(i\text{-Pr}_2\text{POC}_6\text{H}_3\text{CH}_2\text{NBn})\text{Ni})_2]$ (**4.1**; Bn= CH₂Ph) has been investigated by various analytic techniques. Cyclic voltammetry measurements have shown that **4.1** undergoes a quasi-reversible, one electron, Ni-based redox process ($\Delta E_{1/2}^0 = -0.07$ V), and spectroelectrochemical measurements conducted on the product of the electrolytic oxidation, $[\mathbf{4.1}]^+$, have shown electronic transitions in the near IR region. Computational studies using Density Functional Theory (B3LYP) have corroborated the experimentally obtained structure of **4.1**, provided complete MO and structural analyses for $[\mathbf{4.1}]^+$, and helped interpret the experimentally obtained absorption spectra for **4.1** and $[\mathbf{4.1}]^+$. These findings indicate that the radical cation $[\mathbf{4.1}]^+$ is a dimeric, mixed-valent species (class III) wherein most of the spin density is delocalized over the two nickel centers ($\text{Ni}^{+2.5}_2\text{N}_2$), but some spin density is also present over the two nitrogen atoms ($\text{Ni}^{+2}_2\text{N}_2$). Examination of alternative structures for open shell species generated from **4.1** has shown that the spin density distribution is highly sensitive towards changes in the ligand environment of the Ni ions. NMR, UV-Vis, EPR, and single crystal X-ray diffraction analyses have shown that chemical oxidation of **4.1** with *N*-Bromosuccinimide (NBS) follows a complex process that gives multiple products, including the monomeric trivalent species $\kappa^P, \kappa^C, \kappa^N-\{2,6-(i\text{-Pr}_2\text{PO})(\text{C}_6\text{H}_3)(\text{CH}=\text{NBn})\}\text{NiBr}_2$ (**4.2**). These studies also indicate that oxidation of **4.1** with one equivalent of NBS gives an unstable, paramagnetic intermediate that decomposes to a number of divalent species, including succinimide and the monomeric divalent complexes $\kappa^P, \kappa^C, \kappa^N-\{2,6-(i\text{-Pr}_2\text{PO})(\text{C}_6\text{H}_3)(\text{CH}=\text{NBn})\}\text{NiBr}$ (**4.3**) and $\kappa^P, \kappa^C, \kappa^N-\{2,6-(i\text{-Pr}_2\text{PO})(\text{C}_6\text{H}_3)(\text{CH}_2\text{N}(\text{H})\text{Bn})\}\text{NiBr}_2$ (**4.4**); a second equivalent of NBS then oxidizes **4.3** and **4.4** to **4.2** and other unidentified products. The divalent complex **4.3** was synthesized independently and shown to react with NBS or bromine to form its trivalent homologue **4.2**. The new complexes **4.2** and **4.3** have been characterized fully.

4.2 Introduction

Pincer complexes¹ have attracted much attention over the past two decades due, primarily, to their demonstrated potential in catalysis and materials science,² and the burgeoning interest in the chemistry of pincer complexes has led to a significant expansion in the type of pincer systems being investigated. Despite this expanding diversity, however, vast majority of pincer complexes reported to date are monometallic species; moreover, a majority of the multimetallic pincer complexes reported to date feature “spacer-type” ligands as opposed to short bridging ligands that might facilitate interactions between proximate metal centers (e.g., μ -halide, μ -OR, μ -NR₂, etc.).³ Given the important role played by multimetallic complexes in probing paradigms such as cooperative reactivity and various intermetallic electronic interactions (e.g., electron transfer, magnetism, etc.),⁴ multimetallic complexes based on pincer-type ligands should present interesting case studies.

During the course of our studies on pincer complexes of nickel,⁵ we have synthesized the bimetallic species [$\kappa^P, \kappa^C, \kappa^N, \mu^N$ -(2,6-(*i*-Pr₂POC₆H₃CH₂NBn)Ni)₂ (**4.1**; Bn= CH₂Ph) featuring two Ni^{II} centers bridged by the amide moiety of a new POCN-type pincer ligand (Figure 4.1).^{15j} Noteworthy structural features of **4.1** include a puckered, cyclobutane-like Ni₂N₂ core and a *syn* orientation of the *N*-substituents; this compound is also an active catalyst for the Michael addition of ROH to acrylonitrile, which gives anti-Markovnikov products of alcoholysis. Complex **4.1** is a rare example of LXL pincer-type dinickel species, but a number of structurally related “pincer-like” dinickel complexes are known, including the complexes [LNi^{II}₂]^{2+/3+},⁶ [LNi^{II}Ni^{III}(NCCH₃)₂]³⁺,⁷ [(SNS)Ni^{II}]₂,⁸ and [(PNP)Ni^I]₂⁹ depicted in Figure 4.1. The latter species is a diradical featuring weak Ni-Ni interactions, whereas the other systems do not appear to involve any intermetallic interaction. Moreover, EPR measurements and DFT analyses have indicated that the spin density is localized mostly on *one* Ni center in [LNi₂]³⁺ (ca. 70%)^{6b} and [LNi^{II}Ni^{III}(NCCH₃)₂]³⁺ (ca. 90% on the six coordinate Ni).^{6b} These observations

are thought to be relevant for understanding the reactivities of the active site in [NiFe] hydrogenases, for which these complexes are proposed as model systems.

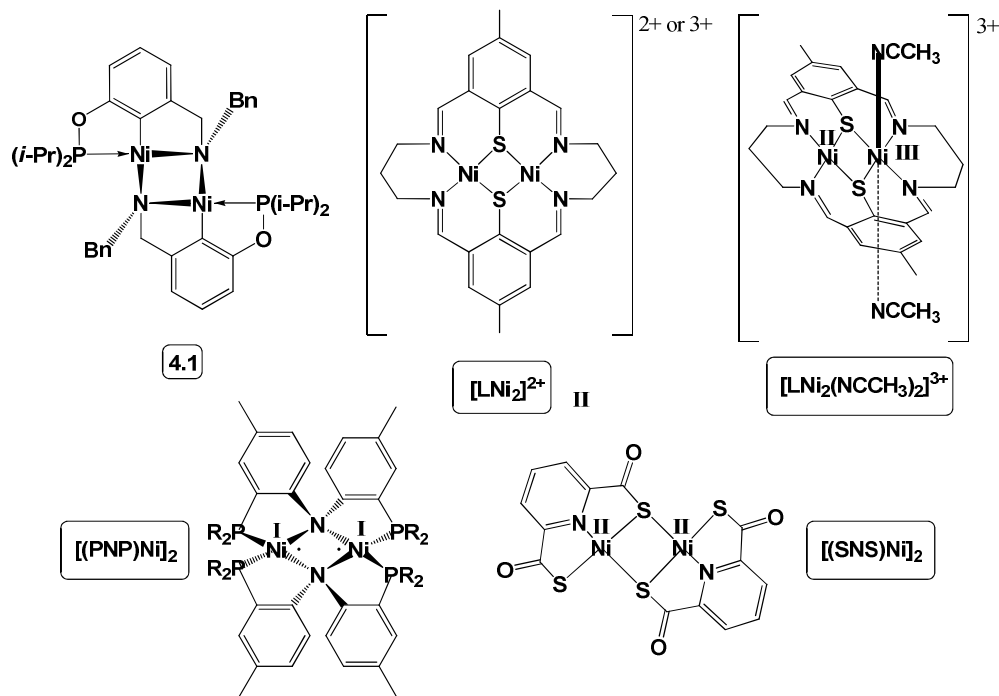


Figure 4.1. Dimeric species **4.1**

Our interest in the chemistry of Ni^{III} pincer complexes^{15e-i} and the relatively facile access to **4.1** prompted us to examine the redox behavior of this dimeric species in order to answer some of the following questions: Would the dimeric structure of **4.1** be preserved upon oxidation? If so, would oxidation take place at both halves of the dimer or just one? In either case, how would the spin density be distributed over the Ni centers and the ligands? The generation of adjacent trivalent centers (or proximate ligand-based radicals) would be expected to give rise to varying degrees of spin-coupling and interesting magnetic properties, while single electron oxidation at nickel would generate a mixed-valent species of localized or delocalized spin density. A combination of spectroscopic, computational, and X-

ray diffraction studies were undertaken to study the electrochemical and chemical oxidation of **4.1**, as reported herein.

4.3 Results and Discussions

4.3.1 Electrochemical oxidation of **4.1**.

Cyclic voltammetry measurements of **4.1** revealed a redox profile (Figure 4.2) that is qualitatively similar to those of its monomeric analogues (POCN)NiBr studied previously¹⁵ⁱ (POCN= 2,6-*i*-Pr₂POC₆H₃CH₂NR₂). This result implies that the observed oxidation of **4.1** is a quasi-reversible, Ni-based, one-electron process,¹⁰ which rules out the possibility that electrochemical oxidation of **4.1** generates a doubly oxidized Ni^{III}/Ni^{III} species or leads to major structural reorganization that might entail collapse of the dimeric structure. The half cell potential $E^{1/2}_0$ of **4.1** (-0.07 V) is much smaller than that of the monomeric amino analogues (POCN)NiBr (ca. +0.60 V for NR₂= NMe₂, NEt₂, and *N*-morpholinyl)¹⁵ⁱ and the above-cited dinickel species [LNi₂]²⁺ (ca. +0.55 V).⁶ The facile oxidation of **4.1** can be attributed to the strongly electron-donating character of the amido moieties as well as the destabilizing (albeit weak) Ni-Ni interactions that would be expected to raise the energy of its HOMO (vide infra).

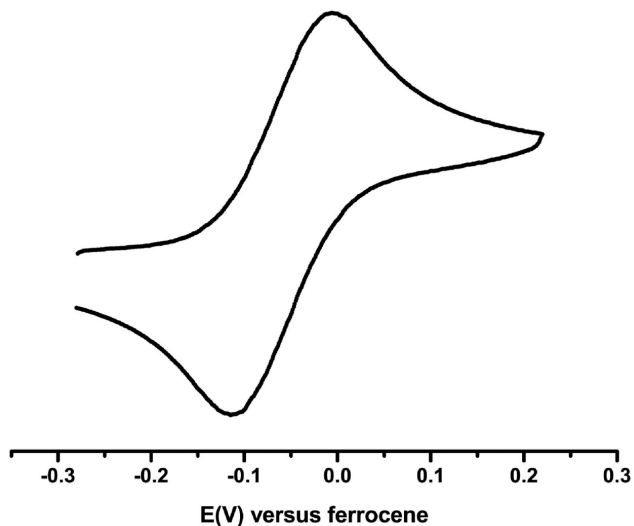
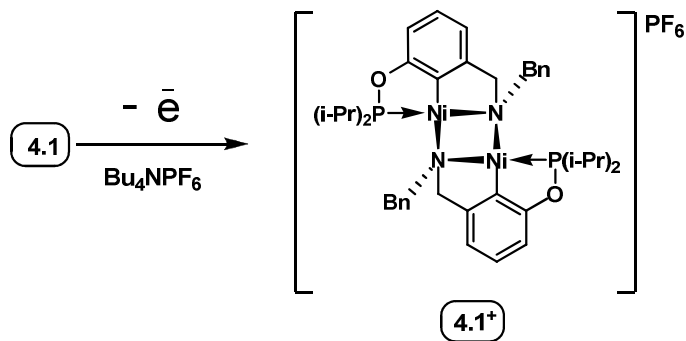


Figure 4.2. Cyclic voltammogram measured at 25 °C for a 1 mM dichloromethane solution of **4.1** containing tetrabutylammonium hexafluorophosphate as supporting electrolyte (0.1 M). The measurements were conducted using a glassy carbon working electrode at a scan rate of 100 mV/s. See Experimental Section for full details on the electrochemical studies.

A spectroelectrochemical investigation of **4.1** was undertaken in an effort to detect the product(s) of its electrochemical oxidation (Scheme 4.1).



Scheme 4.1. Electrochemical oxidation of **4.1**

The electrolysis was carried out at 25 °C and 550 mV over 12 min on a 4 mM dichloromethane (DCM) solution of **4.1** containing (n-Bu)₄NPF₆ as

supporting electrolyte (0.1 M), and observed changes in molar absorbance were monitored by UV-Vis-NIR spectroscopy (Figure 4.3). A gradual darkening of the sample was observed and an intensely dark solution was obtained at the end of the electrolysis. Consistent with the observed color of the solution, the absorption spectrum (Fig. 2b) displayed multiple low-energy transitions in the range of 10000-15000 cm^{-1} ; by comparison, the dinickel species $[\text{LNi}_2]^{3+}$ (Figure 4.1) exhibits a low-intensity absorption band at ca. 11000 cm^{-1} ($\epsilon = 85 \text{ M}^{-1} \text{ cm}^{-1}$),^{6b} whereas the absorption spectra of monomeric complexes $(\text{POCN})\text{Ni}^{\text{III}}\text{Br}_2$ contain only bands higher than 15000 cm^{-1} .¹⁵ⁱ These differences in the absorption spectra imply important structural differences between $[\mathbf{4.1}]^+$ and $(\text{POCN})\text{Ni}^{\text{III}}\text{Br}_2$, suggesting that the dimeric structure of **4.1** survives its electrolytic oxidation. As will be discussed later, computational studies support this assertion and show that electronic transitions from occupied orbitals to the low-lying β -spin LUMO of $[\mathbf{4.1}]^+$ give rise to multiple bands in the near-IR and visible region of its absorption spectrum (vide infra).

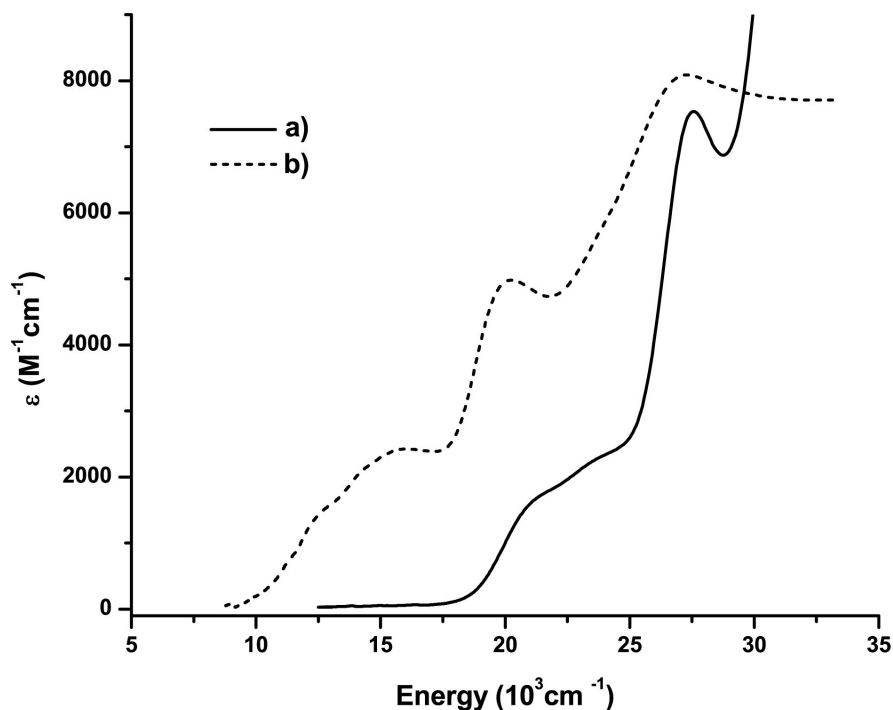
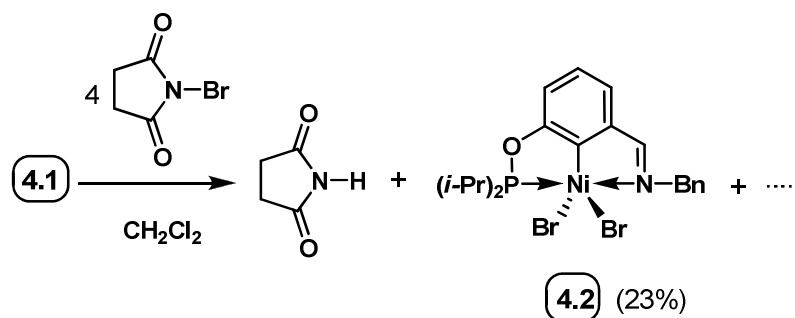


Figure 4.3. Absorption spectra of **4.1** in dichloromethane before (a) and after (b) the electrochemical oxidation at $E_{\text{ox}} = 550 \text{ mV}$.

4.3.2 Chemical oxidation of **4.1**.

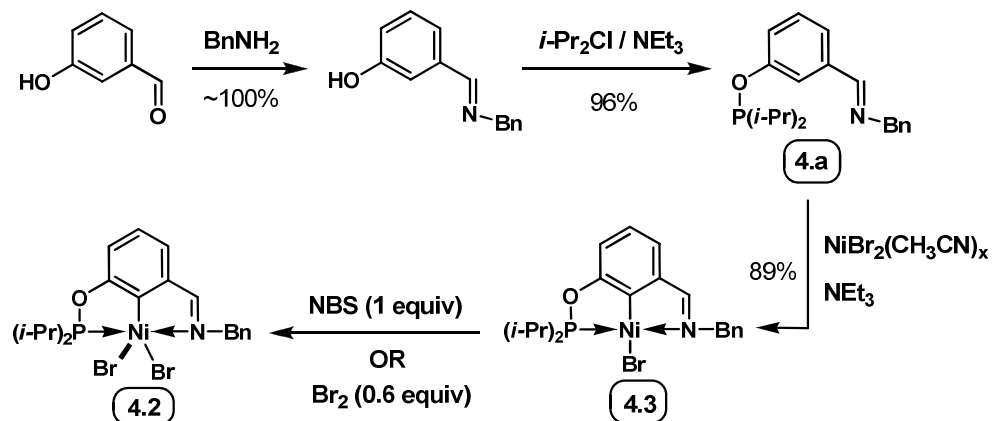
The relatively low oxidation potential of **4.1** and the reversible nature of its redox process encouraged us to attempt a chemical oxidation and isolate the resulting species. Since previous studies had shown that *N*-Bromosuccinimide (NBS) and bromine are suitable oxidants for converting (POCN)NiBr to trivalent species, we investigated the reaction of **4.1** with these oxidants. Portion-wise addition of solid NBS to a concentrated solution of **4.1** in DCM caused an instantaneous darkening of the initially orange solution, and a brown mixture was formed when 2 equiv of NBS had been added; additional NBS resulted in the formation of an increasingly darker reaction mixture. Adding cold hexane to the nearly black reaction mixture containing **4.1** and 4 equiv of NBS resulted in the precipitation of an off-white solid, which was isolated by filtration and identified as succinimide. Storage of the dark filtrate at -18 °C for about one week gave a small crop of purplish-black crystals that were identified as the monomeric Ni^{III} species **4.2** featuring a new, imine-type POCN ligand (Scheme 4.2). The oxidation with bromine also produced **4.2**, but this reaction was less clean, producing a greenish solid that we have not been able to identify.



Scheme 4.2. Chemical oxidation of **4.1**

The observed formation of **4.2** involves oxidation of **4.1** at both the ligand ($\text{ArCH}_2\text{NR} \rightarrow \text{ArCH}=\text{NR}$) and the metal ($\text{Ni}^{\text{II}} \rightarrow \text{Ni}^{\text{III}}$), which raises many questions about how and in which order the individual oxidation steps occur, and whether the entire process proceeds via a cascade-type mechanism or a step-wise mechanism going through observable intermediates. A number of studies have been carried out to answer some of these questions, beginning with the demonstration that the trivalent imine-type species **4.2** can be generated by oxidation of its divalent analogue **4.3**, which was prepared independently as illustrated in

Scheme 4.3. Thus, the requisite imine-type POCN ligand was prepared in two high-yield steps: reaction of benzylamine with 3-hydroxybenzaldehyde gave the corresponding Schiff base, which was then reacted with $(i\text{-Pr})_2\text{PCI}$ in the presence of base to give ligand **4.a** as a colorless oil. Reaction of this new ligand with $\text{NiBr}_2(\text{CH}_3\text{CN})_x$ and NEt_3 gave the corresponding pincer complex **4.3** in good yield, while treatment of the latter with one equivalent of NBS in DCM gave the anticipated oxidation product **4.2** in about 62 % yield; the oxidation gave a much better yield (94%) when 0.6 equiv of Br_2 was used as oxidant. These results demonstrate that the trivalent dibromo species **4.2** can, in principle, arise from its divalent monobromo analogue **4.3**. To determine whether **4.3** is generated during the oxidation of **4.1**, we have examined the reaction of **4.1** with NBS using NMR, EPR, and UV-visible spectroscopy, as described below.

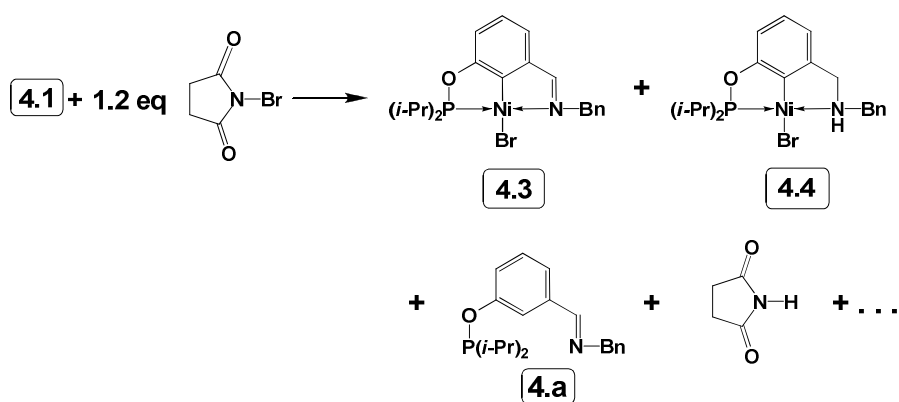


Scheme 4.3. Alternative synthesis of 4.2

4.3.3 Monitoring oxidation of 4.1 by NMR spectroscopy.

A 0.022 M DCM solution of 4.1 containing $\text{O}=\text{PPh}_3$ as internal standard was titrated with a 0.032 M solution of NBS, and the progress of the oxidation reaction was monitored by the changes in the color of the sample and its NMR signals. Thus, an instantaneous darkening of the solution was observed at the point of contact each time an aliquot of NBS was added. The deep brown spot dispersed after 2-3 seconds, but the initial yellow-orange color of the sample darkened gradually to a reddish-brown up to the addition of ca. one equiv of NBS; adding more NBS caused further darkening of the sample, giving a deep-brown/black mixture at the end of the titration. The $^{31}\text{P} \{^1\text{H}\}$ NMR spectrum of the sample containing the first 100 μL aliquot of NBS showed the emergence of a few new peaks in the chemical shift region of ca. 198-202 ppm, whereas subsequent additions of three more aliquots led to increases in the intensities of some of these signals and a commensurate decrease in the intensity of the precursor signal (at δ 193.16 in DCM). Addition of the fifth aliquot (ca. 1.2 equiv of NBS in total) caused complete disappearance of the signal due to the starting material 4.1, while additional aliquots of the oxidant led to a continuous decline

in the signal intensities for all product peaks in comparison to the internal standard (OPPh_3). Finally, addition of the 9-th aliquot (ca. 2.2 equiv of NBS in total) led to a complete disappearance of all ^{31}P signals. The above observations indicate that the oxidation of **4.1** proceeds in two distinct stages. The first, which takes place when less than one equiv of NBS is present in the mixture, involves the initial conversion of **4.1** to an intensely-colored, short-lived species for which no spectral signature was obtained; this species decomposes rapidly to give a few relatively stable and diamagnetic species characterized by the appearance of a less intense color and the emergence of new and persistent ^{31}P signals. Close inspection of the $^{31}\text{P}\{^1\text{H}\}$ NMR spectra showed two major peaks at ca. 202 ppm, very close to the chemical shift region for the ^{31}P signals of the divalent imine-type complex **4.3** (ca. 201.9 ppm in DCM) and the analogous $\text{N}(\text{Bn})\text{H}$ complex **4.4** shown in Scheme 4.4 (202.0 ppm in DCM). These assignments were confirmed later when we noted increases in the intensity of the corresponding NMR signals upon addition of authentic samples of each of **4.3** and **4.4** to solutions containing **4.1** and 1.2 equiv of NBS. The ^1H NMR spectra recorded for samples containing 1equiv each of NBS and **4.1** in dry C_6D_6 were also consistent with the formation of **4.3** (e.g., PhCH_2N and $\text{CH}=\text{N}$ signals at ca. 4.9 and 7.3 ppm, respectively) and **4.4** (e.g., characteristic NH and PhCH_2 signals at 3.2–4.8 ppm).



Scheme 4.4. Monitoring chemical oxidation by NMR

The ^1H NMR spectra also contained the characteristic signals for succinimide and, curiously, the free ligand $\text{PhCH}_2\text{N}=\text{CH}(\text{C}_6\text{H}_4)\text{OP}(i\text{-Pr})_2$ (Scheme 4.4). The next stage of the oxidation, which occurs when the reaction mixture contains more than one equiv of NBS, is characterized by a significant darkening of the sample and the gradual disappearance of all ^{31}P signals, implying the formation of paramagnetic species.

4.3.4 Detection of oxidation products by EPR spectroscopy.

While NMR provides insight into the diamagnetic products of the oxidation reaction, EPR can be used to detect the paramagnetic products. The samples used for the EPR measurements were prepared by dissolving different quantities of NBS in 0.22 mM toluene solutions of **4.1** and the resulting mixtures were kept at ambient temperature for approximately 10 min before being degassed by repeated freeze-pump-thaw cycles and cooled to 120 K in the EPR spectrometer. It is important to note that variations in mixing time or NBS content (up to 3 equiv) did not affect the EPR spectrum.

The EPR spectrum of this sample (Figure 4.4A) is typical of Ni^{III} pincer compounds possessing axial halogen ligands;^{11,15i} therefore, we have simulated it on this basis. The simulation includes an anisotropic g-tensor and hyperfine coupling to one spin 3/2 nucleus; all other hyperfine couplings are simulated as an anisotropic Gaussian linewidth. The simulation shows that the g-tensor has principal values of $g_{xx}=g_{yy} = 2.22$ and $g_{zz} = 2.01$. Arrows above the spectrum indicate the positions of features corresponding to these g-values. The hyperfine coupling constants to the spin 3/2 nucleus are found to be $A_{xx}=A_{yy}= 30$ G and $A_{zz} = 170$ G; the features resulting from the large A_{zz} component of the splitting are also indicated in Figure 4.4A. The feature at ~2950 G is the so-called “anomalous line” which occurs when one of the hyperfine components is similar in magnitude to the g-anisotropy.¹² The g-values and hyperfine couplings obtained from the simulation are consistent with a Ni^{III} complex possessing an axial Br ligand. Note

that the simulation does not take the difference in magnetic moment between ^{79}Br and ^{81}Br into account and the reported couplings therefore represent an average of the coupling for the two isotopes. Additional smaller hyperfine splittings are visible in the experimental spectrum between ~ 3250 G and 3500 G indicating that the other atoms bound to the Ni^{III} center have non-zero nuclear spin.

The experimental and simulated EPR spectra for **4.2** (0.22 M solution in toluene, 120 °K) are shown in Figure 4.4A. The similarity of spectra A and B in Fig. 3 suggests that **4.2** is the main oxidation product observed *in situ*. However, careful inspection of the two spectra reveals some subtle differences. For example, the trough near ~ 3100 G is shifted upfield in the spectrum of **4.2** by ~ 20 G compared to the spectrum of the oxidation reaction mixture. This difference can be accounted for in the simulation by a small shift of the in-plane components of the g-tensor to $g_{xx}=2.23$ and $g_{yy}=2.19$. Slightly more pronounced hyperfine structure, probably due to Br, is also visible at ~ 3000 G in the spectrum of **4.2**. The origin of these differences is uncertain but might be expected if the oxidation reaction mixture contained minor amounts of other Ni^{III} species. We note that the spectrum does not show evidence for any organic radicals indicating that any such species produced by the oxidation are unstable.

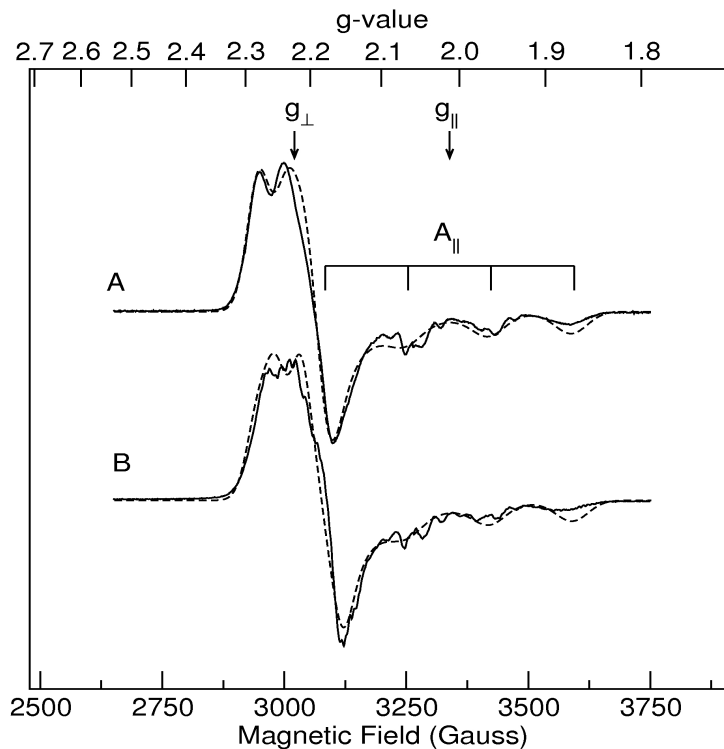


Figure 4.4. X-band (9 GHz) EPR spectra (toluene, 120 K) of the oxidation product(s) of **4.1** with 1 equiv of NBS (A) and compound **2** (B). The solid lines are experimental spectra, the dashed curves are simulations. Simulation parameters A: $g_{xx}=g_{yy}=g_{\perp}=2.22$, $g_{zz}=g_{\parallel}=2.01$, $I=3/2$ nucleus $A_{xx}=A_{yy}=A_{\perp}=30$ G, $A_{zz}=170$ G; B: $g_{xx}=2.23$, $g_{yy}=2.19$, $g_{zz}=2.01$, $I=3/2$ nucleus $A_{xx}=A_{yy}=30$ G, $A_{zz}=170$ G. Microwave frequency: 9.401599 GHz; microwave power: 2 mW; modulation amplitude: 1.0 G.

4.3.5 UV-Vis studies on oxidation of complexes **4.1**, **4.3**, and **4.4** with NBS.

To complement the NMR and EPR studies discussed above, we have used UV-Vis spectroscopy with the objective of identifying the paramagnetic intermediates/products involved in the oxidation of **4.1**. UV-Vis spectra were first recorded for all the complexes as well as the mixtures obtained from NBS oxidation of the divalent species in order to compare the spectral profiles to one another. Not unexpectedly, the spectrum of independently prepared **4.2** was

virtually identical to the spectrum recorded for the mixture of **4.3** and NBS, and closely resembled the spectral profile of the mixture of **4.1** and NBS (Figure 4.5). Interestingly, a similar spectrum was also obtained for the mixture of **4.4** and NBS (Figure 4.5d), but in this case the oxidation product had a limited stability and decomposed over ~5 min to an intractable green species. It is also noteworthy that under similar conditions the NBS oxidation proceeds much more rapidly for **4.1** and **4.4**. Finally, the spectra obtained for the trivalent complex **4.2** and the oxidation mixtures display multiple electronic transitions extending across the visible region (ca. 15000-28000 cm^{-1} , Figure 4.5), whereas the divalent complexes display absorption bands above ca. 20000 cm^{-1} (Figure 4.6).

To monitor the course of the oxidation reaction, we titrated a 0.4 mM DCM solution of **4.1** (initial volume 2.50 mL) at ambient temperature with 50 μL aliquots of a 4 mM NBS solution and the spectra were recorded 20 s after addition of each aliquot. The spectral profile for the entire titration (Figure 4.7) confirms the conclusions drawn from the NMR studies: the oxidation reaction takes place over two stages, each corresponding to the addition of 5-6 aliquots of NBS (approximately one equiv); beyond the 11-th aliquot (550 μL , ca. 2.1 equiv of NBS), the spectral profile remained fairly invariable and very similar to the absorption spectrum observed for complex **4.2** (Figure 4.5c).

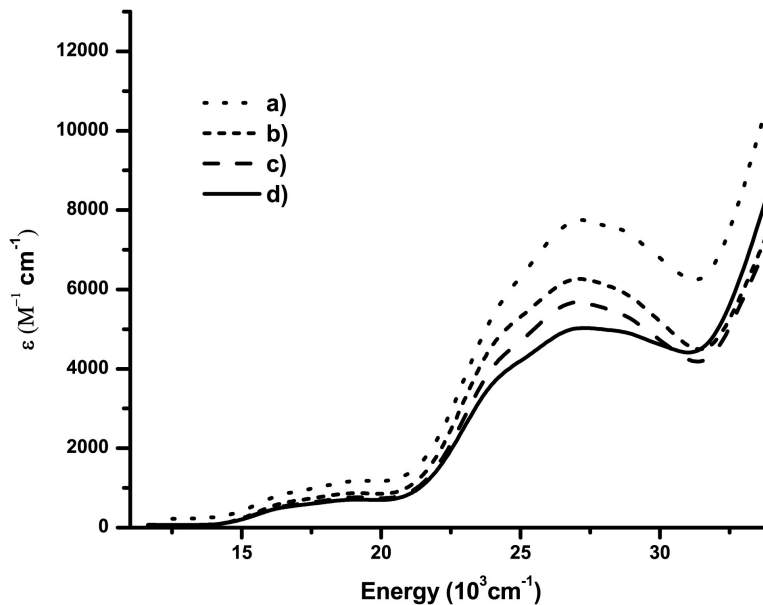


Figure 4.5. UV-Vis spectra of nickel complexes (0.4 mM in DCM, 25 °C) with or without NBS: (a) **4.1** + 4 equiv NBS; (b) **4.3** + **4.4** + 1.1 equiv NBS; (c) complex **4.2** alone; (d) **4.4** + 1.1 equiv NBS.

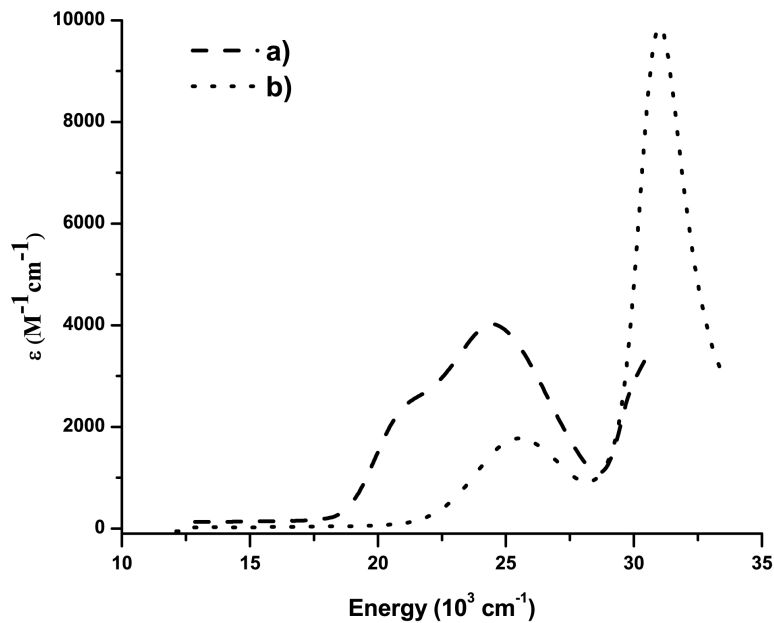


Figure 4.6. UV-Vis spectra (25 °C) of the divalent complexes **4.3** (a) and **4.4** (b); both samples ca. 0.4 mM.

Evolution of the spectral profile for the oxidation of **4.1** can be seen more clearly by examining the set of spectra corresponding to each of these two distinct stages of the titration. Thus, we can see in Figure 4.8 that addition of the first few aliquots of NBS results in a steady decrease in the intensities of the bands belonging to **4.1** (ca. 21000, 27500, and 31000 cm^{-1}), while a new band emerges gradually at ca. 24000-26000 cm^{-1} . Significantly, the absorbance remains fairly constant at ca. 26000 cm^{-1} during this stage of the reaction, but no clear isosbestic point was evident; this is consistent with the initial formation of an unstable intermediate. Beyond the first equiv of NBS (>5 aliquots, Figure 4.9), there is a continued decline of the high-energy absorption at ca. 31000 cm^{-1} and a steady growth of multiple, poorly resolved bands at ca. 15000-20000 and 22000-27000. In contrast to what was observed in the first stage of the oxidation, a fairly clear isosbestic point is found during the second stage (at ca. 30000 cm^{-1} , Figure 4.9), implying a direct and intermediate-free transformation.

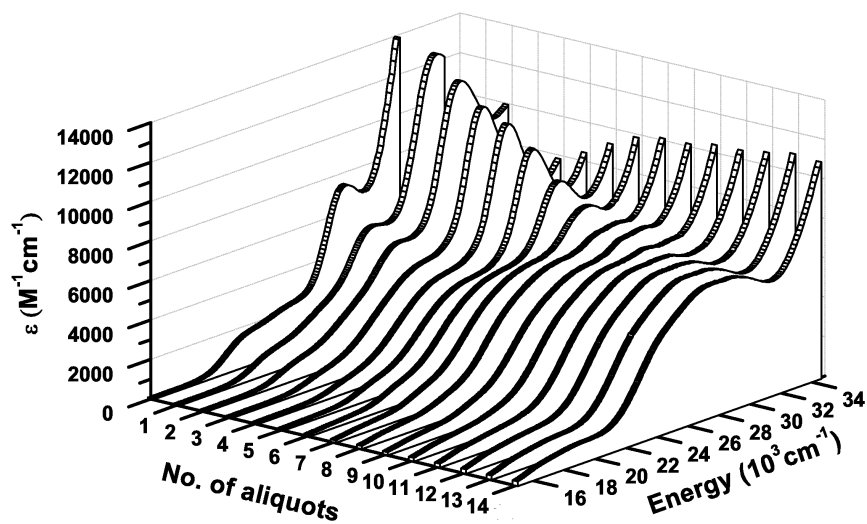


Figure 4.7. UV-Vis spectra (25 °C) of **4.1** (2.5 mL of a 0.4 mM solution in DCM, spectrum 0) with 50 μL aliquots of a 4 mM solution of NBS in DCM (spectra 1-14).

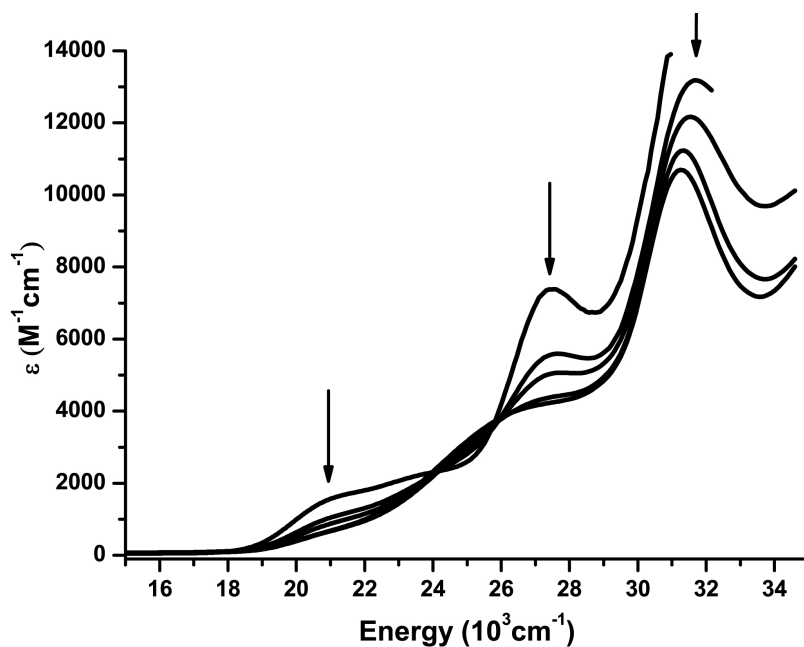


Figure 4.8. UV-Vis spectra (25 °C) recorded during the initial stage of the titration of **4.1** with NBS. See main text for titration details.

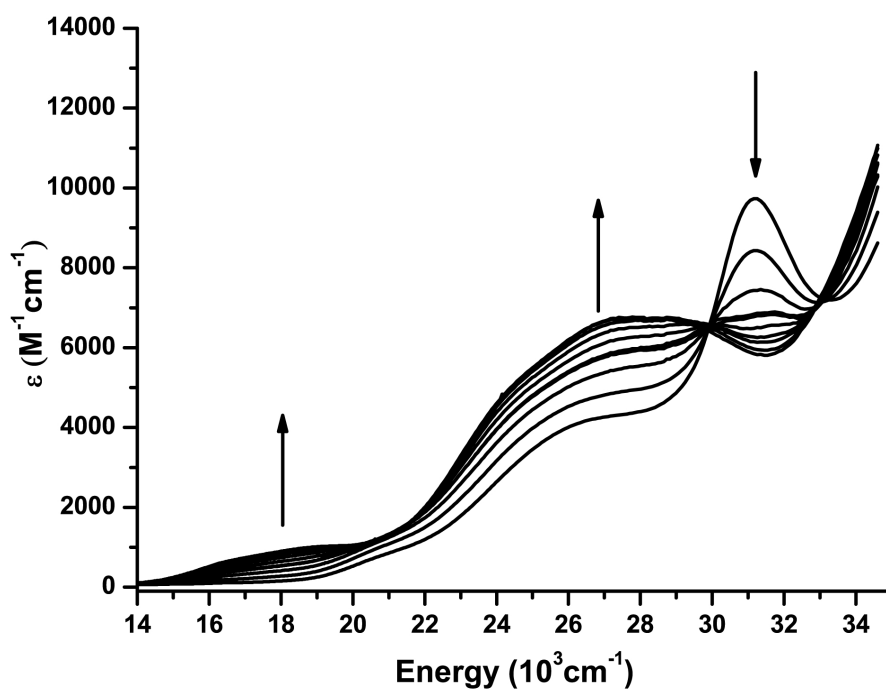


Figure 4.9. UV-Vis spectra (25 °C) recorded during the second stage of the titration of **4.1** with NBS. See main text for titration details.

4.3.6 Computational studies.

Full molecular structures of **4.1** and **[4.1]⁺** have been investigated using density functional theory (DFT) at the B3LYP¹³/TZVP¹⁴ level of the theory, their absorption spectra have been predicted using time-dependent DFT (TD-DFT),¹⁵ and the results compared to the corresponding experimental data. These studies have corroborated the proposed (dimeric) structure of **[4.1]⁺** and provided valuable details on the energies and compositions of the frontier molecular orbitals and spin density distribution in the open shell species arising from the oxidation of **4.1**, as described below.

4.3.6.1 Calculated structures of **4.1** and **[4.1]⁺**.

The calculated structure of **4.1** is in very good agreement with the solid state structure of this compound, which has been established by single crystal diffraction study.^{15j} For instance, the puckered (or cyclobutane-like) arrangement of the Ni₂N₂ core and the *syn* orientation of the *N*-benzyl substituents observed in the solid state structure of **4.1** are reproduced in the calculated structures; more specifically, the angle between two Ni₂N planes is 124° in the X-ray structure of **4.1** and 121.4° in the computed structures of **4.1** and **[4.1]⁺**. There is also good agreement between the experimentally observed (2.512(1) Å) and calculated (2.523 Å) Ni-Ni distances in **4.1**; moreover, the computed bond order (0.13) indicates very little metal-metal interaction in this compound, as can be expected for low-spin d⁸ Ni^{II} ions. On the other hand, a significantly shorter Ni-Ni distance (2.393 Å) and greater bond order (0.43) were found in **[4.1]⁺**, resulting from the diminished occupancy of the Ni-Ni σ* orbital in the oxidized species that reduces the destabilizing character of this interaction.

The shorter Ni-N distances in the experimentally established and calculated structures of **4.1** correspond to the Ni and N atoms belonging to

different halves of the dimer; this structural feature reflects the stronger covalency of the Ni-N bonds between different halves of the dimer (bond order 0.56) vs. those belonging to the same halves (bond order 0.47). In the calculated structure of **[4.1]⁺**, the corresponding bond orders are slightly greater (0.64 and 0.53, respectively) and the Ni-N distances are somewhat shorter (1.985/1.997 vs. 2.006/2.027). The opposite trend was observed for the Ni-C and Ni-P bonds, which were found to be the most covalent metal-ligand bonds (calculated bond orders 1.00 and 0.93, respectively). Thus, the calculated Ni-C distances were 1.885 Å in **4.1** (vs. 1.864(2) Å in the solid state structure) and 1.894 Å in **[4.1]⁺**; the corresponding Ni-P distances were 2.203 Å in **4.1** (vs. 2.122(1) Å in the solid state structure) and 2.268 Å in **[4.1]⁺**. These results can be understood in terms of HSAB theory: the greater compatibilities between a “softer” Ni^{II} ion in **4.1** (NPA-derived charge +0.70 a.u.) and “soft” phosphinite and aryl ligands should lead to more covalent bonds, while the “harder” character of the nickel ions in **[4.1]⁺** (NPA-derived charge +0.84 a.u.) should favor stronger interactions with the “hard” amido ligands. Altogether, the valence index for the Ni atoms is 3.16 in **4.1** and 3.74 in **[4.1]⁺**.

Inspection of the frontier molecular orbitals for **4.1** and **[4.1]⁺** (Figure 4.10 and Figure 4.11) and their compositions and energies (Table 4.1) has allowed us to evaluate the impact of oxidation on the electronic structure of **4.1** and to map out the spin density distribution in the oxidized species. Complete valence delocalization of the Ni₂N₂ core in **[4.1]⁺** is implied from the symmetrical spin density distribution (0.77 e⁻ from two Ni atoms and 0.29 e⁻ from two bridging N atoms, Figure 4.10a); therefore, complex **[4.1]⁺** represents a class III mixed-valence system¹⁶ (Ni^{+2.5}₂N₂) analogously to the oxidized binuclear Cu_A center in bio-inorganic chemistry (Cu^{+1.5}₂S₂).^{4b,h} The observation of symmetrical spin density distribution in these bimetallic systems stands in contrast to the localized spin density distribution reported for [LNi^{II}Ni^{III}(NCCH₃)₂]³⁺ (Figure 4.1).⁷

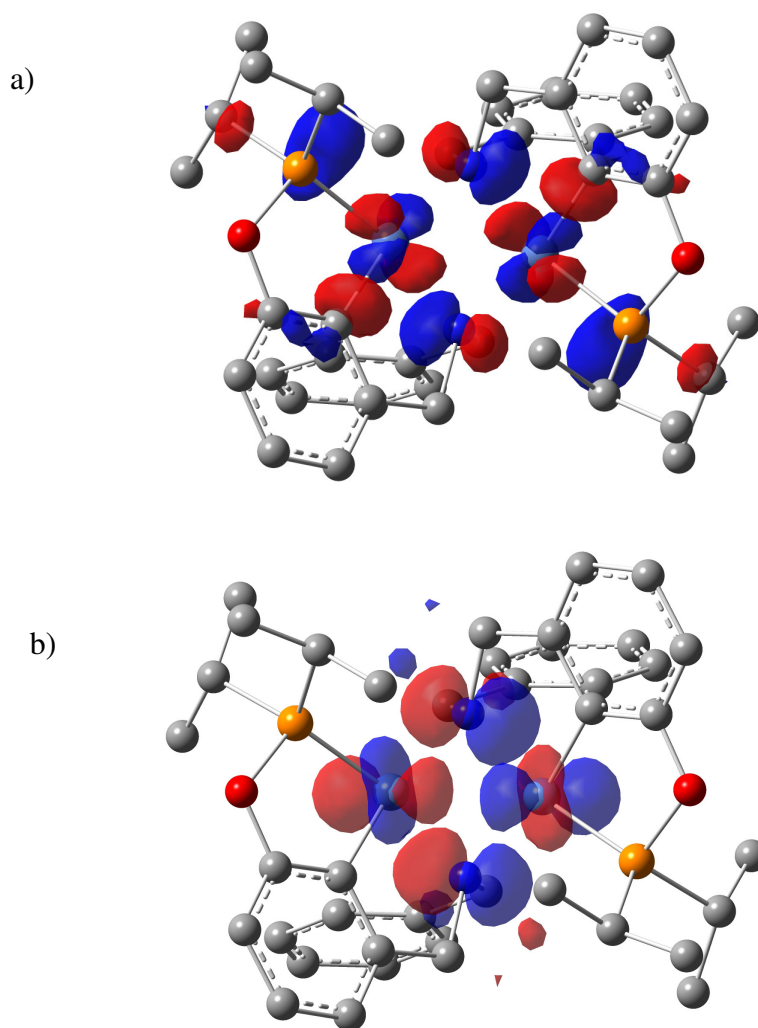
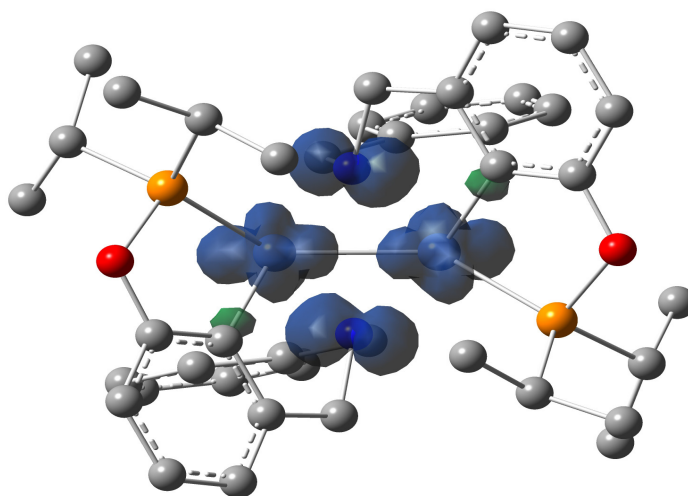
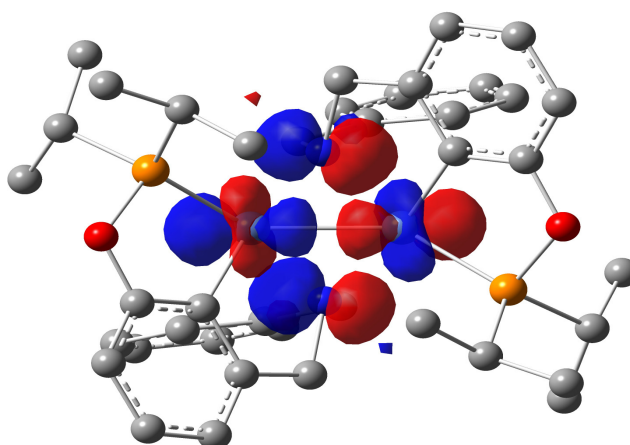


Figure 4.10. Frontier molecular orbitals of **4.1**: LUMO (a) and HOMO (b). Isosurface value of 0.04 a.u. Spheres are coloured to signify the atoms in keeping with convention: grey for carbon, blue for nitrogen, orange for phosphorus, red for oxygen, light-blue for nickel. H atoms are not shown for clarity.

a)



b)



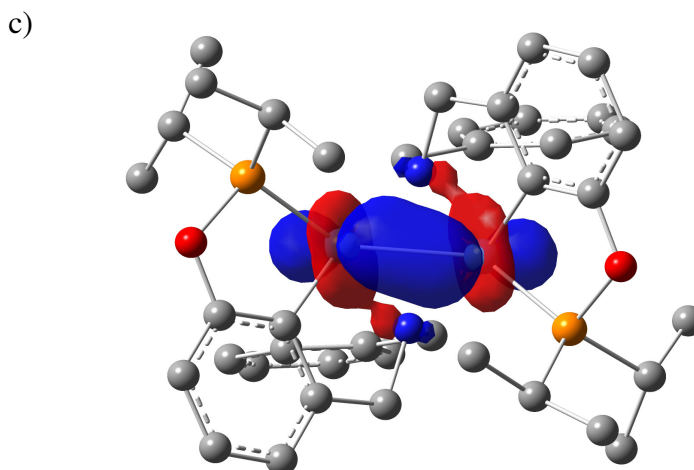


Figure 4.11. Spin density and frontier molecular orbitals of $[4.1]^+$: spin density (a; isosurface value of 0.004 a.u.), β -spin LUMO (b; isosurface value of 0.04 a.u.), β -spin HOMO-10 (c; isosurface value of 0.04 a.u.). Spheres are coloured to signify the atoms in keeping with convention: grey for carbon, blue for nitrogen, orange for phosphorus, red for oxygen, light-blue for nickel. H atoms are not shown for clarity.

Table 4.1. Spin-allowed absorption bands calculated for **4.1** and **[4.1]⁺**.^a

4.1			[4.1]⁺		
Energy (cm ⁻¹)	<i>f^b</i>	Assignment	Energy (cm ⁻¹)	<i>f^b</i>	Assignment
18700	0.0046	HOMO→ LUMO (56%)	6400	0.0003	β-HOMO-4→ LUMO (55%)
19000	0.0010	HOMO→ LUMO+1 (58%)	6700	0.0027	β-HOMO-3→ LUMO (55%)
21000	0.0081	HOMO-3→ LUMO (35%)	8000	0.0019	β-HOMO-13→ LUMO (31%) β-HOMO-10→ LUMO (30%)
24300	0.0143	HOMO-9→ LUMO (25%)	10800	0.0596	β-HOMO-10→ LUMO (38%)
29600	0.0611	HOMO→ LUMO+2 (74%)	11500	0.0020	β-HOMO-12→ LUMO (64%)
			13500	0.0047	β-HOMO-2→ LUMO (28%) β-HOMO→ LUMO (25%)
			14300	0.0020	β-HOMO-2→ LUMO (66%)
			15500	0.0090	β-HOMO-7→ LUMO (22%) β-HOMO-13→ LUMO (21%)

^aTransitions in the near-IR, visible and near-UV region (6,000–30,000 cm⁻¹ for **4.1** and up to 16000 cm⁻¹ for **[4.1]⁺**), calculated at the B3LYP/TZVP level of theory. Excitation contributions greater than 10% are shown, smaller contributions are omitted. ^b*f* = oscillator strength. The complete list of calculated transitions can be found in the Supporting Information.

Table 4.2. Frontier molecular orbital energies and compositions (%) for **4.1** and **[4.1]⁺**.

	Energy (eV)	Ni	N	P
4.1				
LUMO+2	-0.49	16	3	18
LUMO+1	-0.86	44	10	23
LUMO	-1.12	40	11	21
HOMO	-5.08	55	28	2
HOMO-3	-5.70	71	10	4
HOMO-9	-6.47	77	10	5
[4.1]⁺				
β-LUMO	-6.57	68	20	3
β-HOMO	-8.72	7	0	1
β-HOMO-1	-8.81	8	0	1
β-HOMO-2	-8.97	0	0	0
β-HOMO-7	-9.28	3	3	0
β-HOMO-3	-8.98	17	10	0
β-HOMO-10	-9.63	85	13	1
β-HOMO-13	-10.36	72	9	3

In order to probe the influence of axial ligation on spin density distribution in our system, we constructed a smaller model featuring *N*-Me substituents and performed structure optimization for oxidized species bearing either an axial Br ligand attached to one Ni, $(\mu\text{-L})_2\text{Ni}_2\text{Br}$, or a positive charge (analogously to **[4.1]⁺**). Analysis of the electronic structures of these models showed that the latter species has a more symmetrical spin density distribution on the Ni_2N_2 core: 0.26 e^- on each N and 0.23 \bar{e} on each Ni. In contrast, the spin density distribution is entirely localized on the Ni-Br_{ax} moiety of the neutral species $(\mu\text{-L})_2\text{Ni}_2\text{Br}$, with 0.82 \bar{e} on Ni (d_{z^2}) and 0.20 \bar{e} on Br (p_z), which implies that the bimetallic core in this species can best be described as $\text{BrNi}^{\text{III}}\text{N}_2\text{Ni}^{\text{II}}$. The Ni-Br_{ax} bond in this model was found to be quite long (2.547 Å), which is anticipated on the basis of theoretical considerations and consistent with experimental values observed in solid state structures of related pentacoordinate, 17-electron complexes (pincer)NiBr₂ (Ni-Br_{ax}~2.43-2.46 Å).^{15e-i} It appears, therefore, that the spin distribution in these dinickel complexes is highly sensitive towards changes in the ligand environment around the Ni ions. This is in sharp contrast to behaviour of systems with the softer Cu_2S_2 core where high covalency of Cu-thiolate bonds ensures high stability of spin distribution.^{4h}

4.3.6.2 Calculated absorption spectra for **4.1** and **[4.1]⁺**.

The calculated spectra for **4.1** and **[4.1]⁺** are depicted in Figure 4.12, while the spectral details (energies, probabilities, and assignments of bands) are listed in Table 2. The lowest-energy, spin-allowed absorption transition found in the predicted spectrum for **4.1** at 18,700 cm^{-1} is due principally to an electronic transition from the metal-based HOMO to the metal-based LUMO. This transition overlaps with two other transitions, a weak HOMO→LUMO+1 transition at 19000 cm^{-1} and a stronger HOMO-3→LUMO transition at 21000 cm^{-1} , to form a single band at 20500 cm^{-1} with a shoulder at 18,700 cm^{-1} . The second intense band (at 24300 cm^{-1}) is due to the HOMO-9→LUMO transition. For comparison, the corresponding transitions in the experimental spectrum of **4.1** are manifested

by poorly resolved bands at ca. 19000-21000 and 22500-25000 cm^{-1} , respectively (Figure 4.3). In all these transitions, the donor and acceptor orbitals are located primarily on the Ni_2N_2 cluster. A very intense band due to the HOMO \rightarrow LUMO+2 (π^*) transition is also present in the predicted and experimental spectra, at 29,600 and ca. 27500 cm^{-1} , respectively.

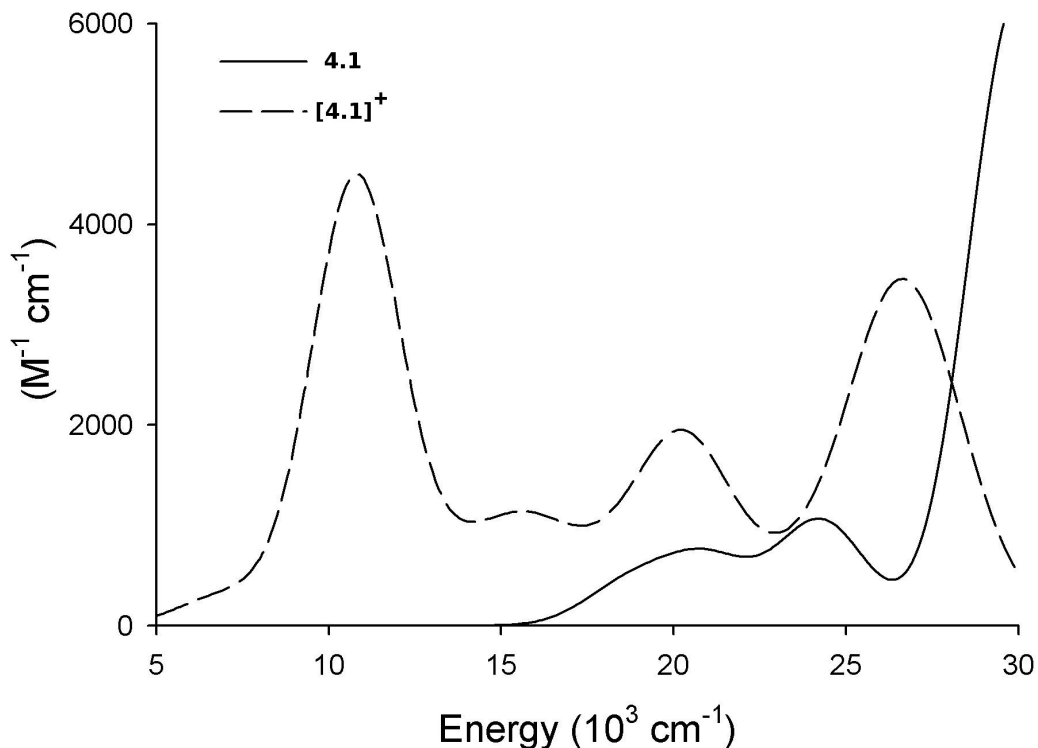


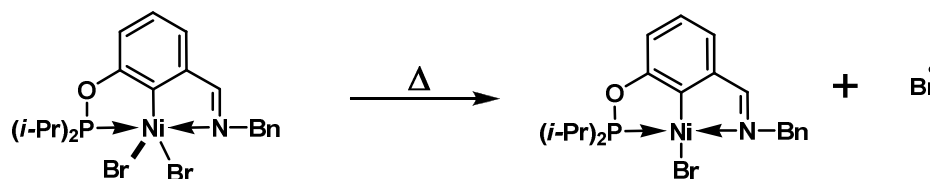
Figure 4.12. TD-DFT-calculated visible absorption spectra of **4.1** (solid line) and **[4.1]⁺** (dash line), calculated at the B3LYP/TZVP level of theory.

Recall that conversion of **4.1** to **[4.1]⁺** involves the removal of an electron from the HOMO (Figure 4.10) and generation of a σ^{*1} ground state configuration featuring a low-energy vacant orbital (β -spin LUMO, Figure 4.11b). This leads to low-energy transitions from the fully-occupied orbitals to the β -spin LUMO, these transitions appearing in the near-IR and visible region of the absorption spectrum of **[4.1]⁺** (Figure 4.12, Table 4.2). The transition from the bonding β -spin HOMO-10 (Ni $d_{z^2} + d_{z^2}$, Figure 4.11c) to the β -spin LUMO is the main

component of the intense absorption band at $10,800\text{ cm}^{-1}$ in the predicted spectrum of $[\mathbf{4.1}]^+$, but a few minor contributions are also found for this transition (Table 4.2).

4.3.7 Characterization of **4.2** and **4.3** by NMR and X-ray diffraction analysis.

Complete characterization of the dimeric complex **4.1** and its monomeric precursor **4.4** has been described previously. This section describes the characterization of complexes **4.2** and **4.3** by single crystal X-ray crystallography and elemental analysis; paramagnetic **4.2** was also analyzed by EPR studies, while the diamagnetic complex **4.3** was characterized by NMR spectroscopy. The $^{31}\text{P}\{^1\text{H}\}$ NMR spectrum of **4.3** (C_6D_6) displays a singlet at 201.4 ppm (201.9 ppm in DCM), downfield of the signals for the free ligand (149 ppm) and **4.1** (191.6 ppm), and very close to the corresponding signal for complex **4.4** (201.7 ppm in C_6D_6 , 202.0 ppm in DCM). The ^1H NMR of this sample showed a singlet at ca. 4.9 ppm for PhCH_2N and a doublet at ca. 7.3 ppm for $\text{CH}=\text{NBn}$ ($^4J_{\text{H-P}} = 4\text{ Hz}$), whereas the $^{13}\text{C}\{^1\text{H}\}$ NMR spectrum showed a doublet at ca. 172 ppm for $\text{CH}=\text{N}$ ($^3J_{\text{C-P}} = 3\text{ Hz}$). As expected, fresh samples of **4.2** were NMR silent, but over time a $^{31}\text{P}\{^1\text{H}\}$ NMR signal was detected at ca. 201 ppm in the spectrum, indicating that this trivalent species undergoes thermal decomposition to form its divalent analogue **4.3** (Scheme 4.5).



Scheme 4.5. Thermal decomposition of **4.2**

The experimental and simulated EPR spectra of a 0.22 M solution in toluene at 120 °K **4.2** are shown in Fig. 4.4B. The simulation parameters are very similar to those obtained for the species generated *in situ* from oxidation of **4.1** (spectrum A in Fig. 3), but careful inspection of the two spectra reveals that the trough near ~3100 G is shifted upfield in the spectrum of **4.2** by ~20 G. The simulation shows that this is because the g-tensor of **4.2** is not axially symmetric and has $g_{xx}=2.23$ and $g_{yy}=2.19$. Slightly more pronounced hyperfine structure, probably due to Br, is also visible at ~3000 G suggesting a possible difference in the ligands or their geometry in the *in situ* oxidation product.

Suitable single crystals were obtained for complexes **4.2** and **4.3** and subjected to single crystal diffraction analyses; the ORTEP diagrams are shown in Figure 12, while selected crystal data and structural parameters are listed in Tables 3 and 4. The nickel center in complex **4.3** adopts a nearly perfect square planar geometry, thanks primarily to the planar configuration adopted by the CH=NBn moiety. The sp²-hybridized and less sterically encumbered imine moiety also forms a shorter bond to the Ni center in comparison to the corresponding distance in previously reported POCN-type complexes featuring amine moieties (1.990 vs. ca. 2.030 Å).¹⁵ⁱ Complex **4.2** displays a square pyramidal geometry where the phosphinito moiety is slightly outside of the plane defined by the atoms C, Ni, and N and the aromatic ring; this is a generally observed deformation that can be attributed to the partially filled dz² orbital and steric repulsions between the P-substituents and the lone pairs of the axial bromine atom. A slight pyramidal distortion is also apparent from a) the out-of-plane displacement of the Ni center in **4.2** (by ca. 0.35 Å) from the basal plane defined by the atoms P1, C1, N1, and Br1, and b) the C(1)-Ni-Br(1) angle that is much smaller in **4.2** than **4.3** (155° vs. 171°). Moreover, the pentacoordinate Ni^{III} center forms significantly longer bonds with C1 and P. Similar pyramidal distortions and stretched bonds were also observed when divalent (POCN)NiBr complexes were converted into the trivalent congeners (POCN)NiBr₂.¹⁵ⁱ

Figure 4.13. ORTEP diagrams for complex **4.2** (a) and **4.3** (b). Thermal ellipsoids are set at the 50% probability level. Hydrogen atoms are omitted for clarity.

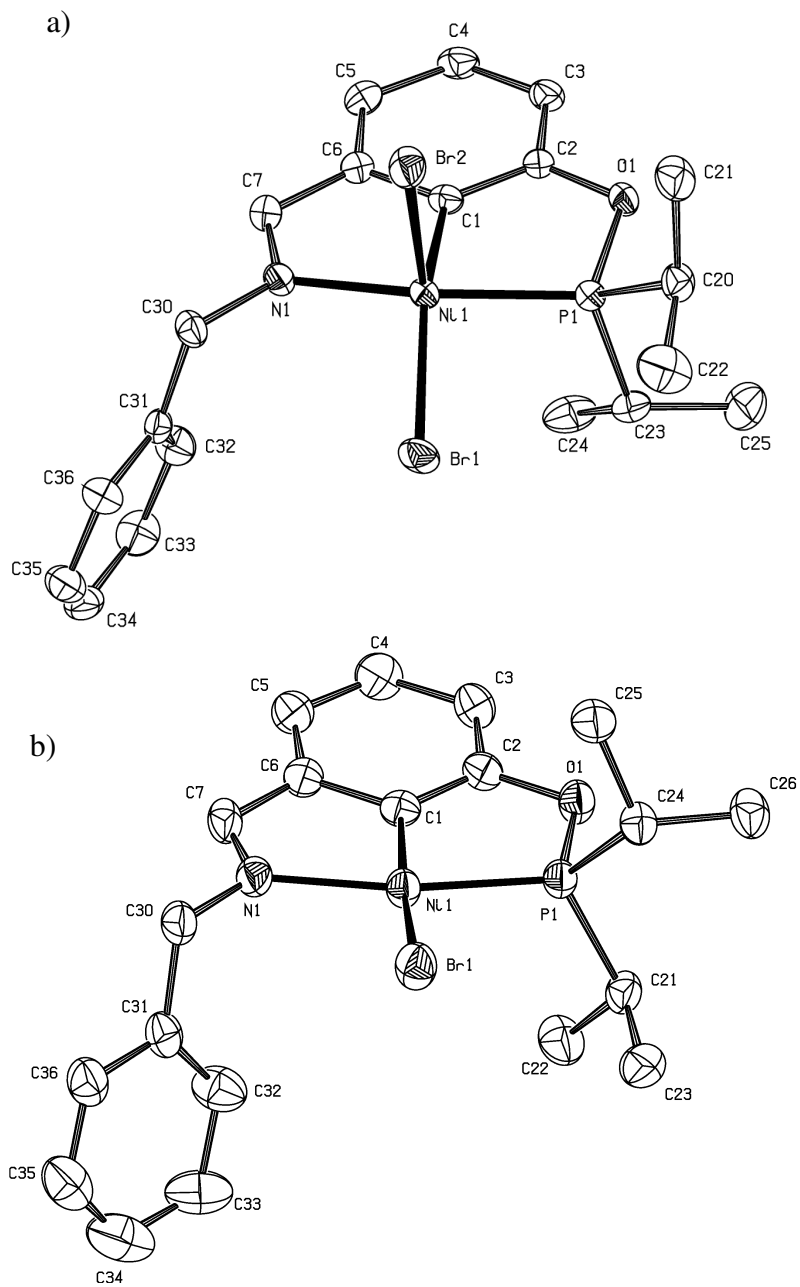


Table 4.3. Crystal Data Collection and Refinement Parameters for Complexes **4.2** and **4.3**.

	4.2	4.3
chemical formula	C ₂₀ H ₂₅ NiPNOBr ₂	C ₂₀ H ₂₅ NiPNOBr
<i>F</i> w	546.93	464.99
<i>T</i> (K)	150	150
wavelength (Å)	0.71073	1.54178
space group	P2 ₁ /n	P2 ₁ /c
<i>a</i> (Å)	8.4257(8)	10.0435(2)
<i>b</i> (Å)	26.053(3)	42.5527(7)
<i>c</i> (Å)	10.051(1)	14.9885(2)
α (deg)	90	90
β (deg)	106.6550(1)	107.425(1)
γ (deg)	90	90
<i>Z</i>	4	12(<i>Z</i> '=3)
<i>V</i> (Å ³)	2113.8(4)	6111.79(2)
ρ _{calcd} (g cm ⁻³)	1.719	1.584
μ (cm ⁻¹)	47.84	45.14
θ range (deg)	1.56–27.54	2.08–72.78
R1 ^a [<i>I</i> > 2σ(<i>I</i>)]	0.0208	0.0656
wR2 ^b [<i>I</i> > 2σ(<i>I</i>)]	0.0450	0.1641
R1 [all data]	0.0288	0.0688
wR2 [all data]	0.0464	0.1658
GOF	0.959	1.139

^a $R_1 = \frac{\sum(|F_o| - |F_c|)}{\sum|F_o|}$

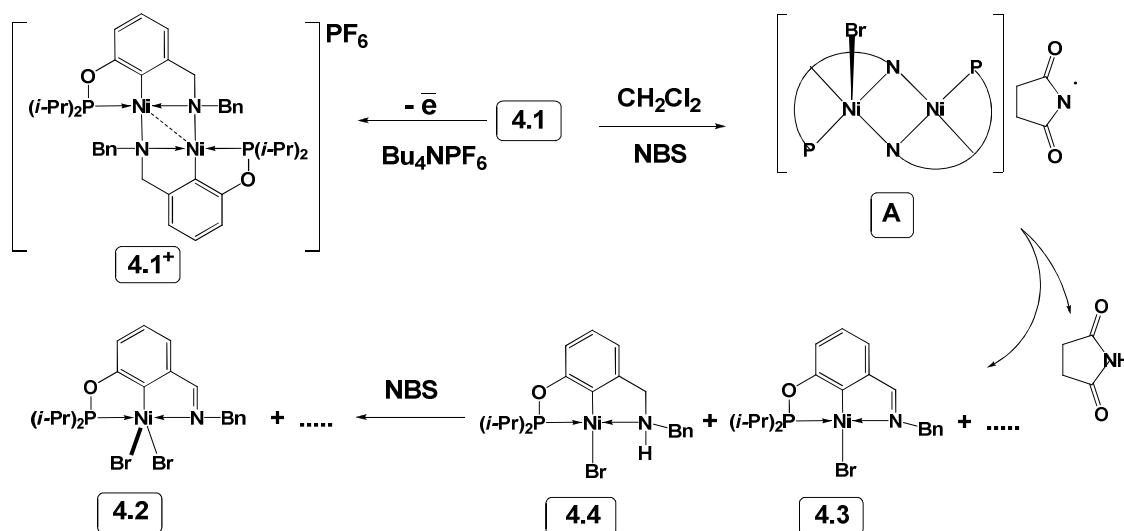
^b $wR_2 = \left\{ \frac{\sum[w(F_o^2 - F_c^2)^2]}{\sum[w(F_o^2)^2]} \right\}^{1/2}$

Table 4.4. Selected Bond Distances (Å) and Angles (deg) for Complexes **4.2** and **4.3**

	4.2	4.3
Ni-C(1)	1.896(2)	1.860(5)
Ni-P	2.192(1)	2.125(2)
Ni-N	2.004(2)	1.990(5)
Ni-Br(1)	2.360(1)	2.338(1)
Ni-Br(2)	2.419(1)	-
C(1)-Ni-Br(1)	155.43(5)	171.1(2)
C(1)-Ni-Br(2)	95.92(5)	-
P-Ni-N	158.25(5)	162.7(2)
N-Ni-Br(1)	100.17(4)	100.2(2)
P-Ni-Br(1)	92.99(2)	97.11(5)
N-Ni-Br(2)	93.14(4)	-
P-Ni-Br(2)	99.13(2)	-
P-Ni-C(1)	78.43(6)	80.3(2)
N-Ni-C(1)	82.52(7)	82.6(2)

4.3.8 Conclusions

The study reported herein has provided a survey of the oxidation pathways traversed by complex **4.1**, a rather rare dimeric compound featuring two Ni^{II} centers held by pincer ligands at sufficiently close proximity to allow electronic interactions. The results described above have demonstrated that electrolytic oxidation converts **4.1** to a radical cation that appears to maintain the original dimeric structure; in contrast, chemically induced oxidation converts **4.1** to an unstable intermediate species that decomposes to give, eventually, the monomeric product **4.2** featuring a trivalent Ni center and an oxidized (imine-type) new ligand (Scheme 4.6).



Scheme 4.6. Mechanism of oxidation of **4.1**

NMR and UV-Vis monitoring of the reaction of **4.1** with NBS revealed the formation of succinimide and two monomeric divalent species, **4.3** and **4.4**, that are among the intermediates generated in the chemical oxidation of **4.1**. The independent synthesis and full characterization of complex **4.3**, and its direct oxidation to **4.2**, provided further support for the postulated pathway shown in

Scheme 2. On the other hand, the initial product of the reaction of **4.1** with NBS, species **A** in Scheme 2, could not be detected. The postulated structure of this species involves formal oxidation at one Ni center and the concomitant formation of a Ni-Br bond; this proposal is based on the observed tendency of POCN-type pincer complexes of nickel complexes to undergo one-electron oxidation at the nickel center as opposed to the ligand.¹⁷

Another ambiguous aspect of the chemical oxidation of **4.1** touches on whether succinimide is generated via H-abstraction from the solvent or from the ArCH₂ moiety in the postulated intermediates **4.A**. One argument against the prevalence of the latter pathway is that succinimide is also generated in the conversion of (POCN)NiBr to (POCN)NiBr₂ with no concomitant oxidation of the POCN ligand.^{15j} It is tempting to argue that succinimide is generated by the H-abstraction from the reaction medium, and to propose a hydrogen transfer mechanism from one ArCH₂N moiety in **4.A** to another, thus generating the CH=NBn moiety in **4.3** and the NH moiety in **4.4**, but other possibilities can not be ruled out.

The results obtained from cyclic voltammetry and spectroelectrochemical measurements as well as computational investigations have allowed us to survey the redox and absorption properties of **4.1** and compare them to the corresponding data reported for monomeric species (POCN)NiBr_{2/3} and related dinickel species [LNi₂]^{2+/3+} and [LNi₂(NCCH₃)₂]³⁺ (L is a “compartmental macrocyclic ligand” shown in Figure 4.1). When combined together, these results point out that electrolytic oxidation of **4.1** removes an electron from the HOMO to generate a dimeric radical cation, [**4.1**]^{+•}. Since the HOMO in **4.1** has anti-bonding character with respect to the Ni-Ni bond, formation of [**4.1**]^{+•} brings about greater Ni-Ni bond order in [**4.1**]^{+•}. DFT studies have established that the experimentally observed and computationally predicted low-energy electronic transitions extending into the near-IR region originate from the presence of low-lying β-LUMO in [**4.1**]^{+•}.

Another important question addressed by the current study pertains to the localization of the spin density on metal centers and ligand atoms. Previous studies have shown that the spin density in the open shell monomeric pincer complexes (POCN)NiBr₂,¹⁵ⁱ (POCOP)NiX₂,^{15e,f} and (PCP)NiX₂^{15g} is entirely localized on the Ni-Br_{ax} moiety, as was found to be the case in complex **4.2**. In the case of the dinickel species [LNi^{II}Ni^{III}(NCCH₃)₂]³⁺, DFT studies have shown that most of the spin density is localized on the six coordinate Ni ion (72% on 3d_z and 16% on 3d_{xy}) as well as the N atoms of the acetonitrile moieties coordinated to it (ca. 15%).⁷ Similarly, a DFT analysis has shown that the presence of an axial Br in our system would localize the spin on the Ni-Br_{ax} moiety, giving a BrNi^{III}Ni^{II}N₂ core; this might explain the diminished thermal stability of the chemical oxidation intermediate **A** illustrated in Scheme 4.6. In contrast, computational analysis of [**4.1**]⁺ (no axial ligands, *N*-Me or *N*-Bn substituents) has revealed a delocalization of spin density over the Ni₂N₂ core, with a substantial amount of spin density residing over the two N atoms. We conclude that [**4.1**]⁺ is best described as a weighted average of two limiting resonance structures featuring (a) anionic amide moieties and Ni^{+2.5} centers, and (b) an amide moiety and an aminyl radical delocalized through the two Ni^{II} centers (Figure 4.14). Thus, the amide-type POCN ligand in **4.1** can be considered a new example of the non-innocent pincer ligands introduced by Grützmacher's¹⁸ and Mindiola's¹⁹ groups.²⁰

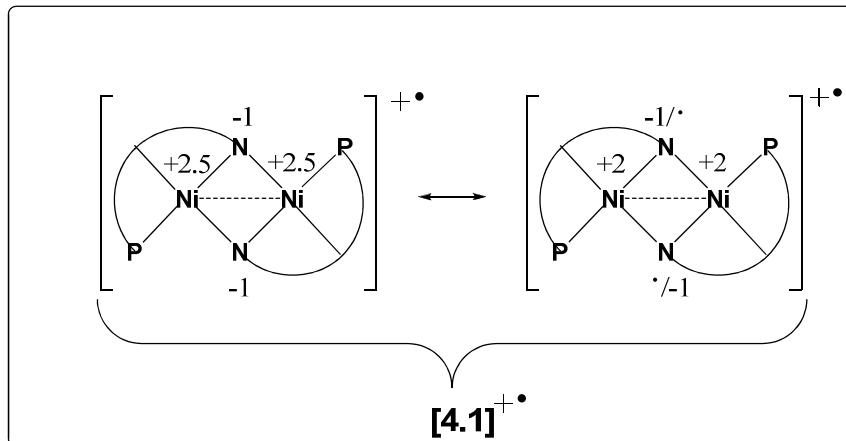


Figure 4.14. Mixvalent species

The unanticipated conversion of the dimeric complex **4.1** into the monomeric 17-electron complex **4.2** featuring a new imine-type POCN ligand and the successful, high-yield synthesis of this species have opened up a new avenue for further exploration of its reactivities, including the possible promotion of radical addition and cyclization reactions. Future studies will also probe the redox behavior of new dinickel analogues of **4.1** in hopes of developing a better understanding of the factors that determine the different oxidation pathways and elucidating the structures of the oxidized species.

4.4 Experimental Section

4.4.1 General.

All manipulations were carried out using standard Schlenk and glove box techniques under nitrogen atmosphere. All solvents used for experiments were dried to water content of less than 10 ppm by passage through activated aluminum oxide (MBraun SPS) and deoxygenated by vacuum-nitrogen extraction. C_6D_6 was dried over molecular sieve (pore size 4 Å) and then deoxygenated by 3-5 freeze-pump-thaw cycles. Quality of the solvents used for experiments was tested using Mettler Toledo C20 coulometric Karl Fischer titrator. The followings

were purchased from Aldrich and used without further purification: Ni (metal), chlorodiisopropylphosphine, N-Bromosuccinimide, 3-hydroxybenzaldehyde, triethylamine, and C₆D₆. A Bruker AV 400 spectrometer was used for recording ¹H, ¹³C{¹H} (101 MHz), and ³¹P{¹H} (162 MHz). ¹H and ¹³C chemical shifts are reported in ppm downfield of TMS and referenced against the residual C₆D₆ signals (7.15 ppm for ¹H and 128.02 ppm for ¹³C); ³¹P chemical shifts are reported in ppm and referenced against the signal for 85% H₃PO₄ (external standard, 0 ppm). Coupling constants are reported in Hz. The correlation and assignment of ¹H and ¹³C NMR resonances were aided by ¹H COSY, HMQC and DEPT. UV-Vis spectra were recorded on Varian Bio 300 equipped with temperature controlling system using standard sampling cells (1 cm optical path length).

4.4.1.1 Synthesis of the $\kappa^P, \kappa^C, \kappa^N$ -{2,6-(*i*-Pr₂PO)(C₆H₃)(CH=NBn)}NiBr₂ (**4.2**).

Method A: To a solution of [$\mu^N((i\text{-Pr})_2\text{POCNBn})\text{Ni}$]₂ (200 mg, 0.260 mmol) in 5 mL of dry and degassed DCM cooled to -78 °C was added 181 mg of NBS (1.04 mmol). The resulting dark brown-black mixture was allowed to stir for an additional 5 min and then treated with 5 mL of cold hexane follow by filtration of formed precipitate. Solvent were reduced to approximately 2 mL in vacuum and resulting mixture was left to crystallize at -18 °C for approximately one week. After this time black crystal was collected washed with cold hexane and dried under vacuum for 1 hour to furnish **4.2** in 23 % (64 mg) yield.

Method B: To a solution of **3** in 5 mL of dry and degassed DCM at -78 °C was added a DCM solution of Br₂ (2 mL, 0.059 mM). Resulting dark brown-black mixture was allowed to stir for additional 5 min and then solvent was removed in vacuum yielding dark purple-black powder (0.110 g, 94 %).

Anal. Calcd for C₂₀H₂₅OPNNiBr₂: C, 44.08; H, 4.62; N, 2.57; Found: C, 43.89; H, 4.77; N, 2.66.

4.4.1.2 Synthesis of the 3-((benzylimino)methyl)phenol (**4.a**).

To a solution of 3-hydroxybenzaldehyde (1.00 g, 8.20 mmol) in 10 mL of methanol at r.t. was added a solution of benzylamine (0.880 g, 8.20 mmol) in 10 mL of methanol. The resulting mixture was stirred for one hour to obtain the anticipated Schiff base as a white suspension. Removal of volatiles under vacuum for 1 hour gave **4.a** as a white powder (1.68 g, 97 %). ^1H NMR (δ , CDCl_3): 4.75 (s, 2H, Bn{CH₂}), 6.84 (d, $^3J = 7$, 1H, {Ar}H⁶), 7.15 – 7.23 (m, 3H), 7.23 – 7.31 (m, 5H, overlapping with CHCl₃), 8.23 (s, 1H, CH=N). $^{13}\text{C}\{^1\text{H}\}$ NMR (δ , CDCl_3): 64.83 (s, 1C, CH₂Ph), 114.13 (s, 1C, {Ar}C⁶), 118.70 (s, 1C, {Ar}C²), 121.72 (s, 1C, {Ar}C⁴), 127.30 (s, 1C, {Ar}C⁵), 128.25 (s, 2C, {Bn}C^{meta}), 128.71 (s, 2C, {Bn}C^{ortho}), 130.04 (s, 1C, {Bn}C^{para}), 137.32 (s, 1C, {Bn}C^{ipso}), 138.86 (s, 1C, {Ar}C³), 156.43 (s, 1C, {Ar}C¹), 162.58 (s, 1C, CH=N).

4.4.1.3 Synthesis of the 3-((benzylimino)methyl)(phosphinito)benzene (**4.b**).

To a solution of **4.a** (1.00 g, 4.73 mmol) and triethylamine (0.788 mL, 5.20 mmol) in THF (35 mL) stirring at 0-5 °C was added chlorodiisopropyl phosphine (96% assay, 0.780 mL, 4.73 mmol). The resulting mixture was allowed to warm to room temperature, stirred for an additional hour, and evaporated under decreased pressure to give an oily residue, which was extracted with hexane (3×25 mL). Evaporation of the combined extracts furnished the product as a colorless oil (1.47 g, 95%). ^1H NMR (δ , C_6D_6): 0.94 (dd, $^3J_{\text{HH}} = 7$, $^3J_{\text{HP}} = 16$, 6H, CHCH₃), 1.10 (dd, $^3J_{\text{HH}} = 7$, $^3J_{\text{HP}} = 11$, 6H, CHCH₃), 1.85 – 1.60 (m, 2H, CHCH₃), 4.56 (s, 2H, {Bn}CH₂), 7.12 – 7.04 (m, 2H, {Ar}H⁵ & {Bn}H^{para}), 7.17 (t, $^3J_{\text{HH}} = 6$, 2H, {Bn}H^{meta}), 7.32 – 7.23 (m, 3H, {Ar}H⁶ & {Bn}H^{para}), 7.37 (d, $^3J_{\text{HH}} = 8$, 1H, {Ar}H⁴), 7.95 (br s, 2H, {Ar}H² & CH=N). $^{13}\text{C}\{^1\text{H}\}$ NMR (δ , C_6D_6): 17.14 (d, $^2J_{\text{CP}} = 9$, 2C, CHCH₃), 17.82 (d, $^2J_{\text{CP}} = 20$, 2C, CHCH₃), 28.60 (d, $^1J_{\text{CP}} = 18$, 2C, CHCH₃), 65.14 (s, 1C, {Bn}CH₂), 118.27 (d, $^3J_{\text{CP}} = 11$, 1C, {Ar}C⁶), 121.08 (d, $^3J_{\text{CP}} = 11$, 1C, {Ar}C⁶), 122.41 (s, 1C, {Ar}C⁴), 127.04 (s, 1C, {Ar}C⁵), 128.27 (s, 2C, {Bn}C^{ortho}), 128.68 (s, 2C, {Bn}C^{meta}), 129.83 (s, 1C, {Bn}C^{para}), 138.69

(s, 1C, {Bn}C^{ipso}), 140.21 (s, 1C, {Ar}C³), 160.27 (d, $J_{CP} = 9$, 1C, {Ar}C³), 161.20 (s, 1C, CH=N). ³¹P{¹H} NMR (δ, C₆D₆): 148.7 (s).

4.4.1.4 Synthesis of the $\kappa^P, \kappa^C, \kappa^N$ -{2,6-(*i*-Pr₂PO)(C₆H₃)(CH=NBn)}NiBr (**4.3**).

A solution of **4.b** (1.47 g, 4.49 mmol) in 20 mL of benzene was slowly added to a stirring suspension of NiBr₂(CH₃CN)_x (1.350 g, 4.49 mmol) and triethylamine (0.625 mL, 4.49 mmol) in toluene (15 mL) at r. t. The resulting dark brown mixture was then heated for 5 h at 60 °C. Removal of the solvent and purification of the solid residues by column chromatography (SiO₂, eluents: hexane followed by 70:30 CH₂Cl₂:Hexane) furnished the product as a brick-red powder (2.08 g, 89 %).

¹H NMR (δ, C₆D₆): 1.12 (dd, $^3J_{HH} = 7$, $^3J_{HP} = 15$, 6H, 2×CHCH₃), 1.41 (dd, $^3J_{HH} = 7$, $^3J_{HP} = 18$, 6H, 2×CHCH₃), 2.28 – 2.03 (m, 2H, 2×CHCH₃), 4.90 (s, 2H, {Bn}CH₂), 6.41 (d, $^3J_{HH} = 7$, 1H, {Ar}H⁵), 6.60 (d, $^3J_{HH} = 8$, 1H, {Ar}H³), 6.70 (t, $^3J_{HH} = 8$, 1H, {Ar}H⁴), 7.02 (t, $^3J_{HH} = 7$, 1H, {Bn}H^{para}), 7.09 (t, $^3J_{HH} = 7$, 2H, 2×{Bn}H^{ortho}), 7.21 (d, $^3J_{HH} = 7$, 2H, 2×{Bn}H^{meta}), 7.29 (d, $^3J_{HP} = 4$, 1H, CH=N). ¹³C{¹H} NMR (δ, C₆D₆): 16.76 (d, $^2J_{CP} = 2$, 2C, CHCH₃), 18.08 (d, $^2J_{CP} = 4$, 2C, CHCH₃), 28.79 (d, $^1J = 23$, 2C, CHCH₃), 60.09 (s, 1C, {Bn}CH₂), 113.14 (d, $^3J_{CP} = 12$, 1C, {Ar}C³), 120.91 (d, $^4J_{CP} = 2$, {Ar}C⁵), 126.51 (s, 1C, {Ar}C⁴), 127.71 (s, 1C, {Bn}C^{para}), 128.88 (s, 2C, 2×{Bn}C^{ortho}), 129.65 (s, 2C, 2×{Bn}C^{meta}), 138.15 (s, 1C, {Bn}C^{ipso}), 148.3 (s, 1C, {Ar}C⁶), 153.40 (d, $^2J = 35$, 1C, {Ar}C¹), 165.76 (d, $^2J = 10$, 1C, {Ar}C²), 172.18 (d, $^2J_{CP} = 3$, 1C, CH=N). ³¹P{¹H} NMR (δ, C₆D₆): 201.35 (s).

Anal. Calcd for C₂₀H₂₅OPNNiBr: C, 51.66; H, 5.42; N, 3.01; Found: C, 51.55; H, 5.59; N, 3.08.

4.4.2 Electrochemical measurements.

Cyclic voltammetry measurements were performed using a BAS Epsilon potentiostat. The electrochemical properties of these compounds were measured

at room temperature in DCM using a standard three electrode system consisting of a glassy carbon working electrode, the Pt auxiliary electrode, and the Ag/AgCl reference electrode. Bu_4NPF_6 was used as electrolyte (0.1 mol/dm^3) and the solutions were bubbled with nitrogen before each experiment. Reversible redox waves of the ferrocenyl moieties were observed under these conditions ($E_{1/2} \{\text{FeCp}_2^+/\text{FeCp}_2\} = +0.48 \text{ V}$).

The spectroelectrochemical (SEC) measurements on complex **4.1** were performed at room temperature using Varian 500 UV-Vis-NIR spectrometer in combination with BAS Epsilon potentiostat in DCM solutions containing $(n\text{-Bu})_4\text{NPF}_6$ as electrolyte (0.1 M). The experiments were carried out on a three electrode set-up consisting of a 5 mm diameter platinum mesh electrode as working electrode, a platinum wire counter electrode, and an Ag/AgCl reference electrode, and using micro sampling cells with a 1 mm optical path length. The chemical reversibility of all processes was confirmed by reversing the applied potential (from 0.07 V to -0.25 V) and regenerating the spectrum of the starting complex **4.1**. The spectrum shown in Figure 2 was obtained at the end of oxidative electrolysis.

4.4.3 EPR Spectroscopy

EPR spectra were collected on a Bruker Elexsys E580 spectrometer operating in cw mode. For compound **2**, a solution ($\sim 0.5 \text{ mM}$) in toluene was prepared, and placed in a 4 mm o.d. EPR tube. The solution was then degassed by repeated freeze-pump-thaw cycles and the tube was sealed under vacuum. The sample was frozen to 120 K in the spectrometer resonator. For the oxidation of **4.1**, a solution of **4.1** (0.67 mM) was mixed with a solution of NBS (6.7 mM) in DCM in the volume ratio needed to give the desired mole ratio and diluted to give a final concentration of **4.1** of 0.22 mM.

4.4.4 Computational Details.

All DFT calculations were performed using the Gaussian 09 package. Stationary points on the potential energy surface were obtained using the B3LYP hybrid density functional method. Geometry optimizations were performed using the TZVP basis set for all atoms. Tight SCF convergence criteria were used for all calculations. The converged wave functions were tested to confirm that they correspond to the ground-state surface. Mayer bond orders and the analysis of molecular orbitals in terms of fragment orbital contributions were carried out using the AOMix program. Absorption spectra were calculated from time-dependent DFT (TD-DFT) simulations at the B3LYP/TZVP level. Calculated excitation energies and oscillator strengths were converted into absorption spectra using the pseudo-Voigt functions (50% Gaussian and 50% Lorentzian) and the 3000 cm⁻¹ half-bandwidths as described before.

4.4.5 Crystal Structure Determinations.

Single crystals of **4.2** and **4.3** were grown from a DCM/hexane solution by slow diffusion of hexanes into a saturated solution of the complex **4.2**, **4.3**. The crystallographic data for complexes **4.1** was collected on a Bruker Microstar generator (rotating anode) equipped with a Helios optics, a Kappa Nonius goniometer and a Platinum135 detector and crystallographic data for complexes **4.3** were collected on a Bruker SMART generator (X-ray sealed tube) a Kappa Nonius goniometer and a APEX II detector.

Cell refinement and data reduction were done using SAINT²¹. An empirical absorption correction, based on the multiple measurements of equivalent reflections, was applied using the program SADABS.²² The space group was confirmed by XPREP routine²³ in the program SHELXTL.²⁴ The structures were solved by direct-methods and refined by full-matrix least squares and difference Fourier techniques with SHELX-97.²⁵ All non-hydrogen atoms

were refined with anisotropic displacement parameters. Hydrogen atoms were set in calculated positions and refined as riding atoms with a common thermal parameter. Publication materials and ORTEP drawings were prepared using LinXTL and the Platon program integrated in it.

4.5 Acknowledgment.

The authors gratefully acknowledge financial support received from Université de Montréal (fellowships to D.M.S.) and NSERC of Canada (Research Tools and Instruments and Discovery grants to D.Z.).

4.6 Supporting Information.

DFT-optimized structure coordinates are available free of charge: <http://pubs.acs.org>. Complete details of the X-ray analyses for complexes **4.2** (788986) and **4.3** (788985) have been deposited at *The Cambridge Crystallographic Data Centre*. These data can be obtained free of charge via www.ccdc.cam.ac.uk/data_request/cif, or by emailing data_request@ccdc.cam.ac.uk, or by contacting The Cambridge Crystallographic Data Centre, 12, Union Road, Cambridge CB2 1EZ, UK; fax: +44 1223 336033.

4.7 References

¹ For some of the pioneering reports on pincer complexes see: (a) Moulton, C. J.; Shaw, B. L. *J. Chem. Soc., Dalton Trans.* **1976**, 1020. (b) Crocker, C.; Errington, R. J.; McDonald, W. S.; Odell, K. J.; Shaw, B. L.; Goodfellow, R. J. *J. Chem. Soc., Chem. Commun.* **1979**, 498. (c) van Koten G.; Timmer, K.; Noltes, J. G.; Spek, A. L. *J. Chem. Soc., Chem. Com.* **1978**, 250. (d) Fryzuk, M. D.; MacNeil, P. A. *J. Am. Chem. Soc.* **1981**, *103*, 3592.

² For a selection of reviews and primary reports describing some applications of pincer complexes see: (a) Albrecht, M.; van Koten, G. *Angew. Chem., Int. Ed.* **2001**, *40*, 375. (b) van der Boom, M. E.; Milstein, D. *Chem. Rev.* **2003**, *103*, 1759. (c) Singleton, J. T. *Tetrahedron* **2003**, *59*, 1837. (d) Liang, L.-C. *Coord. Chem. Rev.* **2006**, *250*, 1152. (e) Nishiyama, H. *Chem. Soc. Rev.* **2007**, *36*, 1133. (f) Leis, W.; Mayer, H. A.; Kaska, W. C. *Coord. Chem. Rev.* **2008**, *252*, 1787. (g) Goldman, A. S.; Roy, A. H.; Huang, Z.; Ahuja, R.; Schinski, W.; Brookhart, M. *Science* **2006**, *312*, 257. (h) van der Ploeg, A. F. M. J.; van Koten, G.; Brevard, C. *Inorg. Chem.* **1982**, *21*, 2878. (i) Batema, G. D.; Lutz, M.; Spek, A. L.; van Walree, C. A.; Donegá, C. d. M.; Meijerink, A.; Havenith, R. W. A.; Pérez-Moreno, J.; Clays, K.; Büchel, M.; van Dijken, A.; Bryce, D. L.; van Klink, G. P. M.; van Koten, G. *Organometallics* **2008**, *27*, 1690. (j) Zweifel, T.; Naubron, J.-V.; Grützmacher, H. *Angew. Chem., Int. Ed.* **2009**, *48*, 559. (k) Ohff, M.; Ohff, A.; van der Boom, M. E.; Milstein, D. *J. Am. Chem. Soc.* **1997**, *119*, 11687. (l) Miyazaki, F.; Yamaguchi, K.; Shibasaki, M. *Tetrahedron Letters* **1999**, *40*, 7379. (m) Naghipour, A.; Sabounchei, S. J.; Morales-Morales, D.; Canseco-González, D.; Jensen, C. M. *Polyhedron* **2007**, *26*, 1445. (n) Gunanathan, C.; Ben-David, Y.; Milstein, D. *Science* **2007**, *317*, 790. (o) Sebelius, S.; Olsson, V. J.; Szabo, K. J. *J. Am. Chem. Soc.* **2005**, *127*, 10478. Bernskoetter, W. H.; Brookhart, M. *Organometallics* **2008**, *27*, 2036. (p) Dijkstra, H. P.; Meijer, M. D.; Patel, J.; Kreiter, R.; van Klink, G. P. M.; Lutz, M.; Spek, A. L.; Canty, A. J.; van Koten, G. *Organometallics* **2001**, *20*, 3159.

³ Examples of bimetallic pincer complexes include the following: (a) [{2,6-(RSCH₂)₂C₆H₃}Rh(H)(μ-Cl)]₂ (Evans, D. R.; Huang, M.; Seganish, W. M.; Chege, E. W.; Lam, Y.; Fettinger, J. C.; Williams, T. L. *Inorg. Chem.* **2002**, *41*, 2633). (b) (CF₃PCP)Pt[κ¹-C,κ³-P,C,P-2,6-(CHP(CF₃)₂)(CH₂P(CF₃)₂)-C₆H₃]PtCl and [{2,6-C₆H₃(CH₂P(CF₃)₂)₂Pt₂(μ-X)]⁺ (X= H, Cl; Adams, J. J.; Arulsamy, N.; Roddick, D. M. *Organometallics* **2009**, *28*, 1148). (c) [{2,6-bis(piperidylmethyl)benzene}Pt]₂⁺(μ-Λ) (Jude, H.; Krause Bauer, J. A.; Connick, W. B. *Inorg. Chem.* **2005**, *44*, 1211 and references therein). For a few reports on

dendrimers based on pincer complexes see the following: (d) Huck, W. T. S.; Snellink-Ruel, B.; van Veggel, F. C. J. M.; Reinhoudt, D. N. *Organometallics* **1997**, *16*, 4287. (e) Kleij, A. W.; Gossage, R. A.; Klein Gebbink, R. J. M.; Brinkmann, N.; Reijerse, E. J.; Kragl, U.; Lutz, M.; Spek, A. L.; van Koten, G. *J. Am. Chem. Soc.* **2000**, *122*, 12112. (f) Gossage, R. A.; Jastrzebski, J. T. B. H.; van Ameijde, J.; Mulders, S. J. E.; Brouwer, A. J.; Liskamp, R. M. J.; van Koten, G. *Tet. Lett.* **1999**, *40*, 1413.

⁴ For a few representative studies on metal-metal interactions and electron transfer processes occurring in mixed-valent bimetallic systems see: (a) Ward, M. D. *Chem. Soc. Rev.* **1995**, 121. (b) Gorelsky, S. I.; Xie, X.; Chen, Y.; Fee, J. A.; Solomon, E. I. *J. Am. Chem. Soc.* **2006**, *128*, 16452. (c) Hagadorn, J. R.; Zahn, T. I.; Que, Jr., L.; Tolman, W. B. *Dalton Trans.* **2003**, 1790. (d) Ernst, S.; Kasack, V.; Kaim, W. *Inorg. Chem.* **1988**, *27*, 1146. (e) Gamelin, D. R.; Randall, D. W.; Hay, M. T.; Houser, R. P.; Mulder, T. C.; Canters, G. W.; de Vries, S.; Tolman, W. B.; Lu, Y.; Solomon, E. I. *J. Am. Chem. Soc.* **1998**, *120*, 5246. (f) Atwood, C. G.; Geiger, W. E. *J. Am. Chem. Soc.* **2000**, *122*, 5477. (g) Lu, C. C.; Bill, E.; Weyhermüller, T.; Bothe, E.; Wieghardt, K. *J. Am. Chem. Soc.* **2008**, *130*, 3181. (h) Xie, X.; Gorelsky, S. I.; Sarangi, R.; Garner, D. K.; Hwang, H. J.; Hodgson, K. O.; Hedman, B.; Lu, Y.; Solomon, E. I. *J. Am. Chem. Soc.* **2008**, *130*, 5194.

⁵ (a) Groux, L.F.; Bélanger-Gariépy, F.; Zargarian, D. *Can. J. Chem.* **2005**, *83*, 634. (b) Castonguay, A.; Sui-Seng, C.; Zargarian, D.; Beauchamp, A. L. *Organometallics* **2006**, *25*, 602. (c) Sui-Seng, C.; Castonguay, A.; Chen, Y.; Gareau, D.; Groux, L. F.; Zargarian, D. *Topics in Catalysis* **2006**, *37*, 81. (d) Castonguay, A.; Beauchamp, A. L.; Zargarian, D. *Acta Cryst.* **2007**, *E63*, m196. (e) Pandarus, V.; Zargarian, D. *Chem. Comm.* **2007**, 978. (f) Pandarus, V.; Zargarian, D. *Organometallics* **2007**, *26*, 4321. (g) Castonguay, A.; Beauchamp, A. L.; Zargarian, D. *Organometallics* **2008**, *27*, 5723. (h) Castonguay, A.; Spasyuk, D. M.; Madern, N.; Beauchamp, A. L.; Zargarian, D. *Organometallics* **2009**, *28*, 2134. (i) Spasyuk, D. M.; Zargarian, D.; van der Est, A. *Organometallics* **2009**, *28*, 6531. (j) Spasyuk, D. M.; Zargarian, D.; *Inorg. Chem.* **2010**, *49*, 6203.

⁶ (a) Atkins, A. J.; Blake, A. J.; Schröder, M. *Chem. Comm.* **1993**, 1662. (b) Branscombe, N. D. J.; Atkins, A. J.; Marin-Becerra, A.; McInnes, E. J. L.; Mabbs, F. E.; McMaster, J.; Schröder, M. *Chem. Comm.* **2003** 1098.

⁷ van Gastel, M.; Shaw, J. L.; Blake, A. J.; Flores, M.; Schröder, M.; McMaster, J.; Lubitz, W. *Inorg. Chem.* **2008**, *47*, 11688.

⁸ (a) op den Brouw, P. M.; van der Linden, J. G. M. *Inorg. Nucl. Chem. Lett.* **1977**, *13*, 149. (b) Huang, D.; Deng, L.; Sun, J.; Holm, R. *Inorg. Chem.* **2009**, *48*, 6159. This complex features a dianionic XLX-type SNS ligand; no structural studies have been conducted on this species due to its limited solubility.

⁹ Adhikari, D.; Mossin, S.; Basuli, F.; Dible, B. R.; Chipara, M.; Fan, H.; Huffman, J. C.; Meyer, K.; Mindiola, D. J. *Inorg. Chem.* **2008**, *47*, 10479. It should be added that, strictly speaking, this compound is not a pincer-type species because the two neutral donor moieties of the PNP ligand are bound to different nickel centers, while it is the central amido moiety that serves as bridge. Thus, the PNP ligand spans across the two nickel centers and does not impose a meridional coordination environment on them.

¹⁰ It should be noted that a wider-than-anticipated peak-to-peak separation on the order of ca. 0.080-1.20 V is a common feature of the cyclic voltammograms obtained for DCM solutions of all nickel pincer complexes examined by us. That one-electron processes are at work in these systems is supported by the results obtained from square-wave-voltammetry experiments and by the fact that, under the experimental conditions employed during our studies, ferrocene also produces similar peak-to-peak separations.

¹¹ (a) Grove, D. M.; van Koten, G.; Mul, P.; Zoet, R.; van der Linden, J. G. M.; Legters, J.; Schmitz, J. E. J.; Murrall, N. W.; Welch, A. J., *Inorg. Chem.* **1988**, *27*, 2466-2473; (b) Grove, D. M.; van Koten, G.; Mul, W. P.; van der Zeijden, A. A. H.; Terheijden, J.; Zoutberg, M. C.; Stam, C. H., *Organometallics* **1986**, *5*, 322-326; (c) Grove, D. M.; van Koten, G.; Zoet, R.; Murrall, N. W.; Welch, A. J., *J. Amer. Chem. Soc.* **1983**, *105*, 1379-1380; (d) Kozhanov, K. A.; Bubnov, M. P.; Cherkasov,

V. K.; Fukin, G. K.; Vavilina, N. N.; Efremova, L. Y.; Abakumov, G. A., *J. Mag. Res.* **2009**, *197*, 36-39.

¹² Kivelson, D.; Neiman, R., *J. Chem. Phys.* **1961**, *35*, 156-161.

¹³ (a) Becke, A. D. *J. Chem. Phys.* **1993**, *98*, 5648. (b) Lee, C.; Yang, W.; Parr, R. G. *Phys. Rev. B* **1988**, *37*, 785.

¹⁴ Godbout, N.; Salahub, D. R.; Andzelm, J.; Wimmer, E. *Can. J. Chem.* **1992**, *70*, 560.

¹⁵ (a) Casida, M. E. "Time Dependent Density Functional Response Theory for Molecules" in *Recent Advances in Density Functional Methods*; Chong, D. P., Ed.; World Scientific: Singapore, **1995**; p 155. (b) Stratmann, R. E.; Scuseria, G. E.; Frisch, M. J. *J. Chem. Phys.* **1998**, *109*, 8218.

¹⁶ Robin, M. B.; Day, P. *Adv. Inorg. Chem. Radiochem.* **1967**, *10*, 247.

¹⁷ We have also considered an alternative reaction pathway involving initial oxidation at the ligand to generate an intermediate featuring a Ni-coordinated aminyl radical. Such a species could undergo H-abstraction by the *in-situ* generated succinimide radical to give **4.3**, or abstract H[•] from the reaction medium to generate **4.4**. However, this scenario would require more than two equiv of oxidant for the formation of the ultimate product, **4.2**.

¹⁸ Buttner, T.; Geier, J.; Frison, G.; Harmer, J.; Calle, C.; Schweiger, A.; Schonberg, H.; Grützmacher, H. *Science* **2005**, *307*, 235.

¹⁹ Adhikari, D.; Mossin, S.; Basuli, F.; Huffman, J. C.; Szilagy, R. K.; Meyer, K.; Mindiola, D. J. *J. Am. Chem. Soc.* **2008**, *130*, 3676.

²⁰ For a recent discussion on the characterization and potential applications of metal complexes bearing aminyl radicals see: Hicks, R. G. *Angew. Chem. Int. Ed.* **2008**, *47*, 7393.

²¹ SAINT (1999) Release 6.06; Integration Software for Single Crystal Data. Bruker AXS Inc., Madison, Wisconsin, USA.

²² Sheldrick, G.M. (1999). SADABS, Bruker Area Detector Absorption Corrections. Bruker AXS Inc., Madison, Wisconsin, USA.

²³ XPREP (1997) Release 5.10; X-ray data Preparation and Reciprocal space Exploration Program. Bruker AXS Inc., Madison, Wisconsin, USA.

²⁴ SHELXTL (1997) Release 5.10; The Complete Software Package for Single Crystal Structure Determination. Bruker AXS Inc., Madison, Wisconsin, USA.

²⁵ (a) Sheldrick, G.M. (1997). SHELXS97, Program for the Solution of Crystal Structures. Univ. of Gottingen, Germany. (b) Sheldrick, G.M. (1997). SHELXL97, Program for the Refinement of Crystal Structures. University of Gottingen, Germany.

Chapter 5: Isonitrile Transformation to Carbene in Reaction With POCN Nickel Dimeric Species.

5.1 Abstract

The new bimetallic pincer complex has been synthesized by the reaction of $[\mu^N; \kappa^P, \kappa^C, \kappa^N\text{-}\{2\text{-}(i\text{-Pr}_2\text{PO}), 6\text{-}(\text{CH}_2\text{NBn})\text{-C}_6\text{H}_3\}\text{Ni}]_2$ (**3.5**) with 2,6-dimethylphenyl isocyanide. Surprisingly, only one amido fragment of **3.5** has undergone the reaction even if 5 equivalents of 2,6-dimethylphenyl isocyanide was used and/or harsher conditions were applied. Obtained complex was characterized structurally and its purity was confirmed by combustion as well as NMR analysis. The crystal structures showed that reaction of **3.5** with 2,6-dimethylphenyl isocyanide did not lead to breakage of dimeric structure of **3.5**, but instead transformed one of the POCN-pincer moieties to POCC-type. The new fragment features a carbene ligand detected at 214 ppm in carbon NMR which exhibits a strong coupling with the phosphorus nucleus. An orange material (**5.1**) was isolated in a high yield. Studies by cyclic voltammetry have shown a quasi-reversible oxidation, which occurs at 0.39 V ($\Delta E_p = 110$ mV) and corresponds to one electron oxidation to Ni^{III} .

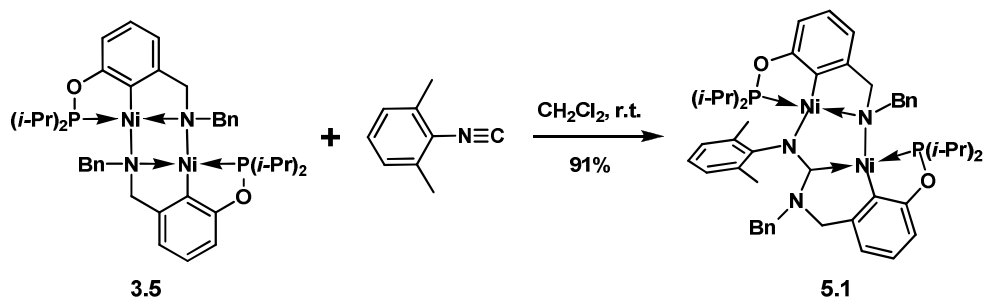
5.2 Introduction

Nucleophilic addition to the coordinated isonitrile or carbonyl ligand has long attracted much attention in the scientific community. This reaction frequently leads to an interesting transformation such as CH activation of coordinated isonitrile or supporting ligands¹. At the same time isonitrile nucleophilic addition is of great interest in organic chemistry since it provides access to imines which are the fundamental compounds for imidazole² and

pyrimidine heterocycles³ preparation. Non catalytic nucleophilic addition to non-coordinated isonitriles is hard to perform; however, the isonitrile coordinated to the metal is much more susceptible toward nucleophilic attack and so use of coordination compound is necessary to achieve this transformation⁴. While nucleophilic addition of amines or amides is fairly well explored in the literature, the reaction of amido complexes with isonitrile ligands remaining little explored. At the same time, reactions of metal alkyl complexes with isonitrile or CO ligands have been reported previously in literature⁵. Generally, these reactions were leading to formation of acyl or formimino complexes which are very reactive species and several examples of isolation of these materials were reported in literature⁶. In this context the reactivities of isonitrile with bisamido $[\mu^N; \kappa^P, \kappa^C, \kappa^N\text{-}\{2\text{-}(i\text{-Pr}_2\text{PO}), 6\text{-}(\text{CH}_2\text{NBn})\text{-C}_6\text{H}_3\}\text{Ni}]_2$ (**3.5**) POCN pincer complex is of interest for better understanding the nature of this organometallic species and for our quest for 14 electron unsaturated species.

5.3 Results and Discussions

No visible color change was noted when one equiv of 2,6-dimethylphenyl isocyanide was allowed to react with a 0.26 M dichloromethane (DCM) solution of **3.5** at ambient temperature, but the ³¹P NMR spectrum of the mixture indicated that the starting material had been consumed completely (vide infra). Interestingly, increase of the quantity of 2,6-dimethylphenyl isocyanide up to the 5 molar excess as well as increasing the temperature of reaction up to 60 °C have not furnished the double insertion product to the second amido fragment and only form **5.1**. Analysis of the orange solid obtained from this reaction confirmed the formation of **5.1** and helped to establish its identity (Scheme 5.1.).



Scheme 5.1. Synthesis of complex **5.1**

Thus, the appearance of two signals in the ^{31}P NMR spectrum of the product implied an unsymmetrical dimeric structure for **5.1**. This was also inferred from the ^1H and ^{13}C NMR spectra that showed two different sets of signals for the proton and carbon nuclei of the pincer ligands; in addition, the appearance of 8 different ^{13}C signals and 5 different ^1H signals for the xylyl moiety indicated the disappearance of the C2 axis present in the isocyanide precursor. Most interestingly, the ^{13}C NMR spectrum displayed a doublet at 214 ppm featuring a very large P-C coupling constant of 106 Hz which is consistent with a new carbene ligand positioned trans to a phosphinite moiety. Interestingly, all $\underline{\text{CH}_2}$ protons of benzyl groups (Figure 5.1) displayed very strong geminal coupling and appear as a pair of AB doublets.

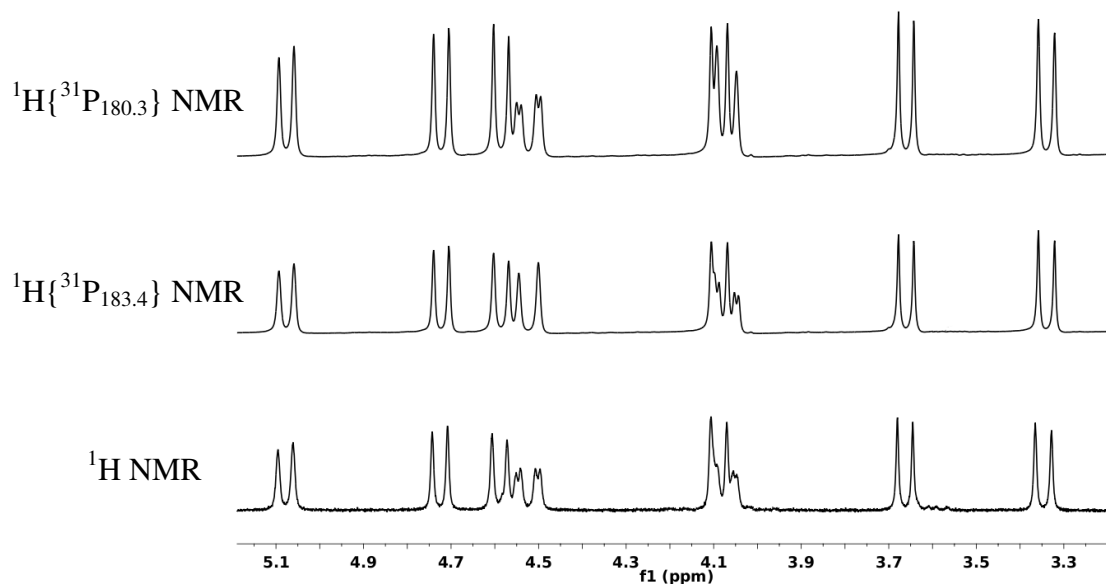


Figure 5.1. The methylene region in the ^1H -NMR spectra (C_6D_6) of complexes **5.1**

It is interesting to note that, additional small coupling was spotted for CH_2 protons at 4.07 and 4.52 ppm. Broad band phosphorus decoupled ^1H NMR experiments together with HMBC and HMQC were conducted in order to understand the nature of such spin-spin interaction. To our surprise, we have found that protons at 4.07 and 4.52 ppm belong to the same carbon nucleus ($\text{NCH}_2\text{Ar-a}$, $\text{a}=\text{POCN}$), however they are coupled to different phosphorus atoms. Complementary crystallographic investigation of this problem helped us to conclude about existence of the short contact between phosphorus nuclear (P2) and one of the hydrogen of $\text{CH}_2\text{Ar-a}$ group resulting in small through space ($J_{\text{HP}} = 5$ Hz, $\text{P2-H7A} = 2.93 \text{ \AA}$) coupling. At the same time, the second hydrogen of $\text{CH}_2\text{Ar-a}$ group displayed small through bond coupling ($J_{\text{HP}} = 4$ Hz) with another phosphorus (P1) nucleus. An X-ray diffraction study unequivocally established the solid state structure of **5.1**, as described below.

The ORTEP diagram for complex **5.1** (Figure 5.2) shows that this compound consists of two Ni centered square planes, linked to each other through a bridging amido moiety and an unusual Fischer-type diamino carbene ligand that binds to one Ni center via the C-centered lone pair and to the other Ni center via one of the amine substituents. Geometrical parameters of the N-C-N carbene moiety (C48-N2=1.363(3), C48-N3=1.330(3)), determined by X-ray crystallography, were correlated with similar literature examples⁷ and allowed us to conclude the formation of a carbene ligand in a POCC type pincer moiety (Figure 5.2). Interestingly, the Ni-P bond distances observed for both POCN and POCC complexes were found to be significantly longer for POCC moiety (2.237(1) Å (Table 5.2) versus 2.177(1) Å), suggesting strong trans influence of the carbene ligand on coordination strength of the phosphinito ligand. Similar characteristic changes were observed for Ni-C bonds, where POCC type moiety displays somewhat longer C41-Ni2 bond compared to similar type of bonding in POCN moiety (C41-Ni2 = 1.910(2) Å versus C1-Ni1 = 1.870 (2) Å).

Figure 5.2. ORTEP diagram for complexes **5.1**. Thermal ellipsoids are shown at the 50% probability level. Hydrogen atoms and benzyl group (C31) are omitted for clarity.

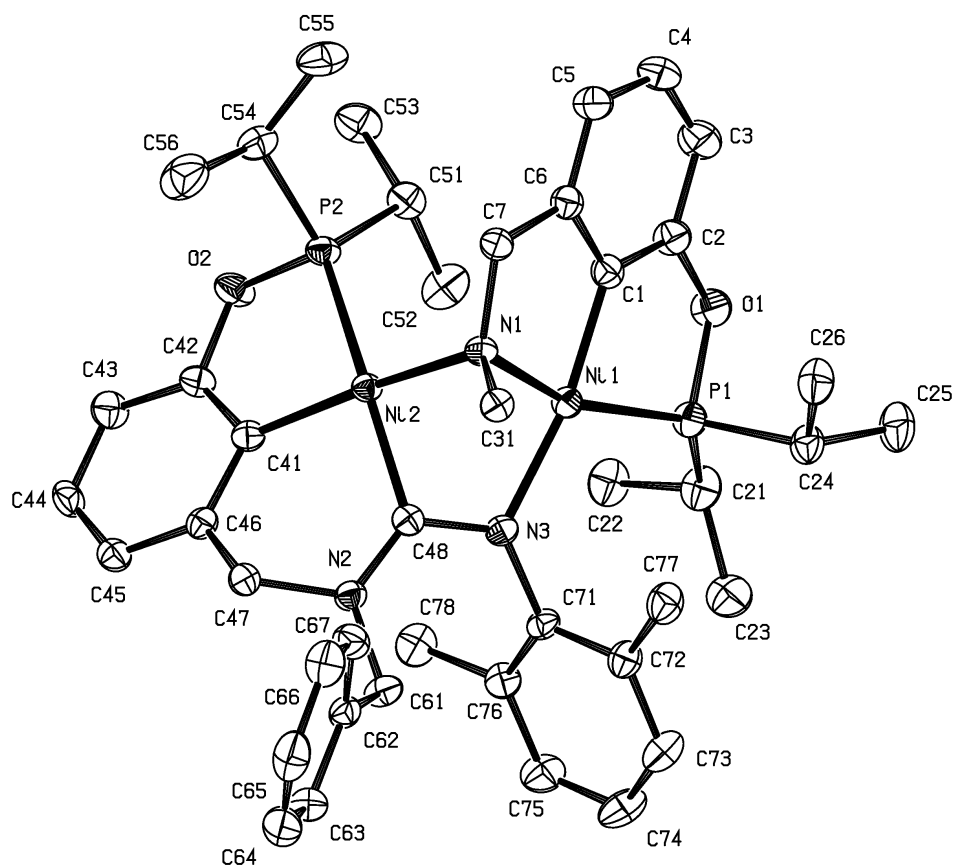


Table 5.1. Crystal Data Collection and Refinement Parameters for Complexes**5.1.**

	5.1
chemical formula	C ₄₉ H ₆₁ N ₃ Ni ₂ O ₂ P ₂
crystal colour	Orange
<i>F</i> _w ; F(000)	903.37; 956
<i>T</i> (K)	150
wavelength (Å)	1.54178
space group	P-1
<i>a</i> (Å)	9.183(1)
<i>b</i> (Å)	12.496(1)
<i>c</i> (Å)	22.267(2)
α (deg)	75.612(3)
β (deg)	78.816(3)
γ (deg)	76.488(3)
<i>Z</i>	2
<i>V</i> (Å ³)	2381.3(3)
ρ _{calcd} (g·cm ⁻³)	1.260
μ (mm ⁻¹)	1.919
θ range (deg); completeness	2.07 – 69.72; 0.978
collected reflections; R _σ	43552; 0.0195
unique reflections; R _{int}	43552; 0.0344
R1 ^a ; wR2 ^b [I > 2σ(I)]	0.0530; 0.1454
R1; wR2 [all data]	0.0545; 0.1469
GOF	1.060
largest diff peak and hole	2.44 and -0.31

$$^a R_1 = \frac{\sum (|F_o| - |F_c|)}{\sum |F_o|}$$

$$^b wR_2 = \left\{ \frac{\sum [w(F_o^2 - F_c^2)^2]}{\sum [w(F_o^2)^2]} \right\}^{1/2}$$

Table 5.2. Selected Bond Distances (Å) and Angles (deg) for Complexes **5.1**.

	5.1
Ni(1)-C(1)	1.871(2)
Ni(1)-P(1)	2.179(1)
Ni(1)-N(1)	1.968(2)
N(1)-Ni(2)	1.976(2)
Ni(1)-N(3)	1.963(2)
Ni(2)-C(41)	1.911(2)
Ni(2)-P(2)	2.237(1)
N(2)-C(48)	1.363(3)
C(48)-N(3)	1.330(3)
Ni(2)-C(48)	1.899(2)
Ni(2)-N(1)	1.976(2)
Ni(1)-Ni(2)	2.751(1)
C(1)-Ni(1)-N(1)	83.93(9)
C(1)-Ni(1)-P(1)	79.94(8)
C(1)-Ni(1)-N(3)	170.15(9)
P(1)-Ni(1)-N(1)	161.84(6)
N(1)-Ni(1)-N(2)	85.81(6)
N(3)-Ni(1)-N(1)	88.86(8)
C(41)-Ni(2)-N(1)	169.43(9)
C(41)-Ni(2)-P(2)	81.94(7)
C(41)-Ni(2)-C(48)	88.37(9)
P(2)-Ni(2)-C(48)	157.30(7)
N(2)- Ni(1)-P(1)	107.72(5)
Ni(1)-N(3)- C(48)	166.43(5)
C(2)-C(1)-C(6)	115.1(2)
C(42)-C(41)-C(46)	117.8(2)

Interesting features of this complex were observed by electrochemistry. Figure 5.3 illustrates the redox properties of complex **5.1** through its cyclic voltammometric responses in dichloromethane solution. Surprisingly, despite the fact that this complex contains two very different nickel nuclei, a single redox event was observed in its voltammogram. The curve appearance and peak separation, $\Delta E_p=110$ mV, were comparable to the ferrocene voltammogram which suggest one electron oxidation process. At the same time, oxidation potential for complex **5.1** (0.39 V) was not significantly lower comparatively to complex **3.5** (0.41 V) described earlier.

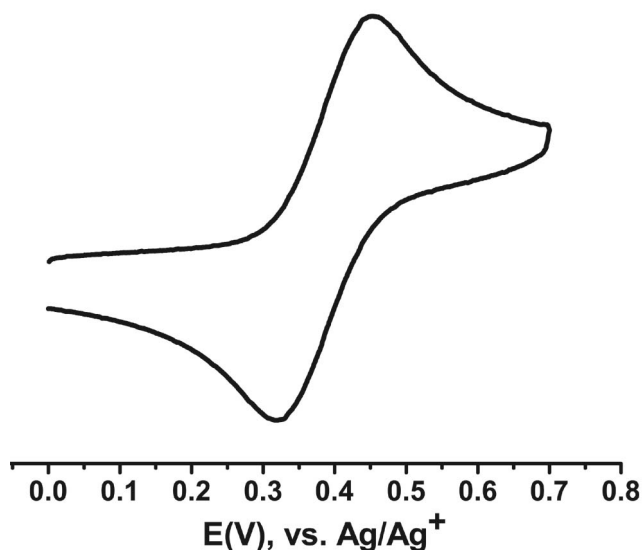


Figure 5.3. Cyclic voltammogram of 1 mmol/dm³ solutions of complex **5.1**, in dichloromethane containing 0.1 mol/dm³ tetrabutylammonium hexafluorophosphate at 25 °C at a scan rate of 100 mV/s on a glassy carbon working electrode.

5.4 Conclusion

To summarize, we have synthesized and fully characterized the new dinuclear nickel species by reaction of isonitrile precursor with complex **3.5**. This transformation demonstrates an interesting way of POCN pincer ligand modification to the unusual POCC-type pincer ligand. The properties of the

carbene fragment were established via single crystal structure determination in combination with NMR spectroscopy. Thus, the carbene moiety displays strong coupling with one phosphorus nucleus as well as a strong trans effect which elongates the P-Ni distance. We have shown that despite the asymmetric nature of dinuclear complex **5.1**, it shows only one quasi-reversible peak in its voltammogram; perhaps suggesting possible communication between the two Ni nuclei. Additional spectroelectrochemical as well as computational studies on this subject might be required in order to better understand the properties of this species (**5.1**).

5.4.1 General

All manipulations were carried out using standard Schlenk and glove box techniques under nitrogen atmosphere. All solvents used for experiments were dried to water content of less than 10 ppm by passage through activated aluminum oxide (MBraun SPS) and deoxygenated by vacuum-nitrogen extraction. C₆D₆ was dried over molecular sieve (pore size 4 Å) and then deoxygenated by 3-5 freeze-pump-thaw cycles. Quality of the solvents used for experiments was tested using Mettler Toledo C20 coulometric Karl Fischer titrator. The following were purchased from Aldrich and used without further purification: Ni (metal), chlorodiisopropylphosphine, N-Bromosuccinimide, 3-hydroxybenzaldehyde, triethylamine, benzylamine, 2,6-dimethylisonitrile and C₆D₆. A Bruker AV 400 spectrometer was used for recording ¹H, ¹³C{¹H} (101 MHz), and ³¹P{¹H} (162 MHz) ¹H and ¹³C chemical shifts are reported in ppm downfield of TMS and referenced against the residual C₆D₆ signals (7.15 ppm for ¹H and 128.02 ppm for ¹³C); ³¹P chemical shifts are reported in ppm and referenced against the signal for 85% H₃PO₄ (external standard, 0 ppm). Coupling constants are reported in Hz. The correlation and assignment of ¹H and ¹³C NMR resonances were aided by ¹H COSY, HMQC, HMBC, DEPT, and ¹H{³¹P} experiments

5.4.2 Synthesis of the complex 5.1

To 17 mg (0.130 mmol) of 2,6-dimethylphenylisonitrile was added a solution of $[\mu^N; \kappa^P, \kappa^C, \kappa^N\text{-}\{2\text{-}(i\text{-Pr}_2\text{PO}), 6\text{-(CH}_2\text{NBn)}\text{-C}_6\text{H}_3\}\text{Ni}]_2$ (100 mg, 0.130 mmol) in dichloromethane (0.5 mL), and the mixture was stirred under nitrogen atmosphere for about 60 min at a room temperature. The complex was isolated by evaporation of the solvent and drying under vacuum to obtain complex **5.1** as an orange solid in a yield of 91 % (107 mg).

^1H NMR (δ , C_6D_6): 0.69 (dd, $^3J_{\text{HH}} = 7$, $^3J_{\text{HP}} = 15$, 3H, CHCH₃), 1.15 – 0.99 (m, 15H, 5×CHCH₃), 1.28 (dd, $^3J_{\text{HH}} = 7$, $^3J_{\text{HP}} = 17$, 3H, CHCH₃), 1.47 – 1.35 (m, 1H, CH), 1.57 – 1.47 (m, 1H, CH), 1.75 – 1.62 (m, 1H, CH), 1.88 (dd, $^3J_{\text{HH}} = 7$, $^3J_{\text{HP}} = 16$, 3H, CHCH₃), 1.96 – 1.92 (m, 1H, CH), 1.97 (s, 3H, CH₃), 2.85 (s, 3H, CH₃), 3.35 (d, $^2J_{\text{HH}} = 15$, 1H, CH₂Bn-b), 3.66 (d, $^2J_{\text{HH}} = 14$, 1H, CH₂Ar-b), 4.07 (dd, $^2J_{\text{HH}} = 19$, $J_{\text{HP}} = 4$, 1H, NCH₂Ar-a), 4.09 (d, $^2J_{\text{HH}} = 14$, 1H, CH₂Bn-b), 4.52 (dd, $^2J_{\text{HH}} = 19$, $J_{\text{HP}} = 5$, 1H, NCH₂Ar-a), 4.59 (d, $^2J_{\text{HH}} = 14$, 1H, CH₂Bn-a), 4.73 (d, $^2J_{\text{HH}} = 14$, 1H, CH₂, CH₂Ar-b), 5.08 (d, $^2J_{\text{HH}} = 14$, 1H, CH₂Bn-a), 6.33 (d, $^3J_{\text{HH}} = 8$, 1H, {Ar-a}H⁵), 6.49 (d, $^3J_{\text{HH}} = 7$, 1H, {Ar-b}H⁵), 6.61 – 6.68 (m, 2H, {Ar-b}H³ & {Ar^{CN}}H^{para}), 6.76 – 6.68 (m, 4H, 2×{Bn-b}H^{ortho} & 2×{Ar^{CN}}H^{meta}), 6.81-6.88 (m, 3H, 2×{Bn-b}H^{meta} & {Ar-a}H³), 7.00 – 6.88 (m, 3H, {Ar-a}H⁴ & {Bn-b}H^{para} & {Ar-b}H⁴), 7.23 (t, $^3J_{\text{HH}} = 7$, 1H, {Bn-a}H^{para}), 7.33 (t, $^3J_{\text{HH}} = 7$, 2H, {Bn-a}H^{meta}), 8.91 (d, $^3J_{\text{HH}} = 7$, 2H, {Bn-a}H^{ortho}).

^{13}C NMR (δ , C_6D_6): 15.92 (d, $^2J_{\text{CP}} = 8$, 1C, CHCH₃), 16.95 (d, $^2J_{\text{CP}} = 3$, 1C, CHCH₃), 17.01 (d, $^2J_{\text{CP}} = 2$, 1C, CHCH₃), 17.53 (d, $^2J_{\text{CP}} = 2$, 1C, CHCH₃), 19.13 (d, $^2J_{\text{CP}} = 4$, 1C, CHCH₃), 19.25 (d, $^2J_{\text{CP}} = 4$, 1C, CHCH₃), 19.51 (d, $^2J_{\text{CP}} = 5$, 1C, CHCH₃), 20.78 (s&d overlapping, 2C, ^{NC}CH₃ & CHCH₃), 21.97 (s, 1C, ^{NC}CH₃), 26.81 (d, $^1J_{\text{CP}} = 15$, 1C, PCH), 28.13 (d, $^1J_{\text{CP}} = 15$, 1C, PCH), 30.94 (d, $J_{\text{CP}} = 17$, 1C, PCH), 31.57 (d, $J_{\text{CP}} = 6$, 1C, PCH), 55.38 (d, $J_{\text{CP}} = 2$, 1C, CH₂Bn-b), 60.45 (s, 1C, CH₂Ar-b), 71.34 (s, 1C, CH₂Bn-a), 77.93 (d, $J_{\text{CP}} = 8$, 1C, NCH₂Ar-a), 106.83 (d, $^3J_{\text{CP}} = 12$, 1C, {Ar-b}C³), 109.68 (d, $^3J_{\text{CP}} = 9$, 1C, {Ar-a}C³), 114.13 (s, 1C, {Ar-a}C⁵), 118.40 (s, 1C, {Ar-b}C⁵), 123.33 (s), 125.50 (s), 126.31 (s), 127.09 (d,

$J_{CP} = 2$, 1C), 128.45 (s), 128.59 (s), 128.89 (s, 1C, $\{^{CN}Ar\}C^{meta}$), 129.04 (s, 1C, $\{^{CN}Ar\}C^{meta}$), 129.34 (s, 2C, $2 \times \{Bn\}C^{ortho}$), 131.08 (s, 1C, $\{^{CN}Ar\}C^{ortho}$), 132.32 (s, 1C, $\{^{CN}Ar\}C^{ortho}$), 136.64 (d, $^2J_{CP} = 18$, 1C, $\{Ar-b\}CNi$), 137.74 (s, 1C, $\{Ar-b\}C^6$), 143.88 (d, $J_{CP} = 4$, 1C, $\{Ar-a\}C^6$), 144.69 (d, $^2J_{CP} = 29$, 1C, $\{Ar-a\}CNi$), 146.08 (d, $J_{CP} = 2$, 1C, $\{Ar-b\}C^6$), 155.63 (d, $J_{CP} = 5$, 1C, $\{^{CN}Ar\}C^{ipso}$), 159.35 (d, $^3J_{CP} = 4$, 1C, $\{Ar-a\}C^6$), 166.03 (d, $^3J_{CP} = 11$, 1C, $\{Ar-b\}C^2$), 167.68 (d, $^3J_{CP} = 14$, 1C, $\{Ar-a\}C^2$), 214.42 (d, $^2J_{CP} = 106$, 1C, $CN\{^{CN}Ar\}$).

^{31}P NMR (δ , C_6D_6): 180.28 (s, 1P, P-b), 183.43 (s, 1P, P-a).

Anal. Calcd for $C_{49}H_{61}N_3Ni_2O_2P_2$: C, 65.15, H, 6.81; N, 4.65; Found: C, 65.11; H, 7.14; N, 4.58

5.4.3 Cyclic voltammetry.

Cyclic voltammetry measurements were performed using a BAS Epsilon potentiostat. The electrochemical properties of compound **5.1** were measured at room temperature in dichloromethane using a standard three-electrode system consisting of a glassy carbon working electrode, a Pt auxiliary electrode, and a Ag/AgCl reference electrode. Bu_4NPF_6 was used as electrolyte (0.1 mol/dm^3) and the solutions were bubbled with nitrogen before each experiment. Quasi-reversible redox waves of the ferrocenyl moieties were observed under these conditions ($E_{1/2} \{FeCp_2^+/FeCp_2\} = +0.48 \text{ V}$).

5.4.4 Crystal Structure Determinations.

Single crystals of **5.1** were grown from a DCM/hexane solution by slow diffusion of hexanes into a saturated solution of the complex **5.1**. The crystallographic data for complexes **5.1** was collected on a Bruker Microstar generator (rotating anode) equipped with a Helios optics, a Kappa Nonius goniometer and a Platinum135 detector.

Cell refinement and data reduction were done using SAINT⁸. An empirical absorption correction, based on the multiple measurements of equivalent reflections, was applied using the program SADABS.⁹ The space group was confirmed by XPREP routine¹⁰ in the program SHELXTL.¹¹ The structures were solved by direct-methods and refined by full-matrix least squares and difference Fourier techniques with SHELX-97.¹² All non-hydrogen atoms were refined with anisotropic displacement parameters. Hydrogen atoms were set in calculated positions and refined as riding atoms with a common thermal parameter. Publication materials as well as ORTEP drawing were prepared by using LinXTL¹³ and Platon in above program.

¹ Zhang, S. W.; Ishii, R.; Motoori, F.; Tanaka, T.; Takai, Y.; Sawada, M.; Takahashi, S. *Inorg. Chim. Acta* **1997**, *265*, 75–82.

² K. Hirano, S. Urban, C. Wang, F. Glorius, *Org. Lett.*, **2009**, *11*, 1019-1022.

³ P. Zhichkin, D. J. Fairfax, S. A. Eisenbein, *Synthesis*, **2002**, 720-722.

⁴ Vujkovic, N.; Ward, B. D.; Maise-Francois, A.; Wadepohl, H.; Mountford, P.; Gade, L. H. *Organometallics* **2007**, *26*, 5522-5534.

⁵ Scheuermann, M. L.; Rheingold, A. L.; Williams, B. S. *Organometallics* **2009**, *28*, 1613-1615.

⁶ For acyl complexes see: (a) Liebeskind, L. S.; Welker, M. E.; Fengl, R. W. *J. Am. Chem. Soc.* **1986**, *108*, 6328-6343. (b) Goldberg, K. I.; Bergman, R. G. *Organometallics* **1987**, *6*, 430-432. For formimino complexes see: (c) Wakatsuki, Y.; Aoki, K.; Yamazaki, H. *J. Chem. Soc., Dalton Trans.* **1986**, 1193.

⁷ Zhang, C.; Wang, Z. *Organometallics* **2009**, *28*, 6507-6514.

⁸ SAINT (1999) Release 6.06; Integration Software for Single Crystal Data. Bruker AXS Inc., Madison, Wisconsin, USA.

⁹ Sheldrick, G.M. (1999). SADABS, Bruker Area Detector Absorption Corrections. Bruker AXS Inc., Madison, Wisconsin, USA.

¹⁰ XPREP (1997) Release 5.10; X-ray data Preparation and Reciprocal space Exploration Program. Bruker AXS Inc., Madison, Wisconsin, USA.

¹¹ SHELXTL (1997) Release 5.10; The Complete Software Package for Single Crystal Structure Determination. Bruker AXS Inc., Madison, Wisconsin, USA.

¹² (a) Sheldrick, G.M. (1997). SHELXS97, Program for the Solution of Crystal Structures. Univ. of Gottingen, Germany. (b) Sheldrick, G.M. (1997). SHELXL97, Program for the Refinement of Crystal Structures. University of Gottingen, Germany.

¹³ LinXTL is the local program and it could be obtained free of charge from <http://sourceforge.net/projects/linxtl/files/>

Chapter 6: POCN pincer complexes of nickel featuring secondary amine ligand arm.

6.1 Introduction

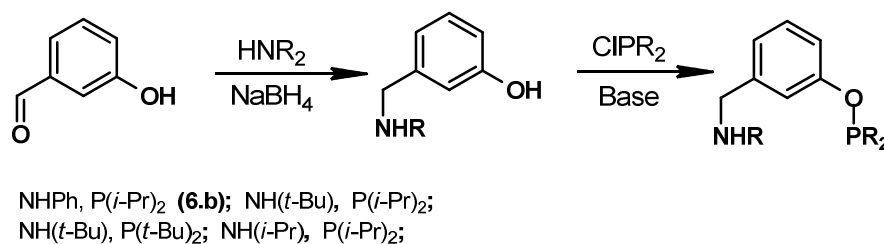
Many symmetric and asymmetric pincer ligands were reported in the literature and their behavior was successfully explored with a large number of different metal ions. Pioneering¹ and further work in this area was mostly concentrated on symmetric pincer ligands featuring tertiary substituted donating ligands. Later, some variations in conventional pincer ligands were demonstrated. Thus, CNS² and PCN^{3,4} pincer ligand were developed and their properties were explored. Despite the variety of pincer system in the literature, there are almost no or little studies conducted concerning reactivities of secondary amine substituted pincer systems.

Previously, we have described POCN-type pincer nickel complexes with various type of coordinating ligand in the amine arm.^{5,6} Some detailed properties of POCN ligands have been described earlier in our previous reports. We have shown that secondary amine-based pincer complexes could be easily prepared by conventional, cyclometallation route. In our quest for 14 electron reactive species, we have investigated the reaction of this type of complexes with various metallo-organic reagents.⁶ However, these reactions did not furnish the 14 electron or nickel alkyl complexes, but rather dimerise two pincer moieties to form bimetallic systems. In the search for alternative ligand structures, we have decided to investigate more bulky or weakly donating coordinating ligands in order to prevent dimerisation. Herein, we describe properties of new POCN pincer complexes featuring a secondary amine arm with different steric bulk of the donating ligands.

6.2 Results and Discussion

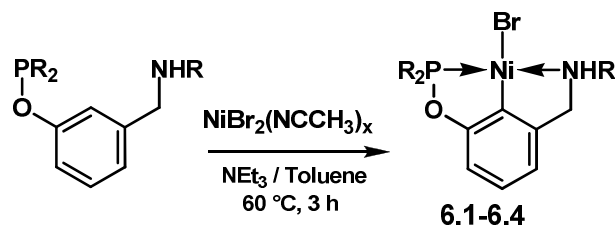
6.2.1 Syntheses.

A three step procedure was applied in order to achieve POCN pincer complexes. The aminophenol precursors for the POCN ligands were prepared by condensation of 3-hydroxybenzaldehyde with the corresponding secondary amines, followed by reduction of the *in situ* formed Schiff base with NaBH₄ in methanol. Finally, phosphination of the obtained aminophenols with *i*-Pr₂PCl or *t*-Bu₂PCl, exclusively furnished POCN pincer ligands as products of OH group phosphination (Scheme 6.1).



Scheme 6.1. Synthesis of POCN-type ligand

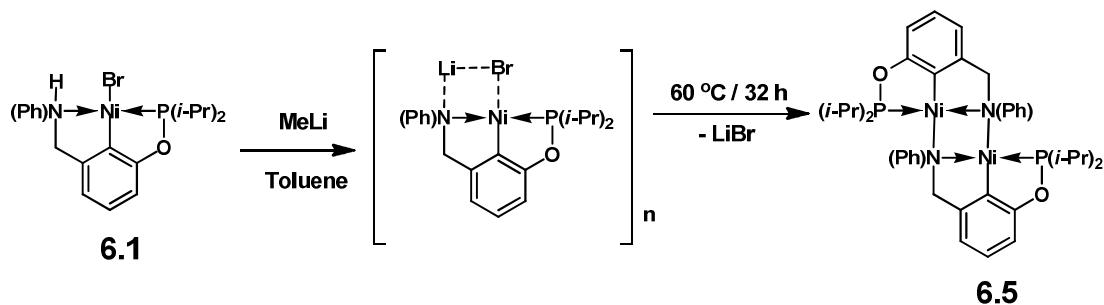
While reaction of the preligand with *i*-Pr₂PCl was smooth in the presence of NEt₃ as a base, the reaction with *t*-Bu₂PCl was somewhat sluggish and much stronger base (NaH) and harsher conditions (reflux CH₃CN 2 days) were implemented for the reaction to occur. Ligand **6.b** was isolated and fully characterized while other POCN ligands were used without isolation. Cyclometalations of POCN ligands were achieved under mild conditions and in the presence of NEt₃ in order to quench *in situ* generated HBr (Scheme 6.2)



NHPh, P(*i*-Pr)₂ (**6.1**); NH(*t*-Bu), P(*i*-Pr)₂ (**6.2**);
 NH(*t*-Bu), P(*t*-Bu)₂ (**6.3**); NH(*i*-Pr), P(*i*-Pr)₂ (**6.4**);

Scheme 6.2. Cyclometallation reaction

The synthesis of **6.5** was performed via reaction of **6.1** with solid methyl lithium in toluene as a solvent (Scheme 6.3). Transformation of **6.1** to **6.5** was monitored by ³¹P NMR spectroscopy over a week. During this time, the mixture was gradually changing in color from yellow-brown to dark red and the peak at 202.6 ppm in phosphorus NMR was gradually disappearing with a grow of another peak at 189.9 ppm. This reaction, as shown previously, was passing through the formation of NMR silent lithium adduct, the identity of which was realized previously⁶ (Scheme 6.3).



Scheme 6.3. Transformation of **6.1** to **6.5**

6.2.2 Characterisation

All precursors for ligand synthesis were fully characterized by NMR and elemental analysis. Noteworthy, the preligand **6.c** displayed somewhat limited solubility in CDCl₃ and its NMR was performed in CD₃OD. As a consequence the

NH and OH signals of this preligand were overlapping with residual OH peak of CD_3OH . The identity of ligand **6.b** was confirmed by NMR spectroscopy while all other ligands were used without isolation. The diamagnetic pincer complexes were fully characterized by NMR, elemental analysis and single crystal structure determination. Due to the complex hydrogen coupling in 1H -NMR some additional HETCOR experiments were performed. Assignments of all carbon and hydrogen signals were carried out by using HMQC and 1H -COSY NMR spectroscopy. Absence of symmetry in complexes **6.1-6.4** makes CH_3 and PCH protons appears as an individual doublet of doublet and multiplet, respectively. The presence of a chiral nitrogen center also complicates the appearance of $ArCH_2$ protons in the complexes. Surprisingly, one of these hydrogens $ArCH_2$ shows strong coupling with NH proton and appears as a doublet of doublet while the other only couples with its germinal neighbor and gives a doublet (1-3 in Figure 6.1).

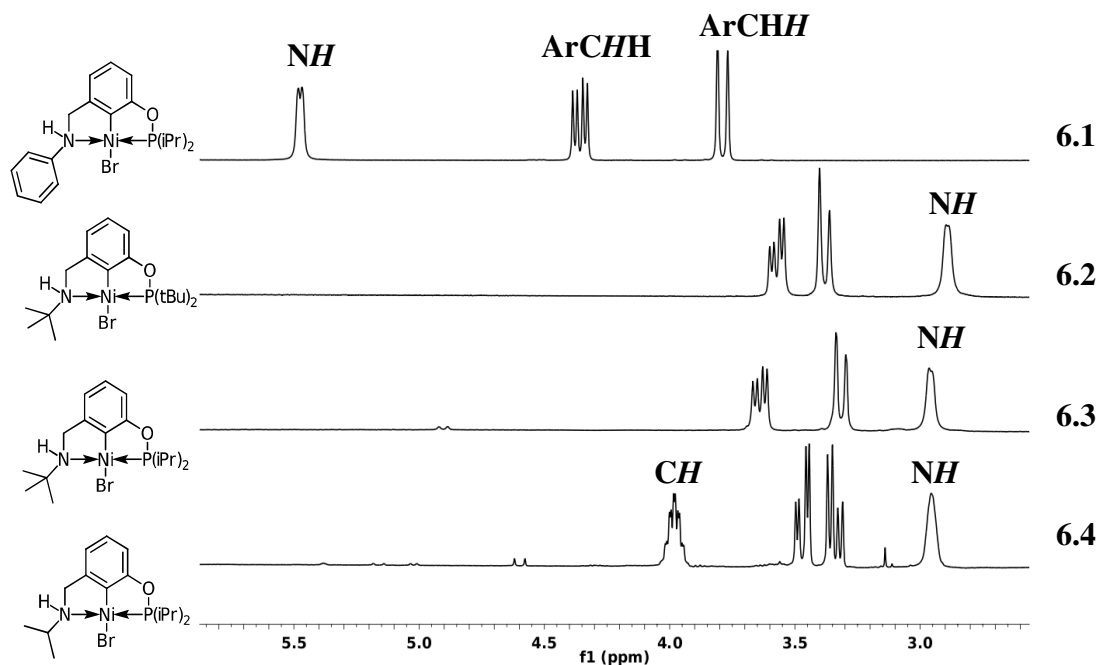


Figure 6.1. The methylene region in the 1H -NMR spectra (C_6D_6) of complexes **6.1-6.4**

An additional complication, in 1H -NMR spectral appearance, was spotted in complex **6.4**. Thus, the $ArCH_2$ protons display strong ($J_{HH} = 16$ Hz) geminal

coupling between each other and typical, non equivalent ($J_{HH} = 8$ Hz, $J_{HH} = 5$ Hz), coupling with the *NH* proton (4 in Figure 6.1). Interestingly, the \underline{CH} proton in the isopropyl group of complex **6.4** exhibits a small coupling to phosphorus ($J_{HP}=2$ Hz) and appears as a doublet of septuplets. It's worth noting, that the *NH* proton for all aliphatic amines appears in ^1H NMR around 3 ppm, while in the case of complex **6.1**, it appears much more downfield (5.5 ppm). Dimeric complex **6.5**, on the other hand, displays only two peaks in the methylene region and appears similar to **6.1**. Also complex **6.5** shows the equivalence of all symmetry-related protons and carbon nuclei.

Analysis of phosphorus NMR spectra of these complexes was straightforward, having a single resonance peak for complexes near 200 ppm (**6.1**, 202.6; **6.2**, 196.6; **6.3**, 195.11; **6.4**, 198.4). Interestingly, more downfield chemical shift in ^{31}P was obtained for complexes with smaller amine or phosphine substituents. However, these observations cannot be correlated with the observed ^{31}P peak for complex **6.5** (190 ppm).

All obtained complexes were additionally characterized by single crystal structure determination in order to obtain their structural parameters. Crystal and data collection details for all complexes are summarised in Table 6.1-6.4. The ORTEP diagram for complexes **6.1-6.4** presented in Figure 6.3 and for complex **6.5** in

Figure 6.4. Due to the presence of chiral nitrogen centers, all presented complexes yielded a racemic mixture of R and S enantiomers.

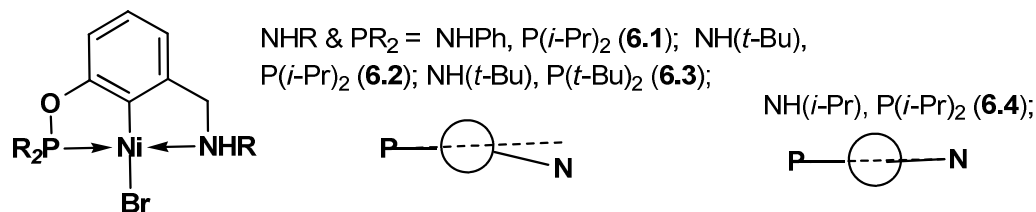


Figure 6.2. Structural features of POCN pincer complexes

X-ray diffraction studies of **6.1-6.4** showed that these complexes adopt moderately distorted square planar geometries in the solid state (Figure 6.3) with the greatest structural distortions appearing in the angles P-Ni-N (163-167°). Additional structural distortions were arising from the tilting of the amine ligand off the plane defined by Ni-C1-C2 (Figure 6.2). However, phosphine ligands in these complexes were always found in the plane. Unique example in this category is the complex **6.4** has both phosphine and amine arms in the plane. This behaviour is more likely a structural artifact which arises from packing of individual molecules in the crystal lattice. The phosphorus-nickel distances in complexes **6.1**, **6.2**, **6.4** were found to be much shorter (~2.11 Å) than in complex **6.3** (2.15 Å) for which (*t*-Bu)₂P was used as a ligand. Similar observations were noted in variation of Ni-N bonds of these complexes. Thus, complex **6.4** displays the shortest Ni-N (2.005(2) Å) bond distances, while complex **6.3** was found to have longest bond distances (2.032(2) Å) in the series. These structural features could be explained from a steric bulk point of view; the bulkier alkyl substituents the smaller pyramidity of the donor ligand and longer the distance to the metal. It is worth mentioning, that complex **6.5** resides on a symmetry element (inversion center) and the second part of this dimeric species was generated by symmetry (part “a”). Contrary to the previously described complex **3.5** complex **6.5** crystallise as “Z” shape, where two pincer moieties are perfectly parallel one to another. At the same time, atomic distances between two pincer moieties were

found to be much longer for complex **6.5** (1.985(2) Å) than for complex **3.5** (1.970(1) Å) reported previously. Similar observations could be seen for Ni-Ni distances. Thus, the Ni-Ni distance in complex **6.5** is much longer (2.838(1) Å) than for complex **3.5** (2.512(1) Å).

Figure 6.3. ORTEP diagrams for complexes **6.1** (a), **6.2** (b), **6.3** (c) and **6.4** (d). Thermal ellipsoids are set at the 50% probability level. Calculated hydrogen atoms are omitted for clarity.

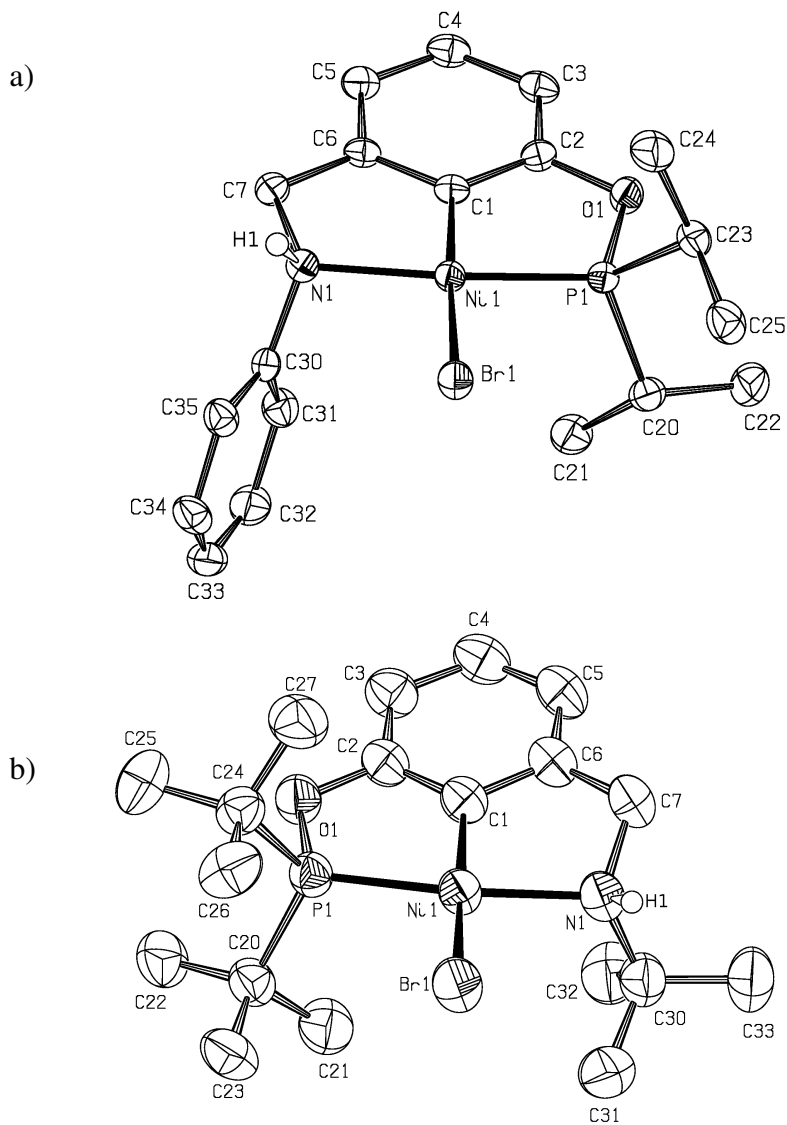


Figure 6.4. ORTEP diagrams for complex **6.5**. Thermal ellipsoids are set at the 50% probability level.

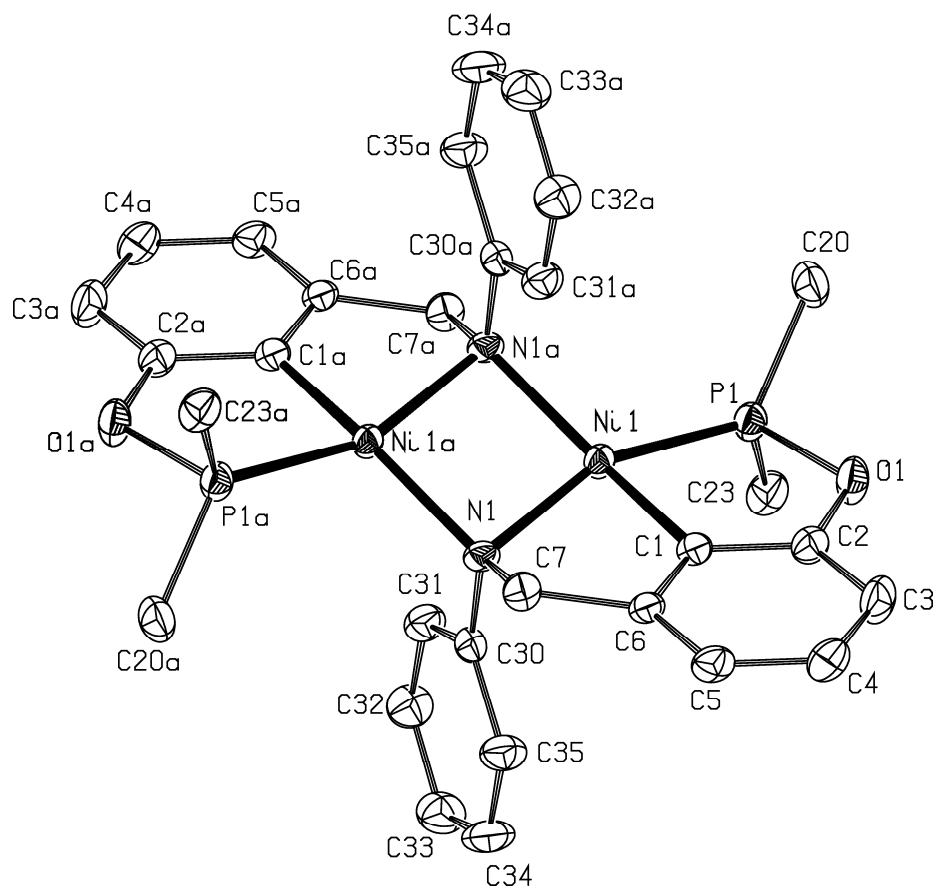


Table 6.1. Crystal Data Collection and Refinement Parameters for Complexes **6.1** and **6.5**.

	6.1	6.5
chemical formula	C ₁₉ H ₂₅ BrNNiOP,0.5(C ₆ H ₆)	C ₃₈ H ₄₈ N ₂ Ni ₂ O ₂ P ₂
crystal colour	Yellow	Red
<i>F</i> _w ; <i>F</i> (000)	492.04; 506	744.14; 784
<i>T</i> (K)	150	150
wavelength (Å)	1.54178	1.54178
space group	P-1	P-1
<i>a</i> (Å)	8.9115(2)	11.1174(2)
<i>b</i> (Å)	10.2997(3)	12.0007(2)
<i>c</i> (Å)	12.6496(3)	14.0031(3)
α (deg)	90.733(1)	107.425(1)
β (deg)	98.863(1)	90.600(1)
γ (deg)	110.671(1)	101.891(1)
<i>Z</i>	2	2
<i>V</i> (Å ³)	1070.50(5)	1739.04(6)
ρ_{calcd} (g·cm ⁻³)	1.527	1.421
μ (mm ⁻¹)	4.281	2.494
θ range (deg); completeness	3.55 – 60.48; 0.890	3.32 – 67.87; 0.862
collected reflections; <i>R</i> _{σ}	16909; 0.0190	25347; 0.0299
unique reflections; <i>R</i> _{int}	16909; 0.0429	25347; 0.0378
<i>R</i> 1 ^a ; <i>wR</i> 2 ^b [<i>I</i> > 2 σ (<i>I</i>)]	0.0278; 0.0775	0.0323; 0.0870
<i>R</i> 1; <i>wR</i> 2 [all data]	0.0280; 0.0777	0.0401; 0.0899
GOF	1.064	1.006
largest diff peak and hole	0.44 and -0.33	0.37 and -0.32

$$^a R_1 = \frac{\sum(|F_o| - |F_c|)}{\sum|F_o|}$$

$$^b wR_2 = \left\{ \frac{\sum[w(F_o^2 - F_c^2)^2]}{\sum[w(F_o^2)^2]} \right\}^{1/2}$$

Table 6.2. Crystal Data Collection and Refinement Parameters for Complexes **6.2-6.4**.

	6.2	6.3	6.4
chemical formula	C ₁₉ H ₃₃ BrNNiOP	C ₁₇ H ₂₉ BrNNiOP	C ₁₆ H ₂₇ BrNNiOP
crystal colour	Yellow	Yellow	Yellow
<i>F</i> _w ; F(000)	461.05; 480	433.00; 896	418.98; 1728
<i>T</i> (K)	150	150	150
wavelength (Å)	1.54178	1.54178	1.54178
space group	P-1	P21/c	Pbca
<i>a</i> (Å)	7.9840(2)	9.3629(3)	10.8825(2)
<i>b</i> (Å)	10.8172(3)	21.4243(6)	16.0131(3)
<i>c</i> (Å)	13.0862(3)	11.3528(3)	21.0574(4)
α (deg)	106.663(1)	90	90
β (deg)	92.922(1)	121.931(2)	90
γ (deg)	94.694(1)	90	90
<i>Z</i>	2	4	8.00(<i>Z'</i> =2)
<i>V</i> (Å ³)	1075.8(1)	1932.7(1)	3669.5(1)
ρ _{calcd} (g·cm ⁻³)	1.423	1.488	1.517
μ (mm ⁻¹)	4.210	4.649	4.878
θ range (deg); completeness	3.54 – 72.68; 0.958	4.13 – 72.83; 0.944	4.20 – 72.34; 0.999
collected reflections; R _σ	14325; 0.0222	20888; 0.0223	45256; 0.0123
unique reflections; R _{int}	14325; 0.0329	20888; 0.0372	45256; 0.0344
R1 ^a ; wR2 ^b [I > 2σ(I)]	0.0383; 0.1017	0.0378; 0.1040	0.0302; 0.0828
R1; wR2 [all data]	0.0399; 0.1031	0.0404; 0.1109	0.0324; 0.0841
GOF	1.091	1.105	1.112
largest diff peak and hole	0.01 and -0.02	0.46 and -0.87	0.55 and -0.90

$$^a R_1 = \frac{\sum(|F_o| - |F_c|)}{\sum|F_o|}$$

$$^b wR_2 = \left\{ \frac{\sum[w(F_o^2 - F_c^2)^2]}{\sum[w(F_o^2)^2]} \right\}^{1/2}$$

Table 6.3. Selected Bond Distances (Å) and Angles (deg) for Complexes **6.1–6.4**.

	6.1	6.2	6.3	6.4
Ni(1)-C(1)	1.851(3)	1.856(2)	1.852(3)	1.853(2)
Ni(1)-P(1)	2.1058(7)	2.1446(6)	2.1133(9)	2.1170(6)
Ni(1)-N(1)	2.012(2)	2.032(2)	2.025(3)	2.005(2)
Ni(1)-Br(1)	2.3552(5)	2.3644(4)	2.3554(6)	2.3471(4)
C(1)-Ni(1)-Br(1)	176.26(7)	169.58(6)	168.8(1)	174.49(6)
P(1)-Ni(1)-N(1)	165.03(7)	163.30(6)	163.33(8)	166.83(5)
P(1)-Ni(1)-Br(1)	95.83(2)	99.82(2)	96.22(3)	96.054(2)
N(1)-Ni(1)-Br(1)	97.96(6)	96.11(6)	99.54(8)	96.73(5)
P(1)-Ni(1)-C(1)	81.95(7)	81.16(7)	81.6(1)	81.96(6)
N(1)-Ni(1)-C(1)	84.57(9)	84.08(8)	83.9(1)	85.02(7)

Table 6.4. Selected Bond Distances (Å) and Angles (deg) for Complex **6.5**.

	6.5
Ni(1)-C(1)	1.854(2)
Ni(1)-N(1)	1.996(2)
Ni(1)-N(1A)	1.9847(2)
Ni(1)-Ni(1A)	2.8377(6)
Ni(1)-P(1)	2.1210(6)
C(1)-Ni(1)-N(1A)	157.68(8)
C(1)-Ni(1)-P(1)	81.38(7)
C(1)-Ni(1)-N(1)	83.79(8)
N(1)-Ni(1)-N(1A)	89.07(8)

6.3 Conclusion.

To summarize, new POCN pincer-type nickel complexes featuring secondary amine ligand have been synthesized. NMR studies of diamagnetic **6.1-6.4** complexes reveal NH moiety intact after cyclometallation and absence of $\{\text{Ar}\}\underline{H}^2$ indicating successful complexation reaction. Structural studies of these materials reveal slightly distorted square planar geometry, with the nitrogen moiety slightly tilted off the plane of coordination. Interestingly, this tilt was absolutely absent in the case of complex **6.4** and more likely arises from the packing of individual molecules in solid state. Additionally, all complexes, despite the presence of chiral center, have crystallized in non chiral space group; therefore indicating presence of mixture of enantiomers in the studied crystalline material. New dimeric complex **6.5** was synthesized and its structural as well as spectroscopic analysis was performed. Structural analysis of this species reveals the presence of two moiety of pincer complexes related one to another by the inversion center. Additionally, atomic distances between two pincer moieties of **6.5** were found to be much greater than in previously discovered complex **3.5**, suggesting easier dissociation of this dimer in solution.

Further investigations of these complexes are needed to better understand their reactivities.

6.4 Experimental Section

6.4.1 General.

All manipulations were carried out using standard Schlenk and glove box techniques under nitrogen atmosphere. All solvents used for experiments were dried to water contents of less than 10 ppm (determined using a Mettler Toledo C20 coulometric Karl Fischer titrator) by passage through activated aluminum oxide columns (MBraun SPS) and freeze-thaw degassed. C_6D_6 was dried over 4 Å molecular sieves and then freeze-thaw degassed. The following were purchased from Aldrich and, unless otherwise noted, used without further purification: Ni

(metal), chlorodiisopropylphosphine, 3-hydroxybenzaldehyde, NBS and triethylamine (was distilled over CaH_2 under nitrogen atmosphere). A Bruker AV 400 spectrometer was used for recording ^1H , $^{13}\text{C}\{^1\text{H}\}$ (101 MHz), and $^{31}\text{P}\{^1\text{H}\}$ (162 MHz). ^1H and ^{13}C chemical shifts are reported in ppm downfield of TMS and referenced against the residual C_6D_6 (7.15 ppm for ^1H and 128.02 ppm for ^{13}C) and CDCl_3 signals (7.26 ppm for ^1H and 77.16 ppm for ^{13}C); ^{31}P chemical shifts are reported in ppm and referenced against the signal for 85% H_3PO_4 (external standard, 0 ppm). Coupling constants are reported in Hz. The correlation and assignment of ^1H and ^{13}C NMR resonances were aided by ^1H COSY, HMQC, HMBC, DEPT, and $^1\text{H}\{^{31}\text{P}\}$ experiments when necessary. GC/MS measurements were made on an Agilent 6890N spectrometer.

6.4.2 Synthesis of ligands.

6.4.2.1 [3-((*N*-phenylamino)methyl)phenol] (**6.a**)

The procedure described⁶ for preparation of 3-((*N*-benzylamino)methyl)phenol was used to prepare current preligand. Compound isolated as off white solid with 87% yield.

^1H NMR (δ , C_6D_6): 3.85 (s, 2H, CH_2), 6.41 (d, $^3J = 8$, 2H, $\{\text{Ph}\}H^{\text{ortho}}$), 6.51 (d, $^3J = 8$, & s overlapping, 2H, $\{\text{Ar}\}H^6$ & $\{\text{Ar}\}H^2$), 6.70 (m, 2H, $\{\text{Ph}\}H^{\text{para}}$ & $\{\text{Ar}\}H^4$), 6.97 (t, $^3J = 8$, 1H, $\{\text{Ar}\}H^5$), 7.10 (t, $^3J = 8$, 2H, $\{\text{Ph}\}H^{\text{meta}}$)

$^{13}\text{C}\{^1\text{H}\}$ NMR (δ , C_6D_6): 47.99 (s, 1C, CH_2), 113.28 (s, 2C, $\{\text{Ph}\}C^{\text{ortho}}$), 114.25 (s, 1C, $\{\text{Ar}\}C^6$), 114.37 (s, 1C, $\{\text{Ar}\}C^2$), 117.90 (s, 1C), 119.53 (s, 1C), 129.50 (s, 2C, $\{\text{Ph}\}C^{\text{meta}}$), 129.93 (s, 1C, $\{\text{Ar}\}C^5$), 141.82 (s, 1C, $\{\text{Ar}\}C^3$), 148.44 (s, 1C, $\{\text{Ph}\}C^{\text{ipso}}$), 156.57 (s, 1C, $\{\text{Ar}\}C^1$)

Anal. Calcd for $\text{C}_{13}\text{H}_{13}\text{NO}$: C, 78.36; H, 6.58; N, 7.03;. Found: C, 78.21; H, 6.73; N, 7.00

6.4.2.2 [3-((*N*-phenylamino)methyl)phosphinitobenzene] (**6.b**)

Synthesis of **6.b** was conducted according to the procedure reported earlier for preparation of 3-((benzylamino)methyl)(phosphinito)benzene⁶. Final ligand isolated as colorless oil with yield more than 96 %.

¹H NMR (δ , C₆D₆): 0.97 (dd, ³J_{HP} = 16, ³J_{HH} = 7, 6H, 2×CH₃), 1.13 (dd, ³J_{HH} = 11, ³J_{HH} = 7, 6H, 2×CH₃), 1.64 – 1.87 (m, 2H, CH), 3.59 (br. s, 1H, NH), 3.94 (s, 2H, CH₂), 6.43 (d, ³J_{HH} = 8, 2H, {Ph}H^{ortho}), 6.71 (t, ³J_{HH} = 7, 1H, {Ph}H^{para}), 6.82 (d, ³J_{HH} = 8, 1H, {Ar}H⁴), 7.03 – 7.13 (m, 3H), 7.28 (s, 1H, {Ar}H²)

¹³C{¹H} NMR (δ , C₆D₆): 17.14 (d, ²J_{CP} = 9, 2C, 2×CH₃), 17.85 (d, ²J_{CP} = 21, 2C, 2×CH₃), 28.59 (d, ²J_{CP} = 18, 2C, 2×CH), 48.07 (s, 1C, CH₂), 113.18 (s, 2C, {Ph}C^{ortho}), 117.45 (d, ²J_{CP} = 11, 1C, {Ar}C⁶), 117.60 (s, 1C), 117.9 (d, ²J_{CP} = 10, 1C, {Ar}C²), 120.9 (s, 1C,) 129.39 (s, 2C, {Ph}C^{meta}), 129.78 (s, 1C, {Ar}C⁵), 141.92 (s, 1C, {Ar}C³), 148.59 (s, 1C, {Ph}C^{ipso}), 160.18 (d, ²J_{CP} = 9, 1C, {Ar}C¹)

³¹P NMR (162 MHz, C₆D₆) δ ppm 147.4 (s, 1P)

6.4.2.3 [3-((*N*-tert-butylamino)methyl)phenol] (**6.c**)

To a solution of 3-hydroxybenzaldehyde (2.5 g, 20.45 mmol) in 40 mL of methanol at r.t. was added a solution of t-butylamine (2.15 mL, 20.45 mmol) in 10 mL of methanol. The resulting mixture was stirred for two hour to obtain a white suspension of Schiff base. The suspension was then cooled to 0 °C and NaBH₄ (0.78 g, 20.45 mmol) was added portionwise over 2 hour. The resulting mixture was concentrated under reduced pressure, treated with 5% HCl until pH~1, and then treated with concentrated aqueous ammonia solution until pH=12 to free up the amine pre-ligand. The obtained suspension of **c** in water was treated with solid KCl (5 g). Filtration of the resulting suspension through a glass frit and drying under vacuum for 2 more hours gave a white powder. (3.67 g, 93 %). The compound was found to have limited solubility in C₆H₆, CHCl₃, and was partially soluble in CH₃OH, THF and CH₃CN.

^1H NMR (δ , CD_3OD): 1.46 (s, 9H, $3\times\text{CH}_3$), 4.08 (s, 2H, CH_2), 4.95 (br. s, 2H, NH & OH overlapping with CD_3OH), 6.86 (dd, $^4J = 2$, $^3J = 8$, 1H, $\{\text{Ar}\}H^6$), 6.97 (d, $^3J = 8$, & s overlapping, 2H, $\{\text{Ar}\}H^4$ & $\{\text{Ar}\}H^2$), 7.27 (t, $^3J = 8$, 1H, $\{\text{Ar}\}H^5$).

$^{13}\text{C}\{^1\text{H}\}$ NMR (δ , CD_3OD): 25.84 (s, 3C, $3\times\text{CH}_3$), 46.63 (s, 1C, CH_2), 58.58 (s, 1C, $\text{C}(\text{CH}_3)_3$), 117.33 (s, 1C, $\{\text{Ar}\}C^6$), 117.75 (s, 1C, $\{\text{Ar}\}C^2$), 121.74 (s, 1C, $\{\text{Ar}\}C^4$), 131.38 (s, 2C, $\{\text{Ar}\}C^5$), 134.43 (s, 1C, $\{\text{Ar}\}C^3$), 159.32 (s, 1C, $\{\text{Ar}\}C^1$).

6.4.2.4 [3-((*N*-iso-propylamino)methyl)phenol] (**6.d**)

The procedure described for preparation of **6.c** was used to prepare current preligand. Compound isolated a white solid with a yield of 79%.

^1H NMR (δ , CDCl_3): 1.16 (t, $^3J = 6$, 6H, $2\times\text{CH}_3$), 2.93 (hept, $J = 6$, 1H), 3.70 (s, 2H, CH_2), 5.49 (br. s, 2H, NH & OH), 6.70 (dd, $^4J = 4$, $^3J = 10$, 1H, $\{\text{Ar}\}H^6$), 6.76 (d, $^3J = 8$, & s overlapping, 2H, $\{\text{Ar}\}H^4$ & $\{\text{Ar}\}H^2$), 7.11 (t, $^3J = 8$, 1H, $\{\text{Ar}\}H^5$).

$^{13}\text{C}\{^1\text{H}\}$ NMR (δ , CDCl_3): 22.05 (s, 2C, $2\times\text{CH}_3$), 48.67 (s, 1C, CH_2), 50.99 (s, 1C, CH), 115.55 (s, 1C, $\{\text{Ar}\}C^6$), 116.24 (s, 1C, $\{\text{Ar}\}C^2$), 120.06 (s, 1C, $\{\text{Ar}\}C^4$), 129.91 (s, 1C, $\{\text{Ar}\}C^5$), 139.95 (s, 1C, $\{\text{Ar}\}C^3$), 157.34 (s, 1C, $\{\text{Ar}\}C^1$).

6.4.3 Synthesis of Complexes 6.1–6.5.

6.4.3.1 κ^P , κ^C , κ^N -{2,6-(*i*-Pr₂PO)(C₆H₃)(CH₂N(Ph)H)}NiBr (**6.1**).

The procedure described previously⁶ for the preparation of κ^P , κ^C , κ^N -{2,6-(*i*-Pr₂PO)(C₆H₃)(CH₂NBnH)}NiBr was used to prepare this complex, which was isolated as yellow powder with a yield of 74%.

^1H NMR (δ , C_6D_6): 1.02 – 1.14 (m, 6H, $2\times\text{CHCH}_3$), 1.19 (dd, $^3J_{\text{HH}} = 7$, $^3J_{\text{HP}} = 18$, 3H, CHCH_3), 1.44 (dd, $^3J_{\text{HH}} = 7$, $^3J_{\text{HP}} = 18$, 3H, CHCH_3), 1.86 – 2.01 (m, 1H, PCH), 2.10 – 2.24 (m, 1H, PCH), 3.79 (d, $^3J_{\text{HH}} = 16$, 1H, CH_2), 4.36 (dd, $^3J_{\text{HH}} = 7$, $^2J_{\text{HH}} = 16$, 1H, CH_2), 5.48 (br. d, $^3J_{\text{HH}} = 5$, 1H, NH), 6.42 (d, $^3J_{\text{HH}} = 7$, 1H, $\{\text{Ar}\}H^5$), 6.63 (d, $J = 8$, 1H, $\{\text{Ar}\}H^3$), 6.86 (t, $^3J_{\text{HH}} = 7$, 1H, $\{\text{Ar}\}H^4$), 6.91 (t, 1H, $\{\text{Ph}\}H^{\text{para}}$), 7.01 (t, $^3J_{\text{HH}} = 7$, 2H, $\{\text{Ph}\}H^{\text{meta}}$), 7.33 (d, 2H, $\{\text{Ph}\}H^{\text{ortho}}$).

$^{13}\text{C}\{^1\text{H}\}$ NMR (δ , C_6D_6): 16.26 (d, $^2J_{\text{CP}} = 3$, 1C, CHCH₃), 17.20 (s, 1C, CHCH₃), 17.90 (d, $^2J_{\text{CP}} = 5$, 1C, CHCH₃), 18.18 (d, $^2J_{\text{CP}} = 4$, 1C, CHCH₃), 28.16 (d, $^2J_{\text{CP}} = 19$, 1C, CHCH₃), 28.40 (d, $^2J_{\text{CP}} = 19$, 1C, CHCH₃), 62.67 (s, 1C, CH₂), 108.52 (d, $^2J_{\text{CP}} = 13$, 1C, {Ar}C³), 114.91 (s, 1C, {Ar}C⁵), 121.76 (s, 2C, {Ph}C^{meta}), 124.84 (s, 1C, {Ph}C^{para}), 127.27 (s, 1C, {Ar}C⁴), 128.99 (s, 2C, {Ph}C^{ortho}), 143.65 (d, $^2J_{\text{CP}} = 33$, 1C, {Ar}C¹-Ni), 146.48 (s, 1C, {Ph}C^{ipso}), 154.48 (s, 1C, {Ar}C⁶), 166.09 (d, $^2J_{\text{CP}} = 10$, 1C, {Ar}C²). ^{31}P NMR (162 MHz, C_6D_6) δ ppm 202.6 (s, 1P)

Anal. Calcd for $\text{C}_{19}\text{H}_{26}\text{NNiOPBr} + \frac{1}{2} \text{C}_6\text{H}_6$: C, 53.70; H, 5.74; N, 2.85;. Found: C, 53.64; H, 5.69; N, 2.93.

6.4.3.2 $\kappa^{\text{P}}, \kappa^{\text{C}}, \kappa^{\text{N}}\text{-}\{2,6\text{-}(i\text{-Pr})_2\text{PO}\}(\text{C}_6\text{H}_3)(\text{CH}_2\text{N}(t\text{-Bu})\text{H})\text{NiBr}$ (**6.2**).

To a stirred solution of **6.c** (0.500 g, 2.79 mmol) and triethylamine (0.400 mL, 2.85 mmol) the $(i\text{-Pr})_2\text{PCl}$ (0.460 mL, 2.79 mmol, 96%) was added at 0-5 °C. The resulting mixture was allowed to warm to r.t. and stirred for additional five hours. After that time, obtained solution was filtered through cannula into a suspension of $\text{NiBr}_2(\text{CH}_3\text{CN})_x$ (0.917 mg, 3.058 mmol) and triethylamine (0.400 mL, 2.85 mmol) in toluene (10 mL) at r. t. The resulting dark brown mixture was then heated for 3 h at 60 °C. After evaporation of the solvent to dryness, crude mixture was resolubilised in DCM and filtered through a short pad of silica gel (eluent: hexane followed by 50:50 CH_2Cl_2 :Hexane). This gave yellow powder of complex **2** (0.818 g, 68 %) after evaporation of the solvent.

^1H NMR (δ , C_6D_6): 1.06 (dd, $^3J_{\text{HH}} = 7$, $^3J_{\text{HP}} = 13$, 3H, CH₃CH), 1.15 (s, 9H, 3×CH₃C), 1.33 – 1.58 (m, 9H, 3×CH₃CH), 2.00 – 2.17 (m, 1H, PCH), 2.27 – 2.47 (m, 1H, PCH), 2.90 (br s, 1H, NH), 3.38 (d, $^3J_{\text{HH}} = 16$, 1H, ArCH₂), 3.57 (dd, $^3J_{\text{HH}} = 7$, $^3J_{\text{HH}} = 16$, 1H, ArCH₂), 6.37 (d, $^3J_{\text{HH}} = 8$, 1H, {Ar}H⁵), 6.58 (d, $^3J_{\text{HH}} = 8$, 1H, {Ar}H³), 6.87 (t, $^3J_{\text{HH}} = 8$, 1H, {Ar}H⁴).

$^{13}\text{C}\{^1\text{H}\}$ NMR (δ , C_6D_6): 15.72 (d, $^2J_{\text{CP}} = 4$, 1C, CH₃CH), 17.94 (m, 3C), 18.49 (d, $^2J_{\text{CP}} = 2$, 1C, CH₃CH), 28.38 (d, $^1J_{\text{CP}} = 23$, 1C, CH₃CH), 30.61 (s, 3C, 3×CH₃), 53.78 (s, 1C, ArCH₂), 57.57 (s, 1C, C(CH₃)₃), 108.14 (d, $^3J_{\text{CP}} = 13$, 1C, {Ar}C³), 114.62 (s, 1C, {Ar}C⁵), 126.98 (s, 1C, {Ar}C⁴), 142.53 (d, $^2J_{\text{CP}} = 36$, 1C, {Ar}C¹-

Ni), 154.36 (s, 1C, {Ar}C⁶), 166.06 (d, ²J_{CP} = 11, 1C, {Ar}C²). ³¹P{¹H} NMR (δ, C₆D₆): 196.90 (s, 1P).

Anal. Calcd for C₁₇H₂₉NNiOPBr: C, 47.16; H, 6.75; N, 3.23;. Found: C, 47.47; H, 6.65; N, 3.06.

6.4.3.3 κ^P, κ^C, κ^N-{2,6-(*t*-Bu₂PO)(C₆H₃)(CH₂N(*t*-Bu)H)}NiBr (**6.3**).

To a stirred solution of **6.c** (0.500 g, 2.79 mmol) the NaH (0.70 mg, 2.79 mmol) was added portionwise (caution H₂ evolution). The obtained mixture was then treated with (*t*-Bu)₂PCl (0.547 mL, 2.79 mmol, 96%) at r.t. and was left to stir at 100 °C overnight. After the obtained solution was filtered through cannula into a suspension of NiBr₂(CH₃CN)_x (0.917 mg, 3.058 mmol) and triethylamine (0.400 mL, 2.85 mmol) in toluene (10 mL) at r. t. The resulting dark brown mixture was then heated for 3 h at 60 °C. After evaporation of the solvent to dryness, crude mixture was resolubilised in DCM and filtered through a short pad of silica gel (eluent: hexane followed by 50:50 CH₂Cl₂:Hexane). This gave yellow powder of complex **6.3** (0.781 g, 61 %) after evaporation of the solvent.

¹H NMR (δ, C₆D₆): 1.14 (s, 9H, 3×CH₃), 1.47 (d, ³J_{HP} = 14, 9H, 3×CH₃P), 1.55 (d, ³J_{HP} = 14, 9H, 3×CH₃P), 2.96 (br. s, 1H, NH), 3.32 (d, ²J_{HH} = 16, 1H, ArCH₂), 3.64 (dd, ³J_{HH} = 7, ²J_{HH} = 16, 1H, ArCH₂), 6.35 (d, ³J_{HH} = 7, 1H, {Ar}H⁵), 6.56 (d, ³J_{HH} = 8, 1H, {Ar}H³), 6.85 (t, ³J_{HH} = 8, 1H, {Ar}H⁴).

¹³C {¹H} NMR (δ, C₆D₆): 28.24 (d, ²J_{CP} = 4, 3C, 3×CH₃C), 28.57 (d, ²J_{CP} = 4, 3C, 3×CH₃C), 30.54 (s, 3C, 3×CH₃C), 38.73 (d, ¹J_{CP} = 16, 1C, CH₃C), 39.76 (d, ¹J_{CP} = 13, 1C, CH₃C), 53.56 (s, 1C, ArCH₂), 57.38 (s, 1C, C(CH₃)₃), 108.20 (d, ³J_{CP} = 12, 1C, {Ar}C³), 114.44 (s, 1C, {Ar}C⁵), 126.85 (s, 1C, {Ar}C⁴), 142.13 (d, ²J_{CP} = 32, 1C, {Ar}C¹-Ni), 154.66 (s, 1C, {Ar}C⁶), 166.70 (d, ²J_{CP} = 10, 1C, {Ar}C²).

³¹P{¹H} NMR (δ, C₆D₆): 195.11 (s, 1P).

Anal. Calcd for C₁₉H₃₃NNiOPBr: C, 49.50; H, 7.21; N, 3.04;. Found: C, 49.44; H, 7.30; N, 2.88

6.4.3.4 $\kappa^P, \kappa^C, \kappa^N$ -{2,6-(*i*-Pr₂PO)(C₆H₃)(CH₂N(*i*-Pr)H)}NiBr (**6.4**).

The procedure described above for the preparation of **6.2** was used to prepare this complex, which was isolated as yellow powder with 75% (0.875 g) yield.

¹H NMR (δ, C₆D₆): 0.62 (d, ³J_{HH} = 7, 3H, NCHCH₃), 1.17 (dd, ³J_{HH} = 7, ³J_{HP} = 14, 3H, NCHCH₃), 1.23 (dd, ³J_{HH} = 7, ³J_{HP} = 15, 3H, PCHCH₃), 1.26 (d, ³J_{HH} = 7, 3H, NCHCH₃), 1.46 (dd, J = 7, ³J_{HP} = 17, 3H, PCHCH₃), 1.53 (dd, ³J_{HH} = 7, ³J_{HP} = 17, 3H, PCHCH₃), 2.07 – 2.20 (m, 1H, PCHCH₃), 2.23 – 2.36 (m, 1H, PCHCH₃), 2.96 (br. s, 1H, NH), 3.34 (dd, ³J_{HH} = 8, ²J_{HH} = 16, 1H, CH₂), 3.47 (dd, ³J_{HH} = 5, ³J_{HP} = 16, 1H), 3.91 – 4.08 (d sept, ³J_{HH} = 7, ³J_{HP} = 2, 1H, CHCH₃), 6.43 (d, ³J_{HH} = 7, 1H, {Ar}H⁵), 6.62 (d, ³J_{HH} = 8, 1H, {Ar}H³), 6.91 (t, ³J_{HH} = 7, 1H, {Ar}H⁴).

¹³C {¹H} NMR (δ, C₆D₆): 16.46 (d, ²J_{CP} = 3, 1C, PCHCH₃), 17.34 (s, 1C, NCHCH₃), 18.14 (d, ²J_{CP} = 5, 1C, PCHCH₃), 18.35 (d, ²J_{CP} = 4, 1C, PCHCH₃), 20.16 (s, 1C, NCHCH₃), 20.83 (d, ²J_{CP} = 2, 1C, PCHCH₃), 28.42 (d, ²J_{CP} = 9, 1C, PCH), 28.66 (d, ²J_{CP} = 9, 1C, PCH), 49.81 (s, 1C, NCH), 52.30 (s, 1C, ArCH₂), 108.10 (d, ³J = 13, 1C, {Ar}C³), 114.84 (s, 1C, {Ar}C⁵), 126.92 (s, 1C, {Ar}C⁴), 142.83 (d, ²J_{CP} = 33, 1C, {Ar}C¹-Ni), 154.52 (s, 1C, {Ar}C⁶), 166.14 (d, ²J_{CP} = 11, 1C, {Ar}C²). ³¹P{¹H} NMR (δ, C₆D₆): 198.04 (s, 1P).

Anal. Calcd for C₁₆H₂₇NNiOPBr: C, 45.87; H, 6.50; N, 3.34;. Found: C, 46.09; H, 6.56; N, 3.18.

6.4.3.5 [$\kappa^P, \kappa^C, \kappa^N$ -{2,6-(*i*-Pr₂PO)(C₆H₃)(CH₂NPh)}Ni]₂ (**6.5**)

To a stirred solution of **6.1** (0.500 g, 1.10 mmol) in dry and degassed toluene (10 mL) at r.t. was added solid MeLi (27.0 mg, 1.21 mmol), and the resulting yellow-brown mixture was stirred for 6 days at r.t. Conversion of **6.1** to **6.5** was monitored by ³¹P{¹H} NMR spectroscopy. At the end of reaction, the mixture was washed with water (3×10 mL) and evaporated under reduced pressure to give a red powder (0.217 g, 53%).

¹H NMR (δ, C₆D₆): 0.47 (dd, ³J_{HH} = 7, ³J_{HP} = 17, 6H, 2×PCHCH₃), 0.71 (dd, ³J_{HH} = 7, ³J_{HP} = 14, 6H, 2×PCHCH₃), 0.91 (dd, ³J_{HH} = 7, ³J_{HP} = 13, 6H, 2×PCHCH₃), 1.25 (dd, ³J_{HH} = 7, ³J_{HP} = 18, 6H, 2×PCHCH₃), 1.32 – 1.45 (m, 2H, 2×PCH), 1.65

– 1.83 (m, 2H, 2×PCH), 4.21 (dd, $^3J_{HP} = 5, 15$, 2H, 2×CHH), 4.84 (d, $^3J_{HH} = 15$, 2H, 2×CHH), 6.46 (d, $^3J_{HH} = 8$, 2H, {Ar}C⁴), 6.79 (t, $^3J_{HH} = 7$, 2H, {Ar}C⁴), 6.88 (d, $^3J_{HH} = 7$, 2H, {Ar}C⁴), 6.93 (t, $^3J_{HH} = 7$, 2H, {Ar}C⁴), 7.00 (d, $^3J_{HH} = 8$, 2H, {Ar}C⁴), 7.05 (d, $^3J_{HH} = 7$, 1H, {Ar}C⁴), 7.09 – 7.20 (m, 16H, {Ar}C⁴).

¹³C {¹H} NMR (δ, C₆D₆): 15.27 (d, $^2J_{CP} = 3$, 11C), 16.09 (s, 15C), 16.58 (s, 12C), 18.27 (d, $^2J_{CP} = 3$, 11C), 27.49 (d, $^2J_{CP} = 18$, 9C), 28.77 (d, $^2J_{CP} = 22$, 8C), 62.36 (s, 9C), 107.50 (d, $^2J_{CP} = 6$, 1C), 115.99 (s, 5C), 118.77 (s, 7C), 120.46 (s, 14C), 125.70 (s, 4C), 126.95 (s, 8C), 128.57 (s, 82C), 129.27 (s, 3C), 129.33 (s, 2C), 137.89 (s, 1C), 144.41 (d, $^2J_{CP} = 30$, 1C), 156.90 (s, 1C), 158.44 (s, 3C), 165.48 (d, $^2J_{CP} = 5$, 1C). ³¹P{¹H} NMR (δ, C₆D₆): 189.95 (s, 2P).

Anal. Calcd for C₃₈H₃₂O₂P₂N₂Ni₂: C, 62.22; H, 6.79; N, 3.63;. Found: C, 61.55; H, 6.75; N, 3.69

6.4.4 Crystal Structure Determinations.

Single crystals of **6.1-6.5** were grown by slow diffusion of hexanes into a saturated DCM (complex **6.2-6.4**) or C₆H₆ (complex **6.1, 6.5**) solution of each complex. The crystallographic data for complexes **6.1-6.5** were collected on a Bruker Microstar generator (rotating anode) equipped with Helios optics, a Kappa Nonius goniometer and a Platinum135 detector.

Cell refinement and data reduction were done using SAINT⁷. An empirical absorption correction, based on the multiple measurements of equivalent reflections, was applied using the program SADABS.⁸ The space group was confirmed by XPREP routine⁹ in the program SHELXTL.¹⁰ The structures were solved by direct-methods and refined by full-matrix least squares and difference Fourier techniques with SHELX-97.¹¹ All non-hydrogen atoms were refined with anisotropic displacement parameters. Hydrogen atoms were set in calculated positions and refined as riding atoms with a common thermal parameter, except for those of the NH moiety of complexes **6.1-6.4**, which were positioned from residual peaks in the difference Fourier map.

6.4.5 References

¹ (a) Moulton, C. J.; Shaw, B. L. *J. Chem. Soc., Dalton Trans.* **1976**, 1020-1024. (b) Van der Ploeg, A. F. M. J.; Van Koten, G.; Vrieze, K.; Spek, A. L.; Duisenberg, A. J. M. *Organometallics* **1982**, *1*, 1066-1070. (c) Grove, D. M.; Van Koten, G.; Ubbels, H. J. C.; Zoet, R.; Spek, A. L. *Organometallics* **1984**, *3*, 1003-1009. (d) Grove, D. M.; Van Koten, G.; Mul, P.; Van der Zeijden, A. A. H.; Terheijden, J.; Zoutberg, M. C.; Stam, C. H. *Organometallics* **1986**, *5*, 322-326.

² Amoedo, A.; Grana, M.; Martinez, J.; Pereira, T.; Lopez-Torres, M.; Fernández, A.; Fernández, J. J.; Vila, J. M. *Eur. J. Inorg. Chem.* **2002**, 613.

³ (a) (1) Poverenov, E.; Gandelman, M.; Shimon, L. J. W.; Rozenberg, H.; Ben-David, Y.; Milstein, D. *Chem. Eur. J.* **2004**, *10*, 4673. (b) Gong, J.; Zhang, Y.; Song, M.; Xu, C. *Organometallics* **2007**, *26*, 6487. (1) Inés, B.; SanMartin, R.; Churruca, F.; Domínguez, E.; Urriaga, M. K.; Arriortua, M. I. *Organometallics* **2008**, *27*, 2833.

⁴ van der Made, A. W.; van der Made, R. H. *J. Org. Chem.* **1993**, *58*, 1262.

⁵ Spasyuk, D. M.; Zargarian, D.; van der Est, A. *Organometallics* **2009**, *28*, 6531.

⁶ Spasyuk, D. M.; Zargarian, D. *Inorg. Chem.* **2010**, *49*, 6203-6213.

⁷ SAINT (1999) Release 6.06; Integration Software for Single Crystal Data. Bruker AXS Inc., Madison, Wisconsin, USA.

⁸ Sheldrick, G.M. (1999). SADABS, Bruker Area Detector Absorption Corrections. Bruker AXS Inc., Madison, Wisconsin, USA.

⁹ XPREP (1997) Release 5.10; X-ray data Preparation and Reciprocal space Exploration Program. Bruker AXS Inc., Madison, Wisconsin, USA.

¹⁰ SHELXTL (1997) Release 5.10; The Complete Software Package for Single Crystal Structure Determination. Bruker AXS Inc., Madison, Wisconsin, USA.

¹¹ (a) Sheldrick, G.M. (1997). SHELXS97, Program for the Solution of Crystal Structures. Univ. of Gottingen, Germany. (b) Sheldrick, G.M. (1997).

SHELXL97, Program for the Refinement of Crystal Structures. University of
Gottingen, Germany.

Chapter 7: Conclusions and perspectives

7.1 General

Undoubtedly, the chemistry of pincer complexes is one of the most valuable part of the organometallic chemistry. It opens a new possibility toward building new materials, exploring catalytic systems and brings us to the new level of multinuclear chemistry. However, pincer chemistry is not free of limitation. There are several challenges in this area such as: accessibilities of pincer ligands, ease of ligand tunability, cyclometalation step of pincer formation, cost of the starting materials and so on. By developing the POCN pincer system, we hoped to overcome these limitations and develop robust and easy accessible ligand structure with multi-diverse possibilities to tune properties of the metal hosting it.

7.2 Synthesis of ligands and complexes

In our work, we have shown that synthesis of POCN pincer ligand could be easily achieved in two simple steps via reductive amination of 3-hydroxybenzaldehyde follow by phosphination of obtained aminophenol by various amines (Scheme 7.1).



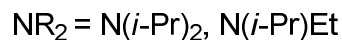
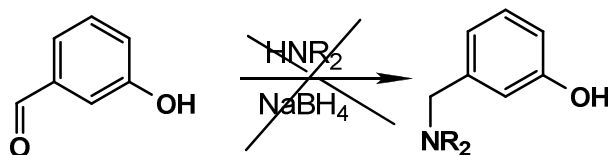
NR₂ = Morpholine, NEt₂, NMe₂, NPh,
NHBn, NH(*i*-Pr), NH(*t*-Bu)

PR₂ = P(*i*-Pr)₂, (*t*-Bu)₂

Scheme 7.1. Synthesis of POCN pincer ligand.

Although, amination reaction was proven to be successful with various primary and secondary amines, it was somewhat limited when using bulkier

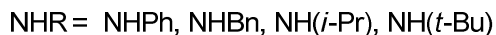
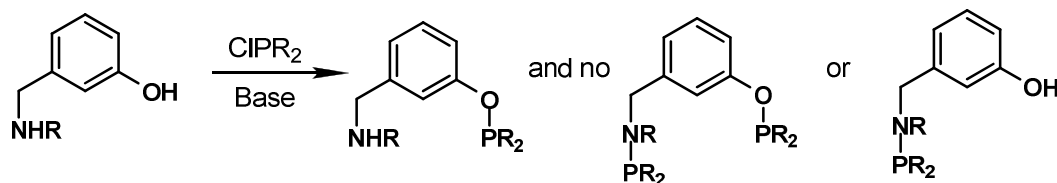
amines like diisopropylamine or isopropylethylamine. As a consequence no products were obtained for this type of starting materials (Scheme 7.2).



Scheme 7.2. Reductive amination with bulkier amines.

Additional complications occurred during reduction of the obtained Schiff base and iminium salt, in a form of 3-hydroxybenzylalcohol, which made the purification process of preligands difficult.

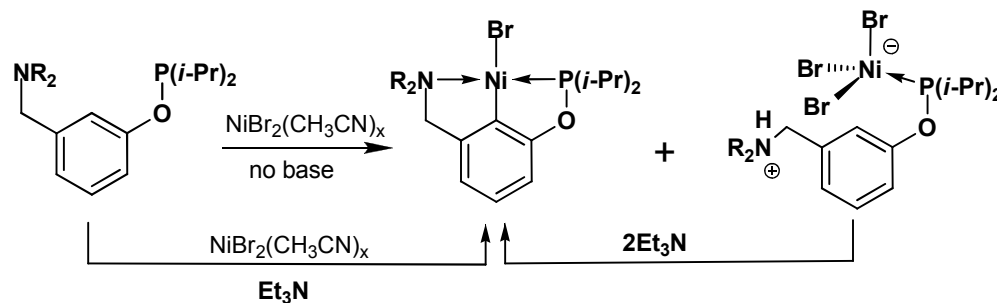
The phosphination of obtained aminophenol with various chlorophosphines furnish POCN ligands in almost quantitative yields. POCN ligands were also isolated in a good yield when the primary amine adducts were subjected to phosphination reaction (Scheme 7.3).



Scheme 7.3. Phosphination of primary amine adducts.

Cyclometalation of all POCN pincer ligands was smoothly achieved by using the $\text{NiBr}_2(\text{CH}_3\text{CN})_x$ precursor which was found to be very reactive and valuable in ligand-assisted C-H activations. Interestingly, cyclometalation of secondary amine POCN ligands did not affect the NH moiety of these ligands and

smoothly furnished final complexes as racemic mixtures of S and R enantiomers in good yield (~70 %).



Scheme 7.4. POCN pincer complex formation.

Also, use of base was necessary for successful cyclometallation and to achieve a high yield of desirable pincer complex. Furthermore, excluding the base from this reaction furnished the targeted pincer complex together with side-product (in 50:50 ratio) arising from protonation of the ligand by the *in situ* generated HBr (Scheme 7.4). The resulting protonated species could then be easily converted to the desirable pincer complex by reaction with two equivalents of the base. The protonated species might be of interest for kinetic studies of cyclometallation, since it excludes the ligand association process.

Depending on ligand structure, the general procedure that was developed for POCN nickel complex allowed high yield (~ 80%) isolations of the final compounds. Ease of wrap-up cyclometallation was in a way comparable with POCOP pincer system where cyclometallation with $\text{NiBr}_2(\text{CH}_3\text{CN})_x$ was as efficient. These findings not only facilitate the exploration of the POCN pincer chemistry, but also make it more attractive from commercial perspective. All nickel complexes and most of the starting ligands were fully characterized by NMR, elemental analysis as well as single crystal structure determination. Interestingly, the nitrogen arm of the POCN ligand was found to be slightly tilted from the Ni-C1-C6 plane (Figure 7.1) while phosphinito moiety was almost perfectly in plane.

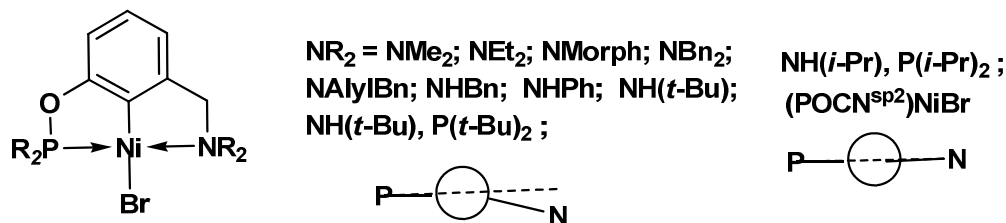


Figure 7.1. Structural features of (POCN)Ni complexes.

Noteworthy, that imino based pincer complex **4.3** and isopropyl complex **6.4** were having their nitrogen moiety perfectly in plane (Figure 7.1). Planarity of nitrogen arm in the complex **4.3** can be explained in term of sp^2 character of nitrogen atom, at the same time isopropyl complex **6.4** displays unusual behavior for this type of complex and more likely appears this way due to packing of individual molecules in a crystal lattice.

7.3 Tertiary amine-based POCN pincer complexes of nickel and their properties

Robust and electronically rich POCN ligand structures and ease of tunability allowed us to explore reactivities and physical properties of these materials. Electrochemical oxidation of $(\text{POCN}^{\text{RR}})\text{NiBr}$ complex by means of cyclic voltammetry showed sets of peaks at 1.0 V and 1.4 V. While, the first peak was found to be pseudo-reversible and corresponded to Ni^{II} to Ni^{III} transformation, the peak at 1.4 V was irreversible. Subsequently, after analysis of electrochemistry obtained for the corresponding ligands and preligand, the second peak was attributed to oxidation of ligand. These observations allowed us to conclude that $(\text{POCN}^{\text{RR}})\text{NiBr}$ pincer complexes are much more electron rich than corresponding $(\text{POCOP})\text{NiBr}$ pincer complexes and somewhat less electron rich than PCP and NCN pincer systems, reported earlier. Additionally, all $(\text{POCN}^{\text{RR}})\text{NiBr}$ complexes demonstrated very similar oxidation potentials from Ni^{II} to Ni^{III} and so the properties of these complexes, as well as ability to furnish stable Ni^{III} species, will depend only on the steric bulk of alkyl substituents in the amino moiety.

Chemical oxidation of $(\text{POCN}^{\text{RR}})\text{NiBr}$ was performed by using Br_2 or NBS. It is important to note, that use of dry solvent under nitrogen atmosphere was essential for successful outcome of reaction; otherwise significant amount of ligand protonated species was obtained arising from *in situ* generated HBr. Thermal stabilities of $(\text{POCN}^{\text{RR}})\text{Ni}^{\text{III}}\text{Br}_2$ complexes were established in solution (UV-Vis) and in solid state (TGA, DSC). Interestingly, complexes with small substituents on the amine moiety, were found to be highly stable in both solid state and in solution while the complex bearing ethyl groups in the amine arm was decaying very rapidly (Figure 7.2). This helped us to conclude that since electronic properties of $(\text{POCN}^{\text{RR}})\text{NiBr}$ complexes are the same, the steric factor is dominant for formation of stable Ni^{III} .

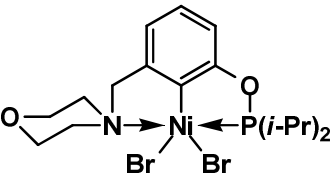
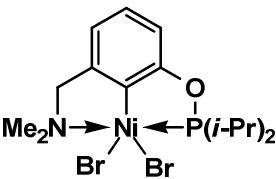
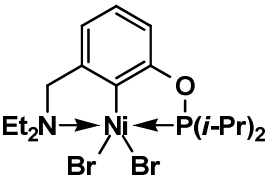
			
Electron richness of Ni^{II}	=	=	=
Stability in solid state	=	>>	>>
Stability in solution	>	>>	>>
Activity of $[\text{Ni}^{\text{II}}]$ in Kharasch addition	50 TON	50 TON	not active

Figure 7.2. Comparison of Ni^{III} stability.

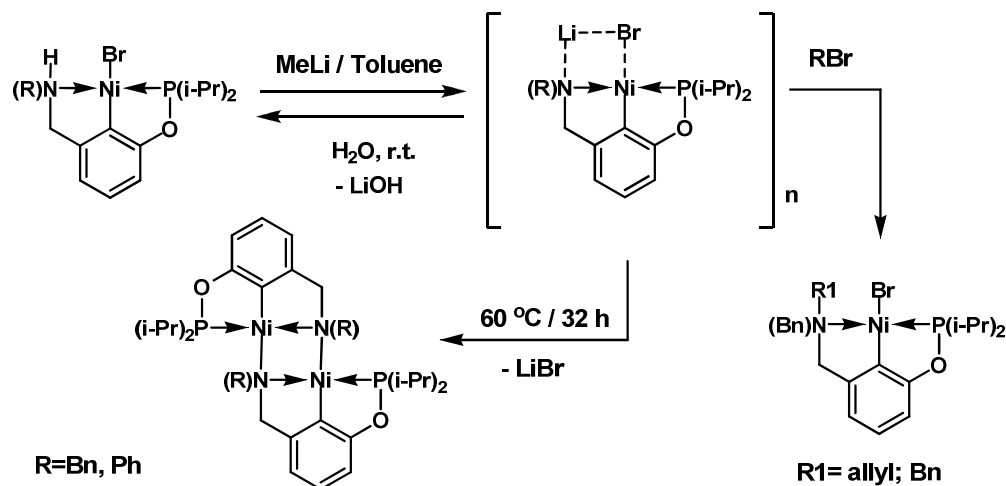
The catalytic activities of $(\text{POCN}^{\text{RR}})\text{NiBr}$ complexes were investigated in reaction of Kharasch addition for which oxidation from Ni^{II} to Ni^{III} is essential. Our findings have shown that the most stable $(\text{POCN}^{\text{RR}})\text{NiBr}$ complex displayed strongest reactivities in Kharasch addition while unstable $(\text{POCN}^{\text{Et}})\text{NiBr}$ or $(\text{POCN}^{\text{Et}})\text{NiBr}_2$ were ineffective in this transformation (Figure 7.2). Based on this observation we have concluded that catalytic efficiency as well as electron

richness of the metal in the nickel pincer complexes, follow the order $\text{NCN} > \text{POC}_{\text{sp}^3}\text{OP} > \text{POCN}$. However, we have shown that the steric bulk of the ligand also greatly influences the reactivities of the pincer nickel complexes in the Kharasch addition. We hope that this new discovery would be the potential guidance to develop new catalysts for this type of transformation.

In addition to these features of POCN pincer complexes we have found that these materials are double luminescent in solid state and further investigation of spectroscopy of these materials will be continued.

7.4 Secondary amine-based POCN pincer complexes of nickel and their properties

Interesting properties of $(\text{POCN}^{\text{RH}})\text{NiX}$ complexes were discovered in reactions with alkyl lithium reagents. Surprisingly, reaction of $(\text{POCN}^{\text{RH}})\text{NiBr}$ with methyl lithium did not furnish any detectable quantities of $(\text{POCN}^{\text{RH}})\text{NiMe}$ complex. However, it led to deprotonation of NH moiety and formation of lithium bromide adduct. Unexpectedly, no methyl complex was obtained even when excess of alkylation reagent was used (Scheme 7.5).

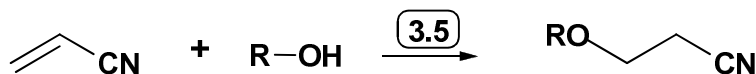


Scheme 7.5. Reactivities of secondary amine complexes.

Unfortunately, we were unable to isolate the lithium bromide adduct, but its identity was confirmed by a series of reactions with alkyl halides and water. Thus, reaction of the lithium bromide adduct with water regenerated the starting (POCN^{RH})NiBr complex while benzyl bromide or allyl bromide furnished corresponding (POCN^{RR})NiBr complexes in good yield (Scheme 7.5). These reactions not only allowed us to conclude about the nature of the lithium adduct but also elegantly demonstrated the ways of ligand transformation associated with metal center. Potentially, this transformation could help to create polymeric pincer complexes suitable for industrial heterogeneous catalysis or introduce unusual functionality close to the metal center.

Heating the lithium bromide adduct for 32 h at 60 °C lead to elimination of LiBr and to generation of dimeric [$\kappa^P, \kappa^C, \kappa^N, \mu^N$ -(2,6-(*i*-Pr)₂PC₆H₃CH₂NR)Ni]₂ species (Scheme 7.5). Interestingly, the properties of these materials are in a way comparable with the properties of amido complex reported by Campora¹. However, the dimeric complex was found to be much more stable toward reaction with water.

The dimeric species **3.5** displayed multi-diverse reactivities with various types of organic ligands. We found that these complexes can easily associate alcohol and react with weak acids like phenyl acetylene or phthalimide. Based on these reactivities, the catalytic hydroalkoxylation of olefin by various alcohols was established (Scheme 7.6).

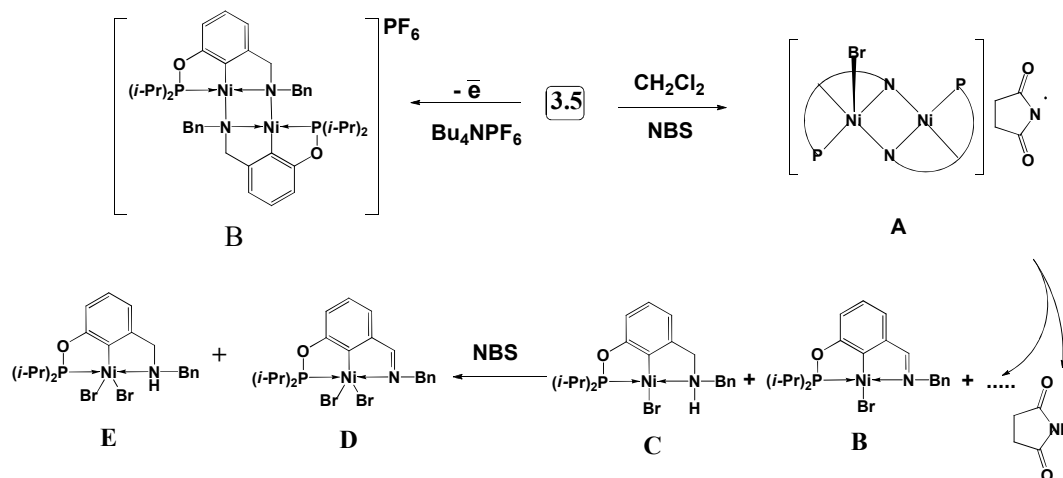


Scheme 7.6. Hydroalkoxylation reaction.

It is noteworthy, that water can also catalytically react with olefins, but the product of such transformation was found only in trace amount. Interestingly,

alcohols with higher acidity were performing much better with up to 2000 catalytic turnovers, while bulkier and less acidic alcohols were less reactive. Mechanism of such transformation is believed to proceed through activation of alcohol by dimeric species via hydrogen bonding with one or two amido moieties followed by reaction with acrylonitrile and elimination of the products. The further investigation of mechanism of this transformation would be simpler with (POCN)NiOR, complexes since it is known that similar alkoxy complexes can easily associate alcohol and can be potential catalysts for this transformations. Also, since dimeric complex **3.5** does not promote hydroamination it would be interesting to investigate possible hydroalkoxylation of amino alcohols.

Unexpected reactivity of dimeric species (**3.5**) were discovered while investigating the oxidation chemistry of this material. Complex **3.5** was found to be much more electron rich and displayed the half cell potential $E^{1/2}_0$ at -0.06 V than monomeric amino analogues $\kappa^P, \kappa^C, \kappa^N$ -(2,6-(*i*-Pr₂POC₆H₃CH₂NR₂)NiBr (ca. 0.60 V for NR₂= NMe₂, NEt₂, and *N*-morpholinyl). Using mild oxidants like NBS or any monomeric (POCN)Ni^{III} complexes we have shown that dimeric species splits into the (POCN^{sp2})NiBr₂ complex (Scheme 7.7). Eventually 23 % of (POCN^{sp2})NiBr₂ (**D**) was recovered from the reaction mixture and fully characterized. Mechanistic insight into this reaction was gained through a series of NMR, EPR, UV-Vis-NIR and spectroelectrochemical experiments.

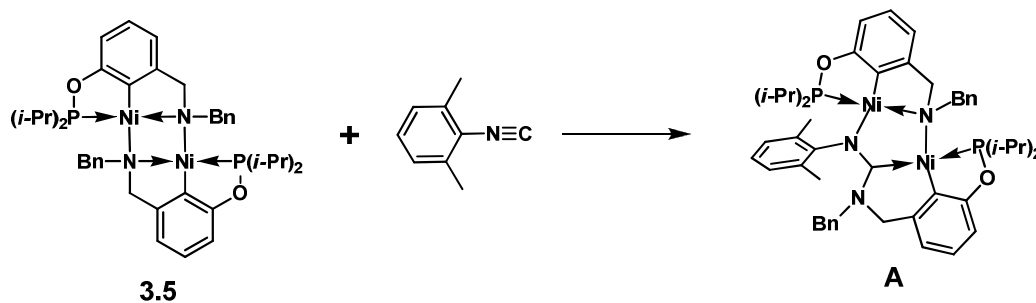


Scheme 7.7. Oxidation of dimeric POCN complex.

Therefore, we have concluded that oxidation of **3.5** to $(\text{POCN}^{\text{sp}2})\text{NiBr}_2$ is a multistep process. It involves oxidation of one of the metal centers in **3.5** and formation of meta-stable intermediate **A**, evidence of which was found by spectroelectrochemistry (**B**). The structural features of intermediate **A** were established by density functional theory. The calculated and experimentally found electronic spectra for intermediate **A** are in good agreement with each other, therefore providing convincing proof of the structure of **A**. The intermediate **A** was found to be unstable and rapidly decayed to monomeric Ni^{II} complexes **B** and **C** as confirmed by ^1H NMR and ^{31}P NMR spectroscopy. The subsequent oxidation of obtained species to Ni^{III} complexes **D** and **E** was monitored by UV-Vis and EPR. Results of these investigations have confirmed the identity of **D** and **E**, where **D** was also isolated in 23 % yield from reaction mixture.

The investigated oxidation chemistry of dimeric species **3.5** is of interest for our further catalytic studies of this unique species in reaction of Kharasch addition and Kumada coupling for which $\text{Ni}(\text{III})$ intermediate is essential.

Unusual reactivity of complex **3.5** was observed in reaction with 2,6-dimethylphenyl isocyanide. Transformation of dimeric nickel species **3.5** resulted in cleavage of coordinate Ni1-N1 and anionic Ni2-N1 bonds of the dimer and formation of new POCC-type 5,6-metalocycles featuring phosphinito and carbene moiety directly coordinated to the metal center.



Scheme 7.8. Transformation of complex **3.5** in reaction with 2,6-(CH₃)₂C₆H₃NC.

Interestingly, increase of the quantity of 2,6-dimethylphenyl isocyanide up to 5 molar excess and increasing the temperature of reaction to 60 °C did not furnish a double insertion product. These findings would be potentially of interest for catalytic amination of isonitrile by amine and formation of amidines as valuable organic materials.

7.5 References

¹ Campora, J.; Palma, P.; del Rio, D.; Conejo, M. M.; Alvarez, E. *Organometallics* **2004**, *23*, 5653-5655.

Chapter 8: Appendices

8.1 General

All supplementary materials such as crystallographic information files and source code of LinXTL were deposited on CD (or online) attached to the present thesis.

8.2 LinXTL

LinXTL is the crystallographic toolbox and text editor combining the power of SHELX and popular sets of programs for crystal structure refinement. LinXTL does not include any of the commercial or non commercial programs or source code used in these programs, however provides GUI environment for these program. LinXTL distributed under terms and conditions of GNU license.

8.2.1 General introduction to LinXTL

LinXTL was originally written for Linux, but I might release a Windows version as well. For those who are familiar with “SHELXTL” software, originally developed by Bruker inc., it would be an easy switch. LinXTL includes basic options of the text editor like Copy, Paste, Delete, Undo (Figure 8.1), program also contains sets of useful options helping to solve X-Ray structures like automatic weight refinement, completion of the structure and many more. It also provides an easy way to prepare tables of crystallographic information and helps to validate, combine, and manipulate the cif files. Some additional tools are currently under development. This software was very useful for me during my studies and for those who tested and gave their feedback about it.

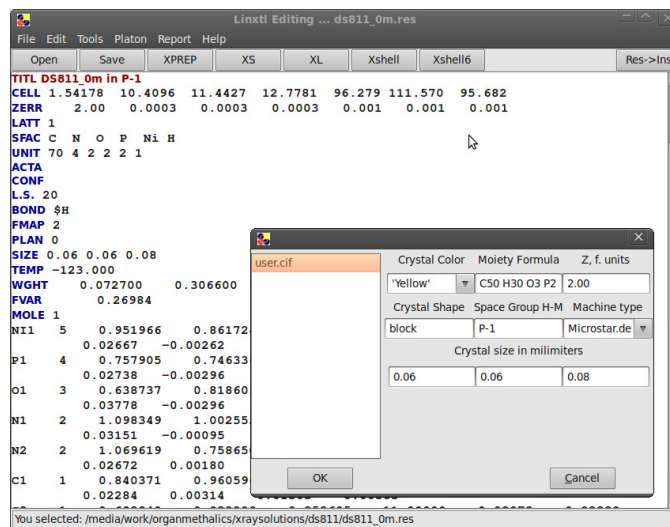


Figure 8.1. Screenshot of LinXtl

For practical purposes, I decided to not include all 50 pages of source code of this software in to this thesis. LinXtl as well as some additional information is available online on my website at <http://dsn.self.com> or at <http://sourceforge.net/projects/linxtl/files/>. Software can be obtained free of charge and distributed under GNU license.

8.2.2 Installation

The current version of LinXtl is available for Linux users only. It was successfully tested on Fedora 9-12¹ and Ubuntu² 8-9.10-10.4. Additional 3rd party programs might be required to use LinXtl. You will need Python³, Tkinter⁴ (wxPython⁵ for version 1.05 and higher), xterm,⁶ SHELX97,⁷ and Platon⁸ installed on your machine. Some additional programs might be quite handy for structural solutions:

Pubcif⁹ – useful for cif validation and publishing

Rasmol¹⁰ – 3D molecular viewer

SADABS^{11,12} - SADABS provides useful diagnostics and can correct for errors such as variation in the volume of the crystal irradiated, incident beam inhomogeneity, and absorption by the crystal support.

XPREP,¹³ **XP**,¹⁴ **XSHELL6**¹⁴ and **XSHELL**¹⁴ (**XSHELL**¹⁴ old version is only available as windows executable via crossover office or wine). The content of the `linxtl.tar` archive must be extracted somewhere on your machine, for example `/home/user/`. All executable files of the above programs must be placed into `~/linxtl/bin` and must have the following names: `xl`, `xp(xpx)`, `xs`, `xprep`, `xh`, `xpro`, `platon`, `xcif`, `cell_now`, `sadabs`, `xshell.exe`. `xpublcif`, `XSHELL` and `brucker` folders of `publcif XSHEEL` must be placed in the `~/linxtl/` folder. To make **XSHELL6** work, you will require `libstdc.so.5` which you will need to place into the `~/linxtl/xshell/lib/` folder.

Finally, if you did everything the right way you can run LinXTL in a terminal like the following: `python /home/user/linxtl/linxtl.pye` or you can make a shortcut to LinXTL with above command on your desktop (this shortcut is available in `linxtl.tar`). If you do not place some executable files in the correct folder or if you do not have them at all, you will not see options available for this program in the menu of LinXTL.

¹ <http://fedoraproject.org/>

² <http://www.ubuntu.com/>

³ <http://www.python.org/>

⁴ <http://tcl.sourceforge.net/>

⁵ <http://www.wxpython.org/>

⁶ <http://invisible-island.net/xterm/xterm.html>

⁷ <http://shelx.uni-ac.gwdg.de/SHELX/>

⁸ <http://www.cryst.chem.uu.nl/spek/platon/pl000000.html>

⁹ <http://journals.iucr.org/services/cif/publcif/>

¹⁰ <http://www.umass.edu/microbio/rasmol/>

¹¹ Sheldrick, **1996**

¹² <http://www.chem.tamu.edu/xray/pdf/manuals/sadabs.pdf>

¹³ <http://shelx.uni-ac.gwdg.de/tutorial/english/xprep.htm>

¹⁴ <http://www.bruker-axs.com/>

